UiT The Arctic University of Norway

Faculty of Engineering, Science and Technology (IVT)
Department of Computer Science and Computational Engineering

Numerical Modelling of Damage Conditions on Herøysund Bridge in Herøy Municipality, Nordland Norway

Christopher Odongo

Master's Thesis in Engineering Design, END-3900
May 2024

Master Thesis in Numerical Modelling of Damage Conditions in the Herøysund bridge found in Herøy Municipality Nordland Norway

Title: Numerical Modelling of Damage Conditions on the Herøysund Bridge in Herøy Municipality, Nordland Norway		***Date of Submission*** 15.05.2024 ***Candidate Number:*** 16
Subject Code: END 3900 -1 – 24V	***Subject Name:*** Master's Thesis	***No. of Report Pages:*** 56 ***No. of Attachment Pages:*** 34 ***Total Number of Pages:*** 90
Author: Christopher Odongo		
Faculty: Engineering Science and Technology	***Department:*** Computer Science and Computational Engineering	
Field of Study: Master of Science in Engineering Design		
Supervisors: Prof. Harpal Singh, UiT Narvik, Norway Dr. Daniel Storni, Wise Technologies, Italy		
Sponsors: Herøy FoU Research, Fylkeskommune, Statens Vegvesen, UiT Narvik, NTNU, and SINTEF		
Keywords: Herøysund bridge, Numerical simulation, Ansys Mechanical, Cracks propagation, Dynamic response, Modal analysis, CAD, SIFS, J-integral, Frequency, Deformation, Equivalent stress, SolidWorks, FEM		

Acknowledgement

Foremost, I express my sincere gratitude to my supervisor, Prof. Harpal Singh, together with Prof Guy Beeri Mauseth for all their support, motivation, and wise counsel during the entire project cycle, without which this master thesis work would not have been successful.

Secondly, my utmost appreciation goes to the Herøy FoU project team in UiT Narvik for the financial support during the execution period and coming out as the main sponsors of this master thesis project.

I equally express special recognition to my dear wife, Madam Norah A. Odongo for holding my hand for the whole period and seeing me through to the dead-end of this master's thesis project.

Finally, I express my indebtedness to all my teachers, mentors and colleagues for the moral support and guidance during the entire studentship life in Narvik.

May 15th, 2024

Ouma Christopher Odongo
UiT- The Arctic University of Norway
Narvik Campus – 2024

Abstract

The usability of bridges is highly dependent on their safety conditions since they are subjected to all sorts of loading that might compromise their ability to withstand stresses over a prolonged period. As a result, dynamic response evaluations and fracture mechanics analysis are essential concepts that can help in monitoring the behaviour of bridges, predicting their lifespan, and planning rehabilitation. Therefore, this research endeavoured to investigate the structural behaviour of Herøysund Bridge through analytical computation and numerical simulation of damage conditions in connection with fracture failure anatomization and dynamic response analysis. The computer-aided design (CAD) model of the bridge, with induced cracks, was developed and assembled in SolidWorks based on the existing 2D drawings and photos taken at the bridge site location.

The 3D model was then exported to Ansys mechanical APDL solver for finite element examination. The overview of analytical computations on structural vibrations and fractural failure study on bridges were handled. Thereafter, Ansys finite element modelling was performed with regards to dynamics of cracks propagation, modal parametric analysis, harmonic response, response spectrum, and random vibration reviews. Results were generated in terms of stress intensity factors (SIFS) and strain energy release rate (J-integral) of cracks, mode shapes, natural frequencies, phase angle, peak response location, total and directional deformations, and equivalent stresses acting on the bridge model. Finally, the obtained results were discussed, and the conclusions drawn.

Keywords:

Herøysund bridge, Numerical simulation, Ansys Mechanical, Cracks propagation, Dynamic response, Modal analysis, CAD, SIFS, J-integral, Frequency, Deformation, Equivalent stress, SolidWorks, FEM

Table of Contents

List of Tables

List of Figures

Abbreviations and Symbols

FEM : Finite Element Modelling

WP : Work Package

ANSYS : Analytical System

SHM : Structural Health Monitoring

LVDT : Linear Variable Differential Transformer

GPR : Ground Penetrating Radar

CAD : Computer Aided Design

FEA : Finite Element Analysis

TEDTL: Total Evenly Distributed Traffic Load

TTLC : Total Traffic Loading at Center

AADTT : Annual Average Daily Truck Traffic

SIFS : Stress Intensity Factors

LEFM : Linear Elastic Fracture Mechanics

SRSS : Square Root Sum of Squares

PSD : Power Spectral Density

NTNU : The Norwegian University of Science and Technology

UiT : University of Tromsø the arctic university of Norway

APDL : Ansys Parametric Design Language

UTS: Ultimate Tensile Strength

YTS: Yield Tensile Strength

RS : Response Spectrum

BBM : Better Bridge Maintenance

RMS: Root Mean Square

3D : Three dimension

2D : Two dimension

EN : European Standards

NS : Standard Norway,

GPa : Gega-Pascal

MPa : Mega Pascal

Pa : Pascal

KPa : Kilo Pascal

K : Stress intensity factors

G_1 : Strain energy release rate

K_{1C} : Fracture toughness

J_C : Critical J-integral value

a : Crack length

kN/m : kilo newtons per metre

$MPa.\sqrt{m}$: Mega Pascal square-root meter

E : Young’s modulus

G : Shear Modulus

v : Poisson’s ratio

σ : Applied stress

σ_c : critical stress

σ_f : fracture stress

ϵ : Elastic strain

Γ: Gamma

1 INTRODUCTION

Bridges are important parts of the transport infrastructure that play a pivotal role in commerce by facilitating the smooth flow of traffic [1]. Different types of bridges serve different purposes and are subjected to different conditions of the environment [2]. As a result, bridges get damaged by stress and other forces resulting in poor conditions hence losing their efficiency over time [3]. Several factors may result in bridge failures and damages. Some include design and structural flaws like it was in Brooklyn Bridge, floods, and erosion as it was in Ovilla road bridge in Texas, earthquakes and extreme events like it was in California bridge, strong winds as it was in Tacoma narrow bridge in Washington [4-6]. Other factors are traffic overload, fatigue, infrastructural issues like concrete deck cracking and steel girders corrosion [4, 7].

Bridge failures may result in catastrophe, economic damage, and human life losses [3, 8]. Therefore, it is paramount to employ cost-effective approaches to monitor the bridges in order to identify the damages [2, 4]. The collapse of Morandi bridge in Genoa, Italy, in August 2018 disclosed that existing infrastructure require constant monitoring [9]. As a result, this master thesis aimed to identify and analyse damage conditions of the Herøysund bridge through finite element modelling of fractures, and vibration conditions.

1.1 Background Information

The Herøysund bridge in Herøy municipality, North Norway is a self-supporting post-tensioned casted girder bridge built-in 1966 [10]. The bridge has been studied extensively by various organizations, like AAS-Jakobsen, Multi-Consult, and NTNU to monitor the damage conditions and maintenance required [11]. In 2017, Multi-Consult performed an evaluation on the Herøysund bridge where they discovered detrimental chlorides on the concrete structure [12, 13]. In 2020, AAS-Jakobsen conducted capacity evaluation and maintenance works to highlight the need for ongoing monitoring of the bridge condition [14, 15]. In 2021, HBK Norge AS built a monitoring system for the Herøysund Bridge [14]. In 2022, NTNU researched on the bridge post-tensioned reinforcement corrosion as part of the Better Bridge Maintenance (BBM) D2 project [10, 16].

Several attempts were made to resuscitate the bridge, but additional damage was discovered in the process. For instance, it was discovered that in several locations the conduits for the post tensioning tendons lacked up to 50% of injection grout and that there was corrosion in the post tensioning tendons [10, 17]. Consequently, the bridge was closed to heavy traffic and instead, it was decided that a new bridge be built next to the old bridge under study [11]. The old bridge was to remain accessible to light traffic with weight restrictions of up to a maximum of 50 tons until the new bridge would be completed later in the year 2024 [16]. Equally, Nordland Fylkeskommune and Statens Vegvesen in partnership with UiT Narvik, NTNU, and SINTEF decided to put the old bridge for scientific research on various technologies that are classified into four work packages that include [10, 11]:

- WP1: Structural health monitoring
- WP2: Corrosion inspection, assessment, and repair
- WP3: Structural assessment with damaged post-tension
- WP4: Reliability and uncertainty quantification

This master thesis project was based on work package (WP1) with main objective of performing finite element modelling of bridge fractures and vibration conditions to determine the extent of damage conditions of the Herøysund bridge. The whole project was under supervision of Herøy FoU team.

1.2 Features of Herøysund bridge

The Herøysund bridge with construction bridge no. 18-1069 is a post-tensioned cast-concrete bridge connecting South and North Herøy to country road 828 along the coast of Helgeland in northern Norway [10, 13, 15, 17, 18]. The bridge design categorization is B250 to B400 and is part of FV828 located at HP3/5991m – 6145m [16]. It has variable heights, a bridge slab, underlying load-bearing beams, and pillars [14]. The bridge features seven axes, five columns, and two land vessels with rock foundations of pillars and earth vessels. It has a total length of 154.5 m and an overall width of 5.30m divided into one carriageway and pavements on both sides [17, 18]. It has concrete density of 2300 kg/m^3 and the ratio of the weight of concrete to importance of cement is 6.57 [12]. The load restrictions for the bridge is according to weight regulations 2/1958, and the bridge was designed using tension control method under the traffic load BK-10/50 [14].

The main span, axes 4 to 5, measures 60 metres in addition to the bridge having cast-in-place pressure plate facing piers 4 and 5 [12, 18]. The primary portion of the bridge, between axes 3 and 6, is braced and tension-reinforced, while the remainder is slack-reinforced [16]. The viaducts are girder structures with lax reinforcement [17]. There is no excess reinforcement along the length of the beams. The bridge was constructed using the stress control method, contrary to modern techniques, such as the partial factor method, which incorporates material and load factors [16, 18]. Figure 1-1 is a layout of Herøysund bridge while figure 1-2 is section profiles variation of the bridge spans.

1.3 Project Description

The modeling of structures is a fundamental step in the design and assessment processes that enable engineers and researchers to understand the behavior of structures subjected to different load conditions. In this master thesis project, the bridge design was developed in SolidWorks while the modeling was performed using commercial software ANSYS based on the Finite Element Modelling (FEM) principles. The critical issues considered during the modeling included the elements used for structural modeling, their schematization, the materials mechanical properties, the applied loads and masses, and the boundary restraints. The choice of these parameters was not trivial given that they affected the response of the model and its reliability in representing the actual structural behavior.

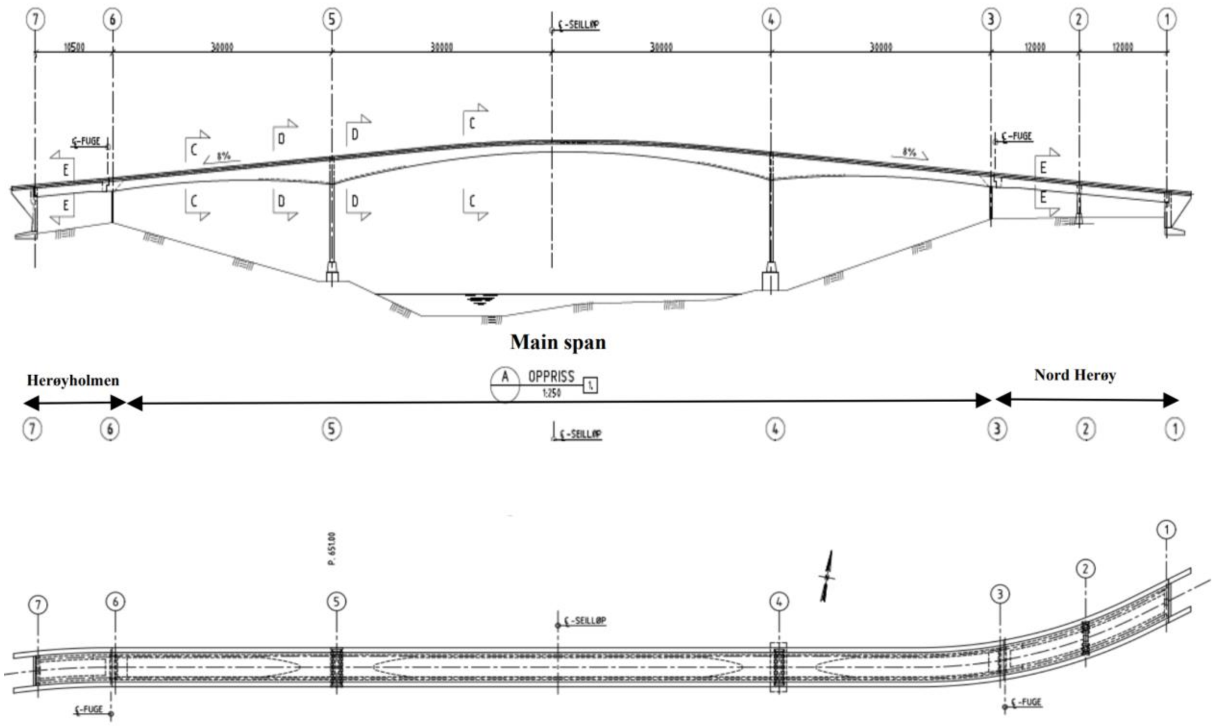

Figure 1-1: Herøysund Bridge layout with dimensions in mm [15, 16, 19]

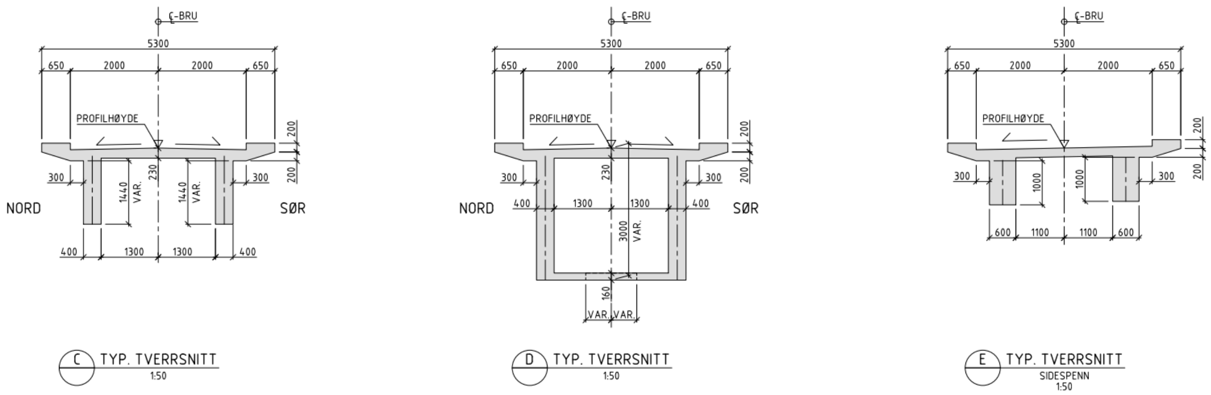

Figure 1-2: Top deck cross section profiles of bridge spans 1-7 all dimensions in mm [15, 16, 19].

To execute the main task of this master thesis project, a detailed 3D solid model of the Herøysund bridge with cracks was developed in SolidWorks design tool. Then, the computer-aided design (CAD) model was transferred to Ansys mechanical APDL solver for structural simulation.

1.4 Regulations

The regulations reference for this study was based on the following standards:

- Standard Norway, NS: 3473 Design of concrete structures - Calculation and construction rules, second edition, 1975.
- Norwegian Public Roads Administration: Handbook 239 Use classification, Load regulations 1920-1973 and bridge standards 1912-1958, 2003.

- Norwegian Public Road Administration: Handbook R-412 Classification of use, 2014, with NA circular 2017.
- EN 1992-1-1 (2004) (English): Eurocode 2: Design of concrete structures, (4)P, Eurocode 2 Part 2, Reinforced and prestressed concrete bridges, EN 1991-1.1 Densities, body mass and external loads.
- ISO 16311-2:2014, Maintenance and repair of concrete structures – Part 2: Assessment of existing concrete structures.
- ISO 13822:2010, Bases for design of structures – Assessment of existing structures.

1.5 Scope of Study

The focus of this master thesis was to develop a clear roadmap in numerical modelling of damage conditions of the Herøysund bridge. This incorporated the identification of damages like fractures on the existing structure, designing the bridge model, and numerical modelling of bridge conditions with respect to structural design analysis, bridge fracture evaluation, and dynamic response review in terms of modal analysis, harmonic response, response spectrum and random vibration study. In order to accomplish this mission, the following were the clear-cut guidelines on the activities lined up to achieve the main goals:-

(i). Study of different nondestructive damage identification methods focusing mainly on vibration-based damage identification methods.

(ii). Analysis of currently available system solutions i.e. analysis of the available beam-based and shell-based finite element models and analysis of requirement specifications, definitions, design requirements, given standards or norms, guidelines, practical experiences, etc.

(iii). Structural design, analytical and numerical examination of the concepts, and establishment of case studies including specifications i.e., physical and design conditions, loading and boundary conditions, requirements for stiffness, strength, weight, materials, and temperatures.

(iv). Physical identification of damage locations on the structures like cracks and corrosions in tendons, girders, decks, and bridge piers.

(v). Finite Element modelling of the structural damage conditions of Herøysund bridge through fracture analysis, modal parametric study, response spectrum evaluation, harmonic response analysis and random vibration anatomisation etc.

1.6 Significance of the Research Work

The significance of this study was attached to the global increasing monetary pressure on bridge authorities to extend the life span of the existing bridges. Identification and analysis of damage conditions of structures like bridge cracks and corrosions help in defining clever maintenance strategies through the detection and correction of fractures in earliest stage and providing accurate remaining lifespan predictions of structures [9].

Globally, inspection and maintenance of bridges is not universal, leading to severe damages in thousands of structures [17]. This equally remains a concern in northern Norway and coastal areas where bridges serve as critical infrastructural components in boosting economies of regions where they are located. In particular, the Herøysund Bridge is very crucial to local fishing industry in Herøy Municipality as it connects North and South Herøy [12]. The intention of this study was to improve the usability of bridges by identifying and detecting damages, analysing the extent of damage through numerical modelling, and providing advisory on the safety and reliability.

1.7 Research Objectives

Based on the mission and vision of this project, this master thesis was anchored on five clear and specific objectives. They include:-

(a). To study structural damage identification and detection methodologies with focus on fractures and vibration analysis.

(b). To identify cracks and corrosions, analyse design requirement specifications, definitions, standards or norms, guidelines, and practical experiences on Herøysund bridge.

(c). To develop Herøysund bridge 3D solid design model in SolidWorks design software based on the available 2D drawings and sketches of the bridge.

(d). To conduct analytical and numerical analysis of the concepts on fracture mechanics, damage identifications and dynamic response evaluations of the bridges.

(e). To perform finite element simulation of the damage conditions of Herøysund bridge structural model through cracks propagation analysis, modal parametric and vibratory analysis using Ansys 2024 R1 program.

1.8 Research Questions

In order to cover the entire scope of this project and achieve all the objectives of this study, the following research questions were to be answered.

(i). What is the current status of damage conditions on the Herøysund Bridge?

(ii). Where are the possible locations of cracks and corrosions on Herøysund Bridge?

(iii). What are the specifications, design features, standards, boundary conditions, and guidelines applicable in the analysis of Herøysund bridge?

(iv). What are the possible causes of cracks and corrosions on the Herøysund bridge?

(v). What are the possible methods applicable in the analysis of cracks and other damages on Herøysund bridge?

1.9 Research Hypothesis

The following hypothesis were developed based on research objectives and questions:

(a). Herøysund bridge is in good shape and usable by all traffic.

(b). Main causes of Herøysund bridge damage condition are traffic overload and structural fatigue.

(c). Vibration-based damage identification methods are the most suitable for analysis of Herøysund bridge damage conditions.

(d). Cracks and corrosion damages are on the top deck of the Herøysund bridge structure.

1.10 Research Project Plan

The master thesis project was scheduled for 18 weeks, from 9th January 2024 to 15th May 2024. The thesis was executed in accordance with the NS-EN standards and Statens Vegvesen directives. Solidworks 2024 was used to develop the 3D design model of the bridge and Ansys 2024 R1 was used for finite element analysis (FEA). Scientific report writing was conducted in MS word, Excel, PowerPoint and Overleaf.com. At the end, all documents were delivered to supervisors and sensors for evaluation. The finite element models and analysis files together with design files developed during the study were included in the project folder.

In order to accomplish all the outlined tasks and objectives, a Gantt chart showing a schedule plan for executing every section of the project was generated as in figure 1-3.

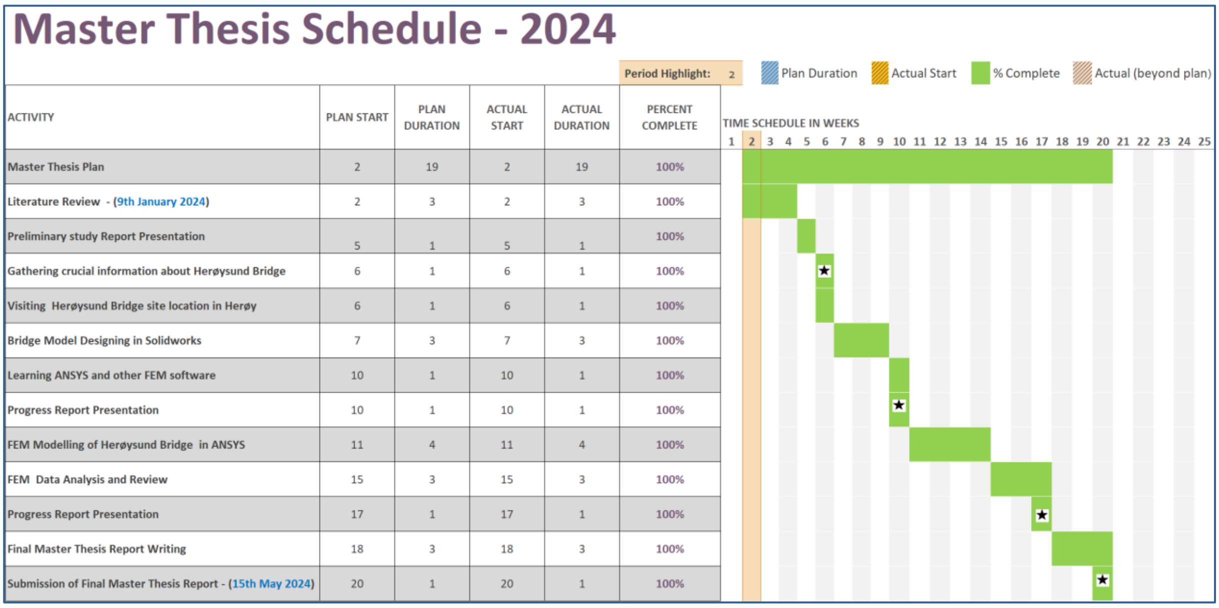

ACTIVITY	PLAN START	PLAN DURATION	ACTUAL START	ACTUAL DURATION	PERCENT COMPLETE
Master Thesis Plan	2	19	2	19	100%
Literature Review - (9th January 2024)	2	3	2	3	100%
Preliminary study Report Presentation	5	1	5	1	100%
Gathering crucial information about Herøysund Bridge	6	1	6	1	100%
Visiting Herøysund Bridge site location in Herøy	6	1	6	1	100%
Bridge Model Designing in Solidworks	7	3	7	3	100%
Learning ANSYS and other FEM software	10	1	10	1	100%
Progress Report Presentation	10	1	10	1	100%
FEM Modelling of Herøysund Bridge in ANSYS	11	4	11	4	100%
FEM Data Analysis and Review	15	3	15	3	100%
Progress Report Presentation	17	1	17	1	100%
Final Master Thesis Report Writing	18	3	18	3	100%
Submission of Final Master Thesis Report - (15th May 2024)	20	1	20	1	100%

Figure 1-3: *Master Thesis Project Execution Plan*

2 LITERATURE REVIEW

The ability to monitor structures and identify damage has gained popularity in the civil engineering world. Different methods for identifying bridge damages and cracks have been proposed based on different theories and laboratory tests [20]. This chapter was set to evaluate different existing methods proposed to identify and analyse damage conditions on bridges. One such method that has gained prominence in recent years is structural health monitoring (SHM) [8].

2.1 Structural Health Monitoring

Bridges are subjected to high-temperature fluctuations, harsh storms, and numerous traffic scenarios when used over a long time [2]. As a result, it is important to identify damage locations and examine their severity in the bridge structures. Structural health monitoring is based on four principles. They include: ascertainment of damage existence, defining damage location, identification of the damage severity, and prediction of the remaining lifetime of the damaged structure [1, 2, 7]. Choosing the best method for monitoring bridges depends on different factors like the type and age of the bridge, the type and extent of the damage, cost, and availability of the materials, etc [2].

Modern bridges are inspected with a variety of sensors [2]. Some of the most widely used sensors include fiber optic sensors, accelerometers, vibrating wire sensors, linear variable differential transformers (LVDT), strain gauges etc [7, 9]. They are used in measuring various parameters such as natural frequencies, acceleration forces, linear displacement, strains, loads and temperature fluctuations [7, 20]. Reliable and effective damage identification techniques are crucial to maintaining safety and integrity of a structure [8].

A broad range of techniques, algorithms, and methods have been developed to solve various problems encountered in different structures, from basic structural components such as beams and plates to complex structural systems like bridges and buildings [7, 8, 21, 22]. Most non-destructive damage detection methods are classified as either local or global [21]. The local detection methods comprise of magnetic field methods, acoustic and ultrasonic methods, radiography, ground penetrating radar (GPR), sonic testing, impulse response etc [4, 9]. These methods are integrated with visual inspections, to compensate for knowledge that may be ignored when only using optical methods [9].

The fundamental idea of global damage detection method is that the damage-induced changes in the physical properties like mass, damping, and stiffness will cause detectable changes in modal properties such as natural frequencies, modal damping, and mode shapes [2, 23]. The frequencies of vibration are directly related to the stiffness and the mass of the structure while the mode shapes are related to the defect location [21]. As a result, the emergence of cracks in a structure is associated with reductions in stiffness. Therefore, it is imperative to identify damages by analysing the changes in vibration features of the structures [8].

2.2 Structural Vibration Evaluation

Vibrations or dynamic motions are regarded as unpleasant and unwanted causing undesirable consequences like discomfort, noise, fatigue, destruction, and collapse [4, 6]. Vibratory systems have means of storing potential energy (spring), a means of storing kinetic energy (mass or inertia) and a means by which energy is gradually lost (damper) [5]. The vibration of a system involve the transfer of potential energy to kinetic energy and kinetic energy to potential energy alternately [24]. However, if the system is damped some energy is lost during vibration and must be replaced by external source in order to maintain steady state of vibration [21].

Structures like bridges receive responses when subjected to dynamic and vibration analysis from external and internal forces [5, 24]. The behaviour of such structures at resonance is a fundamental aspect of structural dynamic analysis [25]. The excitation of resonant frequencies of these structures occur with existence of vibration however small or insignificant the vibration [4, 24]. As a result, there is need of having strong reliable vibration analysis tools that can provide in-depth of structural characteristics, operating conditions, and performance criteria [9].

The vibration features of a structure can be determined by random vibration analysis, response spectrum study, harmonic response investigation, and fatigue failure evaluation. Random vibration is described by three factors; amplitude, time, and frequency [5, 21]. The natural frequency of vibration of a structure corresponds to the resonance frequency of the structure [7, 9]. Maximum displacements are produced when a structure is subjected to vibration at its natural frequency [4]. The excitation and responses are measured in the form of time domain method analysis which can be represented in mathematical Fourier series as outlined in equation (2.1) [6, 26]:

$$f_{\mathrm{P}}(t) = \mathrm{Q} + \sum_{n=1}^{\mathrm{K}} \mathrm{Q}\,\alpha_n \sin(2\pi\, n f t + \emptyset_n) \tag{2.1}$$

where;

Q is the external weight
f is the frequency of the force
n is the harmonic number
K is the total harmonics contribution
α_n is the *nth* harmonic's load factor
$\emptyset_n$ is the *nth* harmonic's phase angle

The major limitation of time domain method is that it is too simple to capture the full complexity of the actual load applied to the system given that loading is heavily dependent on the characteristics of the moving load on the bridge [7]. Other types of domain methods include frequency domain and modal domain.

2.3 Dynamic Response Review

The Vibration-based damage detection methods involve measuring and evaluating the dynamic behaviour of the structure by comparing it to the behaviour simulated by numerical models [27]. It is used to discover damage in bridges by analysing the structure load and response mechanism [21]. Damage detection and location accuracies are influenced by damage extent and type of response. Changes in structures like damages and deteriorations result in a decrease of their load-carrying capacity hence impacting on their dynamic response [4, 9]. The dynamic responses of structures vary depending on their inherent damages [24]. Therefore, dynamic response characteristics can be used to evaluate quality and structural integrity [6, 21]. As a result, there is possibility of identifying the damage conditions from the variation of structural responses before and after the occurrence of the damages [25, 28].

A classification of structures can be developed based on vibration monitoring using modal parameters, natural frequencies, mode shapes, damping values, and vibration intensities [2, 25]. Frequencies and mode shapes of structures under vibration are functions of its mass and stiffness [21]. Since mass is usually constant, any change in the dynamic behaviour is associated with stiffness variation which point to the presence of damage in the structure [7, 9]. Damage detection can be carried out on four types of responses i.e., deflection, inclination angle, strain, and curvature computed from the numerical models [24, 25]. Monitoring of dynamic response of structures makes it possible to get very quick knowledge of damage conditions and locations [8, 28].

2.4 Modal Analysis

The modal domain methods play a pivotal role in structural damage identifications than time or frequency domain methods [8]. This is because the modal properties like natural frequencies, modal damping, mode shapes, etc are easier to interrogate than mathematical features in time and frequency domain [3-5]. The modal domain data can be examined through modal analysis techniques [26].

Modal analysis is an approach of determining the natural frequency, mode shapes and damping properties and using them to formulate mathematical models for dynamic behaviour of structures [4, 28]. The mathematical model formulated is called modal model of the system and the information of properties are known as modal data [26, 28]. Modal testing is the process of testing structures with the sole purpose of obtaining analytical description of dynamic and nature of vibration response [4, 5].

There are two types of structural dynamic testing. They include forced vibration testing and ambient vibration testing [7]. The forced vibration testing is done by dropping a known force on the structure which will induce a condition of free vibration [9]. The ambient vibration testing represent a real operating condition of the structure by utilising the disturbances induced by traffic, wind, or other natural and environmental excitations [5, 26]. Given that structures like bridges are large in size, it is viable to get excitation from ambient vibration methods. In addition, ambient testing does not interrupt service of the test structure hence can be applied for long term health monitoring of structures [2]. Modal-based bridge health monitoring identify damage, according to the variation of modal parameters like natural frequencies and mode shapes [28].

3 METHODOLOGY

In this chapter, the outline of executing the project is discussed and the procedures in which every step was undertaken is explained.

3.1 Design of Experiment

To effectively execute the project, all the available information about Herøysund bridge were gathered and analysed. The initial 2D drawings, designs and regulations of the bridge model were obtained, analysed and other relevant data useful in developing the 3D design were used to come up with CAD design for FEM analysis. Photos taken around the bridge area were keenly studied, to help in visual identification of cracks, their locations, and the extent of damage. SolidWorks 2024, and Ansys Space Claim 2024 R1 were used to develop the CAD model of Herøysund bridge and to insert cracks and fissures on the 3D solid model. Analytical computation of the bridge was conducted through elasticity theory analysis, structural vibratory analysis, and fracture mechanics investigation. In addition, numerical methods, and finite element modelling (FEM) in ANSYS Workbench 2024 R1 and Ansys Mechanical APDL 2024 R1 were employed to study the structural behavior of the Herøysund bridge through fracture mechanics analysis, harmonic response, response spectrum and random vibration evaluation. Figure 3-1 is the outline of the stages used in executing the project.

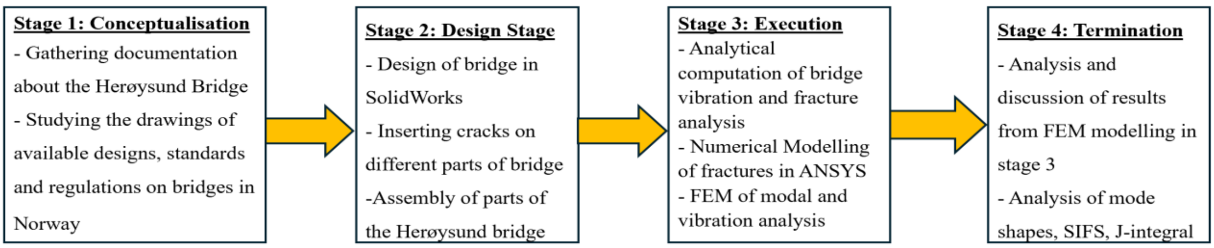

Figure 3-1: *Stages involved in the research design execution.*

3.2 Methodology of 3D-Solid Model

The Eurocode EN 1992-1-1 standardization for concrete structural analysis [29] outlines the use of 3D-Solid, beam, or Shell elements methods for FEM analysis in order to understand experimental and numerical behaviour of concrete structures [30]. As a result, this study chose to use the 3D-solid elements model for FEM analysis.

3.2.1 CAD Modelling

The 2D drawings of the Herøysund bridge were obtained from the UiT research team Herøy FoU group. The AAS-Jakobsen prepared drawings [19] obtained from UiT University were the main materials used for the preparation of the 3D model in SolidWorks. Drawings from the Brutus document directory, provided by SV and NFK, served as a foundation for understanding the bridge structure. Original drawings like in figure 3-2 from the multi-consult were studied to understand main span dimensions and pillar dimensions.

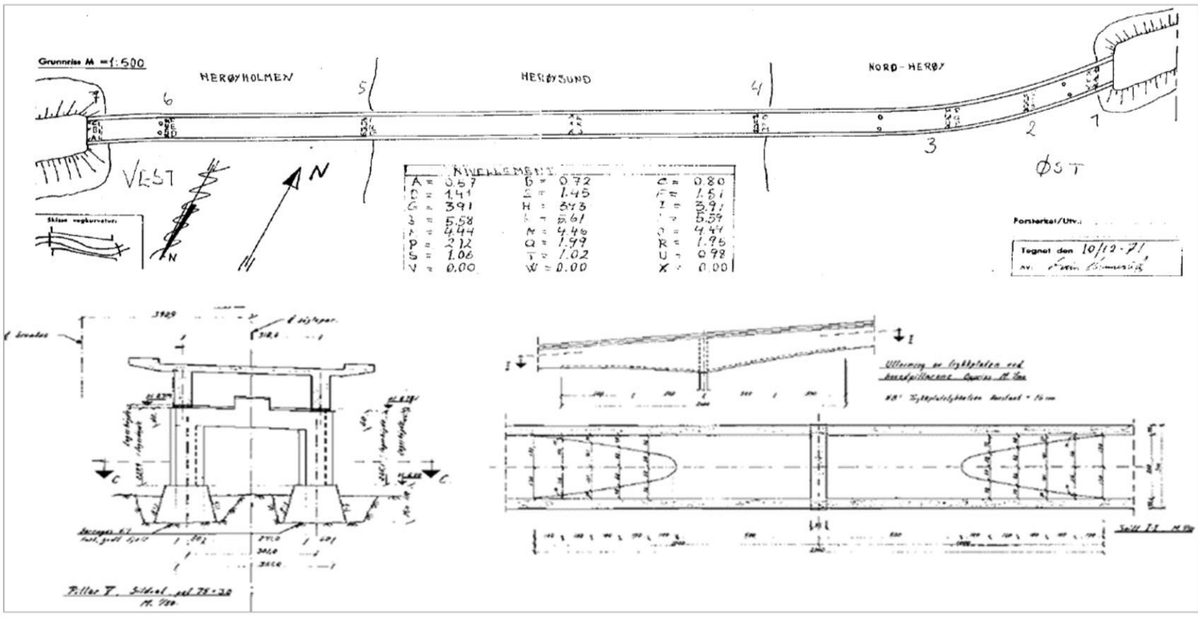

Figure 3-2: *The 1971 Drawings of Herøysund bridge parts [13].*

In addition, the details about pillars, bridge spans, pressure plates, and beam curvatures were extracted from the 2D drawings like one shown in figure 3-3. The CAD models of pillars, and bridge spans developed in SolidWorks were generated separately as shown in figure 3-4.

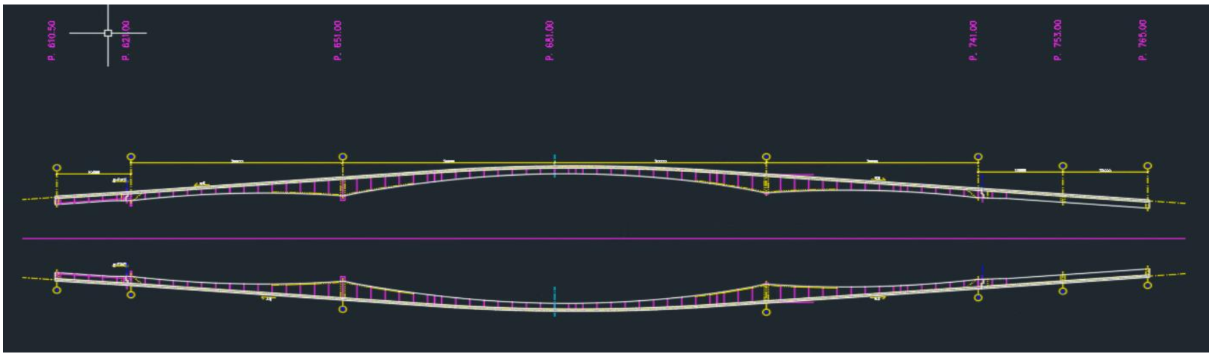

Figure 3-3: *Herøysund Bridge layout drawing [12, 19]*

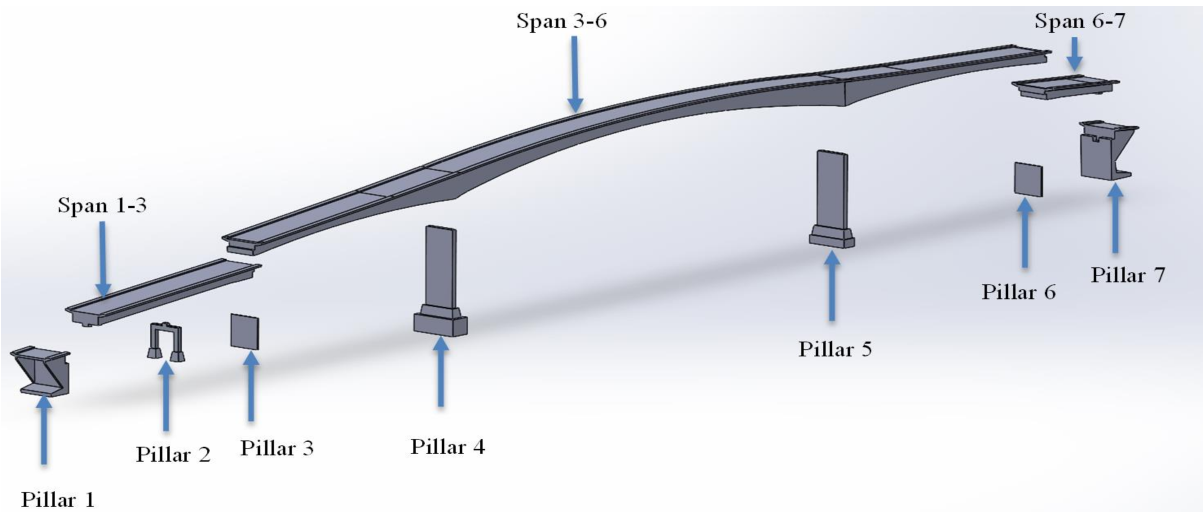

Figure 3-4: *Exploded view of Herøysund bridge parts.*

3.2.2 CAD Assembly

The 3D model parts were assembled with each pillar connected to the spans and spans connected to each other to form a continuous deck as shown in figure 3-5. Pillars 1, 2, 3, 6 and 7 were assembled to the deck with load bearing structural steel plates. Pillars 4 and 5 were assembled to the deck with load bearing structural concrete plates. The 3D model parts, and assembly were submitted as separate files together with this report.

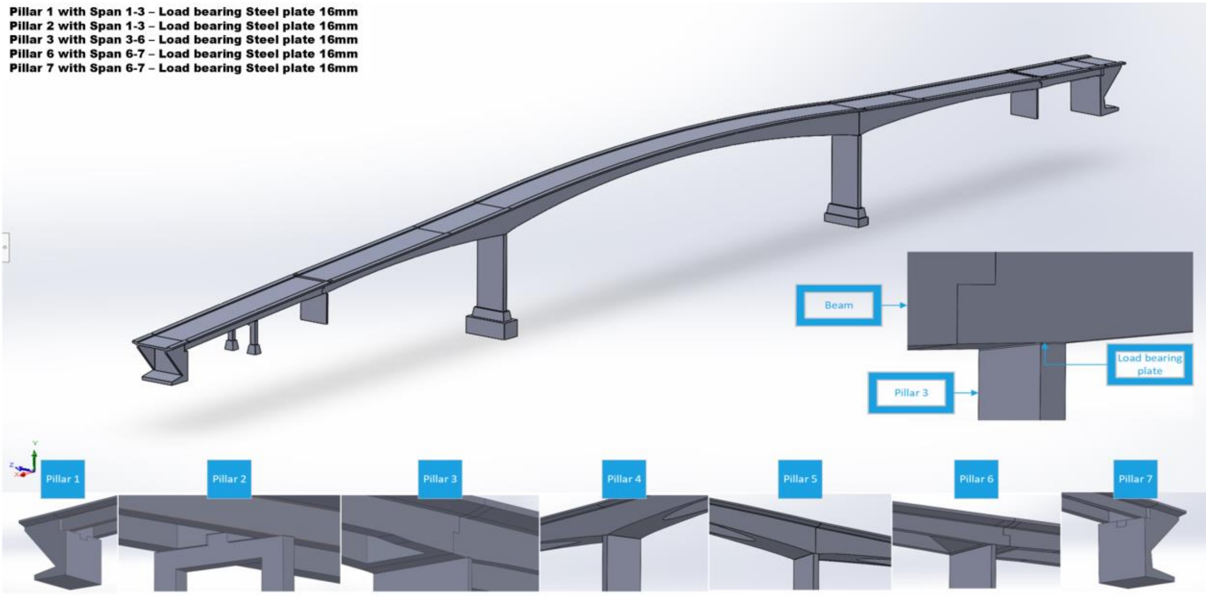

Figure 3-5: *CAD Assembly of Herøysund bridge components*

3.2.3 Cracks on the design

In the process of developing the bridge parts, cracks and fissures identified on the main bridge were incorporated on the different parts of the bridge model. Several fissures were physically identified but only seven cracks that were outstanding were used for the Ansys finite element modelling. Figure 3-6 shows the photos of some of the identified cracks on the Herøysund bridge.

Figure 3-6: *Photos of some of the cracks identified on Herøysund bridge*

The cracks were incorporated in the design as cuts assumed to be of trapezoidal shape. The locations of the cracks can be seen in figures 3-7 and 3-8 where crack 1 is on span 1-3, crack 2 is on pillar 2, crack 3 location is on span 3-6, and crack 4 is on pillar 4. Other cracks are crack 5 on pillar 5, cracks 6 and 7 are on span 6-7 where crack 6 is fissure cutting across the span. The cracks were generated with different crack length (a) values.

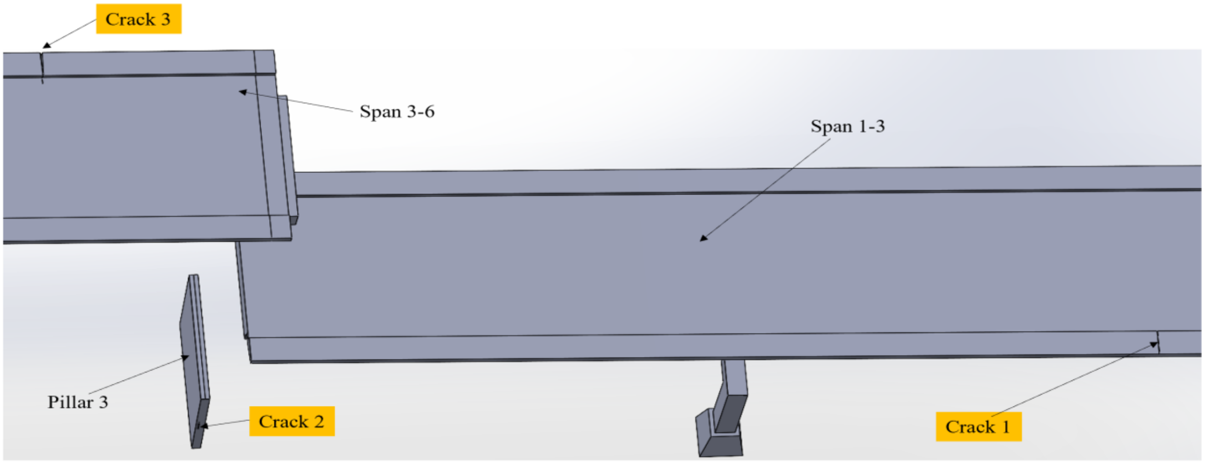

Figure 3-7: *Locations of cracks 1,2 and 3 on Herøysund bridge model.*

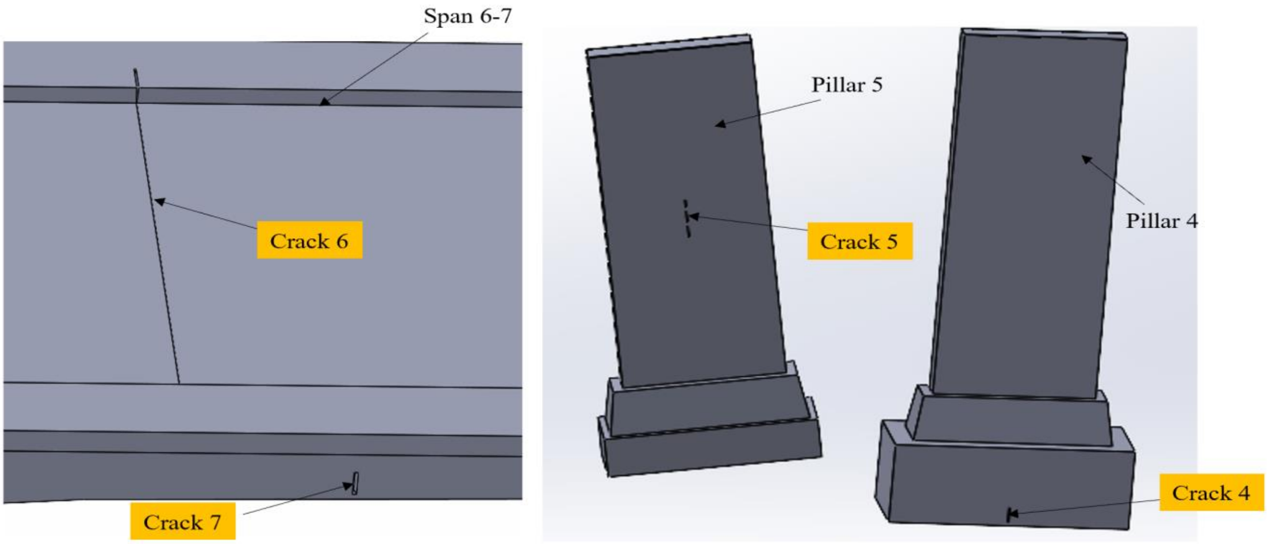

Figure 3-8: *Locations of cracks 4,5,6 and 7on Herøysund bridge model*

3.2.4 CAD Modelling Assumptions

The Solid model created was simplified to meet the project specifications with myriad of assumptions as follows:

(i). Post-tensioning in the bridge were tendons embedded within the structure, hence impossible to physically locate them. To compensate on the limitation, an inward compressive force of $12{,}083{,}400N$ is assumed to act on either side of the main span 3-6.

(ii). The top deck features a 60 mm thick asphalt layer as per [15], that exerts additional load. A uniform load of 7 kN/m is applied to the top deck from pillars 1-7 instead of modelling a layered geometry to avoid FEM contact region errors.

(iii). The design did not consider reinforcements or rebars in pillars and other spans. Therefore, the model was assumed to be entirely concrete with load bearing steel plates between pillars and deck.

(iv). This study assumed existence of seven (7) fissures and cracks at distinct locations of pillars and deck for the purposes of modelling. The cracks were assumed to have different crack lengths. However, some minute cracks which were assumed to be of no effect were ignored.

3.3 Methodology of Finite Element Modelling

FEM approach is usually dependent on geometry, materials, configuration, and simplification. However, there could be circumstances where linear and non-linear analyses are fundamental. The guidelines in Eurocode 2, CEN (2001), recommended using linear or non-linear analysis methods for force distribution determination [31]. This study considered a linear analysis method. As per the Eurocode recommendations, this study focused on loading conditions like self-weight, traffic loading, asphalt load, while the joints were assumed to be frictionless. The bridge was modeled with cracks and the analysis focused on fracture and modal parametric analysis where the structural behavior under loading was observed.

Considering the parameters of this study, Eurocode recommendations, and the linearity parameters, the FEM for Solid models were conducted in a linear elastic analysis using ANSYS 2024 R1. Understanding the correct approach towards using elements for post-tensioned structures such as Herøysund Bridge was considered crucial in laying foundation for the modelling phase. The scope of this study considered only 3D solid model elements. Parameters such as static structural fracture analysis, modal analysis, harmonic response, response spectrum and random vibration were analysed with the objective of finding structural deflection, stress intensity factors and J-integral of cracks, mode shapes and frequencies, participation factors and effective mass. Understanding the bridge behavior characteristics under loading was deemed necessary given that reliability and durability of a structure is dependent on its vibration that may result in damages. Figure 3-9 shows the Ansys project schematic developed while executing the objectives of this master thesis project.

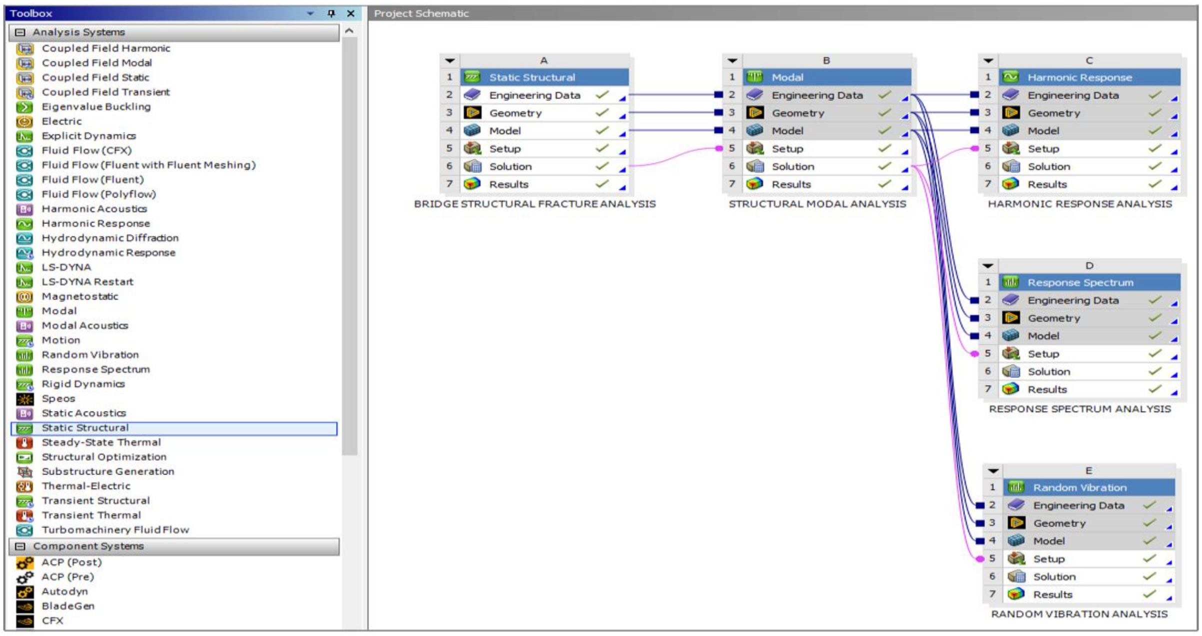

Figure 3-9: *Schematic diagram showing parameters considered in project execution*

4 ANALYTICAL COMPUTATION OF BRIDGE CONDITIONS

The analysis was based upon a dynamical systems approach of mass-spring-damper with multiple degrees-of-freedom. The idea was to model the bridge structure as a system of elastic springs and dampers. The bridge was idealized as Bernoulli-Euler beam having equivalent stiffness [25].

4.1 Elasticity Theory

FEM generate solutions of the deflection based upon a reformulation of Hooke's law [32, 33].

$$\sigma_{ij} = \sum_{k=1}^{3}\sum_{l=1}^{3} c_{ijkl}\,\varepsilon_{kl} \tag{4.1}$$

where σ_{ij} is the stress tensor, ε_{kl} is the strain tensor and c_{ijkl} is the stiffness tensor of the fourth order. The matrix for stress and strain tensor can be expressed as shown [33, 34]:

$$\sigma_{ij} = \begin{bmatrix} \sigma_{11} & \sigma_{12} & \sigma_{13} \\ \sigma_{21} & \sigma_{22} & \sigma_{23} \\ \sigma_{31} & \sigma_{32} & \sigma_{33} \end{bmatrix} \tag{4.2}$$

$$\varepsilon_{kl} = \begin{bmatrix} \varepsilon_{11} & \varepsilon_{12} & \varepsilon_{13} \\ \varepsilon_{21} & \varepsilon_{22} & \varepsilon_{23} \\ \varepsilon_{31} & \varepsilon_{32} & \varepsilon_{33} \end{bmatrix} \tag{4.3}$$

The stiffness tensor c_{ijkl} contains 81 real numbers. However, due to symmetrical properties for the stress and strain tensor the stiffness tensor reduces to 21 values while the stress and strain tensor are reduced to 6 [35].

Since metals and concrete are isotropic materials, their stiffness tensor can be reduced to bulk modulus K and shear modulus G [36]. These moduli can be expressed in terms of the Young's modulus, (E) which is the material's strain response to directional stress, and the Poisson's ratio (v) which is the orthogonal strain response to the directional stress [33, 37]. Relation of these moduli can be expressed as [32, 33, 37];

$$E = 2G(1 + v) = 3K\,(1 - 2v) \tag{4.4}$$

For isotropic materials, Hooke's law eq. (4.1) can be represented as [32, 34, 38]:

$$\begin{bmatrix} \sigma_{11} \\ \sigma_{22} \\ \sigma_{33} \\ \tau_{23} \\ \tau_{13} \\ \tau_{12} \end{bmatrix} = \frac{E}{(1+v)(1-2v)} \begin{bmatrix} 1-v & v & v & 0 & 0 & 0 \\ v & 1-v & v & 0 & 0 & 0 \\ v & v & 1-v & 0 & 0 & 0 \\ 0 & 0 & 0 & \frac{1-2v}{2} & 0 & 0 \\ 0 & 0 & 0 & 0 & \frac{1-2v}{2} & 0 \\ 0 & 0 & 0 & 0 & 0 & \frac{1-2v}{2} \end{bmatrix} \begin{bmatrix} \varepsilon_{11} \\ \varepsilon_{22} \\ \varepsilon_{33} \\ \gamma_{23} \\ \gamma_{13} \\ \gamma_{12} \end{bmatrix} \tag{4.5}$$

FEM uses equations like (4.5) on each element of the meshed 3D geometry to calculate the deformation and stresses in the models [34].

4.2 Equation of Motion

Inertial force, damping force and stiffness force together with externally applied load form the equation of motion that defines the dynamic behaviour of any structure and can be expressed as [4, 5];

$$Inertial\ force\ +\ Damping\ force\ +\ Stiffness\ force\ =\ External\ force$$

According to the theory of structural dynamics, the algebraic form of governing equation of motion of the bridge can be expressed as [5, 39];

$$m\ddot{y} + c\dot{y} + ky = F(t) \tag{4.6}$$

where;

$m\ddot{y}$ is the inertial force
$c\dot{y}$ is the damping force, and c is the damping coefficient
ky is the stiffness force
$F(t)$ is the external dynamic force

The dynamic response can be obtained by solving the equation of motion. The equation is in a matrix form where equation (4.6) becomes [38];

$$[M_b]\{\ddot{\mathrm{y}}\} + [C_b]\{\dot{\mathrm{y}}\} + [K_b]\{\mathrm{y}\} = [F_b] \tag{4.7}$$

where;

$[M_b]$ is the mass matrix
$\{\ddot{\mathrm{y}}\}$ is vibration acceleration (2^{nd} derivative of displacement)
$[C_b]$ is the damping matrix
$\{\dot{\mathrm{y}}\}$ is the vibration velocity (1^{st} derivative of displacement)
$[K_b]$ is the stiffness matrix
$\{\mathrm{y}\}$ is the displacement of the bridge
$[F_b]$ is the force vector

Given that analytical modeling of the bridges may be difficult to realize due to complication of various types of highway bridges, modal synthesis method could be applied to mitigate the challenges. The translation can be given by [28];

$$\{\mathrm{y}\} = [\lambda]\{\mathrm{Z}\} \tag{4.8}$$

where $[\lambda]$ is the mode shape matrix of the bridge and $\{\mathrm{Z}\}$ is the coordinate in the modal coordinate system, which denotes the contribution of every mode shape.

Substituting equation (4.8) into equation (4.7), pre-multiplied by the transpose matrix of the mode shapes, the following equation can be obtained:

$$[M_B]\{\ddot{\mathrm{Z}}\} + [C_B]\{\dot{\mathrm{Z}}\} + [K_B]\{\mathrm{Z}\} = [F_B] \tag{4.9}$$

Where $[M_B]$, $[C_B]$, $[K_B]$, and $[F_B]$ are mass matrix, damping matrix, stiffness matrix, and load vector in the modal coordinate system respectively. They are given by [38]:

$$[M_B] = [\lambda]^T [M_b] [\lambda], \tag{4.10a}$$

$$[C_B] = [\lambda]^T [C_b] [\lambda], \tag{4.10b}$$

$$[K_B] = [\lambda]^T [K_b] [\lambda], \tag{4.10c}$$

$$[F_B] = [\lambda]^T [F_b]. \tag{4.10d}$$

4.3 Free Vibration Analysis of a Bridge

Free vibration refers to the vibration of a system or a structure at its natural frequency without any external force [5]. The behavior of free vibration is determined by the properties of the structure that include mass, stiffness, and damping characteristics [24]. Free vibration analysis is a necessity in the response calculation of bridges by modal analysis [25]. It incorporates global stiffness matrix formation from the free vibration differential equation where eigenvalues and eigenfunctions are determined using nodal displacement and force conditions [20]. The bridge is idealized as a Bernoulli-Euler beam with equivalent stiffness with no external force acting on it as shown in figure 4-1.

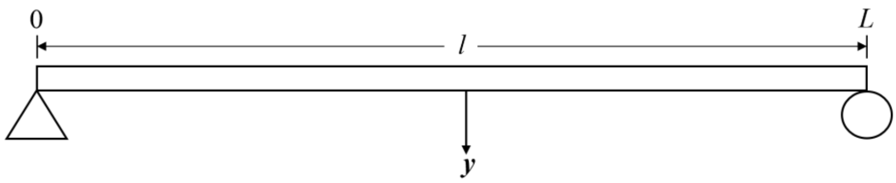

Figure 4-1: *Idealized bridge with no external load on a single span*

The free vibration differential equation of a Euler beam of length, *l* is given by [5, 20]:

$$EI\frac{\partial^4 y}{\partial x^4} + m\frac{\partial^2 y}{\partial t^2} = 0 \tag{4.11}$$

where *EI* is flexural stiffness and *m* is the mass per unit length of the Euler beam.

The vertical displacement, *y* of the Euler beam can be expressed as [24]:

$$y = \varphi(x)\ sin\ \omega t \tag{4.12}$$

where $\varphi(x)$ is the spatial coordinate.

Substituting equation (4.12) into equation (4.11), we can obtain the following equation:

$$\frac{\partial^4 \varphi(x)}{\partial x^4} = \beta^4 \varphi(x), \tag{4.13}$$

where;

$$\beta^4 = \frac{m\omega^2}{EI} \tag{4.14}$$

To find eigenfunctions, the solution of equation (4.12), can be expressed as [20];

$$\varphi(x) = \boldsymbol{A}\ cos\beta x + \boldsymbol{B}\ sin\ \beta x + \boldsymbol{C}\ cosh\ \beta x + \boldsymbol{D}\ sinh\ \beta x \tag{4.15}$$

where integral constants *A, B, C* and *D* can be found by inserting the boundary conditions of the beam.

The rotational angle *θ(x),* the flexural moment *M(x)* and the shear force *S(x)* can be expressed as:

$$\theta(x) = \frac{\mathrm{d}\varphi(x)}{\mathrm{d}x} \tag{4.16}$$

$$M(x) = -EI\frac{\mathrm{d}^2\varphi(x)}{\mathrm{d}x^2} \tag{4.17}$$

$$S(x) = -EI\frac{\mathrm{d}^3\varphi(x)}{\mathrm{d}x^3}. \tag{4.18}$$

The equilibrium equation of the Euler beam considering boundary conditions is given by [34, 38];

$$\begin{Bmatrix} S_1 \\ M_1 \\ S_2 \\ M_2 \end{Bmatrix} = \begin{bmatrix} k_{11} & k_{12} & k_{13} & k_{14} \\ & k_{22} & k_{23} & k_{24} \\ & & k_{33} & k_{34} \\ \text{sym.} & & & k_{44} \end{bmatrix} \begin{Bmatrix} V_1 \\ \theta_1 \\ V_2 \\ \theta_2 \end{Bmatrix} \tag{4.19}$$

where V and θ are the vertical and rotational degrees of freedom of the beam, respectively. Stiffness element components are given as [33]:

$$k_{11} = G(\sin\lambda\cosh\lambda + \cos\lambda\sinh\lambda), \quad k_{22} = \frac{G(\sin\lambda\cosh\lambda - \cos\lambda\sinh\lambda)}{\beta^2},$$
$$k_{12} = \frac{-G(\sin\lambda\sinh\lambda)}{\beta}, \quad k_{23} = -k_{14},$$
$$k_{13} = -G(\sin\lambda + \sinh\lambda), \quad k_{24} = \frac{-G(\sin\lambda - \sinh\lambda)}{\beta^2},$$
$$k_{14} = \frac{G(\cos\lambda - \cosh\lambda)}{\beta}, \quad k_{33} = k_{11}, \quad k_{34} = -k_{12}, \quad k_{44} = k_{22}, \tag{4.20}$$

where;

$$G = \frac{EI\beta^3}{(1 - \cos\lambda\cosh\lambda)}, \quad \lambda = \beta l \tag{4.21}$$

The Integral constants in equation (4.15) can be calculated as shown in equation (4.22) [38]:

$$\begin{Bmatrix} A \\ B \\ C \\ D \end{Bmatrix} = \begin{bmatrix} r_{11} & r_{12} & r_{13} & r_{14} \\ r_{21} & r_{22} & r_{23} & r_{24} \\ r_{31} & r_{32} & r_{33} & r_{34} \\ r_{41} & r_{42} & r_{43} & r_{44} \end{bmatrix} \begin{Bmatrix} V_1 \\ \theta_1 \\ V_2 \\ \theta_2 \end{Bmatrix} \tag{4.22}$$

Where;

$$r_{11} = -H(1 + \sin\lambda\sinh\lambda - \cos\lambda\cosh\lambda), \quad r_{22} = \frac{H(1 - \sin\lambda\sinh\lambda - \cos\lambda\cosh\lambda)}{\beta},$$
$$r_{12} = \frac{H(\sin\lambda\cosh\lambda - \cos\lambda\sinh\lambda)}{\beta}, \quad r_{23} = -H(\sin\lambda + \sinh\lambda), \quad r_{24} = \frac{-r_{13}}{\beta},$$
$$r_{13} = -H(\cos\lambda - \cosh\lambda), \quad r_{31} = -r_{22}\beta, \quad r_{32} = -r_{12},$$
$$r_{14} = \frac{-H(\sin\lambda - \sinh\lambda)}{\beta}, \quad r_{33} = -r_{13}, \quad r_{34} = -r_{14}, \quad r_{41} = -r_{21},$$
$$r_{21} = H(\sin\lambda\cosh\lambda + \cos\lambda\sinh\lambda), \quad r_{42} = \frac{-r_{11}}{\beta}, \quad r_{43} = -r_{23}, \quad r_{44} = \frac{r_{13}}{\beta}$$

and;

$$H = \frac{1}{2(1 - \cos\lambda\cosh\lambda)} \tag{4.23}$$

The eigenvalues, nodal displacements, and nodal forces of Euler-beams can be determined through the procedures described above.

4.4 Ambient Vibration Analysis of Bridge

Forced vibration occurs when an external force or excitation is applied to a structure or system [5]. The vibration frequency in forced vibration matches the frequency of the external force. Given that forced vibration tests are expensive and time-consuming [20], this study assumed ambient vibration testing where vibration arises naturally due to environmental factors such as wind, traffic, or operational use.

This study considered the vibration in Herøysund bridge induced by the forces from passing traffic vehicles as shown in figure 4-2.

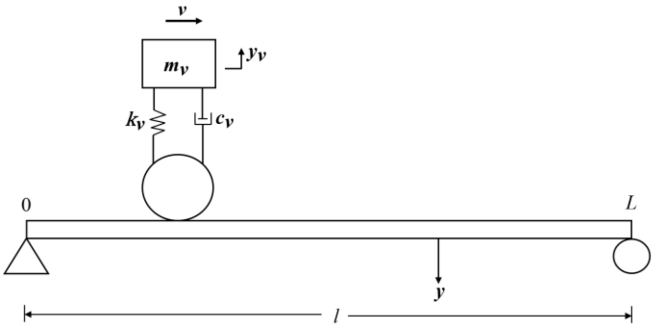

Figure 4-2: *Idealised bridge with a moving vehicle load on one span*

For the formulation of equations of motion, the following assumptions were considered:

(i). the bridge is idealized as a Euler beam having equivalent stiffness;

(ii). only vertical modes of the vehicle are considered;

(iii). the vehicles move at constant velocities, *v* on the bridge.

The equation of motion of the bridge of length, *l* traversed by a vehicle moving at a constant velocity, *v* is expressed as [5, 24]:

$$EI\frac{\partial^4 y}{\partial x^4} + c\frac{\partial y}{\partial t} + m\frac{\partial^2 y}{\partial t^2} = F(x, t) \tag{4.24}$$

where *c* is the damping factor of the bridge and *F(x, t)* is the force transmitted to the bridge by the vehicle.

The equation of motion for the vehicle traversing the bridge is given by [24]:

$$m_v \ddot{y}_v + c_v(\dot{y}_v + \dot{y}) + k_v(y_v + y) = 0 \tag{4.25}$$

where y_v and y are the displacements corresponding to the vehicle and bridge respectively; m_v, c_v and k_v are the mass, damping and spring constant for the vehicle.

To obtain a dynamic response using the eigenvalues and eigenfunctions, the bridge response can be defined as the combination of normal modes and generalised coordinates given by [26]:

$$y(x, t) = \sum_{n=1}^{\infty} q_n(t)\varphi_n(x). \tag{4.26}$$

Applying the boundary conditions of the bridge and substituting equation (4.25) into equation (4.24), we obtain:

$$\ddot{q}_n + 2\zeta_n\omega_n\dot{q}_n + \omega_n^2 q_n = \frac{1}{mM_n^2}\int_0^L F(x, t)\varphi_n(x)\,\mathrm{d}x, \tag{4.27}$$

where

$$M_n^2 = \int_0^L \varphi_n^2\,\mathrm{d}x, \tag{4.28}$$

and m is the mass per unit length of the bridge, ζ_n is the modal damping ratio, ω_n is the natural frequency and $\varphi_n(x)$ is the eigenfunction of the bridge.

The frequency of vibration, ω_v and modal damping ratio, ζ_v of the vehicle is given by [26]:

$$\omega_v = \sqrt{\frac{k_v}{m_v}} \tag{4.29}$$

$$\zeta_v = \frac{c_v}{2 m_v \omega_v} \tag{4.30}$$

To derive non-dimensional equations of motion for the bridge and vehicle, some non-dimensional parameters are introduced as shown below;

$$\varepsilon = \frac{m_v}{ml} \;\; ; \quad \Omega = \omega_v \;\; ; \quad \xi_v = \frac{vt}{l} \;\; ; \quad \xi = \frac{x}{l} \tag{4.31}$$

The static deflection, y_m is defined to make bridge and vehicle displacements non-dimensional where C_{static} for the three-span bridge with equal spans has the value of $(11\pi^4/960)$ [25].

$$y_m = \frac{m_v\, g\, C_{static}}{m\, l\, \omega_v^2} = \frac{\varepsilon\, g\, C_{static}}{\Omega^2} \tag{4.32}$$

$$Y = \frac{y}{y_m} \;\; ; \qquad Y_v = \frac{y_v}{y_m} \;\; ; \qquad u_n = \frac{q_n}{y_m} \tag{4.33}$$

By applying non-dimensional parameters into equations (4.25) and (4.27), the non-dimensional equations of motion for the vehicle and bridge can be expressed as:

$$\Omega^2 Y_v + 2\,\Omega\,\zeta_v\, \varepsilon (Y_v + Y) + \varepsilon\,(Y_v + Y) + \varepsilon\, Y_v = 0 \tag{4.34}$$

$$\ddot{u}_n + 2\zeta_n \left(\frac{\omega_n}{\omega_v}\right) \dot{u}_n + \left(\frac{\omega_n}{\omega_v}\right)^2 u_n = \frac{\Delta l}{M_n^2} \left(\frac{1}{C_{static}} + \varepsilon_v Y_v\right) \varphi_n(\xi_v) \tag{4.35}$$

Where Δ is 1.0 for the forced vibration and 0.0 for the free vibration.

The non-dimensional vertical displacement of the bridge becomes:

$$Y(\xi, \tau) = \sum_{n=1}^{\infty} u_n(\tau) \varphi_n(\xi), \tag{4.36}$$

where $\tau = \omega_v t$

4.5 Bridge Fracture Analysis

Fracture mechanics is based on stress distribution at the tip of a crack derived from elasticity theory [35]. Cracks and other forms of defects might occur on bridge structural materials during service by inducing stresses due to system vibrations [36]. From the continuum mechanics point of view, fracture is governed by the local stress and deformation conditions around the crack tip [40]. Fundamentally, fracture mechanics require stress analysis approach to predict infinite local stresses ($\sigma_{ij} \rightarrow \infty$) at crack tip of most engineering solid materials [41].

The stresses at the crack tip are much higher than the material strength and the high stresses drive the crack to propagate resulting in material failure [36]. Failure due to crack propagation is called fracture failure and is assumed to occur when the maximum normal stress at a point in the material ($\sigma_1 > 0$) exceed its tensile strength (σ_{vs}) i.e $\sigma_1 \geq \sigma_{vs}$, [36, 41].

4.5.1 Crack Theory Analysis

When a solid body is loaded from crack face, the product of the released elastic strain energy density ($\int \sigma d\epsilon$) and the cylindrical volume element ($2\pi a^2 B$) about the crack result in the elastic strain energy that is given by [42];

$$W_e = -2(\pi a^2 B) \int \sigma d\epsilon = -2(\pi a^2 B) \int E' \epsilon d\epsilon \quad (4.37)$$

$$W_e = -2(\pi a^2 B) \left(\frac{E'\epsilon^2}{2}\right) = -(\pi a^2 B) \left(\frac{\sigma^2}{E'}\right) \quad (4.38)$$

where $\sigma = E'\epsilon$ = Hooke's law

$E' = E$ for plane stress

$E' = E/(1 - v^2)$ for plane strain conditions

E = Modulus of elasticity (MPa)

ϵ = Elastic strain

σ = Applied remote stress (MPa)

a = One-half crack length (mm)

v = Poisson's ratio

$4aB = 2(2aB)$ = Total surface crack area (mm^2)

B = Thickness of material (mm)

The factor E' is used in Eq. (4.37) for controlling either plane stress or plain strain condition. Equation (4.38) can be derived by inserting displacement (μ_y) in the y-direction as shown in the following equations [40]:

$$W_e = -4B \int_0^a \frac{1}{2} \sigma \mu_y dx = -4B \int_0^a \frac{1}{2} \sigma \left(\frac{2\sigma}{E'} \sqrt{a^2 - x^2}\right) dx$$

$$W_e = -\left(\frac{4B\sigma^2}{E'}\right) \int_0^a \left(\sqrt{a^2 - x^2}\right) dx = \left(\frac{4B\sigma^2}{E'}\right) \left(\frac{\pi a^2}{4}\right)$$

$$W_e = -\left(\pi a^2 B\right) \left(\frac{\sigma^2}{E'}\right) \quad (4.39)$$

The elastic surface energy for creating new crack surfaces during crack growth is given by [42];

$$W_s = 2(2aB\gamma_s) \quad (4.40)$$

Where γ_s = Specific surface energy (J/mm^2)

For an elastically stressed solid body, Griffith energy balance considered the decrease in potential energy and the increase in surface energy resulting from the growing crack which creates new surfaces [41]. For the energy balance, the total elastic energy of the system i.e the total potential energy takes the mathematical form given by;

$$W = W_s + W_e = 2(2aB\gamma_s) - (\pi a^2 B) \left(\frac{\sigma^2}{E'}\right) \quad (4.41)$$

Dividing Eq. (4.41) by the thickness B to obtain the total potential energy per unit thickness given as;

$$U = U_s + U_e \tag{4.42}$$

$$U = 2(2a\,\gamma_s) - \left(\frac{\pi\, a^2 \sigma^2}{E'}\right) \tag{4.43}$$

where U_s = Elastic surface energy per unit thickness (J/mm)

U_e = Released elastic energy per unit thickness (J/mm)

Therefore, the Griffith energy criterion for crack growth is given by [40];

$$U_e \geq U_s \text{ when } \frac{dU}{da} = 0 \tag{4.44}$$

Taking the second derivative of equation (4.43) with respect to crack length and including material thickness B, we obtain;

$$\frac{d^2(U)}{d\,a^2} = -\frac{2\,\pi\,\sigma^2 B}{E'} \tag{4.45}$$

When $\frac{d^2(U)}{d\,a^2} < 0$, then the system is said to be unstable and the cracks will usually grow [42].

The energy balance gives $4a\gamma_s E' = B\pi\sigma^2 a^2$, from the applied stress (σ), and the crack length (a).

The strain energy release rate (G_1) for solid materials can be derived as [41];

$$\sigma = \sqrt{\frac{(2\,\gamma_s)\,E'}{\pi\,a}} \tag{4.46}$$

$$a = \frac{(2\,\gamma_s)\,E'}{\pi\,\sigma^2} \tag{4.47}$$

$$G_1 = 2\gamma_s = \frac{\pi\,a\,\sigma^2}{E'} \tag{4.48}$$

At fracture, equations (4.46), (4.47) and (4.48) give the critical entities. Rearranging equation (4.48) yields the elastic stress intensity factor given as [40, 41];

$$\sigma\sqrt{\pi\,a} = \sqrt{(2\gamma_s)\,E'} = \sqrt{G_1 E'} \tag{4.49}$$

$$K_1 = \sigma\sqrt{\pi\,a} \tag{4.50}$$

The analysis of Eq. (4.50) suggest that crack extension solids is governed by the critical value of the stress intensity factor [40-42].

Since plastic deformation occur in most engineering solid materials, Irwin modified Griffith's elastic surface energy expression in Eq. (4.48) by adding a plastic deformation energy (γ_p) in the fracture analysis [41]. Therefore, in tension loading, the total elastic-plastic strain energy is called strain energy release rate G_1 which is energy per unit crack surface area available for infinitesimal crack extension [42]. Thus, it can be expressed as;

$$G_1 = 2(\gamma_s + \gamma_p) \tag{4.51}$$

$$G_1 = \frac{\pi\,a\,\sigma^2}{E'}, \qquad \text{where } E' = \frac{E}{B} \tag{4.52}$$

Rearranging equation (4.52) gives the stress equation as;

$$\sigma = \sqrt{\frac{E'\,G_1}{\pi\,a}} \tag{4.53}$$

Combining equations (4.49) and (4.53), we obtain;

$$G_1 = \frac{K_1^2}{E'} \tag{4.54}$$

Crack propagation occurs when $G_1 > G_{1C}$ where G_{1C} is crack driving force or fracture toughness of a material under tension loading [40]. The fracture criterion by G_{1C} establishes crack propagation when $G_1 \geq G_{1C}$ [42]. At this point, the critical stress (σ_c) or fracture stress (σ_f) and the critical driving force (G_{1C}) are derived using equation (4.55) when the crack is unstable [41]. The relation is given by;

$$\sigma_f = \sigma_c = \sqrt{\frac{E' G_{1C}}{\pi a}} \tag{4.55}$$

The maximum applied stress is the critical stress (σ_c) or fracture stress (σ_f) that causes fractures in solid materials and it is less than the yield strength (σ_{ys}) due to the existence of cracks or defects [36].

There are two basic approaches to establish fracture criteria, or crack propagation criteria which include crack tip stress field and energy balance approaches [40].

4.5.2 Crack Growth Analysis based on Stress Field

In crack tip stress field approach, the crack tip stress and displacement are analysed. The parameters governing the near-tip stress and displacement fields are identified as shown in figure 4.3 [36].

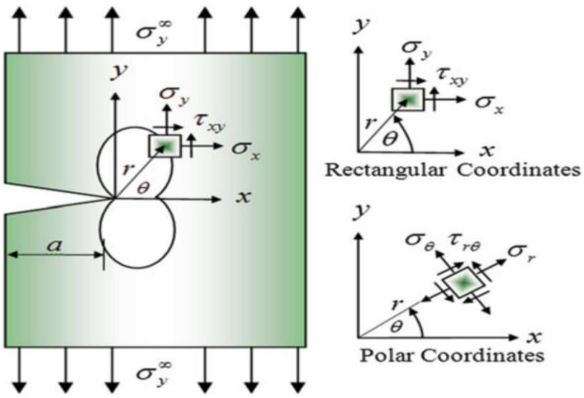

Figure 4-3: crack configuration showing stresses at the crack tip [41]

Linear elastic analysis of a cracked body reveal that stresses around the crack tip vary according to $r^{-1/2}$, where r is the distance from the tip [36]. Stresses become more as r approaches the crack tip [40]. The stresses near the crack tip on elastic solids can be expressed as [36, 40, 41];

$$\sigma_{xx} = \frac{K_1}{\sqrt{2\pi r}} \cos\frac{1}{2}\theta \left(1 - \sin\frac{1}{2}\theta \sin\frac{3}{2}\theta\right)$$
$$\sigma_{yy} = \frac{K_1}{\sqrt{2\pi r}} \cos\frac{1}{2}\theta \left(1 + \sin\frac{1}{2}\theta \sin\frac{3}{2}\theta\right)$$
$$\sigma_{xy} = \frac{K_1}{\sqrt{2\pi r}} \sin\frac{1}{2}\theta \cos\frac{1}{2}\theta \cos\frac{3}{2}\theta \tag{4.56}$$

where K_1 is called stress intensity factor, which depends on the applied load and crack geometry while (r, θ) is the polar coordinates centred at the crack tip as in figure 4.3 [40]. The parameter K_1 has its critical value called fracture toughness, K_{1C} [40, 41]. K_{1C} characterizes the resistance of a material to crack extension [36]. Irwin proposed fracture criteria stating that crack growth occurs when the stress intensity factor reaches a critical value [41, 42] i.e;

$$K_1 = K_{1C} \tag{4.57}$$

The fracture behaviour can be determined from the values of fracture toughness, K_{1C} and the stress intensity factor K_1.

The displacement can be expressed as in equation 4.58 [42];

$$\mu_i = \frac{K_I}{2U_i}\sqrt{\frac{r}{2\pi}}\, g(\theta) \tag{4.58}$$

where K_I is the stress intensity factor (SIF), (r; θ) is the polar coordinates centred at the crack tip, g is the standard gravity and U_i is total potential energy per unit thickness.

4.5.3 Fracture criterion based on energy balance

Crack growth can also be established through potential energy balance during crack extension. Potential energy as a function of crack length is first determined and its variation with a virtual crack extension is then examined [40]. According to Griffith [36, 41], energy decrease in the cracked body is usually absorbed into the newly created crack surface whose energy balance equation is given by;

$$-\,d\Pi = 2da\gamma \qquad \text{or} \qquad -\frac{d\,\Pi}{da} = 2\gamma \tag{4.59}$$

where $-d\Pi$ denote the decrease in the potential energy, a is crack length, γ is the surface energy per unit area, da is crack extension, and $2da\gamma$ is total surface energy of the new crack surface. The energy release rate G_1 proposed by Irwin is defined as the decrease in potential energy per unit crack extension under constant load given by [42];

$$G_1 = -\frac{d\Pi}{da} \tag{4.60}$$

By use of the energy balance approach, the crack growth or failure criterion is given as [40];

$$G_1 = G_{1C} = 2\gamma \tag{4.61}$$

where G_{1C} is a material constant measuring the resistance to fracture.

From equation (4.56), fracture criterion involves the total energy of the cracked body as well as the surface energy of the solid material [36]. Stress intensity factor (K_1) and energy release rate (G_1) are two quantities that distinguish fracture mechanics from the classical failure criteria [36, 40].

In using the stress intensity-based fracture criterion to predict failure of a structure, stress intensity factor is calculated for the given load and geometry [42]. Thereafter, the measure of the fracture toughness is conducted. After stress intensity factor and the fracture toughness are determined, Eq. (4.53) and (4.57) are applied to find the maximum allowable crack length that will not propagate under the design load [40, 41]. Equally, the maximum allowable load that will not cause crack growth can also be determined [40].

5 NUMERICAL MODELLING OF THE BRIDGE CONDITIONS.

Numerical analysis is a powerful tool used to approximate solutions to problems where exact solutions does not exist [34]. Approximation is an iterative process, and the solutions can have very high accuracy depending on the numerical method that is being used. Finite element analysis (FEA) is often applied to analyse geometry with given boundary and initial conditions. The finite element method subdivides the geometry into smaller elements and solves the mathematical problem for each element [38]. Because of the subdivisions of geometry, the method is discrete and can only approximate solutions. In this section, ANSYS 2024 R1 workflow with static structural, fracture, modal, harmonic response, and response spectrum analysis were performed with considerations for geometry, materials, cracks coordinates, mesh attributes and solution metrics.

5.1 Geometry

The model developed in SolidWorks software was transferred to Ansys in parasolid format where it was edited in Ansys Space Claim to produce a 3D solid element model that was utilised in FEM simulations as shown in figure 5-1. The numerical analysis was performed using SI units, with the governing parameters to be studied in the structural and modal analysis were total deformations (m), crack length (m), equivalent stresses (MPa), modal frequencies (Hz), normal elastic strain (m/m), effective mass (kg), J-integral ($\mathrm{J/m^2}$) and stress intensity factor ($MPa.\sqrt{m}$).

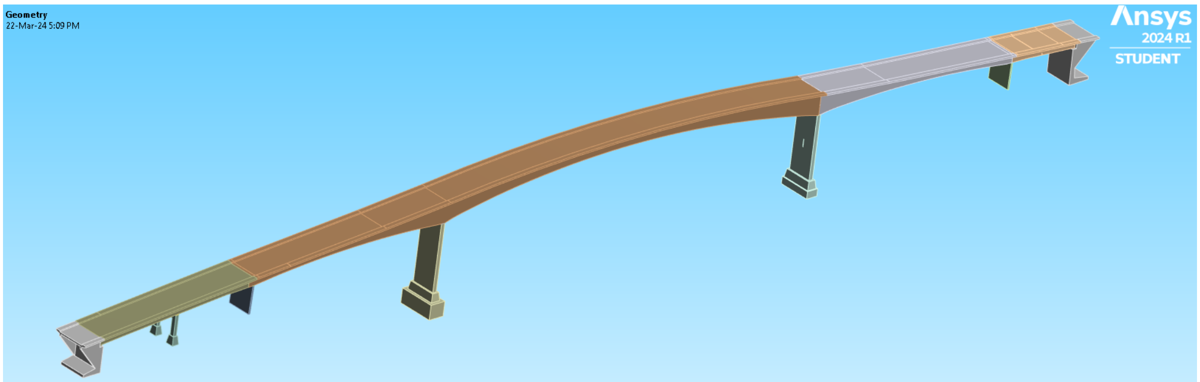

Figure 5-1: *3D-Solid model of bridge geometry*

5.2 Materials

Given that reinforcements on deck and beams were not considered in this project, concrete was used for all pillars, beams, decks and spans 1-7, while structural steel was used for the load-bearing plates on pillars 1, 2, 3, 6 and 7. The materials properties were generated from the CES Granta EduPark materials library in ANSYS 2024 R1 and from materials selection in mechanical design textbook by Ashby [37] which were as shown in table 5-1.

Table 5-1: *Materials properties for model in numerical simulations [37]*

Properties	Concrete	Structural Steel
Density, Kg/mm^3	2.39e-06	7.85e-06
Young's Modulus, MPa	19360	2.00e+05
Poisson's Ratio	0.1414	0.3
Bulk Modulus, MPa	8998	1.67e+05
Shear Modulus, MPa	8480.8	76923
Tensile Ultimate Strength, MPa	1.1960	460
Tensile Yield Strength,MPa	1.0950	250
Isotropic Thermal Conductivity, $W/mm°C$	0.002071	0.06050
Specific heat constant pressure, $mJ/Kg°C$	9.36e+05	4.34e+05
Isotropic Resistivity, $ohm - mm$	5.85e+07	-
Secant Thermal Expansion Coeff.	-	1.20e-05

The mass and volume control for constrained prestressed 3D-Solid bridge structure model used was as in table 5-2.

Table 5-2: *Mass and volume control for 3D-Solid model* [43]

Properties	3D-Solid Model
Mass, kg	$1.3848e + 006$
Volume, mm^3	$5.7891e + 011$

5.3 Meshing

The geometric model was meshed using body sizing for every part of the model. However, face sizing and edge sizing were applied in sections of parts which appeared hidden like cracks and underneath of main span 3-6 which the system could not mesh with body sizing. Solid 186 and 187 were the element types applied in the FEM of the Solid model as they are the default Ansys program controlled meshing types. Solid 186 has reduced integration and is suitable for linear analysis of structures while Solid 187 element type is an improved version of solid 186 with full integration and is suitable for modeling thin-walled structures with high aspect ratios [38].

Figure 5-2 shows the meshed 3D solid model with some mesh details, but extra details are found in appendix A. It must be noted that the Ansys 2024 R1 student version used in this project had meshing limitations. The maximum allowed number of mesh elements was restricted to 32,000 for static structural modelling. Any value above the stated limit gave an error during the simulation. It was such limitations that dictated the choice of the element size, defeature size, number of divisions and growth rate. As earlier mentioned, cracks were meshed with face and edge sizing. The face sizing was applied on the bottom and top faces of the cracks with similar mesh details as in figure 5-2. Edge sizing mesh was applied on the edges of the cracks with different number of divisions depending on the crack length, depth, or height. Figure 5-3 shows the meshing on cracks.

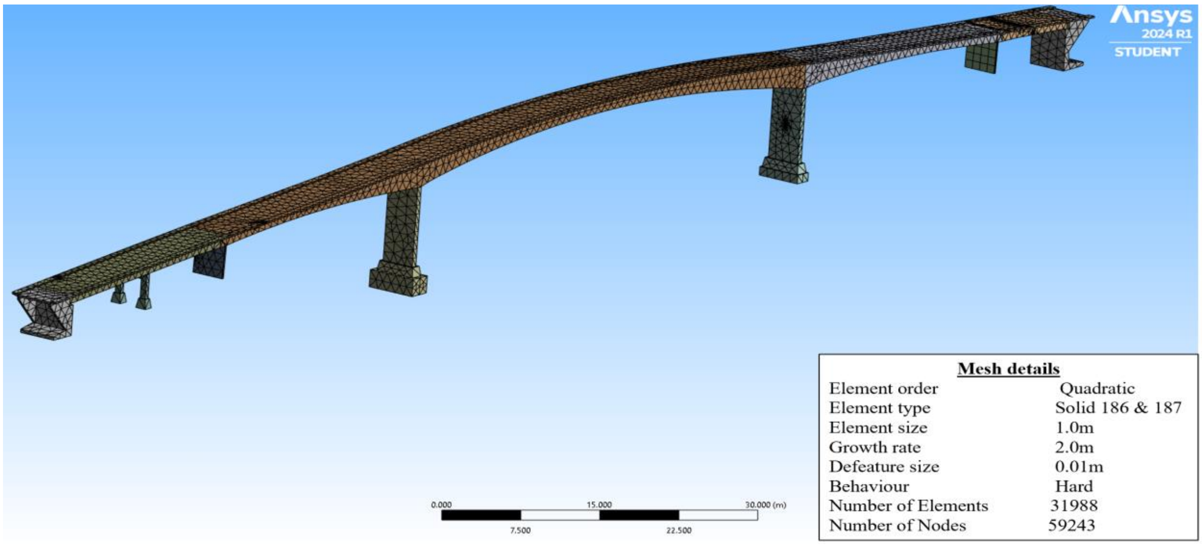

Figure 5-2: *Meshing on the 3D solid model with mesh details*

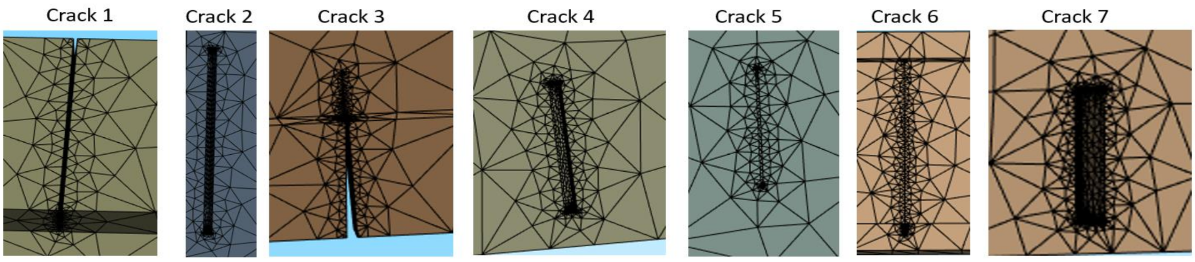

Figure 5-3: *Meshing on different cracks on the 3D solid model*

5.4 Fractures

After meshing, each crack was set up for simulation to determine stress intensity factors and J-integral values. First, the coordinate system of each crack was set where orientation of *x-axis* was set as the principal axis by setting *x-axis* in the direction of the crack tip i.e as a rule of thumb *x-axis* was set to point into the material. The *y-axis* was set perpendicular to the edge of the crack tip i.e perpendicular to the crack plane. By this the *z-axis* was set to be parallel to the edge of the crack tip as shown in figure 5-4. The coordinate details and other details for each crack can be found in appendix B. Thereafter, name selection was applied, and nodal name selection was created to identify the crack tip, top and bottom faces of each crack. The bridge was assumed to be entirely concrete and fracture toughness (K_{1C}) of concrete is usually in the range of 0.2 – 1.4 $MPa.\sqrt{m}$ depending on the specific composition and structure of the concrete [37]. Cracks were set up and crack lengths were assumed as in table 5-3. Four solution contours were set on each crack for comparative analysis.

5.5 Boundary Conditions

Boundary conditions, like fixed supports, and loads are essential for safe and reliable structural analysis. This study considered self-weight of bridge, ambient traffic load, foundation supports and post tensioning of bridge for prestressed modal analysis, fracture analysis, vibration analysis in the structural modelling.

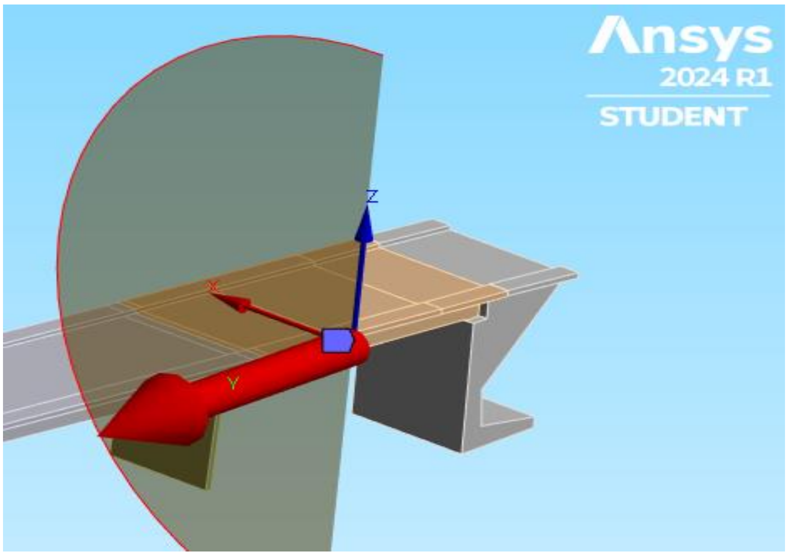

Figure 5-4: *Coordinate system of one of the cracks on the bridge structure*

Table 5-3: *Crack lengths of pre-meshed cracks 1-7*

Crack	Crack Length (m)	Contour solutions
Crack 1	0.15	4
Crack 2	0.07	4
Crack 3	0.9	4
Crack 4	0.08	4
Crack 5	0.1	4
Crack 6	0.2	4
Crack 7	0.06	4

5.5.1 Standard Earth Gravity

The Herøysund bridge structure was considered to be under the action of 9806.6 g/mm^2 (9.8066 m/s^2) gravitational pull acting in the $-$ve (y-axis). Standard earth gravity was used to determine forces and stresses caused by the weight of the bridge structure and loads, and its constant value was used to calculate the self-weight of the Herøysund bridge structure.

5.5.2 Post Tensioned Load

Post-tensioning in the Herøysund Bridge consist of tendons along the longitudinal beams. The tendons in the bridge structure were tensioned while exerting a compressive force on the bridge structure. The tendons were not visible on the external surface of the bridge since they were placed inside the bridge structure. The placement of tendons was as shown in figure 5-5. Given that there was no clarity on the exact locations of tendons across the geometry, an assumption was made that they act as a compressive load on the bridge structure. In the case of Herøysund bridge, the tendons were placed in main span 3-6 [18]. Therefore, it was estimated that compressive loads acting at the front face on either side of span 3-6 represented the post tensioned tendons.

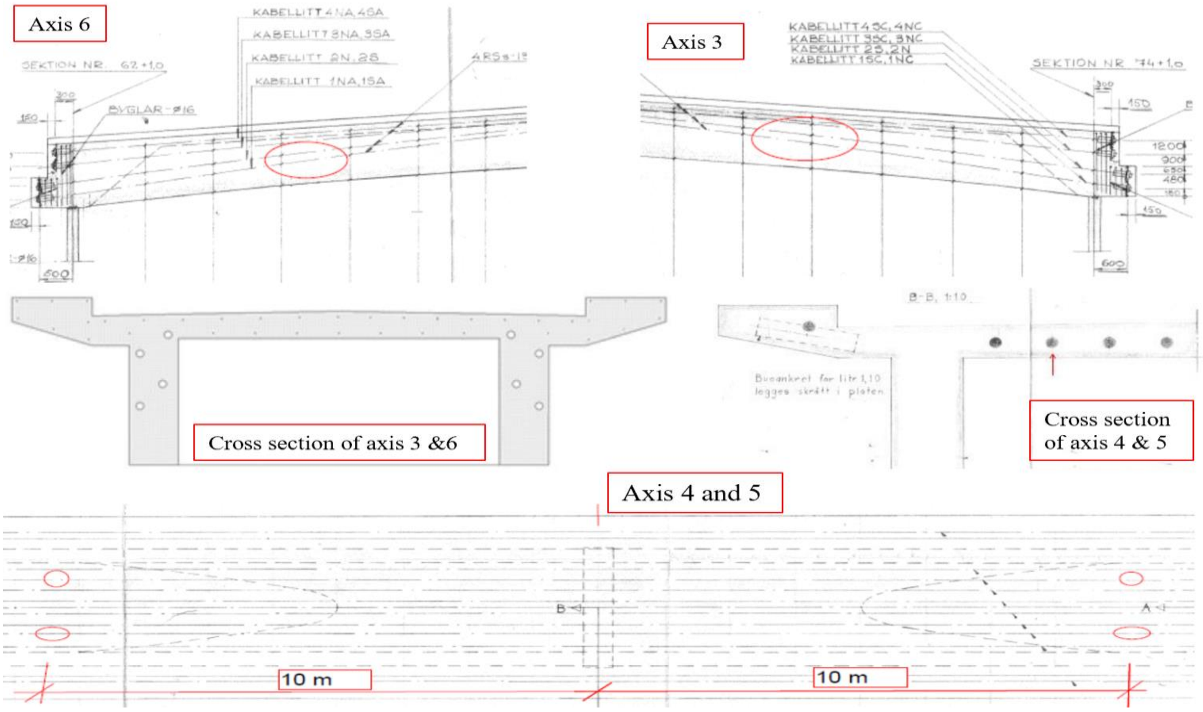

Figure 5-5: *Placement of post tensioned tendons across span 3-6 [18].*

According to Herøysund bridge NovaFrame analysis document from Statens Vegvesen [43], each cable was tensioned with a load of *137* tonnes along the x-axis, i.e., span 3-6 in the longitudinal direction. There are eighteen (18) tendons providing post-tensioning force F_{PT} and as result on each end of the main span, a compressive force C_{PT} act directing towards the centre. The force can be expressed as in equation (5.1) below.

$$F_{PT} = \text{Tension per Cable} \times \text{No. of Cables} \times \text{Gravitational acceleration} \tag{5.1}$$

$$F_{PT} = 137 \times 1000 \times 18 \times 9.8066 = 24{,}166{,}800\text{N}$$

$$C_{PT} = \boldsymbol{12{,}083{,}400N}$$

5.5.3 Railing and Asphalt Load

The bridge under study has *200mm* (*0.2m*) railing, i.e., *0.5kN/m* along with asphalt at the top with a thickness of *60mm* (*0.06m*) throughout the span with a load of $25kN/m^3$ as per the SV V412 Load capacity classification of bridges, and loads [43]. Based on the classification, loads across the bridge in accumulated form can be calculated as a resultant load at the top deck. For 5.3*m* transverse span, asphalt load exerted by asphalt is 7.95 kN/m given by ($5.3m \times 25kN/m^3 \times 0.06m$) while the side rails on both sides exert a load of *1kN/m* given by ($0.5kN/m \times 2$). Therefore, the accumulated load for both asphalt and rail on the bridge deck span 1 – 7 can be expressed as in equations (5.2), (5.3) and (5.4):

$$\text{Asphalt Load: } 0.06\text{m} \times 5.3\text{m} \times 154.5\text{m} \times 25\text{kN/m}^3 = 1228.275\ kN \tag{5.2}$$

$$\text{Railing Load: } 0.5\text{kN/m} \times 154.5\text{m} \times 2 = 154.5kN \tag{5.3}$$

$$\text{The total sum of asphalt and railing load} = \boldsymbol{1382.775\ kN} \tag{5.4}$$

For the whole bridge span this load could be transformed to a resultant force of 1382775 N for bridge length of 154.5 m acting in −ve (y-axis) direction

5.5.4 Traffic Loading

According to NovaFrame analysis document [43] about traffic load on Herøysund bridge, there are four different traffic loading categories. They include load number 701 evenly distributed load P, 801 BK 10A, 901 BK10/50 trailers/lorries and 921 BK10/50 vehicles. The annual average daily truck traffic (AADTT) was used to determine the traffic loading on the Herøysund bridge. According to the report [43], traffic load number 701 and 901 have average loading of *6.0kN/m* and *25.3kN/m* respectively evenly distributed over the *154.5m* span of the bridge deck. Load number 801 BK 10A and 921 BK10/50 vehicles have average magnitude of *40kN* and *75kN* respectively that were assumed to be evenly distributed on the centre span of the Herøysund bridge deck between axis 4 and 5.

Based on the findings, this study considered traffic loading on Herøysund bridge in two ways. First was the consideration of the evenly distributed load over the entire bridge span which was determined as follows:

$$\text{701 evenly distributed load P} = 6.0\text{kN/m} \times 154.5\text{m} = \mathit{927kN} \tag{5.5}$$

$$\text{901 BK10/50 trailers/lorries} = 25.3\text{kN/m} \times 154.5\text{m} = \mathit{3908.85kN} \tag{5.6}$$

$$\text{Total Evenly Distributed Traffic Load, TEDTL} = \boldsymbol{4835.85kN} \tag{5.7}$$

The second consideration was the traffic loading evenly distributed on the centre span of the bridge which was found to be the sum of traffic load of 801 BK 10A and 921 BK10/50 vehicles. This was tabulated as;

$$\text{Total Traffic Loading at Center Span (TTLCS)} = 40\text{kN} + 75\text{kN} = \boldsymbol{115kN} \tag{5.8}$$

The traffic loading was only applied on the carriageway of the Herøysund bridge model as this loading was only considered to have emanated from vehicles and trailers that usually use carriageway. The load was not applied on pedestrians' lanes found on both sides of carriageway.

5.5.5 Applied Loading conditions

The 3D-Solid model loading conditions were presented as shown in figure 5-6. The base of all seven pillars were fixed to the ground, and a force of *1382.775kN* exerted at the top deck across span 1-7 was applied to represent rail and asphalt loading. A loading force of *12083400N* was applied as a compressive load on both ends of main span 3-6 acting horizontally (x-axis) towards the centre of the bridge. The structure in global coordinate system was under the action of standard earth gravity, i.e., $9.8066\ m/s^2$ representing the action of self-weight of bridge acting at its centre of gravity. The traffic loading was also considered in this project simulation. Total evenly distributed traffic load (TEDTL) of *4835.85kN* was applied only on carriageway on top deck across span 1-7 and total traffic loading at centre (TTLC) of *115kN* was applied on carriageway of top deck between span 4 and 5.

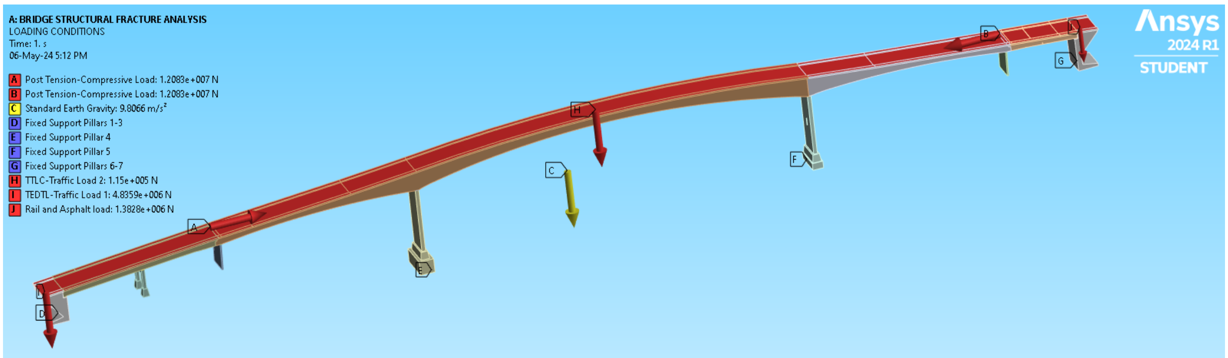

Figure 5-6: *Applied loading conditions on Herøysund bridge*

5.6 Solution Metrics

Numerical modelling is usually applied to accurately observe the structural system behavior. This requires a correct approach in selecting the appropriate parameters to be investigated and finding a balance between reliable results, efficient simulation time, and level of details. Figure 5-7 show the parameters analysed, steps used in solving them and resultant outcomes.

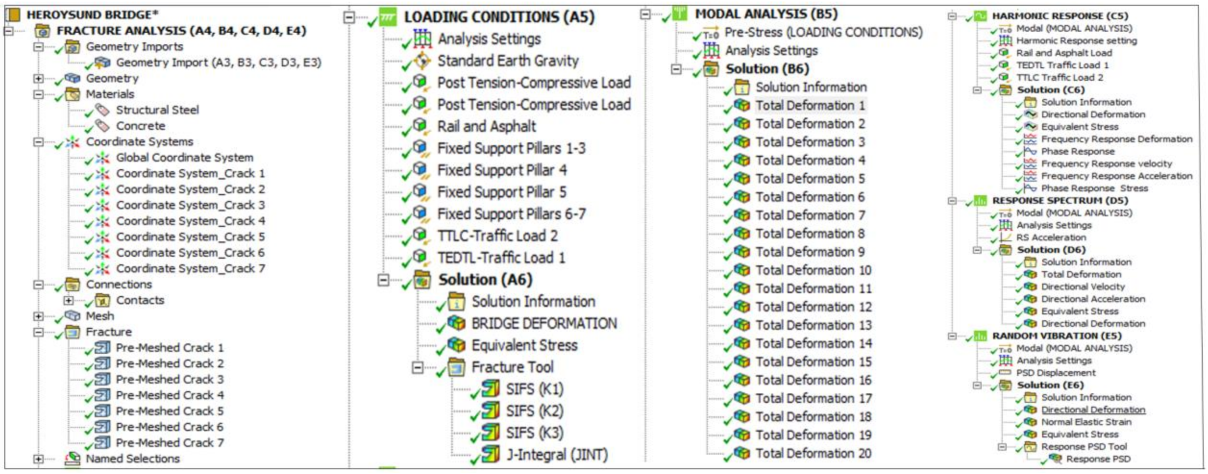

Figure 5-7: *Schematization of applied parameters in numerical simulation*

In this master thesis project, five different parameters were analysed i.e fracture analysis, prestressed modal analysis, harmonic response, response spectrum and random vibration. The outcome of the analysis was generated interms of different result solutions such as bridge structure deformation, equivalent (von mises) stress, normal strain, stress intensity factors, J-integral, mode shapes, natural frequencies, frequency response, phase angles, directional, velocity and acceleration deformation. All these outcomes were geared towards understanding the vibrational behaviour of the bridge structure under loading and the effect of the identified cracks on the structural and behavioural orientation of the bridge.

6 RESULTS AND DISCUSSIONS

This Section presents the structural fracture analysis, prestressed modal and vibratory evaluated results obtained from the simulation using ANSYS 2024 R1. The numerical prestressed modal analysis was carried out for twenty modes while fracture analysis was conducted for each of the seven identified cracks. Fracture analysis results were presented in three different stress intensity factors (K1, K2 and K3) together with J-integral values. In addition, harmonic response, response spectrum and random vibration examinations of the structure were determined based on modal frequency data to observe the vibration condition of the bridge. Most relevant results like structural deformation, equivalent (von mises) stress, normal elastic strain, mode shapes and modal frequencies, stress intensity factors (SIFS) and J-integral were discussed.

6.1 Fracture Analysis Results

Seven main cracks were identified, pre meshed and the bridge model analysed to find the structural deformation, stress intensity factors (SIFS) and J-integral of every crack. Figure 6-1 is an illustration of the Herøysund bridge and cracks locations during the numerical modelling.

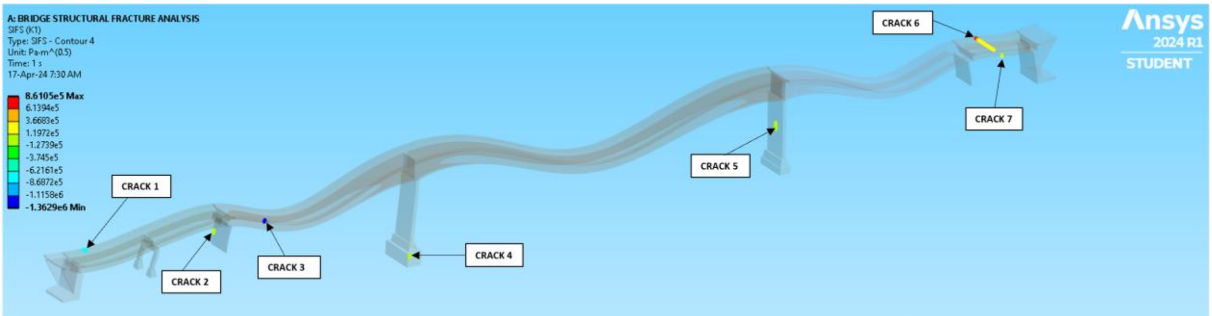

Figure 6-1: Cracks locations during the numerical modelling of the bridge model

6.1.1 Bridge Deformation

Due to loading conditions on the bridge, the structural model was simulated, and its structural deformation was determined. The maximum total deformation of the bridge model structure was found to be *0.054216m* (*54.216mm*). The maximum deformation was experienced on main bridge span 3-6 and minimal deformation was experienced on pillar 7 as shown in figure 6-2.

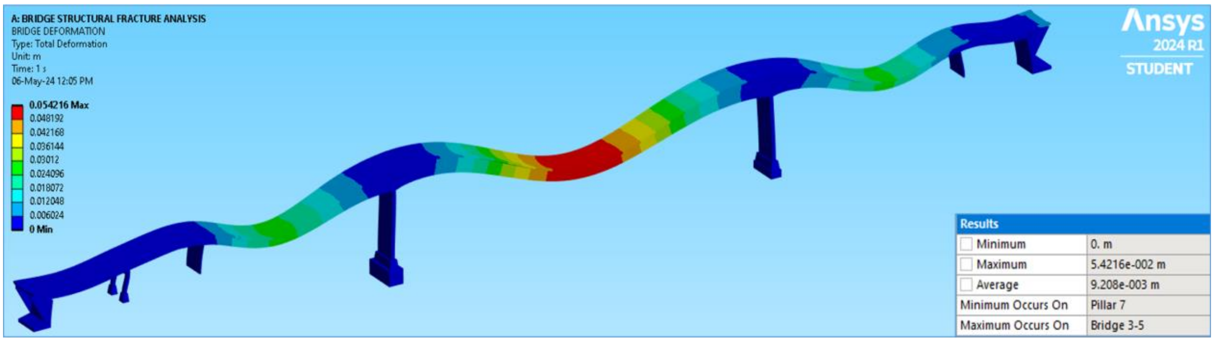

Figure 6-2: The total deformation of the modelled bridge structure

6.1.2 Equivalent (Von Mises) Stress

Equivalent stress provides a measure of the total stress within a material, taking into account all the different types of stresses that may be present such as tensile, compressive, and shear stresses [37]. Comparison of equivalent stress to the tensile ultimate and yield strength of a material is used to determine whether or not a structure will fail under the given loading conditions hence providing an insight into the safety and reliability of a structure. Ultimate tensile strength (UTS) is the maximum stress that a material can withstand when stretched or pulled before it breaks [37]. On the other hand, tensile yield strength which is associated with material stiffness is the maximum stress that a material can withstand without undergoing permanent deformation [33, 37]. If the equivalent stress exceeds the ultimate tensile and yield strength, the material is likely to fail. Such comparisons are applied in safety criteria on structures to prevent failure and ensure safety and reliability. The maximum and minimum equivalent stresses due to loading on the Herøysund bridge model were determined as in figure 6-3.

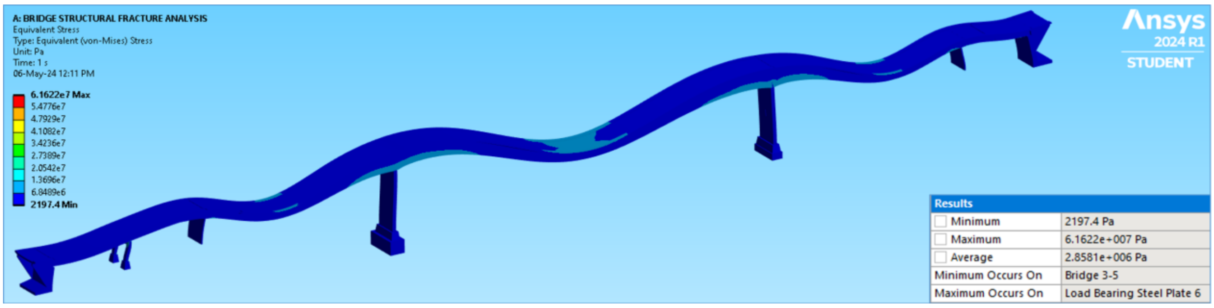

Figure 6-3: *Equivalent stress outline on Herøysund bridge modelled structure*

The maximum von mises stress was obtained as *61.622 MPa* occurring on load bearing steel plate on pillar 6 while the minimum equivalent stress was found to be *2.1974 kPa* occurring on main bridge span 3-5. The bridge was assumed to be made of concrete with load bearing steel plates on pillars 1, 2, 3, 6 and 7. The maximum equivalent stresses of *61.622 MPa* occurring on load bearing steel plate on pillar 6 was compared against the ultimate tensile strength (UTS) and yield tensile strength (YTS) of structural steel. It was found that the maximum equivalent stress was very much lower than UTS (*460MPa*) and YTS (*250MPa*) of structural steel. As a result, there will be no failure of Herøysund bridge due to maximum equivalent stress. On the hand, the minimum equivalent stress of *2.1974 kPa* acting on bridge span 3-5 was compared against the UTS and YTS of concrete. The findings showed that the minimum equivalent stress was way less than UTS (*1.1960 MPa*) and YTS (*1.0950 MPa*) of concrete. Hence, Herøysund bridge will not fail due to the minimum equivalent stress.

The average equivalent stress value of *2.8581MPa* was assumed to act uniformly on the Herøysund bridge. Since the value is greater than the ultimate tensile strength and yield tensile strength of concrete, there is high probability of Herøysund bridge failure due to loading conditions.

6.1.3 Cracks Propagation Analysis

In this section, only maximum and minimum stress intensity factors (SIFS) and J-integral values were considered for overall effect on all the cracks. Stress intensity factor (SIF) represents the vulnerability of each crack to propagation while J-integral is the energy required to grow the crack [42]. For crack propagation to occur, the SIF value must be equal or greater than fracture toughness of the material. The J-integral is the energy release rate i.e the energy flow into the crack tip and characterizes the energy required to create a unit area of new crack surface [41]. Three different stress intensity factors (K1, K2, and K3) and a single value of J-integral were evaluated on each crack with four different solution contours for comparative analysis. Tables 6-1 and table 6-2 illustrate the maximum and minimum values generated from the stress intensity factors and J-integral results for all the cracks that were involved in the analysis. The rest of the figures, tables, and graphs of SIF (K1, K2, and K3) and J-integral results for each crack are attached in appendix C.

Table 6-1: *Maximum Stress Intensity Factors and J-integral values of Cracks*

Cracks	SIFS (K1) (KPa.√m)	SIFS (K2) (KPa.√m)	SIFS (K3) (KPa.√m)	J-Integral (J/m^2)
Crack 1	-675.78	-37.333	27.031	22.565
Crack 2	8.3074	1.4307	-3.2576	0.27816
Crack 3	-1222.5	451.58	72.796	83.936
Crack 4	-3.789	0.29941	0.27559	0.0075869
Crack 5	4.7439	0.02161	2.7984	0.483
Crack 6	861.81	-76.548	177.92	22.203
Crack 7	172.43	4.9792	65.012	0.82119
All Cracks Combined	861.81	451.58	177.92	83.936

Table 6-2: *Minimum Stress Intensity Factors and J-integral values of Cracks*

Cracks	SIFS (K1) (KPa.√m)	SIFS (K2) (KPa.√m)	SIFS (K3) (KPa.√m)	J-Integral (J/m^2)
Crack 1	-762.33	-105.97	3.6886	-6.4919
Crack 2	1.7976	0.1583	-5.3857	-0.026034
Crack 3	-1445.9	393.29	-38.891	45.169
Crack 4	-13.095	-0.024031	-0.43919	0.00018075
Crack 5	-0.0084024	-0.35338	-0.084997	-0.4511
Crack 6	174.72	-245.16	-164.15	-5.4713
Crack 7	107.98	-5.1754	20.925	-0.12156
All Cracks Combined	-1445.9	-245.16	-164.15	-6.4919

The maximum SIF and J-integral values in tables 6-1 and 6-2 were equated against the fracture toughness (K_{1C}) and critical J-integral value (J_C) of concrete to determine which of the cracks is likely to propagate and factors of safety of the structure based on effect on each crack.

Stress Intensity Factors (SIFS)

Stress intensity factor (SIF) describe the stress state near the tip of a crack and is related to the rate of crack growth [41]. SIF is calculated as a function of applied load, crack size and geometry of material [40]. When SIF exceeds the fracture toughness of a material, failure will occur due to rapid and unstable crack growth [36, 40]. There are three different types of cracking modes i.e mode I is an opening (tensile) where the crack surfaces move apart, mode II is sliding where crack surfaces slide over each other [42]. Mode III is tearing where crack surfaces move relative to one another [40]. The sign of SIF (K) indicate the type of stress state at the crack tip e.g. positive K value represent tensile stress state associated with mode I while negative K value is a compressive stress state [41].

From tables 6-1 and 6-2, the SIF (K1) results showed negative values for crack 1 in all the four contours revealing compressive stress state. SIF (K1) results for crack 2 are all positive in all the contours hence tensile stress state. SIF(K1) results for crack 3 and crack 4 are all negative thus stress state is compressive. On the hand, SIF(K1) results for crack 6 and crack 7 indicate positive K values hence tensile stress state. SIF(K1) results for crack 5 is a mixture of positive and negative values in the contours indicating a combination of tensile and compressive stress states experienced on a crack. The second SIF (K2) results show that cracks 1 and 6 have negative values manifesting compressive stress mode while cracks 2 and 3 have positive K values exhibiting tensile stress state. However, cracks 4, 5 and 7 have both negative and positive values hence tensile and compressive stress states in the cracks. The third SIF (K3) results in all contour solutions reveal that cracks 1 and 7 had positive values of K and the rest of cracks had both positive and negative K values.

The fracture toughness of concrete is approximated as $K_{1C} = 0.2 – 1.4\ MPa.\sqrt{m}$ ($200 – 1400\ kPa.\sqrt{m}$) and critical J-integral is approximated to be $2.0656 – 101.24 J/m^2$. The study analogized the results against fracture toughness and critical J-integral values. The assumption made was that results within and above the limits of fracture toughness (K_{1C}) and critical J-integral (J_C) values elicit crack propagation while values below the lower limit does not precipitate crack growth as illustrated in figure 6-4. A further assumption was that in the set of K1, K2 and K3 values, the highest value of K for every crack was compared against fracture toughness to show probabilities of crack propagation.

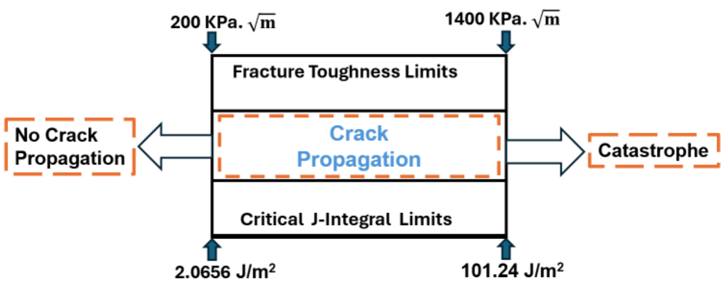

Figure 6-4:*Illustration of where Crack propagation is likely to occur*

Comparing absolute SIF (K) values against the K_{1C} values of concrete i.e $200 – 1400\ kPa.\sqrt{m}$. The absolute SIF K1 values in table 6-1 for cracks 1, 3, and 6 were within the limit but values for cracks 2, 4, 5 and 7 were below the fracture toughness limit. In table 6-2, the absolute SIF K1 values for cracks 1 and 3 were within the limits while those for cracks 2, 4, 5, 6 and 7 were below. A glance at absolute values of SIF K2 results in table 6-1 show that only crack 3 results are within the limit of $200 –1400\ kPa.\sqrt{m}$ and in table 6-2, results for cracks 3 and 6 are within the range. The absolute values for SIF

K3 results in both tables 6-1 and 6-2 revealed that none of the cracks had the results within the range of *200 –1400* $KPa.\sqrt{m}$ and therefore none of the cracks will propagate. The SIF K3 results were abandoned and only K1, K2 and J-integral results were utilised for further analysis.

SIFS K1 and K2 results show that crack 1 is in a compressive stress state. Since cracks do not propagate in compressive stress state, crack 1 will not propagate based on the stress intensity factor (SIF) results obtained from the numerical simulation. According to stress intensity factor (SIF) K1 and K2 results in tables 6-1 and 6-2, cracks 2, 4, 5 and 7 had values below the fracture toughness range of 200 – 1400 $KPa.\sqrt{m}$ thus the cracks will not propagate. Moreover, according to maximum stress intensity factor results in table 6-1, cracks 3 and 6 had absolute K1 values of *1222.5* $KPa\sqrt{m}$ and *861.81* $KPa\sqrt{m}$ respectively. However, crack 3 value showed a compressive stress state while crack 6 was a tensile stress state value. Accordingly, crack 6 will propagate while crack 3 will not propagate based on SIF (K1) results. A further look into second SIF (K2) results revealed that crack 3 had tensile stress state result of *451.58* $KPa\sqrt{m}$. Actually, SIF K2 results in both table 6-1 and 6-2 showed tensile stress state in crack 3 with maximum and minimum stress intensity factor results within the propagation range. Therefore, crack 3 is likely to propagate according to SIF (K2) results.

Maximum SIF (K2) results suggested that crack 3 will propagate while maximum SIF (K1) results connoted that crack 6 will propagate. Therefore, based on stress intensity factor results, cracks 3 and 6 on Herøysund bridge will propagate. The findings were further confirmed through strain energy fracture failure analysis using J-integral results.

J-Integral analysis

J-integral represents the strain energy release rate and accounts for mixed-mode loading i.e., combinations of tension, shear, and bending [40]. It is the measure of the intensity of stress and deformation fields near the crack tip [42]. Its crucial for analyzing complex loading conditions since it is the mesure of the energy available for crack propagation and used to predict the onset of crack growth on a material [41, 42]. J-integral values depend on loading conditions, geometry of crack in the material and the mechanical properties of the materials [41]. J-integral equation is defined by [36];

$$J \equiv \int_{\Gamma} (W n_1 - T_i \frac{\partial u_i}{\partial x_1}) \, ds \tag{6.1}$$

where W is strain energy density

n_1 is normal to the curve (Γ)

T_i is surface traction vector

u_i is displacement vector

x_1 is the coordinate direction

ds is the differential element along the path (Γ)

When the J-integral reaches a critical value (J_C), the crack will propagate leading to failure of the material i.e crack propagates when $J \geq J_C$ [40].

Critical value J_C can be determined through analytical method called Linear Elastic Fracture Mechanics (LEFM) which is given by [42];

$$J_C = \frac{K_{IC}^2}{E} \tag{6.2}$$

The critical J-integral (J_C) value range of concrete was calculated, given K_{1C} = 0.2 – 1.4 MPa.$\sqrt{\text{m}}$ and Young's modulus, E = 19360 MPa, as follows:

Taking lower limit of fracture toughness as 0.2 MPa.$\sqrt{\text{m}}$ and converting into Pa.$\sqrt{\text{m}}$ we get;

$K_{1c} = 0.2MPa \cdot \sqrt{m} = 0.2 \times 10^6 Pa \cdot \sqrt{m}$

$E = 19360MPa = 19360 \times 10^6 Pa$

Calculating critical J-integral based on equation (6.2) we obtain;

$$J_c = \frac{{K_1}_c^2}{E} = \frac{(0.2 \times 10^6)^2}{19360 \times 10^6} = \frac{0.04 \times 10^{12}}{19360 \times 10^6} = 2.0656 Pa.m \tag{6.3}$$

$J_c \approx 2.0656\ J/m^2$

The lower limit value of critical J-integral of concrete is approximately *2.0656* J/m^2.

Taking the upper limit of fracture toughness as 1.4 MPa.$\sqrt{\text{m}}$, we can get;

$K_{1c} = 1.4MPa \cdot \sqrt{m} = 1.4 \times 10^6 Pa \cdot \sqrt{m}$

$$J_c = \frac{{K_1}_c^2}{E} = \frac{(1.4 \times 10^6)^2}{19360 \times 10^6} = \frac{1.96 \times 10^{12}}{19360 \times 10^6} = 101.24 Pa.m \tag{6.4}$$

$J_c \approx 101.24\ J/m^2$

The upper limit value of critical J-integral (J_C) of concrete material is approximately *101.24* J/m^2. Critical J-integral (J_C) value of concrete materials is in the range of 2*.0656 – 101.24*J/m^2.

This research considered maximum J-integral values for each crack generated in table 6-1 and compared against the critical J-integral (J_C) range of *2.0656 – 101.24*J/m^2 and observations were drawn on which cracks would propagate. Table 6-1 showed that cracks 2, 4, 5 and 7 had lower maximum J-integral values than the critical J-integral (J_C) limits of *2.0656 – 101.24*J/m^2. Actually, cracks 2, 4, 5, and 7 had maximum J-integral values of *0.27816* J/m^2, *0.0075869* J/m^2, *0.483* J/m^2 and *0.82119* J/m^2 respectively. These results demonstrate that cracks 2, 4, 5 and 7 on Herøysund bridge would not propagate based on strain energy release rate on crack growth analysis. This was a confirmation that the outlined cracks would not propagate just as it was affirmed under stress intensity factor (SIFS) results analysis.

On the contrary, maximum J-integral results for cracks 1, 3 and 6 in table 6-1 were within the required critical J-integral (J_C) range of *2.0656 – 101.24* J/m^2. Indeed, the cracks 1, 3 and 6 had maximum J-integral values of *22.565* J/m^2, *83.936* J/m^2 and *22.203* J/m^2 respectively. These results proved that cracks 1, 3 and 6 on Herøysund bridge would likely propagate when the bridge is subjected to loading. Comparing these findings with the stress intensity factor evaluations, it confirmed that cracks 3 and 6 have high probability of propagation.

In summary, cracks 2, 4, 5 and 7 on Heroysund bridge structure would likely not propagate under loading based on both stress intensity factor and J-integral findings from numerical modelling of the fractures. Therefore, there would be no structural failure of Herøysund bridge due to the presence of cracks 2, 4, 5 and 7. On the other hand, cracks 3 and 6 have high probability of propagation based on both stress intensity factors and J-integral results hence structural failure of the bridge. For crack 1, the stress intensity factor (K1) and (K2) results exhibited compressive stress state that might jeopardise its propagation but J-integral results presented high probability of propagation. Therefore, because of high strain energy release rate on crack 1 compared to the critical J-integral value of concrete, this study settled that crack 1 is likely to propagate. As a result, cracks 1, 3 and 6 are likely to cause structural failure of Herøysund bridge under dynamic loading hence must be urgently revamped.

6.2 Modal Analysis Results

In complex structures like the Herøysund Bridge, FEM calculates the natural frequency and identifies mode shapes. In this project twenty (20) modes were generated, and their natural frequencies were found as shown in table 6-3. The mode shapes for the first six modes were as given in figure 6-4. The mode shapes for the rest of the modes i.e mode shapes for modes 7 to 20 are found in Appendix D.

6.2.1 Modal Natural Frequencies

Natural frequencies represent the oscillation of the structure at each mode.The natural frequencies for the 20 modes were as shown in table 6-3.

Table 6-3: *Modes with corresponding natural frequencies*

Modes and Natural Frequencies					
Modes	**1**	**2**	**3**	**4**	**5**
Frequency (Hz)	1.4232	1.6801	2.9455	3.3111	3.5452
Modes	**6**	**7**	**8**	**9**	**10**
Frequency (Hz)	3.5876	4.2984	4.6805	5.2245	6.3200
Modes	**11**	**12**	**13**	**14**	**15**
Frequency (Hz)	6.8002	7.3868	7.5485	7.7091	9.0028
Modes	**16**	**17**	**18**	**19**	**20**
Frequency (Hz)	9.8222	10.351	10.598	10.776	11.492

6.2.2 Mode shapes

Mode shapes characterize the displacement patterns of a structure and are classified into three categories that include flexural (bending), transverse, and torsional (twisting) [28]. Table 6-4 is a brief overview of the three types of mode shapes. The significance of each mode type vary depending on the design, materials, location, and load types of the structures. Figure 6-5 convey the primary mode shapes for the 3D-solid model of Herøysund bridge displaying general patterns of modes of structures.

Table 6-4: *Types of Modes and some of their characteristics [28]*

Characteristics	**Types of Modes**		
	Flexural (Bending)	**Transverse**	**Torsional (Twist)**
Nature of Motion	Up and down	Side to side	Twisting
Primary Causes	Self-weight and load	Self-weight and load	Uneven weight distribution
Impact on Structure	Deflection, cracking	Lateral instability	Twisting, warping
Frequency	Lowest	Higher than flexural	Higher than flexural and transverse
Design Considerations	Material selection, geometry	Wind barriers, damping	Symmetry, torsional stiffness

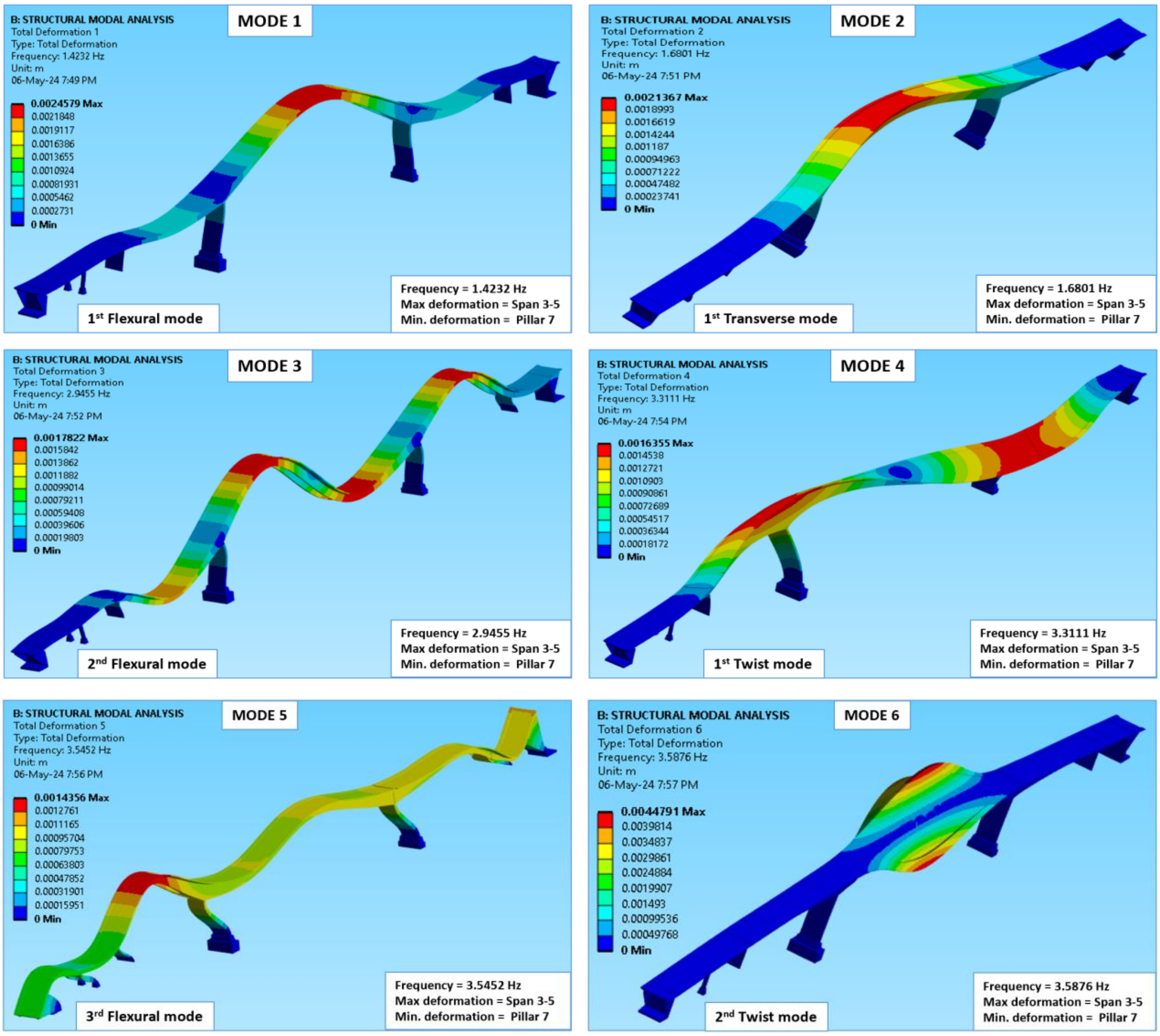

Figure 6-5: *Mode shapes of the first 6 modes*

Flexural modes are primary vibrational modes that require the least energy for excitation with equal mass distribution. As a result, the first mode of Herøysund bridge was flexural mode. The lowest energy state is the energy required to oscillate a structure. The first flexural mode shown in figure 6-5 was the first fundamental mode 1 with the least resonant frequency magnitude of *1.4232 Hz* and highest wavelength required to cause longitudinal bending. High wavelengths exhibit variation in modal displacements across the structure. The first flexural mode presented deformation in one section only, i.e., maximum deformation of *2.4579 mm* in mid-span 3-6. Similarly, the second and third flexural modes represented two and three crests oscillating in opposite direction.

The second lowest excitation energy state illustrated the first transverse mode at *1.6801Hz* represented by mode 2 in figure 6-5. The third and fourth lowest energy states were found to be the second flexural mode at *2.9455Hz* and the first torsional (twist) mode at *3.3111Hz* represented by modes 3 and 4 respectively. The fifth and sixth lowest energy states were the third flexural mode at *3.5452 Hz* and second torsional mode at *3.5876 Hz* characterized by modes 5 and 6 respectively. The rest of the modes and their shapes are found in appendix D.

In general, the excitation frequency for each mode shape increased with decrease in wavelength. Similarly, the displacement variation (oscillation amplitude) increased with increasing frequency. In addition, the modes at higher frequencies had a mix of flexure, transverse, and torsional mode shapes.

6.2.3 Mode Participation Factors, Effective Mass, and Modal Excitation

For complex structures, there can be several degrees of freedom in modal analysis implying creation of several natural frequencies. Participation factor and effective mass are applied to determine the number of modes to extract and identify the most important modes [20]. Mode participation factor and effective mass measure the amount of mass moving in each direction for each mode [26]. A high value in a direction denote that the mode will be excited by forces or excitations in that direction.

Participation factor is a measure of response of a structure at a given frequency. It represents how much each mode contributes to the deflections and corresponding stresses and strains in a particular direction. Participation factor can be determined by an equation expressed as [28];

$$\text{Participation factor, } \gamma_i = \{\emptyset\}_i^T[\mathrm{M}]\{\mathrm{D}\} \tag{6.5}$$

Where $\{\emptyset\}_i^T$ is mode shape

[M] is the mass matrix

{D} is Excitation directional vector.

Effective mass is expressed as [26];

$$\text{Effective mass, } M_{eff,\,i} = \gamma_i^2 \tag{6.6}$$

Modes that contribute significantly to deformation of a structure in any direction have high magnitude of participation factor and effective mass [20]. Such modes most easily get exciting vibration forces in any particular direction.

The mode coefficient (A_i) is the factor that is multiplied by the eigenvector to give actual displacement in each mode. Mode coefficient can be determined from participation factors (γ_i) and spectrum values (S_i) given by [28];

$$\text{Mode Coefficient, } \mathrm{A}_i = (S_i)\,(\gamma_i) \tag{6.7}$$

The response (displacement, velocity, and acceleration) for each mode can be found considering frequency, mode coefficient and mode shapes. Table 6-5 illustrate the translational and rotational participation factors and effective mass of all modes generated in x, y, and z. The participation factor and effective mass together with their ratio for each coordinate can be found in appendix E.

Table 6-5: *Participation factor and effective mass for all modes generated in x,y,z directions*

Participation Factor

Mode	Frequency [Hz]	X Direction	Y Direction	Z Direction	Rotation X	Rotation Y	Rotation Z
1	1.4232	47.08	374.38	5.3645	-1236.5	585.72	-31393
2	1.6801	-1.0125	-1.1678	725.24	4983.2	59134	78.171
3	2.9455	206.32	11.687	0.38238	-38.053	701.06	-9094.
4	3.3111	-4.5109	-3.8709	4.5565	285.72	-24826	469.79
5	3.5452	1003.6	140.85	-0.16435	-478.99	3280.7	-13669
6	3.5876	-2.6376	-1.5098	34.25	-405.45	3086.3	142.
7	4.2984	-297.31	465.25	4.5736	-1566.2	-706.57	-38713
8	4.6805	4.1388	-3.2792	527.34	2188.7	42619	21.525
9	5.2245	-67.177	24.047	5.3529	-59.989	325.46	18184
10	6.32	-0.57169	-0.84423	29.312	177.1	-8108.7	47.536
11	6.8002	-0.86419	-1.408	41.502	284.82	-13585	124.28
12	7.3868	-0.29114	2.008	-97.91	204.67	-7720.3	-175.33
13	7.5485	-0.25742	6.1108	-17.355	-283.7	2485.2	-493.88
14	7.7091	50.871	-317.93	1.425	1087.9	450.48	25658
15	9.0028	-0.91563	-0.57741	298.2	1284.4	11625	-28.146
16	9.8222	88.305	165.12	3.3525	-547.08	322.03	-12492
17	10.351	0.38785	-0.60736	127.74	26.199	4713.7	54.357
18	10.598	29.825	36.919	-9.1426	-152.71	782.32	-2901.
19	10.776	-2.4568	-1.398	-84.587	-194.24	11860	110.47
20	11.492	-25.015	-231.41	6.4396	807.3	329.44	18586

Effective Mass

Mode	Frequency [Hz]	X Direction [kg]	Y Direction [kg]	Z Direction [kg]	Rotation X [kg m m]	Rotation Y [kg m m]	Rotation Z [kg m m]
1	1.4232	2216.5	1.4016e+005	28.778	1.529e+006	3.4307e+005	9.8553e+008
2	1.6801	1.0251	1.3637	5.2597e+005	2.4832e+007	3.4968e+009	6110.8
3	2.9455	42566	136.59	0.14621	1448.	4.9148e+005	8.2701e+007
4	3.3111	20.348	14.984	20.762	81636	6.1635e+008	2.207e+005
5	3.5452	1.0072e+006	19839	2.7012e-002	2.2943e+005	1.0763e+007	1.8683e+008
6	3.5876	6.9571	2.2794	1173.	1.6439e+005	9.5252e+006	20165
7	4.2984	88391	2.1645e+005	20.917	2.4531e+006	4.9924e+005	1.4987e+009
8	4.6805	17.13	10.753	2.7809e+005	4.7906e+006	1.8164e+009	463.31
9	5.2245	4512.7	578.25	28.654	3598.7	1.0592e+005	3.3067e+008
10	6.32	0.32683	0.71272	859.2	31364	6.5751e+007	2259.7
11	6.8002	0.74682	1.9826	1722.4	81124	1.8455e+008	15446
12	7.3868	8.4765e-002	4.0319	9586.3	41891	5.9604e+007	30741
13	7.5485	6.6263e-002	37.341	301.2	80487	6.176e+006	2.4392e+005
14	7.7091	2587.9	1.0108e+005	2.0306	1.1836e+006	2.0294e+005	6.5835e+008
15	9.0028	0.83838	0.3334	88923	1.6498e+006	1.3515e+008	792.18
16	9.8222	7797.8	27264	11.239	2.993e+005	1.037e+005	1.5605e+008
17	10.351	0.15043	0.36889	16318	686.37	2.2219e+007	2954.7
18	10.598	889.54	1363.	83.587	23319	6.1202e+005	8.4156e+006
19	10.776	6.036	1.9545	7154.9	37728	1.4065e+008	12204
20	11.492	625.74	53552	41.469	6.5173e+005	1.0853e+005	3.4546e+008
Sum		1.1569e+006	5.6051e+005	9.3033e+005	3.8166e+007	6.5664e+009	4.2533e+009

In modal analysis, participation factor and effective mass are parameters for assessing the mass movement of each mode along the x, y, and z-direction and they identify modes with maximum contribution. From table 6-5, the modes with significant excitation on the Herøysund bridge structure were established in any particular direction. Table 6-6 is the summary of the level of excitational participation of each mode in all the directions.

Table 6-6: *Participating modes for translational and rotatonal excitations*

Excitation	Participating modes	Effective mass ratio
X-Direction	1, 3, 5, 7, 9, 14, 16, 18, 20	83.52%
Y-Direction	1, 3, 5, 7, 9, 14, 16, 18, 20	40.46%
Z-Direction	2, 6, 8, 10, 11, 12, 15, 17, 19	67.16%
X-Rotation	1, 2, 5, 6, 7, 8, 14, 15, 16, 20	68.49%
Y-Rotation	2, 4, 5, 6, 8, 10, 11, 12, 13, 15, 17, 19	56.41%
Z-Rotation	1, 3, 4, 5, 7, 9, 13, 14, 16, 18, 20	36.48%

The participation factor and effective mass analysis showed significant excitation from flexural mode 5 in *x-direction*. Flexural modes 7, 1 and 14 had notable contribution in *y-axis* translation direction and *z-axis* rotation. Similarly, transverse modes 2 and 8 had exceptional excitation in *z-direction* and *y-axis* rotation. In addition, transverse mode 2 had outstanding contribution in *x-axis* rotatation.

6.3 Harmonic Response Analysis

Harmonic response analysis is crucial in the design and maintenance of structures. It is frequency based analysis used to simulate structural response to sinusoidally repeating dynamic loading [5]. It is very useful in understanding important structural behaviors like resonance, where excessive motion, stress, noise, and vibrations occur at a particular frequency [20]. Steady state response of Herøysund bridge was solved assuming harmonic loads were acting for a particular period.

Table 6-7: *Modal mass, Kinetic energy, and translational effective mass for extracted modes*

***** MODAL MASSES, KINETIC ENERGIES, AND TRANSLATIONAL EFFECTIVE MASSES SUMMARY *****

					EFFECTIVE MASS				
MODE	FREQUENCY	MODAL MASS	KENE	X-DIR	RATIO%	Y-DIR	RATIO%	Z-DIR	RATIO%
1	1.423	0.1655E+06	0.6619E+07	2217.	0.16	0.1402E+06	10.12	28.78	0.00
2	1.680	0.2333E+06	0.1300E+08	1.025	0.00	1.364	0.00	0.5260E+06	37.97
3	2.945	0.3260E+06	0.5583E+08	0.4257E+05	3.07	136.6	0.01	0.1462	0.00
4	3.311	0.4034E+06	0.8731E+08	20.35	0.00	14.98	0.00	20.76	0.00
5	3.545	0.7632E+06	0.1893E+09	0.1007E+07	72.71	0.1984E+05	1.43	0.2701E-01	0.00
6	3.588	0.5021E+05	0.1276E+08	6.957	0.00	2.279	0.00	1173.	0.08
7	4.298	0.1484E+06	0.5412E+08	0.8839E+05	6.38	0.2165E+06	15.63	20.92	0.00
8	4.680	0.2965E+06	0.1282E+09	17.13	0.00	10.75	0.00	0.2781E+06	20.08
9	5.224	0.1927E+06	0.1038E+09	4513.	0.33	578.2	0.04	28.65	0.00
10	6.320	0.1440E+06	0.1135E+09	0.3268	0.00	0.7127	0.00	859.2	0.06
11	6.800	0.1122E+06	0.1024E+09	0.7468	0.00	1.983	0.00	1722.	0.12
12	7.387	0.2982E+05	0.3211E+08	0.8477E-01	0.00	4.032	0.00	9586.	0.69
13	7.548	0.3116E+05	0.3504E+08	0.6626E-01	0.00	37.34	0.00	301.2	0.02
14	7.709	0.1974E+06	0.2315E+09	2588.	0.19	0.1011E+06	7.30	2.031	0.00
15	9.003	0.2368E+06	0.3789E+09	0.8384	0.00	0.3334	0.00	0.8892E+05	6.42
16	9.822	0.5700E+06	0.1086E+10	7798.	0.56	0.2726E+05	1.97	11.24	0.00
17	10.35	0.9923E+05	0.2099E+09	0.1504	0.00	0.3689	0.00	0.1632E+05	1.18
18	10.60	0.1854E+06	0.4110E+09	889.5	0.06	1363.	0.10	83.59	0.01
19	10.78	0.2519E+06	0.5773E+09	6.036	0.00	1.955	0.00	7155.	0.52
20	11.49	0.1559E+06	0.4063E+09	625.7	0.05	0.5355E+05	3.87	41.47	0.00
sum				0.1157E+07	83.52	0.5605E+06	40.46	0.9303E+06	67.16

The input loads of *1382.775 kN*, *4835.85 kN* and *115 kN* representing rail and asphalt load, total evenly distributed traffic load (TEDTL) and total traffic loading at centre (TTLC) respectively were assumed to act sinusoidally at same frequency along the top deck of bridge span 1–7. The equation of motion in harmonic response analysis for input loads is given by [24];

$$F_i = (F_i)_{max}\ Sin\ (\omega t\ +\ \theta_i) \tag{6.8}$$

Where F_i is the input load

ω is frequency of input load

t is the time domain

θ_i is input load phase angle

Since input load is sinusoidal, the output solution is expected to be sinusoidal at frequency given by the equation of motion as [5];

$$u_i = (u_i)_{max}\ Sin\ (\omega t + \varphi_i) \tag{6.9}$$

Where u_i is output solution

φ_i is phase angle of solution

The difference between input load phase angle (θ_i) and phase angle of solution (φ_i) is caused by damping and out of phase loads resulting in phase shift [24].

This study assumed damping of 2.5% with prestressed modal analysis as the pre-requisite in performing harmonic response simulation. The natural frequency results obtained in section 6.1 were utilised in determining the harmonic response behaviour of the Herøysund bridge model. The 20 modes with natural frequency ranging between *1.4232 Hz* and *11.492 Hz* were used thus the frequency sweep was set between 0 and *12Hz* with spatial resolution set to maximum. The displacement in vertical (y-axis) direction was of interest and solution intervals were set to 6. This implied that results set was calculated for every *0.5Hz* from 0 to *12Hz*. The objective was to predict maximum response location, frequency, phase angle and stresses. The first thing to check was the largest response location in the structure and at what frequency and phase angle. The frequency response plot was inserted to check displacement that correspond to frequency and phase angle at the location of peak response. Thereafter, local results such as directional deformation and equivalent stresses at maximum response frequency were determined based on acceptance criteria in this analysis.

6.3.1 Frequency Response

The deformation frequency response data was generated as found in table 6-8. The data was used to find the maximum amplitude and phase angle. Frequency response graphs of amplitude against natural frequency was retrieved as in figure 6-6. The results in table 6-8 and figure 6-6 showed that the maximum response amplitude was *0.62093m* at frequency of *1.418 Hz* and phase angle of 93.944°.The values insinuate that the highest response was attained at a frequency of *1.418 Hz* and phase angle of 93.944°. The maximum response frequency of *1.418 Hz* was used to determine the phase response of the structure and maximum response location as well as the phase shift between the input loads and the output resonance.

Table 6-8: *Frequency response data of Amplitude and phase angles*

Tabular Data

	Frequency [Hz]	Amplitude [m]	Phase Angle [°]
1	0.	7.9628e-002	180.
2	1.0735	0.17515	168.25
3	1.2866	0.35672	149.42
4	1.3756	0.56143	119.74
5	1.4073	0.61696	100.95
6	1.418	0.62093	93.944
7	1.4232	0.61948	90.489
8	1.4284	0.61577	87.034
9	1.4392	0.60142	80.029
10	1.4724	0.51958	61.239
11	1.5516	0.32152	35.632
12	1.617	0.22827	26.029
13	1.6581	0.19008	22.303
14	1.6726	0.17915	21.259
15	1.6801	0.17387	20.76
16	1.6876	0.16883	20.285
17	1.7023	0.15969	19.431
18	1.7456	0.13709	17.357
19	1.8733	9.4217e-002	13.587
20	2.2499	4.3051e-002	10.329
21	2.3128	3.8669e-002	10.301
22	2.5463	2.9842e-002	170.16
23	2.7734	3.0156e-002	163.82
24	2.8748	3.004e-002	160.37
25	2.9171	2.9876e-002	159.06
26	2.9455	2.9747e-002	158.3
27	2.9741	2.9998e-002	168.72
28	3.0179	3.0784e-002	167.2
29	3.1283	3.2579e-002	162.39
30	3.2199	3.3818e-002	157.82
31	3.2731	3.4436e-002	155.
32	3.3111	3.483e-002	153.17
33	3.3496	3.518e-002	150.99
34	3.4049	3.5567e-002	147.69
35	3.4282	3.5682e-002	146.34
36	3.4392	3.5727e-002	145.7
37	3.5	3.5861e-002	142.27
38	3.5452	3.5867e-002	139.86
39	3.5664	3.5856e-002	138.79
40	3.5876	3.5843e-002	137.75
41	3.6348	3.6316e-002	140.77
42	3.6998	3.7569e-002	137.93
43	3.8544	4.0986e-002	129.67
44	3.943	4.3007e-002	123.73
45	3.9492	4.3143e-002	123.27
46	4.1355	4.6106e-002	107.56
47	4.2242	4.626e-002	98.98
48	4.2984	4.5567e-002	91.628
49	4.3738	4.4119e-002	84.245
50	4.4676	4.1486e-002	75.549
51	4.4894	4.0781e-002	73.644
52	4.5879	3.7345e-002	65.65
53	4.6805	3.4006e-002	59.126
54	4.7749	3.0722e-002	53.424
55	4.8865	2.7161e-002	47.797
56	4.9525	2.5253e-002	45.039
57	4.9711	2.4741e-002	44.3
58	5.101	2.149e-002	39.84
59	5.2245	1.8879e-002	36.584
60	5.351	1.7632e-002	12.357
61	5.4907	1.6479e-002	9.4116
62	5.7722	1.4568e-002	4.2945
63	5.9283	1.3693e-002	1.5468
64	6.1152	1.2773e-002	-1.6697
65	6.32	1.1882e-002	-5.2594
66	6.5316	1.105e-002	-9.1383
67	6.5601	1.0943e-002	-9.6774
68	6.8002	1.0065e-002	-14.395
69	7.0588	9.1407e-003	-19.89
70	7.0935	9.0163e-003	-20.631
71	7.3868	7.9517e-003	-26.932
72	7.4676	7.655e-003	-28.637
73	7.5485	7.358e-003	-30.306
74	7.6288	7.0638e-003	-31.916
75	7.7091	6.7716e-003	-33.468
76	8.0746	5.5032e-003	-39.493
77	8.356	5.2351e-003	29.564
78	8.473	5.115e-003	28.141
79	9.0028	4.5271e-003	22.059
80	9.4125	4.0757e-003	17.992
81	9.8222	3.6578e-003	14.474
82	10.087	3.4096e-003	12.455
83	10.351	3.1784e-003	10.61
84	10.474	3.0782e-003	11.347
85	10.598	2.9817e-003	10.639
86	10.687	2.9139e-003	10.147
87	10.776	2.8478e-003	9.6705
88	11.134	2.599e-003	7.927
89	11.492	2.3813e-003	8.4306
90	12.	2.1178e-003	8.991

6.3.2 Phase response

Using the maximum response frequency of *1.418Hz* and sweeping angle range of 0 to 720°, the phase response data and graph of the structure were generated as in appendix F and figure 6-7 respectively. The orientation was set to y-axis as vertical displacement of the structure was the point of interest. The maximum amplitude was achieved at phase angle of 93.944° at frequency of *1.418 Hz*.

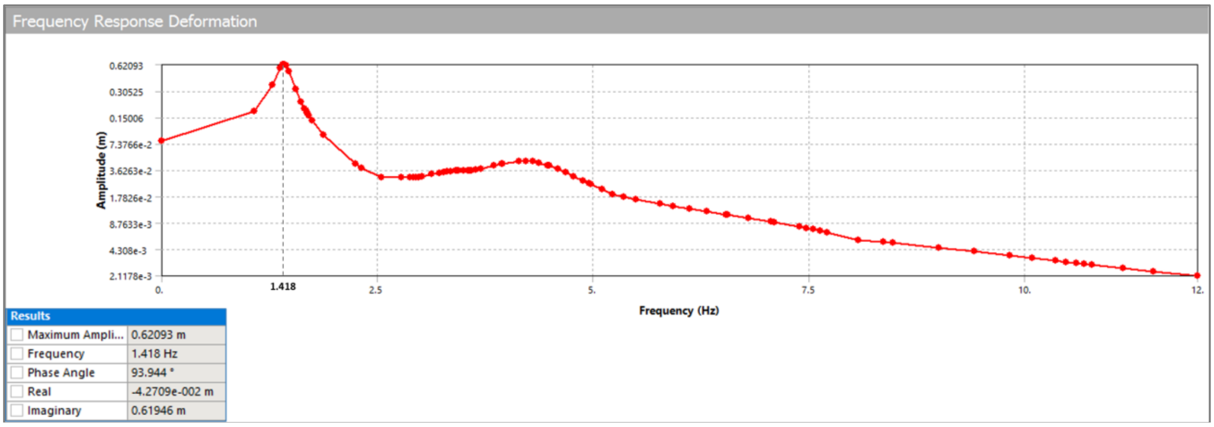

Figure 6-6: *Frequency response graphs of amplitude against frequency*

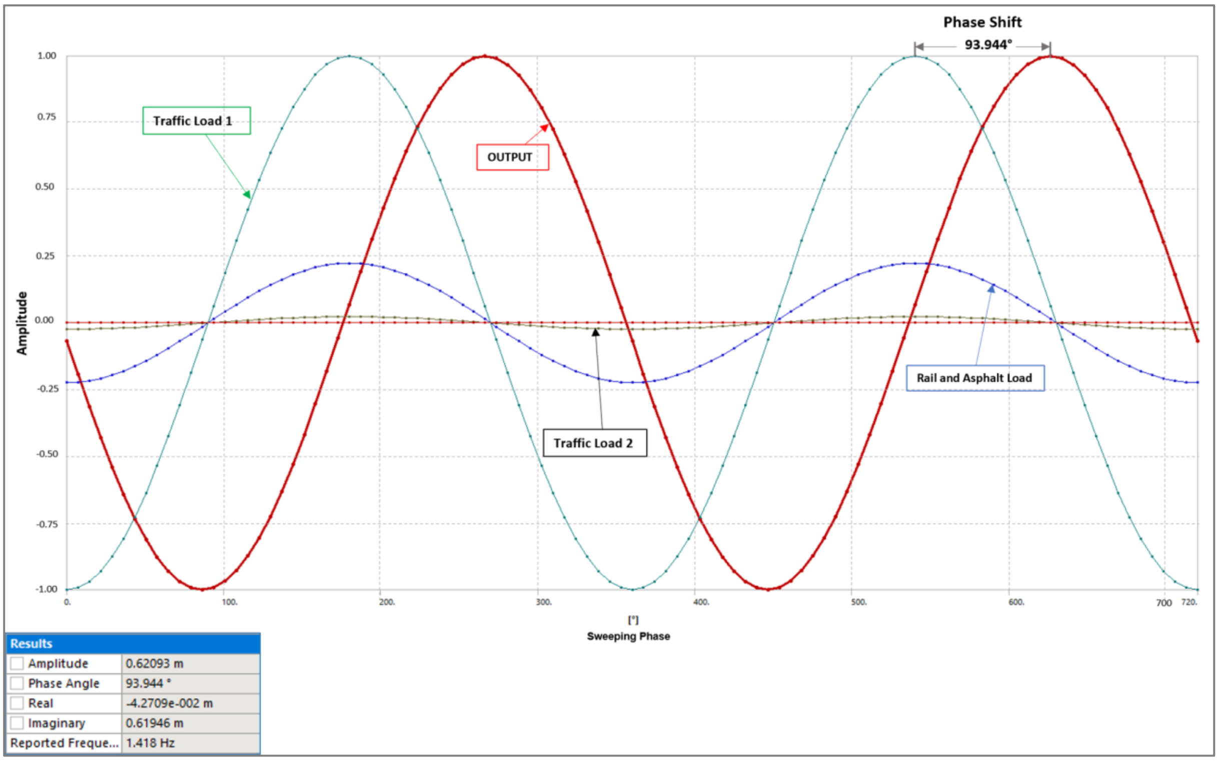

Figure 6-7: *Phase response graph showing phase shift between input loads and response output*

The phase angle of 93.944° represented the phase shift between the sinusoidal input loads and the corresponding response output at damping ratio of 2.5% in the system. The sinuisoidal input loads had similar frequencies and wavelengths but differed in amplitude as shown in figure 6-7. The input loads and output response were 93.944° in-phase.

The frequency and phase response results were utilised to find velocity, acceleration and stress response of the structure as shown in figures 6-8 and 6-9 with tabulated data attached in appendix F. Directional deformation and equivalent stress were equally determined. The maximum amplitude for velocity frequency response was found as *5.5395 m/s* at maximum frequency response of *1.4232 Hz* and phase angle of −179.51°. The angle represented the phase shift between input loads and output velocity response which were 179.51° out-of-phase.

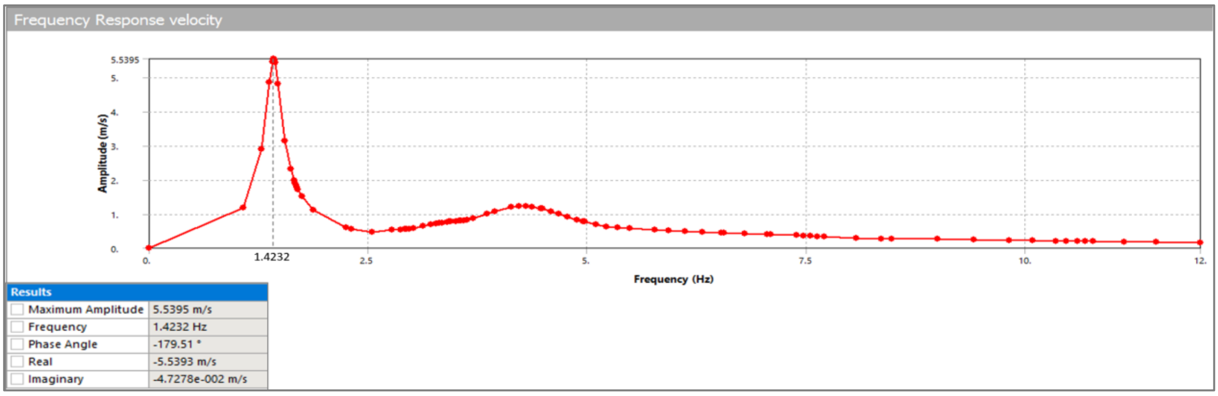

Figure 6-8: *Frequency response velocity graph*

The acceleration frequency response was also determined as in figure 6-9 which gave maximum acceleration amplitude of *49.6* m/s^2 at a response frequency of *1.4284 Hz* and out-of-phase angle of −92.966°. At maximum frequency of *1.418 Hz*, the maximum stress response was found to be *61.116 MPa* at in-phase angle of 92.935° as illustrated by figures and tables in appendix F.

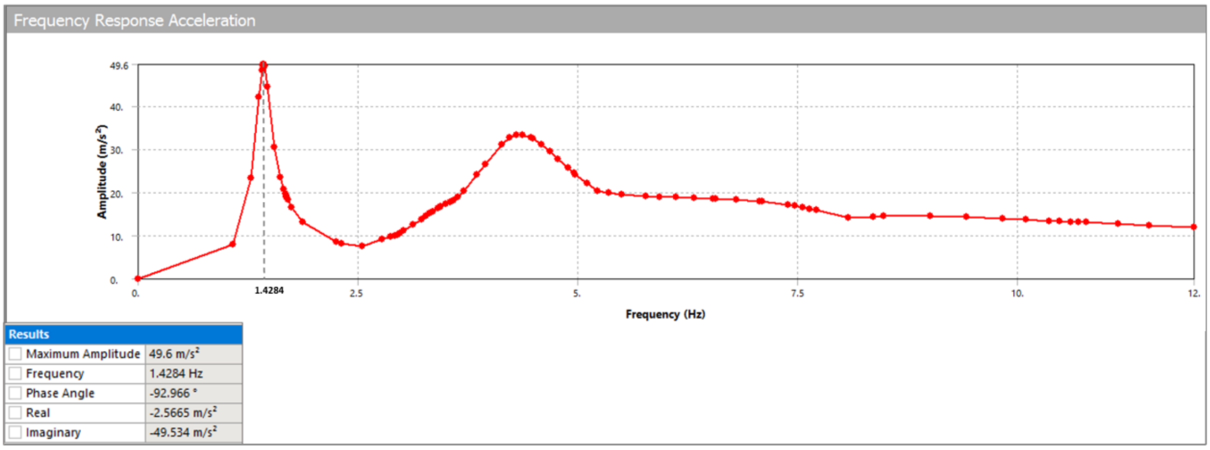

Figure 6-9: *Frequency response acceleration graph*

6.3.3 Directional deformation

Maximum frequency response of *1.418 Hz* and sweeping angle of 93.944° were used to determine directional deformation in y-axis. The maximum directional deformation was obtained as *0.17047m* as shown in figure 6-10. The directional deformations concentrated on bridge span 3-5. This depicted main bridge span 3-5 as the peak response location of the Herøysund bridge.

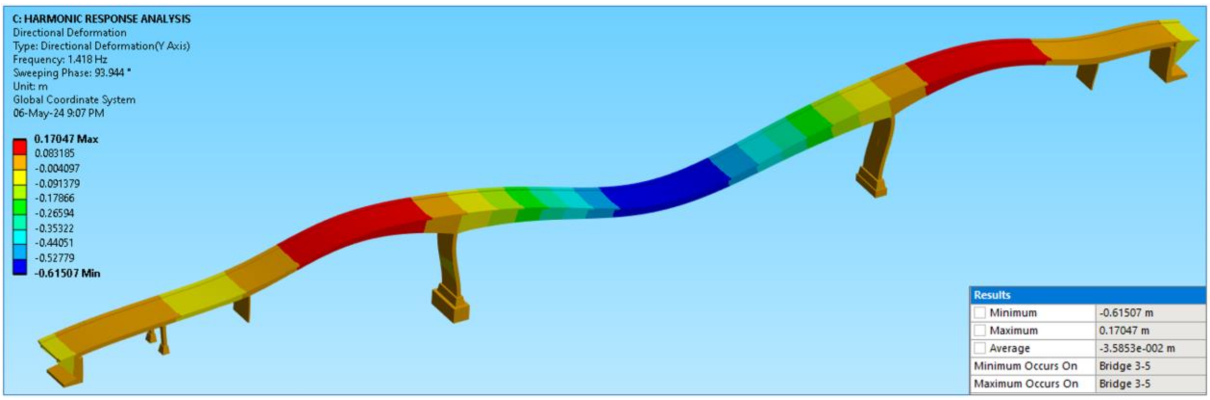

Figure 6-10: *Directional deformation at maximum frequency response and phase angle*

6.3.4 Equivalent (Von Mises) Stress

Under similar conditions like section 6.3.3, equivalent stress on Herøysund bridge was derived. The maximum equivalent stress was *226.64 MPa* on load bearing steel plates in pillar 6. The minimum equivalent stress attained was *1009.7Pa* occurring on bridge span 3-5 as in figure 6-11. The simulation gave an average von mises stress of *11.081 MPa* under maximum frequency and phase response.

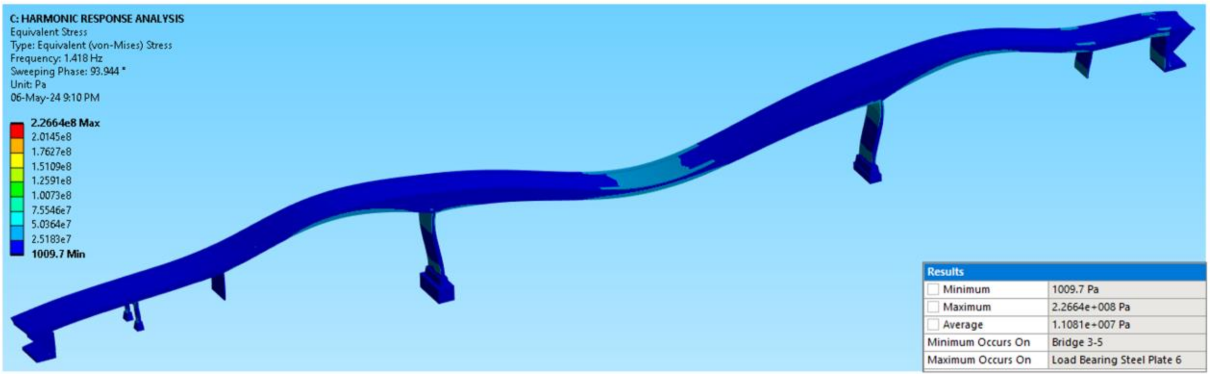

Figure 6-11: *Equivalent stress under harmonic response*

6.4 Response Spectrum Analysis

Response spectrum is used in place of time history analysis to determine quick approximation of peak response of structures exposed to short, non-deterministic, time dependent loading conditions e.g. earthquake and shock loading events [20]. It is a mode superposition analysis that utilize results from modal analysis with known spectrum to determine deformation and stresses in the model [24]. This study considered response spectrum analysis of Herøysund bridge to evaluate its response to shock loading conditions. Maximum response was determined based on response input spectrum. Just like harmonic response, modal analysis was a pre-requisite in response spectrum analysis and natural frequencies from the corresponding modes 1 to 20 were utilised. The response of each mode was calculated, and the results combined to estimate total and directional deformation.

The boundary conditions considered were fixed support of the pillars 1-7 that defined fixed degree of freedom of the structure. The input excitation was assumed to act uniformly on all support points. Response spectrum estimates the maximum displacement and stress response in the structure through mode combination i.e combining responses from each mode. The mode combination type applied in this project was Square Root Sum of Squares (SRSS) and spectrum type used was multiple points.

Participation factor and effective mass magnitudes for mode 1 in table 6-7 revealed that the mode dominated excitation in y-axis direction thus orientation was set in y-axis. Even though there were some closely spaced modes, there participation in the y-direction was considered insignificant. In addition, Response spectrum (RS) acceleration data was fed into the system with direction set to y-axis to complete analytical setting. RS acceleration data was as in table 6-9 and parameters analysed were total deformation, directional deformation in (*y-axis* direction), directional velocity and acceleration in (*y-axis* direction), and equivalent stress.

Table 6-9: *RS acceleration input data*

MODE	FREQUENCY	INPUT SPECTRA	MODE COEF.
1	1.42	5.43770	-25.4596
2	1.68	674.990	7.07373
3	2.95	0.407963	-0.139206E-01
4	3.31	4.26514	0.381450E-01
5	3.55	24.0240	-6.81976
6	3.59	32.4810	0.965110E-01
7	4.30	4.72196	-3.01190
8	4.68	507.203	1.92315
9	5.22	5.61617	-0.125329
10	6.32	29.2194	0.156439E-01
11	6.80	41.4507	0.319697E-01
12	7.39	4.65668	-0.434069E-02
13	7.55	2.61455	-0.710251E-02
14	7.71	1.49152	0.202111
15	9.00	294.489	0.531415E-01
16	9.82	3.38137	-0.146593
17	10.4	123.165	0.176844E-01
18	10.6	66.3852	-0.552771
19	10.8	41.2621	0.125832E-01
20	11.5	6.60931	0.293344

6.4.1 Total and Directional Deformation

In response spectrum analysis, the total deformation of Herøysund bridge structure had a maximal value of *64.889 mm* as shown in figure 6-12. On the other hand, the maximum directional deformation on *y-axis* direction of the bridge was found to be *62.839 mm* as shown in figure 6-13. The maximum total and directional deformation response were highly experienced on bridge span 3-5 while minimum total and directional deformation were experienced on pillars 1 and 7 respectively.

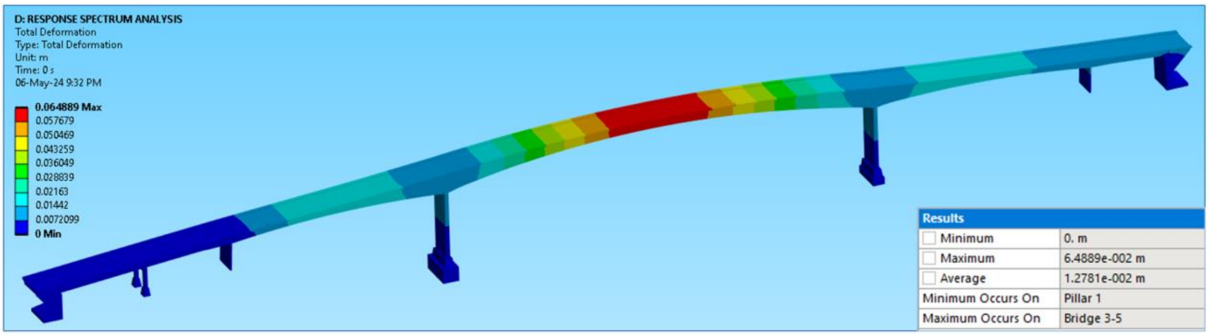

Figure 6-12: *Total deformation results in response spectrum analysis*

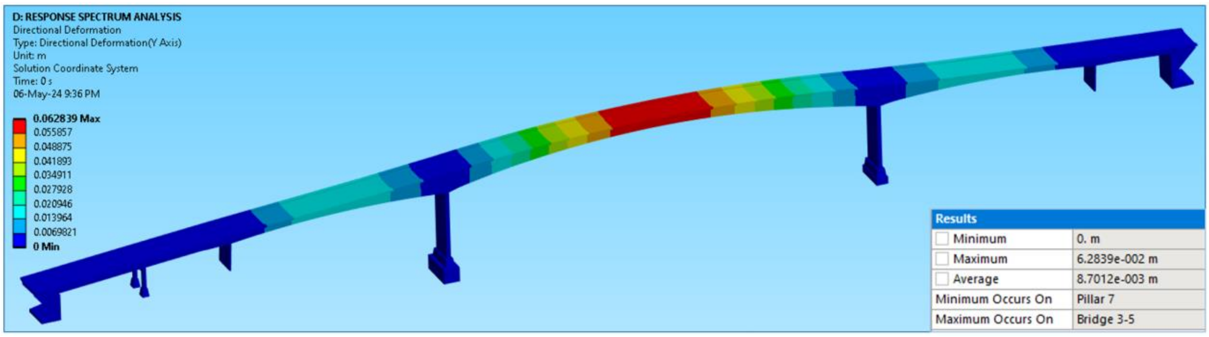

Figure 6-13: *Directional deformation results in response spectrum analysis*

6.4.2 Directional Velocity and Acceleration

The directional velocity and acceleration results were obtained in the *y-axis* direction. The directional velocity result was obtained as in figure 6-14 with maximum value of *0.57507 m/s*. The maximum and minimum directional velocities were experienced on bridge span 3-5 and pillar 7 respectively. On the other hand, maximum directional acceleration was obtained as *8.2312m/s²* and highly experienced on bridge span 5-6 as shown in figure 6-15. Minimal directional acceleration occurred on pillar 7. The obtained average directional velocity and acceleration were *0.10486 m/s* and *2.4371 m/s²* respectively.

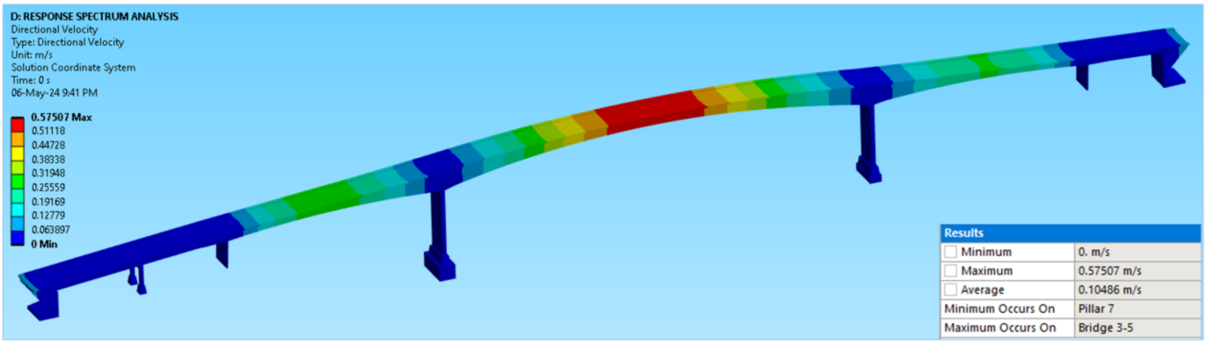

Figure 6-14: *Directional velocity results in response spectrum simulation*

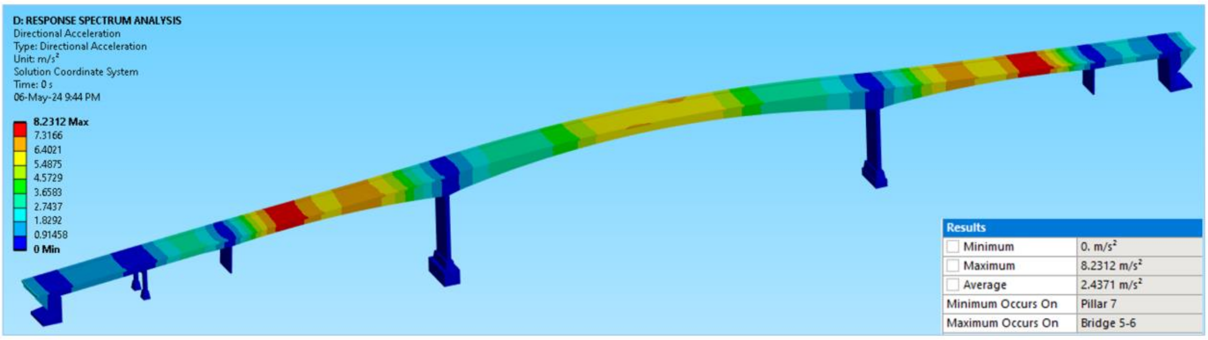

Figure 6-15: *Directional acceleration in response spectrum analysis*

6.4.3 Equivalent Stress

The maximum and minimum von mises stress attained were *29.23 MPa* and *499.02 Pa* respectively giving an average equivalent stress of *1.8614 MPa* as shown in figure 6-16. Maximum and minimum equivalent stress occurred on load bearing steel plate on pillar 6 and bridge span 3-5 respectively.

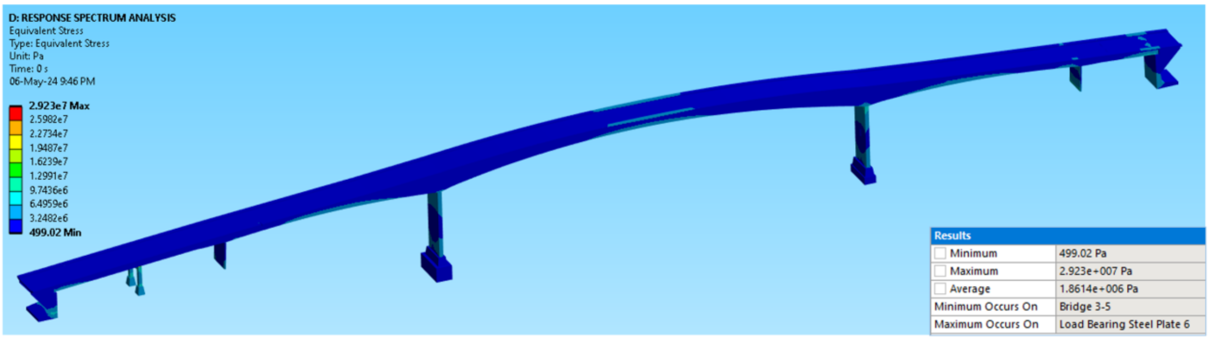

Figure 6-16: *Equivalent stress results in response spectrum analysis*

There were no deformed shapes in response spectrum analysis as it only involved quick calculation to approximate peak results from mode shapes and response spectra input. The mode coefficients were calculated by the Ansys mechanical APDL solver from mode participation factors and input spectra. This was used to combine modes to estimate the overall peak responses. The solver calculated the magnitude of displacements and stresses hence no output as a function of time or frequency obtained.

6.5 Random Vibration Analysis

This analysis helps in determining the structural response to vibration loads that are random in nature e.g., ocean wave loads on offshore structures [20]. Given that Herøysund bridge was built across the arctic ocean with pillars on sea water, this project considered random vibration analysis of the bridge to study the vibratory effect of ocean waves on the bridge pillars and the entire bridge. The frequency content of the spectrum was captured together with statistics and used as the load in the analysis. The spectrum is called power spectral density (PSD) that captures the frequency and mean square amplitude of time history of the load [24].

The random vibration analysis is a mode superposition method [5] therefore, Power spectral density (PSD) displacement values were used based on the frequency values from the prestressed modal analysis. Base excitation and PSD displacement type were applied in this analysis. The base excitation was applied in *x-axis* direction on all the pillars since the load usually propagate from the fixed support. Table 6-10 display the PSD displacement and base excitation values. The PSD displacement input values together with natural frequency values utilised in this analysis were for the 20 modes.

Table 6-10: *PSD Displacement input and participation factors for base excitation*

Tabular Data

	Frequency [Hz]	Displacement [(m^2)/Hz]
1	3.589	4.4784e-003
2	3.9475	2.4583e-003
3	6.3065	2.1352e-003
4	8.5587	5.7816e-003
5	9.0061	1.4357e-003
6	10.357	1.6356e-003

***** PARTICIPATION FACTORS FOR BASE EXCITATION NO. 1 ***** TABLE NO. 1

MODE	VALUE	MODE	VALUE	MODE	VALUE	MODE	VALUE
1	-47.080	2	1.0125	3	-206.32	4	4.5109
5	-1003.6	6	2.6376	7	297.31	8	-4.1388
9	67.177	10	0.57169	11	0.86419	12	0.29114
13	0.25742	14	-50.871	15	0.91563	16	-88.305
17	-0.38785	18	-29.825	19	2.4568	20	25.015

Since the input excitations were statistical in nature, the output responses like displacement and stresses were equally statistical. Stiffness coefficient was defined by damping vs frequency with damping ratio set to 0.025 and frequency set to *12Hz* since the highest prestressed modal natural frequency obtained was *11.492 Hz*.

Results of the analysis in terms of directional deformation (x and z direction), equivalent stress and normal elastic strain were determined at scale factor value of 3-sigma (3σ) with probability of 99.73%. The total deformation could not be determined since the input loads were random and statistical in nature. The response PSD for a vertex in pillar 4 was also determined. In addition, 1-sigma (1σ) and 2-sigma (2σ) scale factor values though not considered in this analysis, were performed and findings were as in appendix G.

6.5.1 Directional deformation

The directional deformation on x-axis at scale factor value of 3-sigma (3σ) was found as *1.5314 m* at a probability of 99.73% as shown in figure 6-17. This show that in 99.73% of time the maximum directional deformation response of Herøysund bridge will not exceed *1.5298m* in *x-axis* direction. Maximum and minimum directional deformation in x-axis direction concentrated on pillar 7.

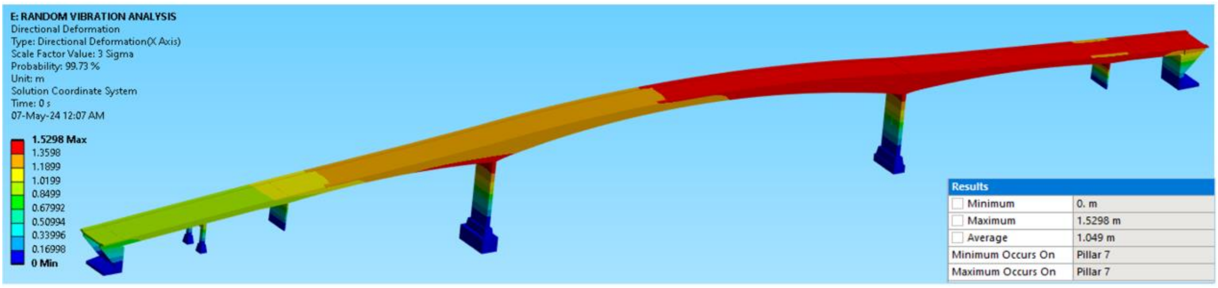

Figure 6-17: *Directional deformation on x axis orientation at scale factor value of 3- sigma (σ)*

The directional deformation response on y and z axis at scale factor value of 3-sigma (3σ) was also determined. The maximum directional deformation in y-axis was *1.9963 m* at a probability of 99.73% as shown in figure 6-18. Similarly, the maximum directional deformation in *z-axis* was *0.023823m* as shown in figure 6-19. It showed that in 99.73% of the time the maximum directional deformation in *y* and *z-axes* will not exceed *1.9963m* and *0.023823m* respectively. The directional deformations of the bridge in both y and z-axes were found to be maximum on bridge span 3-5 and minimal on pillar 7.

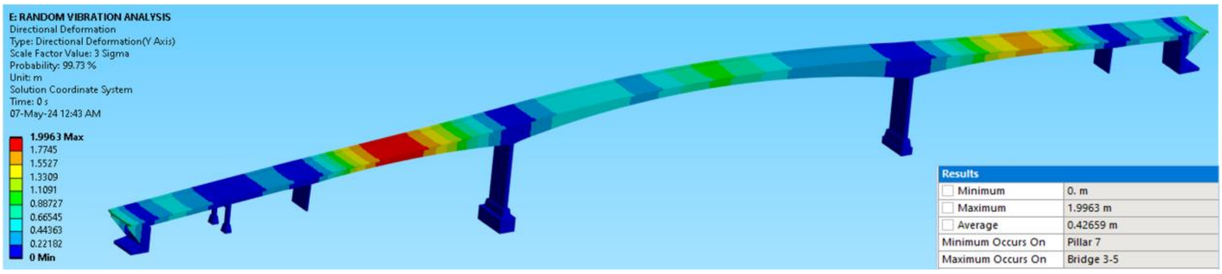

Figure 6-18: *Directional deformation on y axis orientation at scale factor value of 3- sigma (σ)*

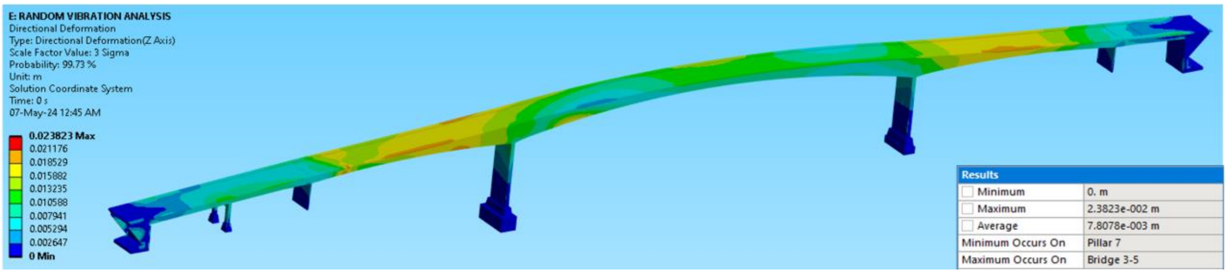

Figure 6-19: *Directional deformation on z axis orientation at scale factor value of 3- sigma (σ)*

In all the three-coordinate axes (x, y, and z), the minimum directional deformation of Herøysund bridge was found to be on pillar 7. Therefore, pillar 7 had the least random vibration response.

6.5.2 Equivalent stress

The maximum von mises stress on Herøysund bridge due to random vibration in *x-axis* direction was determined and found to be *5.6604 GPa* at scale factor value of 3-sigma (3*σ*). The minimum von mises stress was found to be *99.064 KPa* under similar conditions giving an average equivalent stress of *244.22 MPa* as shown in figure 6-20. This showed that the maximum equivalent stress experienced by the Herøysund bridge from any random vibratory source on *x-axis* direction would be less than *5.6604 GPa* but greater than *99.064 KPa* in 99.73% of the time. The result also unveiled that in 99.73% of the time the maximum and minimum equivalent stresses would be experienced on load bearing steel plates on pillar 2 and on bridge span 3-5 respectively.

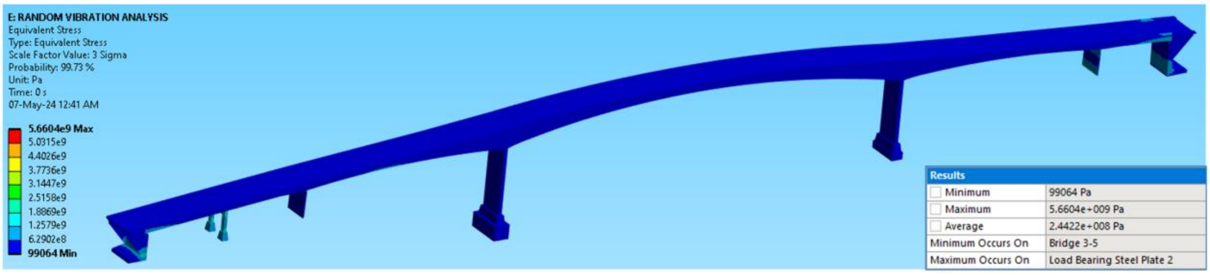

Figure 6-20: *Equivalent stress on x axis orientation of bridge structure at scale factor value of 3σ*

6.5.3 Normal elastic strain

The normal elastic strain was determined in x, y, and z axis orientation for a scale factor value of 3-sigma (3σ). The maximum normal elastic strain was found to be experienced on bridge span 6-7 at a value of *0.10486m/m* in the *x-axis* orientation as shown in figure 6-21. The maximum normal elastic strain in y and z axis orientation at 3-sigma (3σ) was *0.097703 m/m* highly experienced on pillar 6 and *0.058174m/m* highly felt on bridge span 3-5 respectively as shown in figures in appendix G. This revealed that for 99.73% of the time the random vibration on the Herøysund bridge structure would likely result in normal elastic strain of values less than *0.10486 m/m* in x-axis, *0.097703 m/m* in y-axis and *0.058174 m/m* in z-axis respectively.

Figure 6-21: *Normal elastic strain on x axis direction of bridge structure at scale factor value of 3σ*

6.5.4 Response PSD Results

Finally, PSD response simulation was performed on a point node ID 23169 at the foot of pillar 4 as shown in figure 6-22. The maximum response PSD of 5.7816×10^{-3} m^2/Hz was attained at maximum frequency of 8.5587 Hz as shown in tables and figures in appendix G. In addition, the PSD response displacement was established with maximum root-mean square (RMS) value of *0.13607m* at 100%.

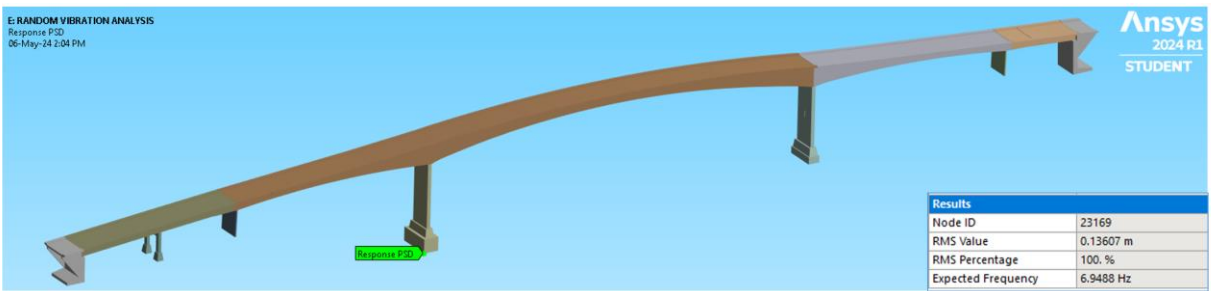

Figure 6-22: *Response PSD analysis on a node of pillar 4*

7 CONCLUSION AND FURTHER RESEARCH

7.1 Conclusion

This master thesis project sought to investigate damage conditions of the Herøysund bridge through structural design modelling and finite element simulation. The project was accomplished through 3D modelling of Herøysund bridge and numerical simulation of static structural parametric evaluation of fracture mechanics, modal and vibratory analysis. The structure was designed in SolidWorks program considering all the 2D drawings available. Thereafter, numerical simulation of fractures, modal and vibratory parameters like harmonic response, response spectrum and random vibration were executed.

Seven cracks were induced on the structure and their analysis was based on stress intensity factors (SIFS) and strain energy release rate J-integral values. Structural deformation and equivalent stress on the bridge due to loading was also determined. The maximum bridge total deformation was found to be *0.054216m* (*54.216mm*) occurring on main bridge-span 3-5 while the maximum von mises stress was obtained as *61.622 MPa* occurring on load bearing steel plate on pillar 6. The average equivalent stresses obtained were much higher compared to ultimate tensile strength and tensile yield strengths of concrete, which implied high probability of structural failure on Herøysund bridge under the given loading conditions. Furthermore, SIFS and J-integral values were analogized against the fracture toughness (K_{1C}) and critical J-integral (J_C) values of concrete to determine which cracks were likely to propagate. From the analysis, it was ascertained that cracks 2, 4, 5, and 7 had zero probability of propagation while cracks 1, 3 and 6 showed very high probability of propagation. Therefore, a conclusion was drawn that cracks 2, 4, 5 and 7 would not have structural failure effect on Herøysund bridge while cracks 1, 3 and 6 would likely cause structural failure effect on Herøysund bridge due to propagation.

In addition, dynamic response analysis of the bridge was conducted through modal analysis, harmonic response, response spectrum and random vibration to investigate the bridge behavioral response under loading. In modal analysis, flexural, transverse, and torsional deformation mode shapes were generated at varying frequencies. The lowest energy level mode 1 had frequency of *1.4232 Hz* and highest energy level mode 20 with frequency of *11.492 Hz*. Participation factor and effective mass ratios were used to determine the translational and rotational excitation of the modes. The analysis demonstrated significant excitation from flexural mode 5 in *x-axis* direction and transverse mode 2 in *x-axis* rotatation. Flexural modes 7, 1 and 14 had notable contribution in *y-axis* direction and *z-axis* rotation. Similarly, transverse modes 2 and 8 had exceptional excitation in *z-direction* and *y-axis* rotation.

Harmonic response analysis was performed to find the peak response location. The study disclosed that peak response frequency of *1.418Hz* and phase angle of 93.944° produced maximum deformational amplitude of *0.62093m* on bridge span 3-5. The research affirmed main bridge span 3-6 as the peak response location of the bridge. Frequency response velocity and acceleration were equally performed with peak response velocity found to be *5.5395 m/s* at frequency of *1.4232 Hz* while peak response acceleration was *49.60*m/s^2 at frequency of *1.4284Hz*. The peak response frequency of *1.418Hz* also gave maximum stress response of *61.116 MPa* and phase response of 92.935° which was in-phase. The maximum stress response value from harmonic response analysis was almost equal to the above outlined maximum von mises stress of the bridge. Total and directional deformation and equivalent stress on the bridge structure were investigated. Maximum directional and total deformation were experienced on bridge span 3-5 and low on bridge pillars 1 and 7. The maximum and minimum equivalent stresses on the bridge were found to occur on load bearing steel plate on pillar 6 and on bridge span 3-5 respectively.

Further, response spectrum and random vibration analysis of the Herøysund bridge under loading were conducted. In response spectrum analysis, RS acceleration data was used to determine total and directional deformation and directional velocity and acceleration of the bridge. In the analysis total deformation, directional deformation, directional velocity were found to be optimal on main bridge span 3-5 while directional acceleration was high on span 5-6. Maximum equivalent stress was experienced on load bearing steel plate on pillar 6. In random vibration analysis, input power spectral data (PSD) was applied to investigate probable deformation, stresses and strain on the bridge. The 3-sigma (3σ) scale factor values with probability of 99.73% were applied in this analysis. It was deduced that in 99.73% of the time, the directional deformation of the bridge would be greater than zero (0) but would not exceed *1.5298m* in the x-axis direction and *1.9963m* in y-axis direction. Similarly, the equivalent von mises stress on the bridge would be greater than *99.064 KPa* but less than *5.6604 GPa* in x-axis direction. Further, the normal elastic strain of the bridge would be less than *0.10486 m/m* in x-axis, *0.097703 m/m* in y-axis and *0.058174 m/m* in z-axis direction respectively.

To sum up, it was observed that the structural deformations would be highly prevalent in main bridge span 3-6 and minimal on bridge pillars 1 and 7 for all the parameters considered for evaluation. However, for equivalent stresses analysis it was identified that maximum equivalent stresses would be experienced by load bearing steel plates on pillars 2 and 6 and minimal on main bridge span 3-6. In general, the structural deformations would be dominant on the Herøysund bridge top deck where the equivalent stresses would be very dismal. On the other hand, equivalent stresses would be eminent on the Herøysund bridge piers but would be inferior on the bridge deck. The findings affirmed that the Herøysund bridge is at a high risk of structural failure and precautionary measures must be undertaken to avert prospects of adversities.

7.2 Further Research

- This study applied linear analysis method, however further research applying non-linear methods for an in-depth numerical modelling of the bridge could be developed with consideration of non-linear effects caused by friction, post-tensioned tendons, and dynamic loads.

- The study considered only seven (7) major cracks but ignored all the other minor cracks. A dynamic simulation of bridge could be performed with all cracks and corrosions induced.

- This study considered traffic load as static load spread on top of the bridge deck. This may not be effective and further research is proposed based on transient structural analysis with traffic loads and other loading conditions like seismic and wind incorporated.

- Finally, in this master thesis project, tendons were presented as compressive post tensioning forces acting longitudinally on both ends of the bridge span 3-6. The method worked well on the 3D solid model, but its precision could be improved. This study proposes further research on the entire post tensioning system with conduits and cables imbedded on the bridge.

8 REFERENCES

[1] R. Niyirora, W. Ji, E. Masengesho, J. Munyaneza, F. Niyonyungu, and R. Nyirandayisabye, "Intelligent damage diagnosis in bridges using vibration-based monitoring approaches and machine learning: A systematic review," *Results in Engineering*, vol. 16, p. 100761, 2022.

[2] B. Bakht and A. Mufti, *Bridges : Analysis, Design, Structural Health Monitoring, and Rehabilitation*, 2nd ed. 2015. ed. Cham: Springer International Publishing : Imprint: Springer, 2015.

[3] Z. Mišković, S. Al-Wazni, and A. Alalikhan, "Damage detection for civil structural health monitoring application-a case study of the steel grid bridge structural model," *Tehnički vjesnik*, vol. 25, no. Supplement 2, pp. 266-275, 2018.

[4] A. A. Rahman, "Theoretical Model for Damage and Vibration Response in Concrete Bridges," Final Research Report, Faculty of Civil Enigneering, Universiti Teknologi …, 2009.

[5] S. S. Rao, "Mechanical vibrations fifth edition," ed, 2011.

[6] F. Fu, *Advanced modelling techniques in structural design*, Chichester, England: Wiley Blackwell, 2015.

[7] S. Karimi and O. Mirza, "Damage identification in bridge structures: review of available methods and case studies," *Australian Journal of Structural Engineering*, vol. 24, no. 2, pp. 89-119, 2023.

[8] W. Fan and P. Qiao, "Vibration-based damage identification methods: a review and comparative study," *Structural health monitoring*, vol. 10, no. 1, pp. 83-111, 2011.

[9] A. C. Neves, "Structural health monitoring of bridges: data-based damage detection method using machine learning," KTH Royal Institute of Technology, 2020.

[10] NTNU. "Herøy FoU Project." https://www.ntnu.edu/kt/research/concrete/projects/heroy-fou (accessed 29 January, 2024).

[11] SINTEF. "Herøysund Bridge." https://www.sintef.no/prosjekter/2022/heroysund-bru/ (accessed 29 January, 2024).

[12] Z. Azad, "Shell-based Finite Element Modeling of Herøysund Bridge," Engineering Design Master thesis, Faculty of Engineering Science and Technology, UiT The Arctic University of Norway, Narvik, Norway, 2023.

[13] L. H. Fredheim, "MULTICONSULT SPESIALINSPEKSJON RAPPORT: 18-1069 HERØYSUND BRU " *STATENS VEGVESEN REGION NORD*, vol. 713789-18-1069-RAP-01, 23 October 2017.

[14] Andreas Karlsson, Erik Boström, and P. Jilderda, "Post-tensioned concrete bridges Inspection manual: R&D program Better Bridge Maintenance 2017-2021," in *NPRA REPORTS-Norwegian Public Roads Administration*: DEKRA Industrial AB TECHNICAL REPORT, 15. mars 2021.

[15] AAS-JAKOBSEN, "BEREGNINGSRAPPORT:18-1069 Herøysund bru. Bæreevneberegninger," *STATENS VEGVESEN RAPPORT*, vol. 12019-03 Herøysund bru, 09.11.2020.

[16] R. Johnsen, "Herøysund bru, korrosjon av etterspent armering: FoU-programmet Bedre Bruvedlikehold 2017-2021 " in *STATENS VEGVESENS RAPPORTER*, SINTEF Ed.: NTNU-Institutt for Maskinteknikk og Produksjon (MTP), 2022.

[17] P. N. Berg, "Beam based Finite element modelling of Herøysund bridge," Engineering Design Master Thesis, Faculty of Engineering Science and Technology, UiT The Arctic University of Norway, Narvik, Norway, 2023.

[18] M. Holmqvist, R. Antonsen, A. Karlsson, and B. Täljsten, "Herøysund bridge Report: Locating voids in grouted tendon ducts with NDT," *DEKRA Industrial AB, Invator AB and Statens Vegvesen*, vol. REPORT: Ref. 7204-R-584522-Ver.1, 2020 February-18.

[19] AAS-JAKOBSEN, "HERØYSUND BRIDGE AUTOCAD 2D DRAWINGS," *STATENS VEGVESEN RAPPORT*, 24.01.2019.

[20] Y. Bai and Z.-D. Xu, *Structural dynamics*, Beverly, MA, USA: Scrivener Publishing: Wiley, 2019.

[21] Y.-B. Yang, C. Lin, and J. Yau, "Extracting bridge frequencies from the dynamic response of a passing vehicle," *Journal of Sound and Vibration*, vol. 272, no. 3-5, pp. 471-493, 2004.

[22] Y. Yang and J. P. Yang, "State-of-the-art review on modal identification and damage detection of bridges by moving test vehicles," *International Journal of Structural Stability and Dynamics*, vol. 18, no. 02, p. 1850025, 2018.

[23] I. Talebinejad, C. Fischer, and F. Ansari, "Numerical evaluation of vibration‐based methods for damage assessment of cable‐stayed bridges," *Computer‐Aided Civil and Infrastructure Engineering*, vol. 26, no. 3, pp. 239-251, 2011.

[24] D. J. R. Michel Geradin, *Mechanical vibrations: theory and application to structural dynamics*, Third edition. ed. New York: New York: Wiley, 2015.

[25] H.-C. Kwon, M.-C. Kim, and I.-W. Lee, "Vibration control of bridges under moving loads," *Computers & structures*, vol. 66, no. 4, pp. 473-480, 1998.

[26] R. B. Carlos Ventura, *Introduction to Operational Modal Analysis*, 1 ed. Newark: Newark: Wiley, 2015.

[27] P. Cawley and R. D. Adams, "The location of defects in structures from measurements of natural frequencies," *The Journal of Strain Analysis for Engineering Design*, vol. 14, no. 2, pp. 49-57, 1979.

[28] J. He and Z.-F. Fu, *Modal analysis*, Oxford ;,Boston: Butterworth-Heinemann, 2001.

[29] EN, "1992-1-1 (English): Eurocode 2: Design of concrete structures - Part 1-1: General rules and rules for buildings [Authority: The European Union Per Regulation 305/2011, Directive 98/34/EC, Directive 2004/18/EC]" 2004. [Online].

Available: https://www.phd.eng.br/wp-content/uploads/2015/12/en.1992.1.1.2004.pdf.

[30] Eurocode2:, "Design of concrete structures | Eurocodes: Building the future'." [Online]. Available: https://eurocodes.jrc.ec.europa.eu/EN-Eurocodes/eurocode-2-design-concrete-structures.

[31] En and BS, "1-1. Eurocode 2: Design of concrete structures–Part 1-1: General rules and rules for buildings," *European Committee for Standardization (CEN)*, 2004.

[32] V. Molotnikov and A. Molotnikova, *Theory of Elasticity and Plasticity: A Textbook of Solid Body Mechanics*, 1st Edition 2021 ed. Cham: Cham: Springer International Publishing AG, 2021.

[33] T. G. Sitharam and L. Govindaraju, *Theory of elasticity*, Singapore: Springer, 2021.

[34] J. J. Ågotnes, "Analytical Approach to Describe Properties in Transition Zones Between Ballasted and Non-Ballasted Track: Analytical Solution to a Beam Resting on a Spring and Damped Foundation with a Moving Load," master Master, Faculty of Engineering Science and Technology, UiT the Arctic University of Norway, Narvik, May 2022.

[35] A. Maceri, *Theory of Elasticity*, 1st ed. 2010. ed. Berlin, Heidelberg: Springer Berlin Heidelberg : Imprint: Springer, 2010.

[36] C. T. Sun and Z. H. Jin, *Fracture mechanics*, Waltham, Mass.: Butterworth-Heinemann/Elsevier, 2012.

[37] M. F. Ashby, *Materials selection in mechanical design, fourth edition*, 4th ed. ed. Burlington, Mass,Amsterdam,Boston: Burlington, Mass: Butterworth-Heinemann, 2011.

[38] M. Moatamedi and H. A. Khawaja, *Finite Element Analysis*, First edition. ed. Boca Raton, FL: CRC Press, 2018.

[39] Q. Gao, Z. Wang, B. Guo, and C. Chen, "Dynamic responses of simply supported girder bridges to moving vehicular loads based on mathematical methods," *Mathematical Problems in Engineering*, vol. 2014, 2014.

[40] D. P. Miannay, *Fracture Mechanics*, 1st ed. 1998. ed. New York, NY: Springer New York : Imprint: Springer, 1998.

[41] N. Perez, *Fracture Mechanics*, 2nd ed. 2017. ed. Cham: Springer International Publishing : Imprint: Springer, 2017.

[42] A. T. Zehnder, *Fracture Mechanics*, 1st ed. 2012. ed. Dordrecht: Springer Netherlands : Imprint: Springer, 2012.

[43] STATENSVEGVESEN, "Herøysund bru: Vedlegg E NovaFrame analysis document."

9 APPENDICES

9.1 Appendix A: Mesh Details

- Mesh
  - Body Sizing
  - Automatic Method
  - Edge Sizing
  - Edge Sizing 2
  - Body Sizing 2
  - Automatic Method 2
  - Body Sizing 3
  - Automatic Method 3
  - Edge Sizing 3
  - Edge Sizing 4
  - Body Sizing 4
  - Automatic Method 4
  - Edge Sizing 5
  - Face Sizing 3
  - Face Sizing 4
  - Automatic Method 5
  - Edge Sizing 6
  - Body Sizing 5
  - Automatic Method 6
  - Edge Sizing 7
  - Body Sizing 6
  - Automatic Method 7
  - Body Sizing 7
  - Automatic Method 8
  - Body Sizing 8
  - Automatic Method 9
  - Edge Sizing 8
  - Edge Sizing 9
  - Face Sizing 7
  - Body Sizing 9
  - Automatic Method 10
  - Edge Sizing 10
  - Body Sizing 10
  - Automatic Method 11

Details of "Mesh"

Display	
Display Style	Use Geometry Setting
Defaults	
Physics Preference	Mechanical
Element Order	Quadratic
Element Size	1.0 m
Sizing	
Use Adaptive Sizing	No
Growth Rate	2.0
Max Size	3.0 m
Mesh Defeaturing	Yes
Defeature Size	1.e-002 m
Capture Curvature	Yes
Curvature Min Size	1.e-002 m
Curvature Normal Angle	Default (70.395°)
Capture Proximity	No
Bounding Box Diagonal	161.84 m
Average Surface Area	8.4675 m²
Minimum Edge Length	1.1511e-004 m
Quality	
Check Mesh Quality	Yes, Errors
Error Limits	Aggressive Mechanical
Target Element Quality	Default (5.e-002)
Smoothing	Medium
Mesh Metric	None
Inflation	
Advanced	
Statistics	
Nodes	59243
Elements	31988
Show Detailed Statistics	No

9.2 Appendix B: Details of Cracks

Coordinate system details of cracks

Details of "Coordinate System_Crack 1"

Definition	
Type	Cartesian
Coordinate System	Program Controlled
APDL Name	
Suppressed	No
Origin	
Define By	Geometry Selection
Geometry	Click to Change
Origin X	-1.2889 m
Origin Y	2.8547 m
Origin Z	5.7269 m
Principal Axis	
Axis	X
Define By	Global X Axis
Orientation About Principal Axis	
Axis	Y
Define By	Default
Directional Vectors	
X Axis Data	[0. -1. 0.]
Y Axis Data	[1. 0. 0.]
Z Axis Data	[0. 0. 1.]
Transfer Properties	
Source	
Read Only	No
Transformations	
Base Configuration	Absolute
Rotate Z	-90. °
Offset X	-3.e-002 m
Transformed Configuration	[-1.2889 2.8847 5.7269]

Details of "Coordinate System_Crack 2"

Definition	
Type	Cartesian
Coordinate System	Program Controlled
APDL Name	
Suppressed	No
Origin	
Define By	Geometry Selection
Geometry	Click to Change
Origin X	-22.168 m
Origin Y	1.1168 m
Origin Z	5.0549 m
Principal Axis	
Axis	X
Define By	Global X Axis
Orientation About Principal Axis	
Axis	Y
Define By	Default
Directional Vectors	
X Axis Data	[0. 0. -1.]
Y Axis Data	[1. 0. 0.]
Z Axis Data	[0. -1. 0.]
Transfer Properties	
Source	
Read Only	No
Transformations	
Base Configuration	Absolute
Rotate Y	90. °
Rotate X	90. °
Offset X	-1.e-002 m
Transformed Configuration	[-22.168 1.1168 5.0649]

Details of "Coordinate System_Crack 3"

Definition	
Type	Cartesian
Coordinate System	Program Controlled
APDL Name	
Suppressed	No
Origin	
Define By	Geometry Selection
Geometry	Click to Change
Origin X	-27.034 m
Origin Y	4.8065 m
Origin Z	1.6519 m
Principal Axis	
Axis	X
Define By	Global X Axis
Orientation About Principal Axis	
Axis	Y
Define By	Default
Directional Vectors	
X Axis Data	[0. 0. 1.]
Y Axis Data	[-1. 0. 0.]
Z Axis Data	[0. -1. 0.]
Transfer Properties	
Source	
Read Only	No
Transformations	
Base Configuration	Absolute
Rotate Y	-90. °
Rotate X	90. °
Offset X	-0.1 m
Transformed Configuration	[-27.034 4.8065 1.5519]

Details of "Coordinate System_Crack 4"

Definition	
Type	Cartesian
Coordinate System	Program Controlled
APDL Name	
Suppressed	No
Origin	
Define By	Geometry Selection
Geometry	Click to Change
Origin X	-53.16 m
Origin Y	-8.3207 m
Origin Z	3.4033 m
Principal Axis	
Axis	X
Define By	Global X Axis
Orientation About Principal Axis	
Axis	Y
Define By	Default
Directional Vectors	
X Axis Data	[1. 0. 0.]
Y Axis Data	[0. 0. -1.]
Z Axis Data	[0. 1. 0.]
Transfer Properties	
Source	
Read Only	No
Transformations	
Base Configuration	Absolute
Rotate X	-90. °
Offset X	-1.e-002 m
Transformed Configuration	[-53.17 -8.3207 3.4033]

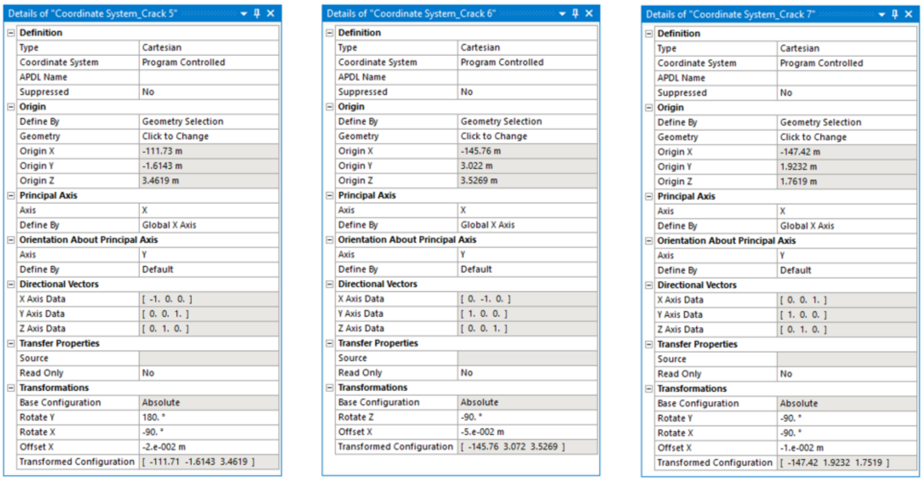

Details of "Coordinate System_Crack 5"	
Definition	
Type	Cartesian
Coordinate System	Program Controlled
APDL Name	
Suppressed	No
Origin	
Define By	Geometry Selection
Geometry	Click to Change
Origin X	-111.73 m
Origin Y	-1.6143 m
Origin Z	3.4619 m
Principal Axis	
Axis	X
Define By	Global X Axis
Orientation About Principal Axis	
Axis	Y
Define By	Default
Directional Vectors	
X Axis Data	[-1. 0. 0.]
Y Axis Data	[0. 0. 1.]
Z Axis Data	[0. 1. 0.]
Transfer Properties	
Source	
Read Only	No
Transformations	
Base Configuration	Absolute
Rotate Y	180. °
Rotate X	-90. °
Offset X	-2.e-002 m
Transformed Configuration	[-111.71 -1.6143 3.4619]

Details of "Coordinate System_Crack 6"	
Definition	
Type	Cartesian
Coordinate System	Program Controlled
APDL Name	
Suppressed	No
Origin	
Define By	Geometry Selection
Geometry	Click to Change
Origin X	-145.76 m
Origin Y	3.022 m
Origin Z	3.5269 m
Principal Axis	
Axis	X
Define By	Global X Axis
Orientation About Principal Axis	
Axis	Y
Define By	Default
Directional Vectors	
X Axis Data	[0. -1. 0.]
Y Axis Data	[1. 0. 0.]
Z Axis Data	[0. 0. 1.]
Transfer Properties	
Source	
Read Only	No
Transformations	
Base Configuration	Absolute
Rotate Z	-90. °
Offset X	-5.e-002 m
Transformed Configuration	[-145.76 3.072 3.5269]

Details of "Coordinate System_Crack 7"	
Definition	
Type	Cartesian
Coordinate System	Program Controlled
APDL Name	
Suppressed	No
Origin	
Define By	Geometry Selection
Geometry	Click to Change
Origin X	-147.42 m
Origin Y	1.9232 m
Origin Z	1.7619 m
Principal Axis	
Axis	X
Define By	Global X Axis
Orientation About Principal Axis	
Axis	Y
Define By	Default
Directional Vectors	
X Axis Data	[0. 0. 1.]
Y Axis Data	[1. 0. 0.]
Z Axis Data	[0. 1. 0.]
Transfer Properties	
Source	
Read Only	No
Transformations	
Base Configuration	Absolute
Rotate Y	-90. °
Rotate X	-90. °
Offset X	-1.e-002 m
Transformed Configuration	[-147.42 1.9232 1.7519]

Pre-meshed cracks set up details

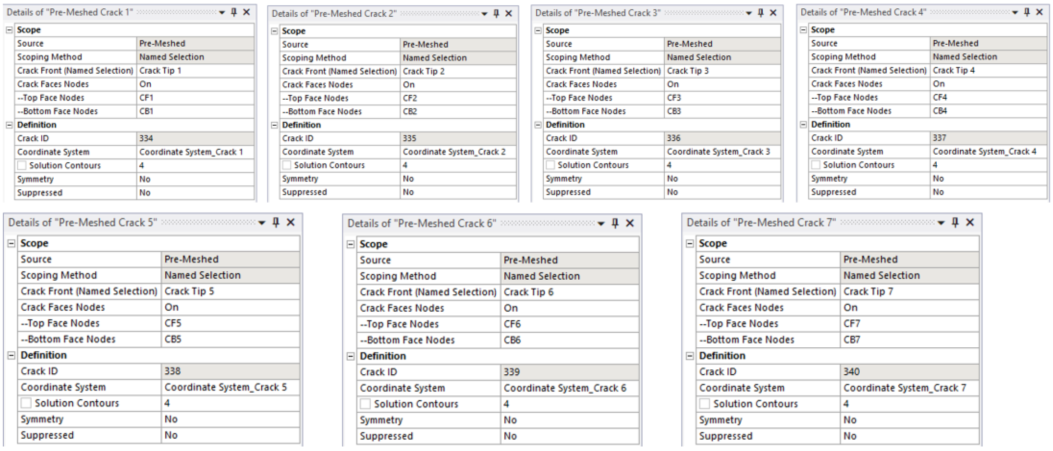

	Details of "Pre-Meshed Crack 1"	Details of "Pre-Meshed Crack 2"	Details of "Pre-Meshed Crack 3"	Details of "Pre-Meshed Crack 4"	Details of "Pre-Meshed Crack 5"	Details of "Pre-Meshed Crack 6"	Details of "Pre-Meshed Crack 7"
Scope							
Source	Pre-Meshed	Pre-Meshed	Pre-Meshed	Pre-Meshed	Pre-Meshed	Pre-Meshed	Pre-Meshed
Scoping Method	Named Selection	Named Selection	Named Selection	Named Selection	Named Selection	Named Selection	Named Selection
Crack Front (Named Selection)	Crack Tip 1	Crack Tip 2	Crack Tip 3	Crack Tip 4	Crack Tip 5	Crack Tip 6	Crack Tip 7
Crack Faces Nodes	On	On	On	On	On	On	On
--Top Face Nodes	CF1	CF2	CF3	CF4	CF5	CF6	CF7
--Bottom Face Nodes	CB1	CB2	CB3	CB4	CB5	CB6	CB7
Definition							
Crack ID	334	335	336	337	338	339	340
Coordinate System	Coordinate System_Crack 1	Coordinate System_Crack 2	Coordinate System_Crack 3	Coordinate System_Crack 4	Coordinate System_Crack 5	Coordinate System_Crack 6	Coordinate System_Crack 7
Solution Contours	4	4	4	4	4	4	4
Symmetry	No	No	No	No	No	No	No
Suppressed	No	No	No	No	No	No	No

Numerical Modelling Project Set Up

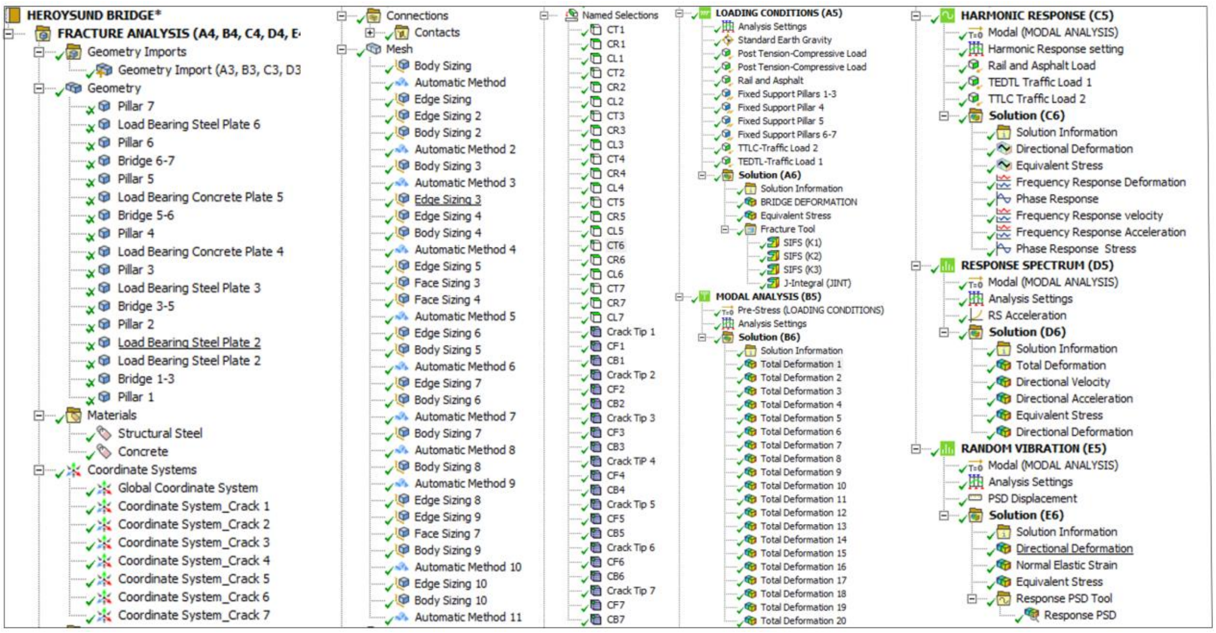

9.3 Appendix C: Fracture Analysis Results

Maximum and Minimum SIF and J-integral Values

CRACK 1

Details of "SIFS (K1)"	
Definition	
Type	SIFS
Subtype	K1
Contour Start	1
Contour End	4
Active Contour	Last
By	Time
Display Time	Last
Separate Data by Entity	No
Calculate Time History	Yes
Suppressed	No
Results	
Minimum	-7.6233e+005 Pa·m^(0.5)
Maximum	-6.7578e+005 Pa·m^(0.5)
Minimum Occurs On	Bridge 1-3
Maximum Occurs On	Bridge 1-3

Details of "SIFS (K2)"	
Definition	
Type	SIFS
Subtype	K2
Contour Start	1
Contour End	4
Active Contour	Last
By	Time
Display Time	Last
Separate Data by Entity	No
Calculate Time History	Yes
Suppressed	No
Results	
Minimum	-1.0597e+005 Pa·m^(0.5)
Maximum	-37333 Pa·m^(0.5)
Minimum Occurs On	Bridge 1-3
Maximum Occurs On	Bridge 1-3

Details of "SIFS (K3)"	
Definition	
Type	SIFS
Subtype	K3
Contour Start	1
Contour End	4
Active Contour	Last
By	Time
Display Time	Last
Separate Data by Entity	No
Calculate Time History	Yes
Suppressed	No
Results	
Minimum	3688.6 Pa·m^(0.5)
Maximum	27031 Pa·m^(0.5)
Minimum Occurs On	Bridge 1-3
Maximum Occurs On	Bridge 1-3

Details of "J-Integral (JINT)"	
Definition	
Type	J-Integral (JINT)
Contour Start	1
Contour End	4
Active Contour	Last
By	Time
Display Time	Last
Separate Data by Entity	No
Calculate Time History	Yes
Suppressed	No
Results	
Minimum	-6.4919 J/m^2
Maximum	22.565 J/m^2
Minimum Occurs On	Bridge 1-3
Maximum Occurs On	Bridge 1-3

CRACK 2

Details of "SIFS (K1)"	
Definition	
Type	SIFS
Subtype	K1
Contour Start	1
Contour End	4
Active Contour	Last
By	Time
Display Time	Last
Separate Data by Entity	No
Calculate Time History	Yes
Suppressed	No
Results	
Minimum	1797.6 Pa·m^(0.5)
Maximum	8307.4 Pa·m^(0.5)
Minimum Occurs On	Pillar 3
Maximum Occurs On	Pillar 3

Details of "SIFS (K2)"	
Definition	
Type	SIFS
Subtype	K2
Contour Start	1
Contour End	4
Active Contour	Last
By	Time
Display Time	Last
Separate Data by Entity	No
Calculate Time History	Yes
Suppressed	No
Results	
Minimum	158.3 Pa·m^(0.5)
Maximum	1430.7 Pa·m^(0.5)
Minimum Occurs On	Pillar 3
Maximum Occurs On	Pillar 3

Details of "SIFS (K3)"	
Definition	
Type	SIFS
Subtype	K3
Contour Start	1
Contour End	4
Active Contour	Last
By	Time
Display Time	Last
Separate Data by Entity	No
Calculate Time History	Yes
Suppressed	No
Results	
Minimum	-5385.7 Pa·m^(0.5)
Maximum	-3257.6 Pa·m^(0.5)
Minimum Occurs On	Pillar 3
Maximum Occurs On	Pillar 3

Details of "J-Integral (JINT)"	
Definition	
Type	J-Integral (JINT)
Contour Start	1
Contour End	4
Active Contour	Last
By	Time
Display Time	Last
Separate Data by Entity	No
Calculate Time History	Yes
Suppressed	No
Results	
Minimum	-2.6034e-002 J/m^2
Maximum	0.27816 J/m^2
Minimum Occurs On	Pillar 3
Maximum Occurs On	Pillar 3

CRACK 3

Details of "SIFS (K1)"	
Definition	
Type	SIFS
Subtype	K1
Contour Start	1
Contour End	4
Active Contour	Last
By	Time
Display Time	Last
Separate Data by Entity	No
Calculate Time History	Yes
Suppressed	No
Results	
Minimum	-1.4459e+006 Pa·m^(0.5)
Maximum	-1.2225e+006 Pa·m^(0.5)
Minimum Occurs On	Bridge 3-5
Maximum Occurs On	Bridge 3-5

Details of "SIFS (K2)"	
Definition	
Type	SIFS
Subtype	K2
Contour Start	1
Contour End	4
Active Contour	Last
By	Time
Display Time	Last
Separate Data by Entity	No
Calculate Time History	Yes
Suppressed	No
Results	
Minimum	3.9329e+005 Pa·m^(0.5)
Maximum	4.5158e+005 Pa·m^(0.5)
Minimum Occurs On	Bridge 3-5
Maximum Occurs On	Bridge 3-5

Details of "SIFS (K3)"	
Definition	
Type	SIFS
Subtype	K3
Contour Start	1
Contour End	4
Active Contour	Last
By	Time
Display Time	Last
Separate Data by Entity	No
Calculate Time History	Yes
Suppressed	No
Results	
Minimum	-38891 Pa·m^(0.5)
Maximum	72796 Pa·m^(0.5)
Minimum Occurs On	Bridge 3-5
Maximum Occurs On	Bridge 3-5

Details of "J-Integral (JINT)"	
Definition	
Type	J-Integral (JINT)
Contour Start	1
Contour End	4
Active Contour	Last
By	Time
Display Time	Last
Separate Data by Entity	No
Calculate Time History	Yes
Suppressed	No
Results	
Minimum	45.169 J/m^2
Maximum	83.936 J/m^2
Minimum Occurs On	Bridge 3-5
Maximum Occurs On	Bridge 3-5

CRACK 4

Details of "SIFS (K1)"	
Definition	
Type	SIFS
Subtype	K1
Contour Start	1
Contour End	4
Active Contour	Last
By	Time
Display Time	Last
Separate Data by Entity	No
Calculate Time History	Yes
Suppressed	No
Results	
Minimum	-13095 Pa·m^(0.5)
Maximum	-3789. Pa·m^(0.5)
Minimum Occurs On	Pillar 4
Maximum Occurs On	Pillar 4

Details of "SIFS (K2)"	
Definition	
Type	SIFS
Subtype	K2
Contour Start	1
Contour End	4
Active Contour	Last
By	Time
Display Time	Last
Separate Data by Entity	No
Calculate Time History	Yes
Suppressed	No
Results	
Minimum	-24.031 Pa·m^(0.5)
Maximum	299.41 Pa·m^(0.5)
Minimum Occurs On	Pillar 4
Maximum Occurs On	Pillar 4

Details of "SIFS (K3)"	
Definition	
Type	SIFS
Subtype	K3
Contour Start	1
Contour End	4
Active Contour	Last
By	Time
Display Time	Last
Separate Data by Entity	No
Calculate Time History	Yes
Suppressed	No
Results	
Minimum	-439.19 Pa·m^(0.5)
Maximum	275.59 Pa·m^(0.5)
Minimum Occurs On	Pillar 4
Maximum Occurs On	Pillar 4

Details of "J-Integral (JINT)"	
Definition	
Type	J-Integral (JINT)
Contour Start	1
Contour End	4
Active Contour	Last
By	Time
Display Time	Last
Separate Data by Entity	No
Calculate Time History	Yes
Suppressed	No
Results	
Minimum	1.8075e-004 J/m^2
Maximum	7.5869e-003 J/m^2
Minimum Occurs On	Pillar 4
Maximum Occurs On	Pillar 4

CRACK 5

Details of "SIFS (K1)"	
Definition	
Type	SIFS
Subtype	K1
Contour Start	1
Contour End	4
Active Contour	Last
By	Time
Display Time	Last
Separate Data by Entity	No
Calculate Time History	Yes
Suppressed	No
Results	
Minimum	-8.4024 Pa·m^(0.5)
Maximum	4743.9 Pa·m^(0.5)
Minimum Occurs On	Pillar 5
Maximum Occurs On	Pillar 5

Details of "SIFS (K2)"	
Definition	
Type	SIFS
Subtype	K2
Contour Start	1
Contour End	4
Active Contour	Last
By	Time
Display Time	Last
Separate Data by Entity	No
Calculate Time History	Yes
Suppressed	No
Results	
Minimum	-353.38 Pa·m^(0.5)
Maximum	21.61 Pa·m^(0.5)
Minimum Occurs On	Pillar 5
Maximum Occurs On	Pillar 5

Details of "SIFS (K3)"	
Definition	
Type	SIFS
Subtype	K3
Contour Start	1
Contour End	4
Active Contour	Last
By	Time
Display Time	Last
Separate Data by Entity	No
Calculate Time History	Yes
Suppressed	No
Results	
Minimum	-84.997 Pa·m^(0.5)
Maximum	2798.4 Pa·m^(0.5)
Minimum Occurs On	Pillar 5
Maximum Occurs On	Pillar 5

Details of "J-Integral (JINT)"	
Definition	
Type	J-Integral (JINT)
Contour Start	1
Contour End	4
Active Contour	Last
By	Time
Display Time	Last
Separate Data by Entity	No
Calculate Time History	Yes
Suppressed	No
Results	
Minimum	-0.4511 J/m^2
Maximum	0.483 J/m^2
Minimum Occurs On	Pillar 5
Maximum Occurs On	Pillar 5

CRACK 6

	Details of "SIFS (K1)"	Details of "SIFS (K2)"	Details of "SIFS (K3)"	Details of "J-Integral (JINT)"
Definition				
Type	SIFS	SIFS	SIFS	J-Integral (JINT)
Subtype	K1	K2	K3	
Contour Start	1	1	1	1
Contour End	4	4	4	4
Active Contour	Last	Last	Last	Last
By	Time	Time	Time	Time
Display Time	Last	Last	Last	Last
Separate Data by Entity	No	No	No	No
Calculate Time History	Yes	Yes	Yes	Yes
Suppressed	No	No	No	No
Results				
Minimum	1.7472e+005 Pa·m^(0.5)	-2.4516e+005 Pa·m^(0.5)	-1.6415e+005 Pa·m^(0.5)	-5.4713 J/m²
Maximum	8.6181e+005 Pa·m^(0.5)	-76548 Pa·m^(0.5)	1.7792e+005 Pa·m^(0.5)	22.203 J/m²
Minimum Occurs On	Bridge 6-7	Bridge 6-7	Bridge 6-7	Bridge 6-7
Maximum Occurs On	Bridge 6-7	Bridge 6-7	Bridge 6-7	Bridge 6-7

CRACK 7

	Details of "SIFS (K1)"	Details of "SIFS (K2)"	Details of "SIFS (K3)"	Details of "J-Integral (JINT)"
Definition				
Type	SIFS	SIFS	SIFS	J-Integral (JINT)
Subtype	K1	K2	K3	
Contour Start	1	1	1	1
Contour End	4	4	4	4
Active Contour	Last	Last	Last	Last
By	Time	Time	Time	Time
Display Time	Last	Last	Last	Last
Separate Data by Entity	No	No	No	No
Calculate Time History	Yes	Yes	Yes	Yes
Suppressed	No	No	No	No
Results				
Minimum	1.0798e+005 Pa·m^(0.5)	-5175.4 Pa·m^(0.5)	20925 Pa·m^(0.5)	-0.12156 J/m²
Maximum	1.7243e+005 Pa·m^(0.5)	4979.2 Pa·m^(0.5)	65012 Pa·m^(0.5)	0.82119 J/m²
Minimum Occurs On	Bridge 6-7	Bridge 6-7	Bridge 6-7	Bridge 6-7
Maximum Occurs On	Bridge 6-7	Bridge 6-7	Bridge 6-7	Bridge 6-7

ALL CRACKS

	Details of "SIFS (K1)"	Details of "SIFS (K2)"	Details of "SIFS (K3)"	Details of "J-Integral (JINT)"
Definition				
Type	SIFS	SIFS	SIFS	J-Integral (JINT)
Subtype	K1	K2	K3	
Active Contour	Last	Last	Last	Last
By	Time	Time	Time	Time
Display Time	Last	Last	Last	Last
Separate Data by Entity	No	No	No	No
Calculate Time History	Yes	Yes	Yes	Yes
Suppressed	No	No	No	No
Results				
Minimum	-1.4459e+006 Pa·m^(0.5)	-2.4516e+005 Pa·m^(0.5)	-1.6415e+005 Pa·m^(0.5)	-6.4919 J/m²
Maximum	8.6181e+005 Pa·m^(0.5)	4.5158e+005 Pa·m^(0.5)	1.7792e+005 Pa·m^(0.5)	83.936 J/m²
Minimum Occurs On	Bridge 3-5	Bridge 6-7	Bridge 6-7	Bridge 1-3
Maximum Occurs On	Bridge 6-7	Bridge 3-5	Bridge 6-7	Bridge 3-5
Tabular and Graph Display				
Crack Selection	Pre-Meshed Crack 1	Pre-Meshed Crack 1	Pre-Meshed Crack 1	Pre-Meshed Crack 1

Crack 1 – Stress intensity factors

Crack 1 – SIF, K1

Tabular Data

	Length [m]	SIFS (K1) Contour 1 [Pa·m^(0.5)]	SIFS (K1) Contour 2 [Pa·m^(0.5)]	SIFS (K1) Contour 3 [Pa·m^(0.5)]	SIFS (K1) Contour 4 [Pa·m^(0.5)]
1	0.	-6.1491e+005	-6.6795e+005	-6.8059e+005	-6.9293e+005
2	9.5153e-003	-6.1491e+005	-6.6795e+005	-6.8059e+005	-6.9293e+005
3	1.9031e-002	-6.2348e+005	-6.7476e+005	-6.8849e+005	-6.9633e+005
4	3.7929e-002	-6.2886e+005	-6.8157e+005	-6.9503e+005	-6.9893e+005
5	5.6827e-002	-6.3424e+005	-6.8838e+005	-7.0158e+005	-7.0153e+005
6	8.778e-002	-6.3982e+005	-6.9667e+005	-7.0691e+005	-7.0521e+005
7	0.11873	-6.454e+005	-7.0496e+005	-7.1225e+005	-7.0889e+005
8	0.15202	-6.5757e+005	-7.197e+005	-7.2349e+005	-7.205e+005
9	0.18531	-6.6975e+005	-7.3445e+005	-7.3473e+005	-7.321e+005
10	0.22014	-6.8205e+005	-7.4793e+005	-7.4608e+005	-7.4456e+005
11	0.25497	-6.9436e+005	-7.6141e+005	-7.5742e+005	-7.5702e+005
12	0.2898	-7.0072e+005	-7.6406e+005	-7.5919e+005	-7.5967e+005
13	0.32463	-7.0708e+005	-7.6671e+005	-7.6095e+005	-7.6233e+005
14	0.35946	-7.1122e+005	-7.6517e+005	-7.5827e+005	-7.6032e+005
15	0.39429	-7.1536e+005	-7.6363e+005	-7.5558e+005	-7.583e+005
16	0.42912	-7.1989e+005	-7.6467e+005	-7.5593e+005	-7.5816e+005
17	0.46395	-7.2441e+005	-7.6572e+005	-7.5628e+005	-7.5801e+005
18	0.49878	-7.1992e+005	-7.6014e+005	-7.5266e+005	-7.5277e+005
19	0.53361	-7.1542e+005	-7.5457e+005	-7.4904e+005	-7.4753e+005
20	0.56537	-6.9806e+005	-7.377e+005	-7.3545e+005	-7.3253e+005
21	0.59712	-6.8069e+005	-7.2083e+005	-7.2186e+005	-7.1752e+005
22	0.61476	-6.646e+005	-7.0543e+005	-7.0876e+005	-7.0361e+005
23	0.63239	-6.485e+005	-6.9004e+005	-6.9566e+005	-6.8969e+005
24	0.6412	-6.324e+005	-6.7465e+005	-6.8256e+005	-6.7578e+005
25	0.65	-6.324e+005	-6.7465e+005	-6.8256e+005	-6.7578e+005

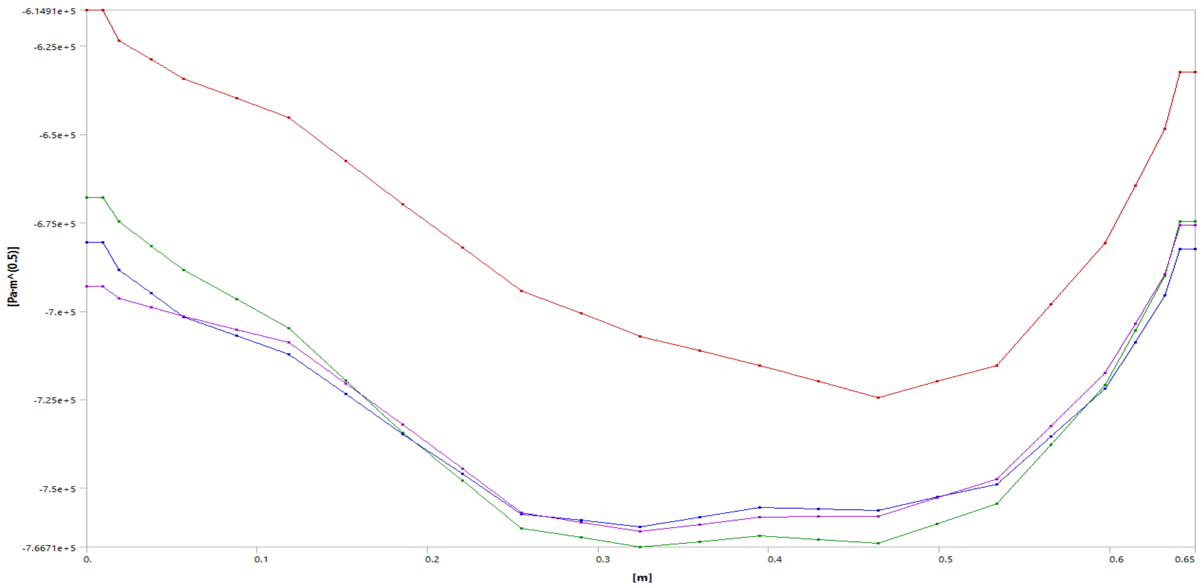

Crack 1 – SIF, K2

Tabular Data

	Length [m]	SIFS (K2) Contour 1 [Pa·m^(0.5)]	SIFS (K2) Contour 2 [Pa·m^(0.5)]	SIFS (K2) Contour 3 [Pa·m^(0.5)]	SIFS (K2) Contour 4 [Pa·m^(0.5)]
1	0.	-62626	-53376	-53980	-48227
2	9.5153e-003	-62626	-53376	-53980	-48227
3	1.9031e-002	-60634	-51260	-49578	-44688
4	3.7929e-002	-58871	-49042	-45270	-41011
5	5.6827e-002	-57109	-46824	-40961	-37333
6	8.778e-002	-57421	-46387	-41110	-37709
7	0.11873	-57733	-45950	-41259	-38086
8	0.15202	-59356	-47960	-45680	-41793
9	0.18531	-60978	-49970	-50102	-45500
10	0.22014	-61764	-53219	-54971	-49340
11	0.25497	-62550	-56467	-59841	-53180
12	0.2898	-62025	-58353	-61434	-55127
13	0.32463	-61499	-60238	-63027	-57074
14	0.35946	-64019	-64134	-65846	-60910
15	0.39429	-66539	-68030	-68666	-64747
16	0.42912	-72601	-79090	-79475	-75999
17	0.46395	-78663	-90151	-90285	-87251
18	0.49878	-80832	-1.0129e+005	-99807	-96612
19	0.53361	-83000	-1.1243e+005	-1.0933e+005	-1.0597e+005
20	0.56537	-80719	-1.1472e+005	-1.075e+005	-1.0334e+005
21	0.59712	-78438	-1.1702e+005	-1.0567e+005	-1.007e+005
22	0.61476	-76378	-1.1504e+005	-1.0015e+005	-94343
23	0.63239	-74318	-1.1306e+005	-94624	-87983
24	0.6412	-72258	-1.1108e+005	-89102	-81624
25	0.65	-72258	-1.1108e+005	-89102	-81624

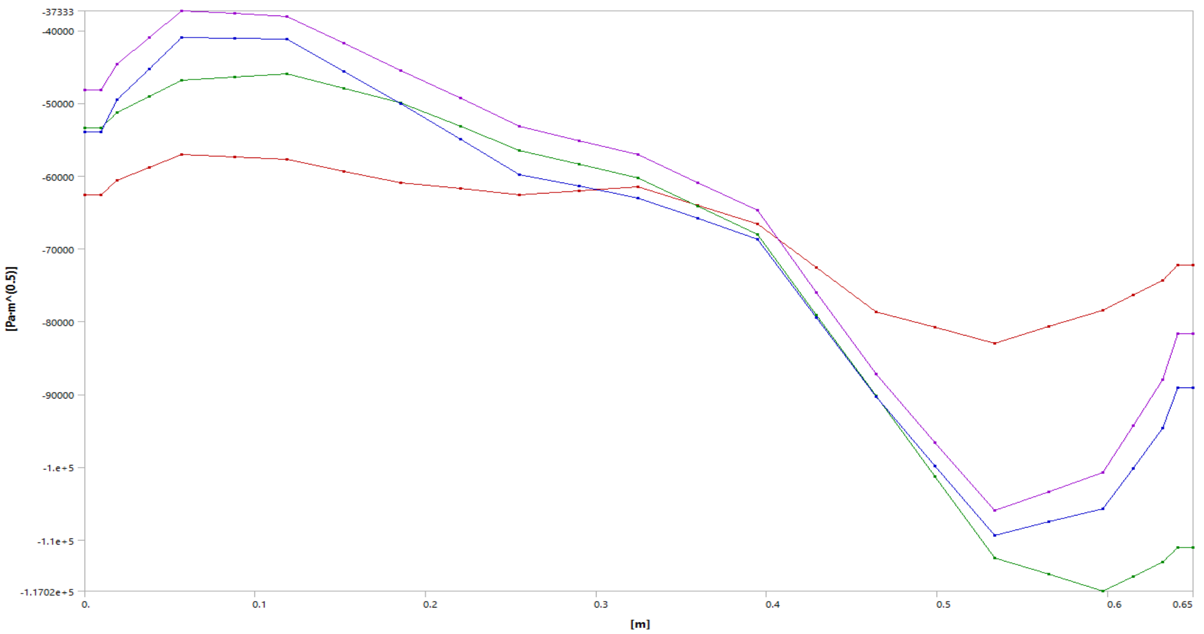

Crack 1 – SIF, K3

Tabular Data

	Length [m]	SIFS (K3) Contour 1 [Pa·m^(0.5)]	SIFS (K3) Contour 2 [Pa·m^(0.5)]	SIFS (K3) Contour 3 [Pa·m^(0.5)]	SIFS (K3) Contour 4 [Pa·m^(0.5)]
1	0.	16288	21895	20483	27031
2	9.5153e-003	16288	21895	20483	27031
3	1.9031e-002	17180	21226	19553	24817
4	3.7929e-002	18171	20862	19121	23124
5	5.6827e-002	19161	20499	18689	21432
6	8.778e-002	19536	20349	18786	20564
7	0.11873	19910	20199	18882	19697
8	0.15202	19438	19578	18880	19258
9	0.18531	18965	18957	18878	18818
10	0.22014	18435	18328	18771	18741
11	0.25497	17905	17700	18665	18664
12	0.2898	17458	17250	18266	18287
13	0.32463	17011	16799	17867	17910
14	0.35946	16266	16040	16965	16950
15	0.39429	15521	15281	16064	15990
16	0.42912	14733	14528	15244	15094
17	0.46395	13945	13775	14424	14198
18	0.49878	12732	12583	13239	13050
19	0.53361	11518	11391	12054	11901
20	0.56537	9856.6	9553.7	9970.4	10070
21	0.59712	8195.4	7716.5	7886.8	8239.9
22	0.61476	6976.7	6302.1	6114.5	6722.8
23	0.63239	5758.	4887.7	4342.2	5205.7
24	0.6412	4539.2	3473.2	2569.9	3688.6
25	0.65	4539.2	3473.2	2569.9	3688.6

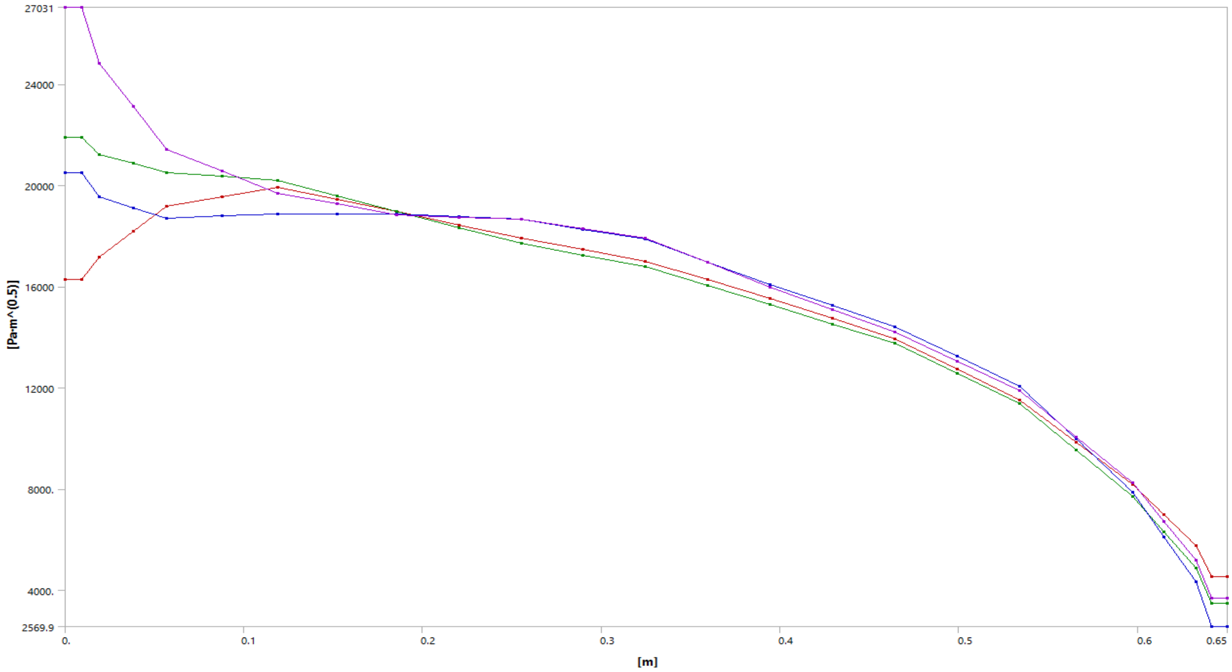

Crack 1 – J-Integral

Tabular Data

	Length [m]	J-Integral (JINT) Contour 1 $[J/m^2]$	J-Integral (JINT) Contour 2 $[J/m^2]$	J-Integral (JINT) Contour 3 $[J/m^2]$	J-Integral (JINT) Contour 4 $[J/m^2]$
1	0.	4.5684	8.5242	10.631	7.6001
2	9.5153e-003	4.5684	8.5242	10.631	7.6001
3	1.9031e-002	4.8663	9.8956	10.988	8.6816
4	3.7929e-002	4.2707	10.478	10.406	8.2936
5	5.6827e-002	3.6752	11.06	9.8245	7.9056
6	8.778e-002	3.0117	11.347	10.04	8.0633
7	0.11873	2.3483	11.634	10.256	8.2211
8	0.15202	2.6175	13.623	12.985	10.644
9	0.18531	2.8866	15.612	15.715	13.066
10	0.22014	3.4859	17.881	18.217	15.344
11	0.25497	4.0851	20.151	20.72	17.621
12	0.2898	4.5763	21.26	21.145	18.685
13	0.32463	5.0676	22.369	21.57	19.748
14	0.35946	6.3663	23.357	21.855	20.726
15	0.39429	7.665	24.345	22.141	21.704
16	0.42912	9.5997	24.92	22.634	22.135
17	0.46395	11.534	25.495	23.128	22.565
18	0.49878	11.362	23.893	21.126	20.298
19	0.53361	11.189	22.292	19.124	18.031
20	0.56537	8.2417	18.396	13.999	12.765
21	0.59712	5.2948	14.501	8.8739	7.4997
22	0.61476	2.4906	11.049	4.312	2.8358
23	0.63239	-0.31364	7.5972	-0.24985	-1.828
24	0.6412	-3.1178	4.1452	-4.8117	-6.4919
25	0.65	-3.1178	4.1452	-4.8117	-6.4919

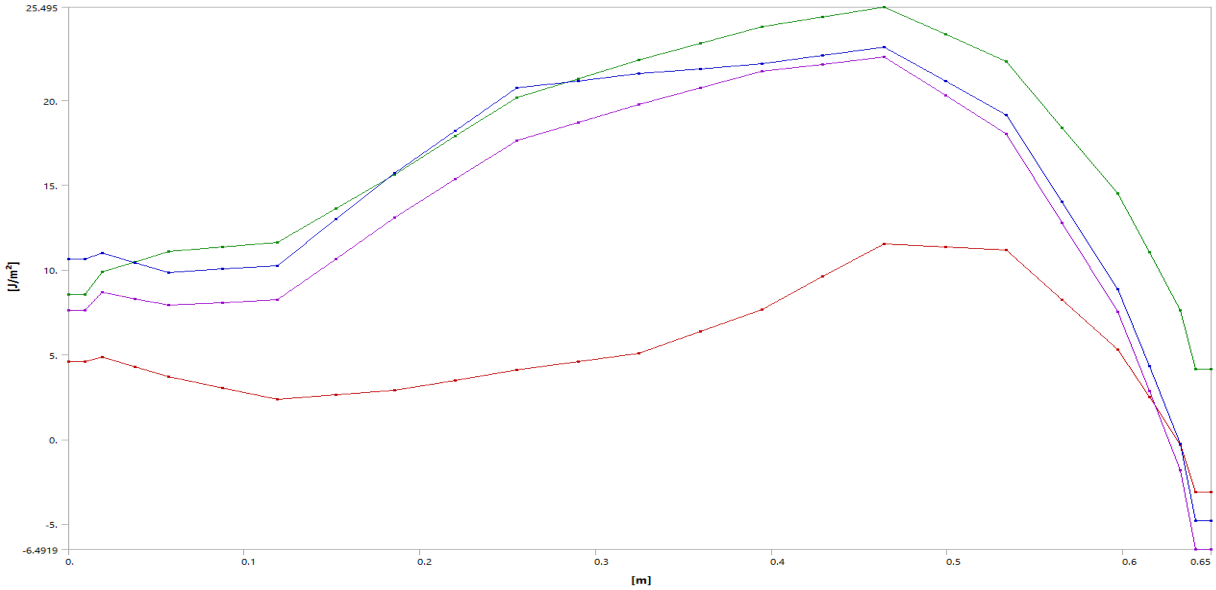

Crack 2 – Stress intensity factors

Crack 2 – SIF, K1

Tabular Data

	Length [m]	SIFS (K1) Contour 1 [Pa·m^(0.5)]	SIFS (K1) Contour 2 [Pa·m^(0.5)]	SIFS (K1) Contour 3 [Pa·m^(0.5)]	SIFS (K1) Contour 4 [Pa·m^(0.5)]
1	0.	7180.8	7570.5	7514.9	7999.1
2	4.0933e-003	7180.8	7570.5	7514.9	7999.1
3	8.1866e-003	7359.1	7601.	7660.5	7993.2
4	1.8206e-002	7145.9	7266.5	7373.7	7585.
5	2.8226e-002	6932.7	6931.9	7086.9	7176.7
6	5.0153e-002	6253.4	6176.2	6326.7	6379.1
7	7.208e-002	5574.1	5420.4	5566.4	5581.5
8	9.7319e-002	4756.1	4549.9	4690.4	4700.3
9	0.12256	3938.1	3679.3	3814.3	3819.1
10	0.1478	3277.	3012.4	3140.4	3142.1
11	0.17304	2615.9	2345.4	2466.5	2465.2
12	0.19828	2275.6	2024.	2136.8	2131.4
13	0.22351	1935.2	1702.6	1807.1	1797.6
14	0.24875	2016.5	1787.3	1887.8	1873.7
15	0.27399	2097.7	1872.	1968.4	1949.7
16	0.29923	2705.3	2466.8	2562.7	2546.7
17	0.32447	3313.	3061.6	3156.9	3143.6
18	0.34971	4292.1	4069.2	4198.	4165.
19	0.37495	5271.2	5076.7	5239.1	5186.4
20	0.40019	6072.3	5936.6	6234.2	6102.
21	0.42543	6873.3	6796.5	7229.3	7017.6
22	0.44853	7210.	7133.3	7760.3	7450.1
23	0.47164	7546.6	7470.	8291.3	7882.6
24	0.48187	7644.9	7534.9	8497.	8024.2
25	0.49211	7743.2	7599.8	8702.6	8165.8
26	0.49605	7841.4	7664.6	8908.2	8307.4
27	0.5	7841.4	7664.6	8908.2	8307.4

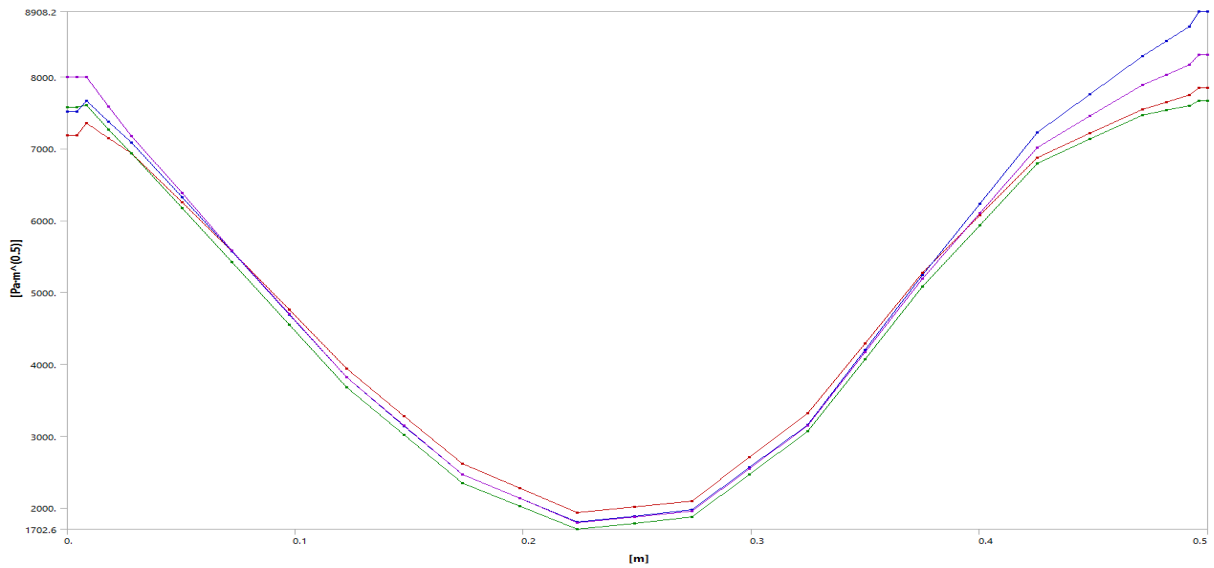

Crack 2 – SIF, K2

Tabular Data

	Length [m]	SIFS (K2) Contour 1 [Pa·m^(0.5)]	SIFS (K2) Contour 2 [Pa·m^(0.5)]	SIFS (K2) Contour 3 [Pa·m^(0.5)]	SIFS (K2) Contour 4 [Pa·m^(0.5)]
1	0.	507.32	247.11	-80.354	158.3
2	4.0933e-003	507.32	247.11	-80.354	158.3
3	8.1866e-003	800.06	607.97	359.59	606.96
4	1.8206e-002	1046.3	856.64	658.58	881.16
5	2.8226e-002	1292.5	1105.3	957.57	1155.4
6	5.0153e-002	1314.1	1079.3	963.16	1113.8
7	7.208e-002	1335.8	1053.4	968.76	1072.2
8	9.7319e-002	1240.9	915.38	854.88	928.13
9	0.12256	1146.	777.38	741.01	784.1
10	0.1478	1074.1	696.71	671.2	709.66
11	0.17304	1002.3	616.04	601.4	635.21
12	0.19828	970.96	603.92	596.22	628.18
13	0.22351	939.59	591.8	591.05	621.15
14	0.24875	966.53	625.83	635.16	655.16
15	0.27399	993.47	659.85	679.27	689.17
16	0.29923	1120.3	750.44	776.58	781.64
17	0.32447	1247.	841.02	873.89	874.11
18	0.34971	1396.2	1005.5	1022.6	1015.8
19	0.37495	1545.4	1170.	1171.3	1157.5
20	0.40019	1570.4	1322.6	1339.4	1275.6
21	0.42543	1595.4	1475.3	1507.4	1393.8
22	0.44853	1511.	1495.4	1618.7	1412.3
23	0.47164	1426.5	1515.4	1730.	1430.7
24	0.48187	1348.5	1472.8	1778.1	1402.6
25	0.49211	1270.5	1430.2	1826.2	1374.4
26	0.49605	1192.5	1387.5	1874.2	1346.2
27	0.5	1192.5	1387.5	1874.2	1346.2

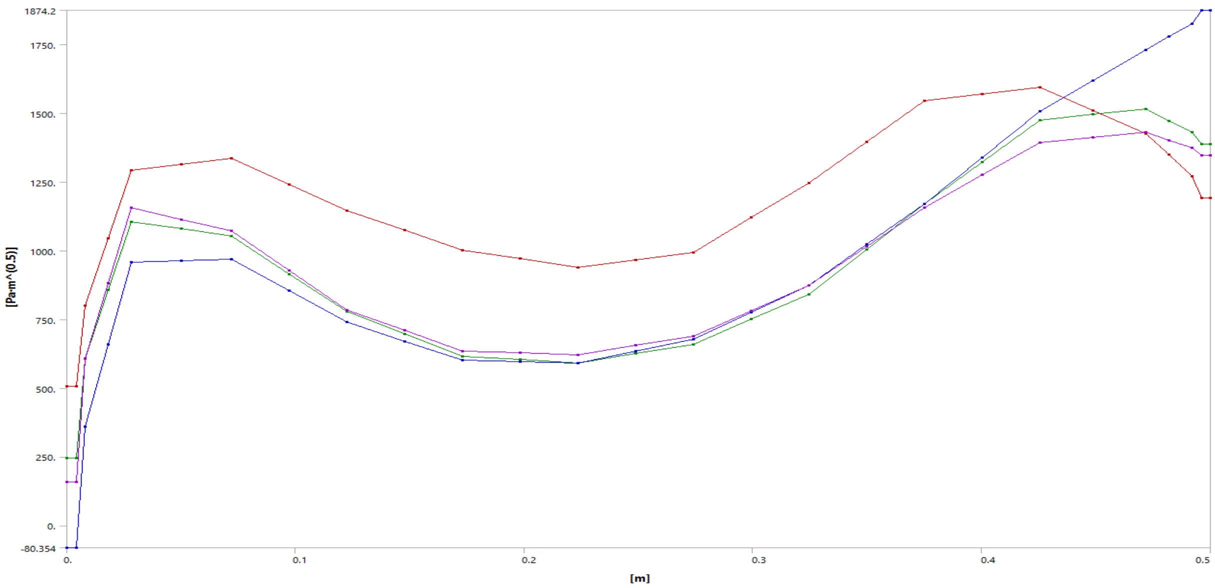

Crack 2 – SIF, K3

Tabular Data

	Length [m]	SIFS (K3) Contour 1 [Pa·m^(0.5)]	SIFS (K3) Contour 2 [Pa·m^(0.5)]	SIFS (K3) Contour 3 [Pa·m^(0.5)]	SIFS (K3) Contour 4 [Pa·m^(0.5)]
1	0.	-3170.2	-2641.8	-3328.5	-4271.9
2	4.0933e-003	-3170.2	-2641.8	-3328.5	-4271.9
3	8.1866e-003	-3398.	-2822.2	-3413.9	-4104.9
4	1.8206e-002	-3583.3	-3016.7	-3500.1	-3959.3
5	2.8226e-002	-3768.6	-3211.2	-3586.2	-3813.7
6	5.0153e-002	-3901.	-3437.4	-3744.1	-3872.1
7	7.208e-002	-4033.4	-3663.5	-3902.	-3930.6
8	9.7319e-002	-4168.5	-3907.3	-4124.3	-4154.6
9	0.12256	-4303.6	-4151.2	-4346.5	-4378.5
10	0.1478	-4431.3	-4361.4	-4521.8	-4626.3
11	0.17304	-4559.1	-4571.6	-4697.1	-4874.1
12	0.19828	-4673.1	-4739.2	-4781.8	-4973.3
13	0.22351	-4787.1	-4906.7	-4866.6	-5072.6
14	0.24875	-4869.1	-5065.9	-5053.8	-5189.2
15	0.27399	-4951.	-5225.	-5241.1	-5305.8
16	0.29923	-4950.7	-5246.3	-5297.3	-5345.8
17	0.32447	-4950.5	-5267.6	-5353.4	-5385.7
18	0.34971	-4695.7	-4899.7	-4875.9	-4915.8
19	0.37495	-4441.	-4531.9	-4398.4	-4445.9
20	0.40019	-3912.8	-4063.5	-3948.2	-3909.8
21	0.42543	-3384.5	-3595.2	-3497.9	-3373.7
22	0.44853	-2920.9	-3523.8	-3627.4	-3315.6
23	0.47164	-2457.4	-3452.4	-3756.8	-3257.6
24	0.48187	-2215.3	-3588.2	-4058.5	-3391.8
25	0.49211	-1973.2	-3724.	-4360.3	-3526.1
26	0.49605	-1731.1	-3859.8	-4662.	-3660.3
27	0.5	-1731.1	-3859.8	-4662.	-3660.3

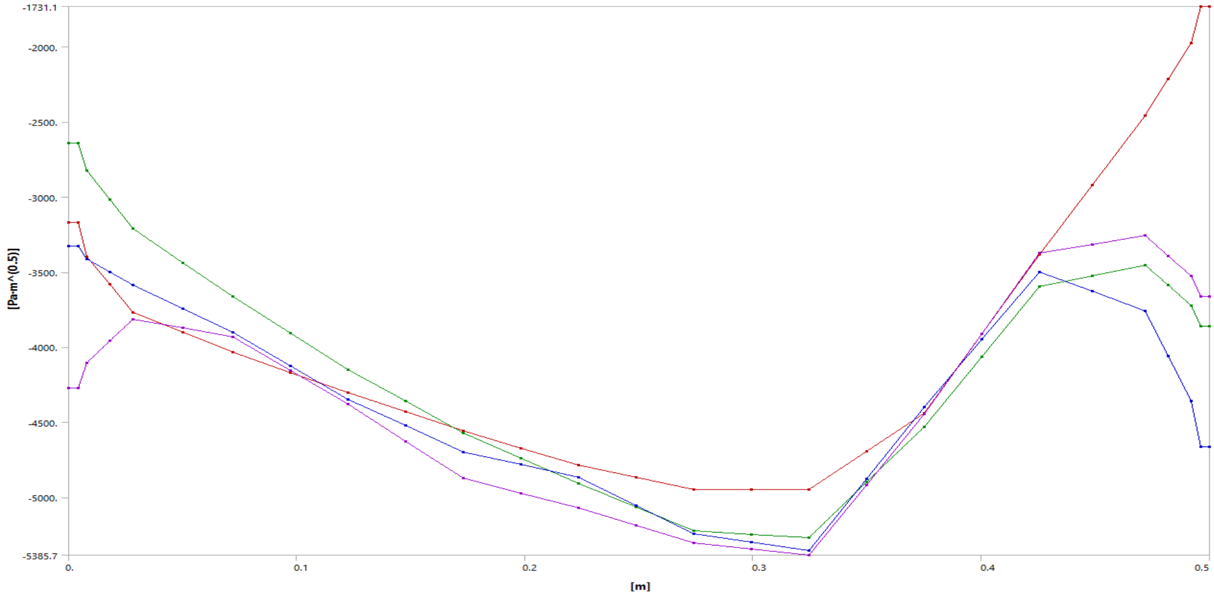

Crack 2 – J-Integral

Tabular Data

	Length [m]	J-Integral (JINT) Contour 1 [J/m²]	J-Integral (JINT) Contour 2 [J/m²]	J-Integral (JINT) Contour 3 [J/m²]	J-Integral (JINT) Contour 4 [J/m²]
1	0.	-2.0536e-002	-5.5113e-002	-7.2055e-002	-2.6034e-002
2	4.0933e-003	-2.0536e-002	-5.5113e-002	-7.2055e-002	-2.6034e-002
3	8.1866e-003	-1.4147e-002	-6.2578e-002	-4.8473e-002	1.0051e-002
4	1.8206e-002	-1.0864e-002	-5.7092e-002	-2.1115e-002	7.9664e-002
5	2.8226e-002	-7.581e-003	-5.1605e-002	6.2425e-003	0.14928
6	5.0153e-002	-9.0249e-003	-3.7377e-002	1.8663e-002	0.12612
7	7.208e-002	-1.0469e-002	-2.3148e-002	3.1084e-002	0.10297
8	9.7319e-002	-1.0479e-002	-1.7062e-002	2.3096e-002	3.8941e-002
9	0.12256	-1.049e-002	-1.0975e-002	1.5108e-002	-2.5083e-002
10	0.1478	-5.857e-003	-9.1687e-003	2.2989e-003	2.766e-002
11	0.17304	-1.2241e-003	-7.362e-003	-1.051e-002	8.0403e-002
12	0.19828	9.8953e-004	6.7059e-003	-1.7708e-002	0.16444
13	0.22351	3.2031e-003	2.0774e-002	-2.4905e-002	0.24848
14	0.24875	5.0865e-003	2.7632e-002	-1.9786e-002	0.26332
15	0.27399	6.9699e-003	3.4491e-002	-1.4666e-002	0.27816
16	0.29923	1.3785e-002	2.1869e-002	1.4141e-002	0.2685
17	0.32447	2.0601e-002	9.2475e-003	4.2948e-002	0.25884
18	0.34971	2.3805e-002	-8.9936e-004	6.8128e-002	0.24445
19	0.37495	2.7009e-002	-1.1046e-002	9.3309e-002	0.23006
20	0.40019	2.0952e-002	-1.5424e-002	8.0082e-002	0.19564
21	0.42543	1.4895e-002	-1.9802e-002	6.6856e-002	0.16122
22	0.44853	5.0877e-003	-2.1324e-002	4.9083e-002	0.127
23	0.47164	-4.7193e-003	-2.2846e-002	3.1311e-002	9.2779e-002
24	0.48187	-1.1784e-002	-2.1536e-002	2.9311e-002	7.5141e-002
25	0.49211	-1.8849e-002	-2.0226e-002	2.7311e-002	5.7502e-002
26	0.49605	-2.5914e-002	-1.8915e-002	2.5311e-002	3.9863e-002
27	0.5	-2.5914e-002	-1.8915e-002	2.5311e-002	3.9863e-002

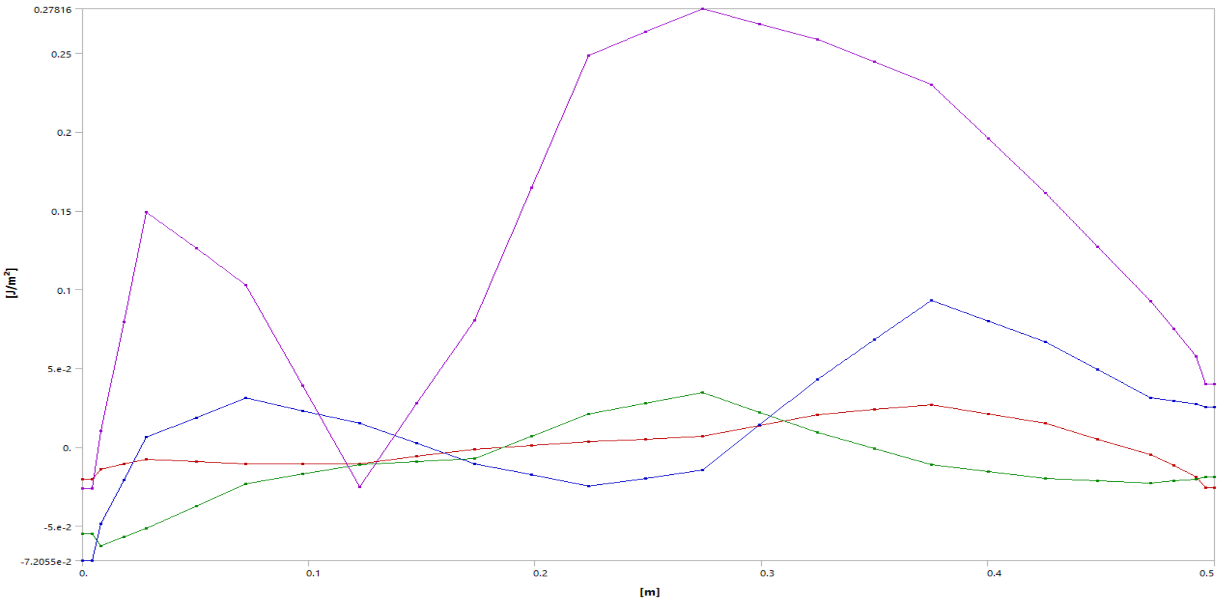

Crack 3 – Stress intensity factors

Crack 3 – SIF, K1

Tabular Data

	Length [m]	SIFS (K1) Contour 1 [Pa·m^(0.5)]	SIFS (K1) Contour 2 [Pa·m^(0.5)]	SIFS (K1) Contour 3 [Pa·m^(0.5)]	SIFS (K1) Contour 4 [Pa·m^(0.5)]
1	0.	-1.2862e+006	-1.4274e+006	-1.4095e+006	-1.4459e+006
2	1.6116e-002	-1.2862e+006	-1.4274e+006	-1.4095e+006	-1.4459e+006
3	3.2232e-002	-1.2492e+006	-1.4065e+006	-1.3887e+006	-1.421e+006
4	4.7955e-002	-1.2143e+006	-1.3715e+006	-1.3597e+006	-1.3836e+006
5	6.3678e-002	-1.1794e+006	-1.3365e+006	-1.3308e+006	-1.3462e+006
6	7.9507e-002	-1.1702e+006	-1.3156e+006	-1.3187e+006	-1.3273e+006
7	9.5336e-002	-1.161e+006	-1.2947e+006	-1.3067e+006	-1.3084e+006
8	0.11116	-1.1627e+006	-1.2934e+006	-1.3107e+006	-1.3099e+006
9	0.12699	-1.1644e+006	-1.2921e+006	-1.3146e+006	-1.3114e+006
10	0.1427	-1.1607e+006	-1.2835e+006	-1.3095e+006	-1.3038e+006
11	0.15841	-1.1569e+006	-1.2748e+006	-1.3043e+006	-1.2963e+006
12	0.1739	-1.1559e+006	-1.2561e+006	-1.2906e+006	-1.2786e+006
13	0.18939	-1.1548e+006	-1.2373e+006	-1.2769e+006	-1.2609e+006
14	0.20456	-1.1574e+006	-1.2233e+006	-1.2674e+006	-1.2481e+006
15	0.21973	-1.16e+006	-1.2094e+006	-1.2579e+006	-1.2353e+006
16	0.23449	-1.1626e+006	-1.1955e+006	-1.2483e+006	-1.2225e+006
17	0.24925	-1.1626e+006	-1.1955e+006	-1.2483e+006	-1.2225e+006

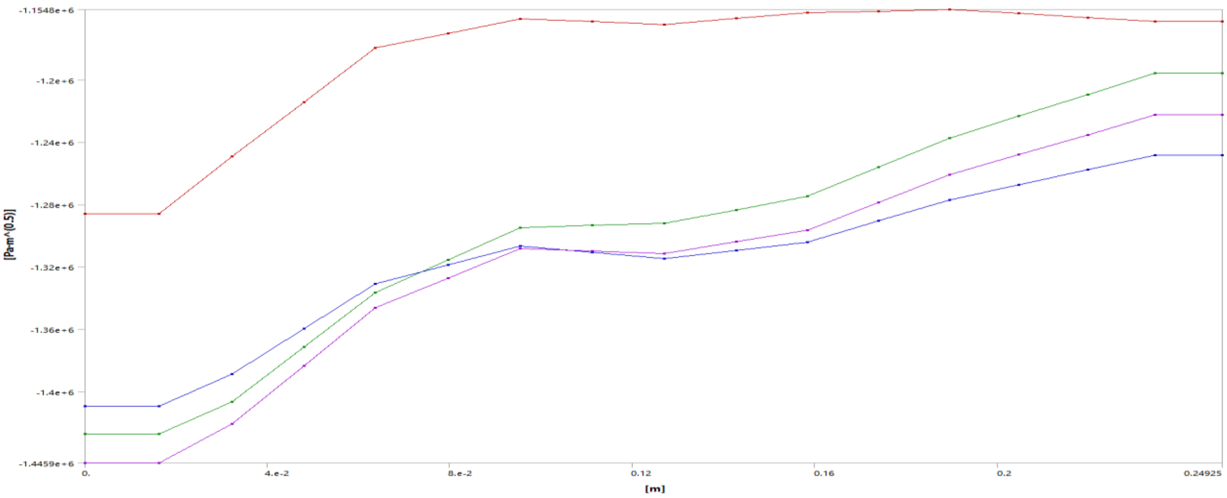

Crack 3 – SIF, K2

Tabular Data

	Length [m]	SIFS (K2) Contour 1 [Pa·m^(0.5)]	SIFS (K2) Contour 2 [Pa·m^(0.5)]	SIFS (K2) Contour 3 [Pa·m^(0.5)]	SIFS (K2) Contour 4 [Pa·m^(0.5)]
1	0.	5.5688e+005	4.6287e+005	4.5072e+005	4.5125e+005
2	1.6116e-002	5.5688e+005	4.6287e+005	4.5072e+005	4.5125e+005
3	3.2232e-002	5.5065e+005	4.5869e+005	4.4677e+005	4.5158e+005
4	4.7955e-002	5.4934e+005	4.5533e+005	4.4444e+005	4.5138e+005
5	6.3678e-002	5.4803e+005	4.5196e+005	4.4211e+005	4.5117e+005
6	7.9507e-002	5.5016e+005	4.5045e+005	4.395e+005	4.503e+005
7	9.5336e-002	5.523e+005	4.4894e+005	4.369e+005	4.4944e+005
8	0.11116	5.4641e+005	4.3978e+005	4.2705e+005	4.4029e+005
9	0.12699	5.4053e+005	4.3062e+005	4.172e+005	4.3113e+005
10	0.1427	5.3016e+005	4.1808e+005	4.0788e+005	4.1861e+005
11	0.15841	5.1979e+005	4.0554e+005	3.9855e+005	4.0609e+005
12	0.1739	5.14e+005	4.0241e+005	3.9865e+005	4.0085e+005
13	0.18939	5.0821e+005	3.9929e+005	3.9875e+005	3.9561e+005
14	0.20456	5.0602e+005	4.0134e+005	4.0206e+005	3.9484e+005
15	0.21973	5.0384e+005	4.0339e+005	4.0537e+005	3.9406e+005
16	0.23449	5.0166e+005	4.0545e+005	4.0867e+005	3.9329e+005
17	0.24925	5.0166e+005	4.0545e+005	4.0867e+005	3.9329e+005

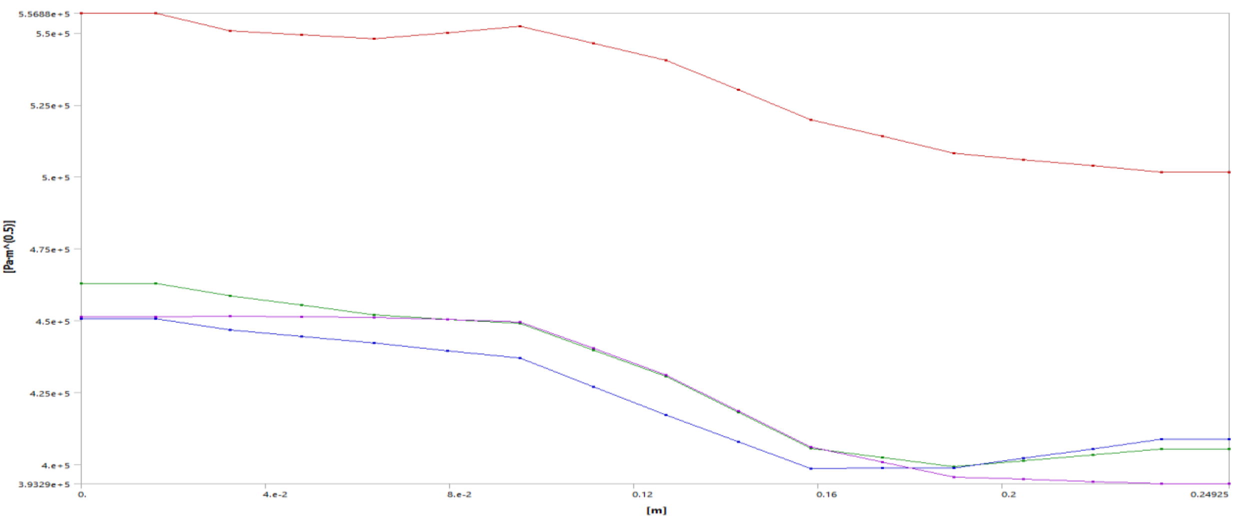

Crack 3 – SIF, K3

Tabular Data

	Length [m]	SIFS (K3) Contour 1 [Pa·m^(0.5)]	SIFS (K3) Contour 2 [Pa·m^(0.5)]	SIFS (K3) Contour 3 [Pa·m^(0.5)]	SIFS (K3) Contour 4 [Pa·m^(0.5)]
1	0.	-31213	-37252	-38764	-38891
2	1.6116e-002	-31213	-37252	-38764	-38891
3	3.2232e-002	-24795	-28428	-29376	-30002
4	4.7955e-002	-14738	-17486	-18196	-19799
5	6.3678e-002	-4681.3	-6542.8	-7015.1	-9596.4
6	7.9507e-002	5012.5	2241.3	1580.1	-881.71
7	9.5336e-002	14706	11025	10175	7832.9
8	0.11116	23498	19529	18910	17352
9	0.12699	32289	28032	27646	26871
10	0.1427	41327	37372	37575	36708
11	0.15841	50365	46712	47505	46545
12	0.1739	57986	54656	55304	53696
13	0.18939	65608	62600	63103	60847
14	0.20456	70247	67587	67557	64830
15	0.21973	74886	72574	72012	68813
16	0.23449	79525	77561	76466	72796
17	0.24925	79525	77561	76466	72796

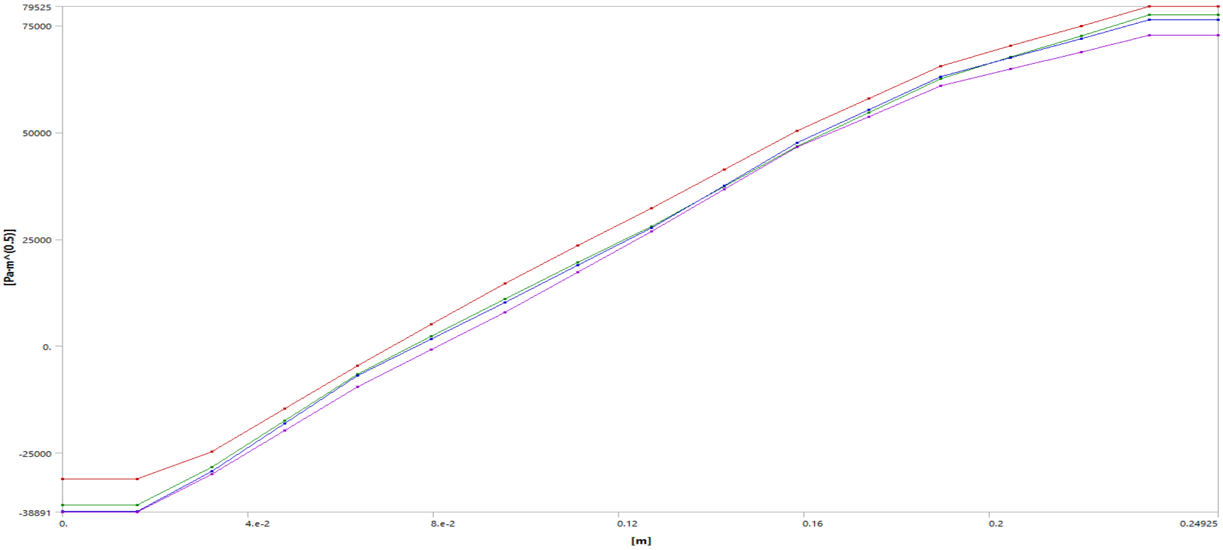

Crack 3 – J-Integral

Tabular Data

	Length [m]	J-Integral (JINT) Contour 1 [J/m²]	J-Integral (JINT) Contour 2 [J/m²]	J-Integral (JINT) Contour 3 [J/m²]	J-Integral (JINT) Contour 4 [J/m²]
1	0.	34.603	78.964	75.852	83.936
2	1.6116e-002	34.603	78.964	75.852	83.936
3	3.2232e-002	25.338	76.14	72.928	80.131
4	4.7955e-002	18.246	70.186	68.373	73.463
5	6.3678e-002	11.155	64.233	63.817	66.795
6	7.9507e-002	11.828	61.521	63.159	64.305
7	9.5336e-002	12.501	58.809	62.502	61.814
8	0.11116	15.417	59.81	64.638	63.186
9	0.12699	18.333	60.812	66.774	64.558
10	0.1427	19.271	59.05	65.663	62.92
11	0.15841	20.21	57.289	64.553	61.283
12	0.1739	21.364	53.004	61.112	57.332
13	0.18939	22.518	48.719	57.672	53.382
14	0.20456	23.946	45.599	55.233	50.644
15	0.21973	25.373	42.479	52.794	47.906
16	0.23449	26.8	39.359	50.355	45.169
17	0.24925	26.8	39.359	50.355	45.169

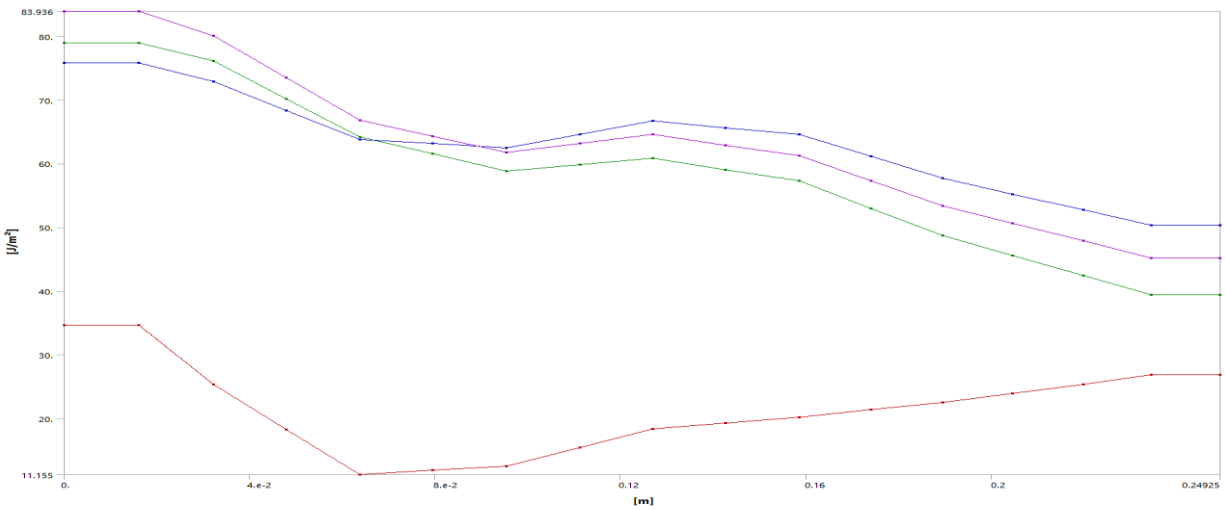

Crack 4 – Stress intensity factors

Crack 4 – SIF, K1

Tabular Data

	Length [m]	SIFS (K1) Contour 1 [Pa·m^(0.5)]	SIFS (K1) Contour 2 [Pa·m^(0.5)]	SIFS (K1) Contour 3 [Pa·m^(0.5)]	SIFS (K1) Contour 4 [Pa·m^(0.5)]
1	0.	-9726.9	-10537	-11435	-11950
2	6.0464e-003	-9726.9	-10537	-11435	-11950
3	1.2092e-002	-10300	-11150	-12000	-12434
4	2.6082e-002	-10807	-11690	-12417	-12765
5	4.0071e-002	-11314	-12230	-12834	-13095
6	6.3923e-002	-11458	-12406	-12863	-13050
7	8.7775e-002	-11601	-12582	-12893	-13005
8	0.11179	-11401	-12378	-12584	-12680
9	0.13581	-11202	-12175	-12275	-12355
10	0.15983	-10619	-11532	-11591	-11710
11	0.18385	-10037	-10889	-10907	-11064
12	0.20787	-9243.6	-10036	-10061	-10229
13	0.23189	-8450.5	-9182.9	-9214.7	-9392.6
14	0.25591	-7608.1	-8262.7	-8322.5	-8489.8
15	0.27992	-6765.6	-7342.5	-7430.3	-7586.9
16	0.30394	-5917.9	-6384.6	-6501.3	-6667.9
17	0.32796	-5070.1	-5426.6	-5572.3	-5748.9
18	0.34297	-4467.6	-4741.	-4903.6	-5095.6
19	0.35799	-3865.1	-4055.4	-4235.	-4442.3
20	0.36399	-3262.7	-3369.8	-3566.4	-3789.
21	0.37	-3262.7	-3369.8	-3566.4	-3789.

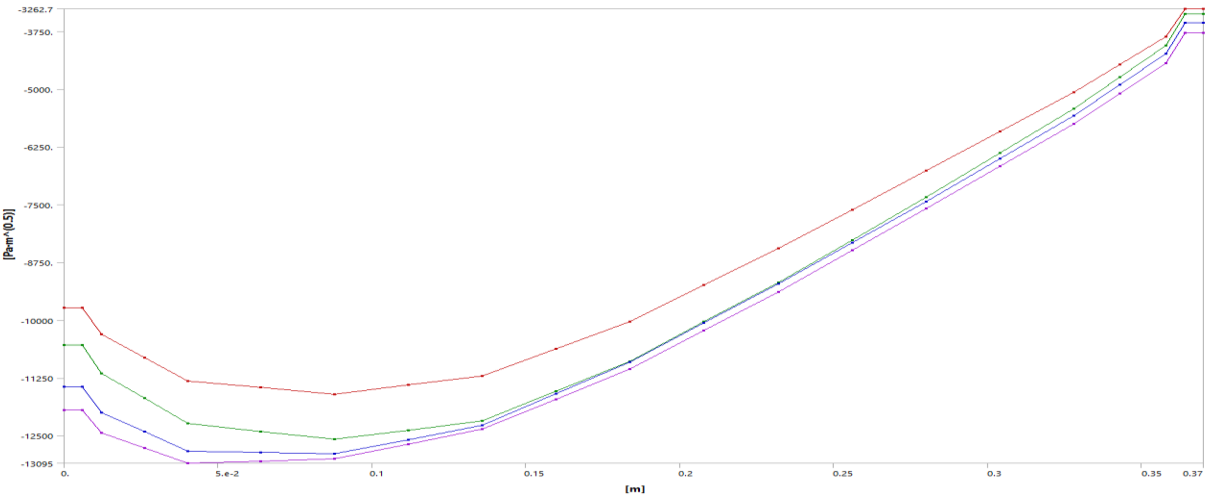

Crack 4 – SIF, K2

Tabular Data

	Length [m]	SIFS (K2) Contour 1 [Pa·m^(0.5)]	SIFS (K2) Contour 2 [Pa·m^(0.5)]	SIFS (K2) Contour 3 [Pa·m^(0.5)]	SIFS (K2) Contour 4 [Pa·m^(0.5)]
1	0.	163.02	-57.199	-152.84	-24.031
2	6.0464e-003	163.02	-57.199	-152.84	-24.031
3	1.2092e-002	150.99	70.928	8.0376	147.04
4	2.6082e-002	135.18	127.42	66.227	223.22
5	4.0071e-002	119.37	183.91	124.42	299.41
6	6.3923e-002	116.86	154.79	104.46	254.09
7	8.7775e-002	114.36	125.67	84.511	208.78
8	0.11179	106.19	102.23	69.932	157.56
9	0.13581	98.025	78.785	55.352	106.34
10	0.15983	71.507	74.268	37.576	68.68
11	0.18385	44.988	69.751	19.8	31.024
12	0.20787	30.211	64.322	21.046	16.033
13	0.23189	15.434	58.892	22.292	1.0425
14	0.25591	6.7621	51.156	21.274	11.967
15	0.27992	-1.91	43.421	20.255	22.892
16	0.30394	-20.041	27.682	-8.0568	29.418
17	0.32796	-38.171	11.944	-36.369	35.943
18	0.34297	-52.985	-4.0831	-62.553	35.976
19	0.35799	-67.799	-20.111	-88.736	36.009
20	0.36399	-82.613	-36.138	-114.92	36.042
21	0.37	-82.613	-36.138	-114.92	36.042

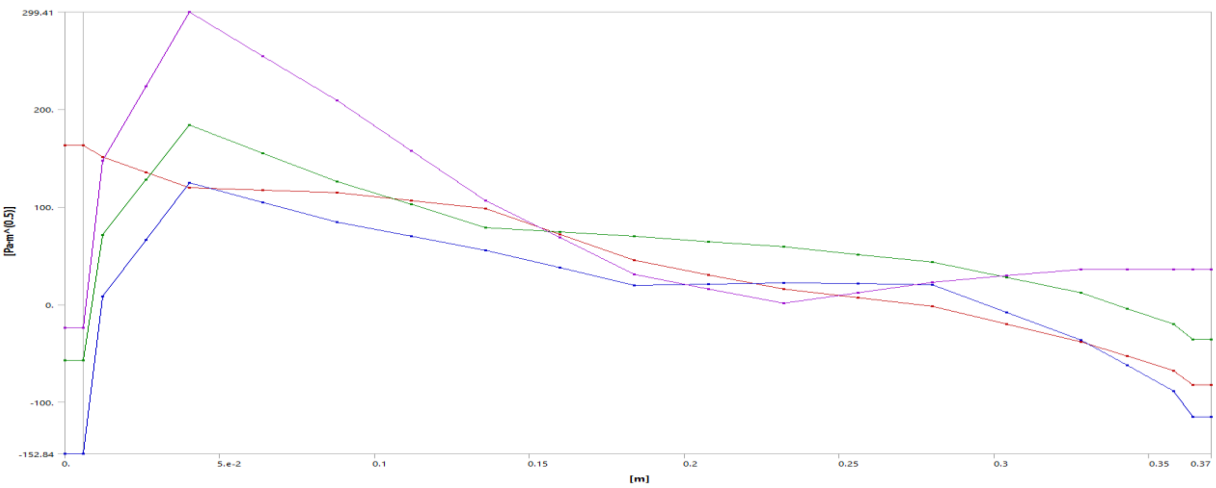

Crack 4 – SIF, K3

Tabular Data

	Length [m]	SIFS (K3) Contour 1 [Pa·m^(0.5)]	SIFS (K3) Contour 2 [Pa·m^(0.5)]	SIFS (K3) Contour 3 [Pa·m^(0.5)]	SIFS (K3) Contour 4 [Pa·m^(0.5)]
1	0.	121.87	-70.425	-255.16	20.006
2	6.0464e-003	121.87	-70.425	-255.16	20.006
3	1.2092e-002	177.72	20.758	-81.547	126.17
4	2.6082e-002	219.73	87.6	9.3916	176.21
5	4.0071e-002	261.75	154.44	100.33	226.26
6	6.3923e-002	260.07	161.05	119.84	232.81
7	8.7775e-002	258.38	167.65	139.35	239.37
8	0.11179	249.56	171.37	171.02	249.08
9	0.13581	240.74	175.08	202.69	258.8
10	0.15983	243.27	196.95	230.33	267.19
11	0.18385	245.81	218.81	257.97	275.59
12	0.20787	235.62	221.13	260.4	273.29
13	0.23189	225.44	223.45	262.83	271.
14	0.25591	194.93	183.07	220.53	208.05
15	0.27992	164.42	142.7	178.23	145.1
16	0.30394	127.98	78.152	102.43	15.757
17	0.32796	91.53	13.605	26.631	-113.58
18	0.34297	65.535	-35.772	-32.666	-222.12
19	0.35799	39.54	-85.148	-91.964	-330.65
20	0.36399	13.545	-134.52	-151.26	-439.19
21	0.37	13.545	-134.52	-151.26	-439.19

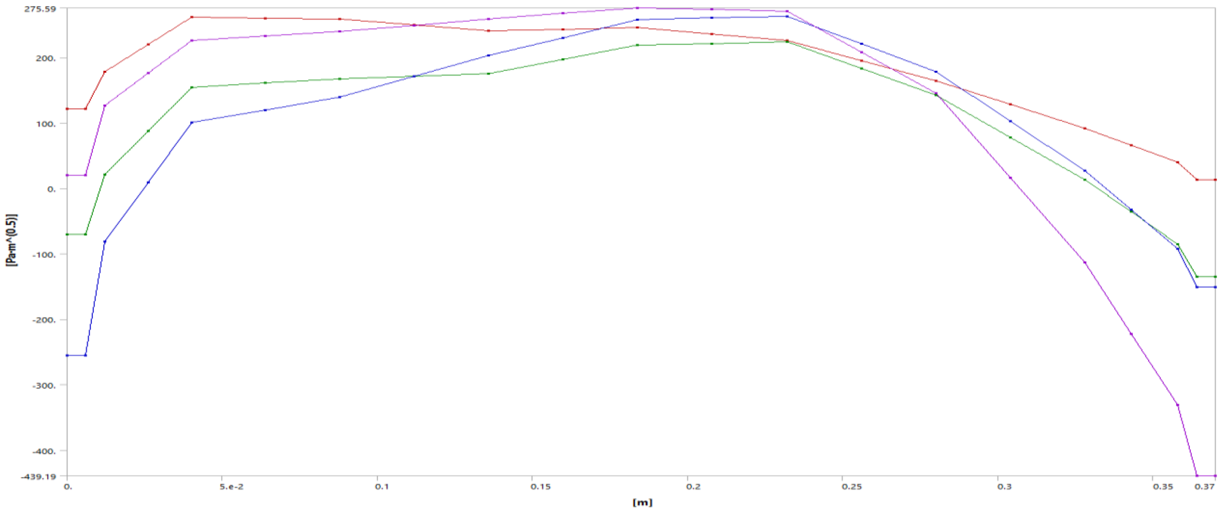

Crack 4 – J-Integral

Tabular Data

	Length [m]	J-Integral (JINT) Contour 1 [J/m²]	J-Integral (JINT) Contour 2 [J/m²]	J-Integral (JINT) Contour 3 [J/m²]	J-Integral (JINT) Contour 4 [J/m²]
1	0.	1.016e-003	4.6011e-003	3.9901e-003	7.5869e-003
2	6.0464e-003	1.016e-003	4.6011e-003	3.9901e-003	7.5869e-003
3	1.2092e-002	1.2725e-003	4.6782e-003	4.5035e-003	5.8304e-003
4	2.6082e-002	1.3938e-003	4.7519e-003	4.3192e-003	4.1837e-003
5	4.0071e-002	1.5151e-003	4.8257e-003	4.1349e-003	2.5369e-003
6	6.3923e-002	1.4228e-003	4.7073e-003	3.9285e-003	2.6621e-003
7	8.7775e-002	1.3305e-003	4.5889e-003	3.7221e-003	2.7873e-003
8	0.11179	1.3017e-003	4.3631e-003	3.9182e-003	3.6354e-003
9	0.13581	1.2729e-003	4.1373e-003	4.1142e-003	4.4834e-003
10	0.15983	1.1063e-003	3.8974e-003	3.9673e-003	4.3933e-003
11	0.18385	9.3974e-004	3.6576e-003	3.8204e-003	4.3032e-003
12	0.20787	6.495e-004	3.3471e-003	3.356e-003	3.7066e-003
13	0.23189	3.5926e-004	3.0367e-003	2.8915e-003	3.1101e-003
14	0.25591	2.4163e-004	2.7161e-003	2.5107e-003	2.7327e-003
15	0.27992	1.2399e-004	2.3955e-003	2.1299e-003	2.3552e-003
16	0.30394	9.2207e-005	2.1614e-003	1.8448e-003	1.9261e-003
17	0.32796	6.0422e-005	1.9272e-003	1.5596e-003	1.4969e-003
18	0.34297	2.9843e-005	1.7941e-003	1.3725e-003	1.0582e-003
19	0.35799	-7.3556e-007	1.6609e-003	1.1854e-003	6.1946e-004
20	0.36399	-3.1314e-005	1.5277e-003	9.983e-004	1.8075e-004
21	0.37	-3.1314e-005	1.5277e-003	9.983e-004	1.8075e-004

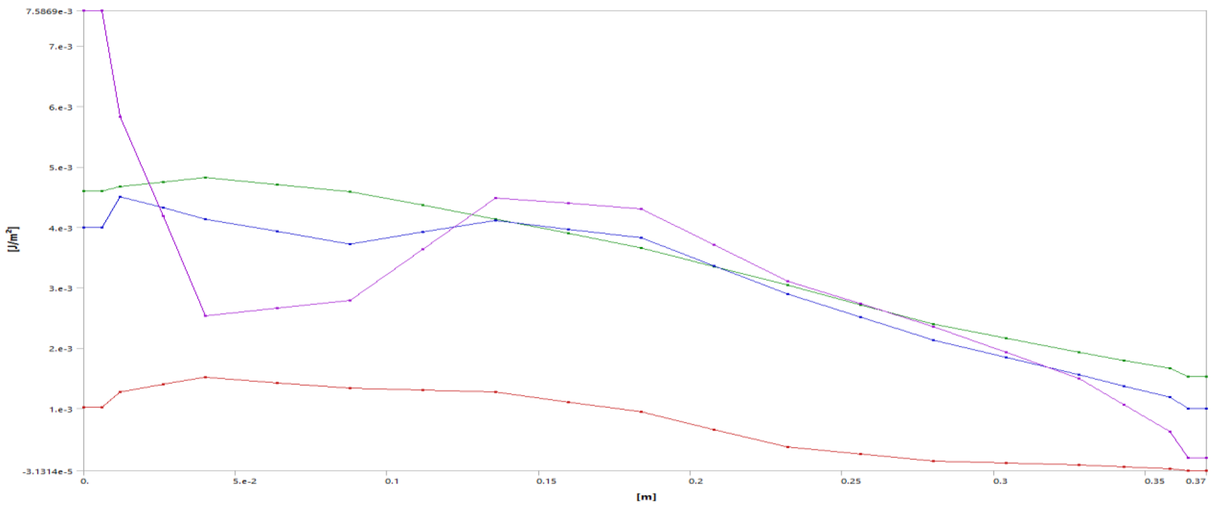

Crack 5 – Stress intensity factors

Crack 5 – SIF, K1

Tabular Data

	Length [m]	SIFS (K1) Contour 1 [Pa·m^(0.5)]	SIFS (K1) Contour 2 [Pa·m^(0.5)]	SIFS (K1) Contour 3 [Pa·m^(0.5)]	SIFS (K1) Contour 4 [Pa·m^(0.5)]
1	0.	4480.6	4380.4	4929.9	4743.9
2	5.7162e-003	4480.6	4380.4	4929.9	4743.9
3	1.1432e-002	4218.1	4199.6	4606.	4397.2
4	2.5975e-002	3709.3	3762.8	4067.	3860.1
5	4.0518e-002	3200.5	3325.9	3528.	3322.9
6	7.7077e-002	2624.9	2788.5	2947.4	2762.4
7	0.11364	2049.3	2251.1	2366.9	2201.8
8	0.16249	1592.8	1807.	1898.4	1758.1
9	0.21134	1136.3	1363.	1429.9	1314.4
10	0.26085	825.38	1047.8	1108.2	1009.6
11	0.31035	514.43	732.63	786.49	704.88
12	0.36163	316.89	524.5	576.04	500.53
13	0.41292	119.35	316.37	365.59	296.18
14	0.4642	9.3168	199.75	241.96	184.53
15	0.51549	-100.71	83.129	118.33	72.877
16	0.56677	-137.75	45.821	71.472	32.238
17	0.61806	-174.79	8.5133	24.609	-8.4024
18	0.66934	-81.182	95.791	82.207	63.984
19	0.72062	12.423	183.07	139.8	136.37
20	0.77165	333.31	490.64	390.61	434.39
21	0.82268	654.19	798.2	641.42	732.4
22	0.87083	1122.9	1266.3	1129.2	1228.2
23	0.91899	1591.6	1734.4	1616.9	1723.9
24	0.94876	1988.5	2150.1	2184.7	2224.5
25	0.97853	2385.3	2565.8	2752.4	2725.
26	0.98915	2616.4	2816.	3151.6	3056.3
27	0.99977	2847.5	3066.2	3550.9	3387.6
28	1.0049	3078.7	3316.4	3950.2	3718.8
29	1.01	3078.7	3316.4	3950.2	3718.8

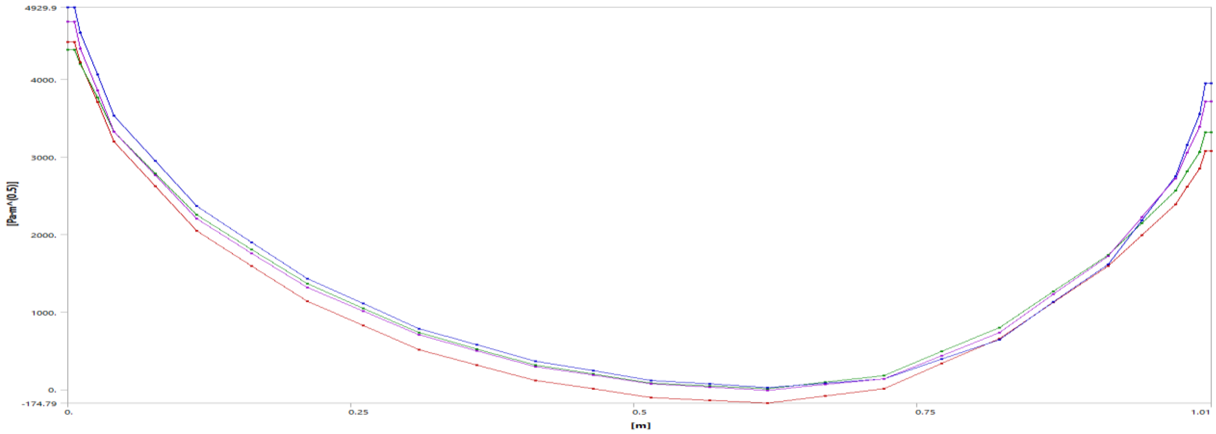

Crack 5 – SIF, K2

Tabular Data

	Length [m]	SIFS (K2) Contour 1 [Pa·m^(0.5)]	SIFS (K2) Contour 2 [Pa·m^(0.5)]	SIFS (K2) Contour 3 [Pa·m^(0.5)]	SIFS (K2) Contour 4 [Pa·m^(0.5)]
1	0.	-326.13	-486.86	-587.54	-353.38
2	5.7162e-003	-326.13	-486.86	-587.54	-353.38
3	1.1432e-002	-270.25	-423.15	-478.09	-299.95
4	2.5975e-002	-218.05	-329.12	-357.12	-224.2
5	4.0518e-002	-165.85	-235.1	-236.16	-148.44
6	7.7077e-002	-141.59	-174.14	-169.95	-118.47
7	0.11364	-117.34	-113.19	-103.74	-88.495
8	0.16249	-111.63	-94.613	-80.862	-63.084
9	0.21134	-105.93	-76.038	-57.979	-37.674
10	0.26085	-106.34	-71.597	-53.476	-13.769
11	0.31035	-106.76	-67.155	-48.974	10.136
12	0.36163	-104.78	-63.406	-47.346	-5.9759
13	0.41292	-102.8	-59.656	-45.719	-22.088
14	0.4642	-97.239	-55.921	-35.875	-23.193
15	0.51549	-91.677	-52.187	-26.031	-24.299
16	0.56677	-91.118	-50.268	-20.749	-6.9219
17	0.61806	-90.559	-48.349	-15.467	10.455
18	0.66934	-88.112	-50.094	-20.758	8.9676
19	0.72062	-85.664	-51.839	-26.049	7.4802
20	0.77165	-84.396	-58.202	-11.239	12.32
21	0.82268	-83.127	-64.564	3.571	17.16
22	0.87083	-96.637	-75.863	9.8051	19.385
23	0.91899	-110.15	-87.163	16.039	21.61
24	0.94876	-117.69	-109.53	-53.998	-10.123
25	0.97853	-125.22	-131.9	-124.04	-41.856
26	0.98915	-121.61	-153.7	-209.41	-77.606
27	0.99977	-117.99	-175.51	-294.78	-113.36
28	1.0049	-114.37	-197.31	-380.15	-149.11
29	1.01	-114.37	-197.31	-380.15	-149.11

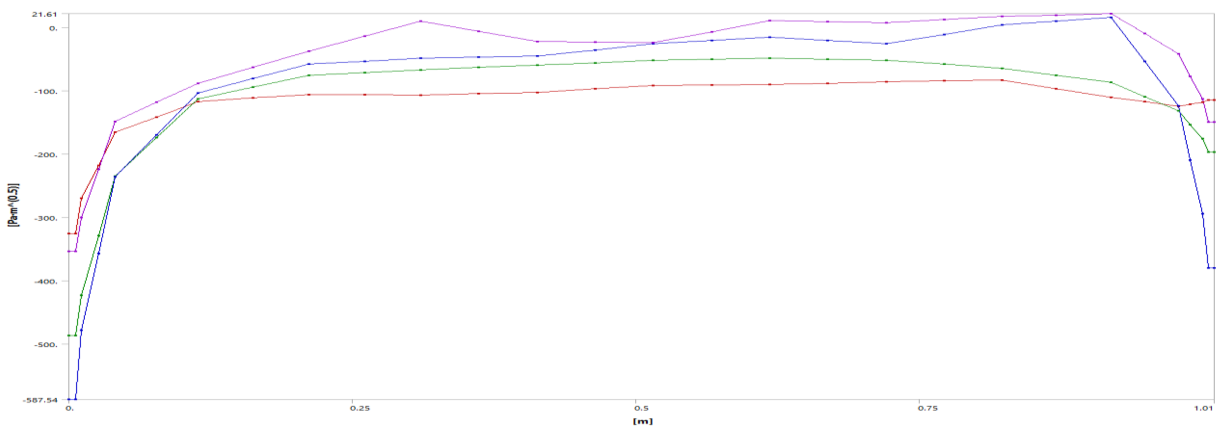

Crack 5 – SIF, K3

Tabular Data

	Length [m]	SIFS (K3) Contour 1 [Pa·m^(0.5)]	SIFS (K3) Contour 2 [Pa·m^(0.5)]	SIFS (K3) Contour 3 [Pa·m^(0.5)]	SIFS (K3) Contour 4 [Pa·m^(0.5)]
1	0.	252.47	1462.9	2165.2	2798.4
2	5.7162e-003	252.47	1462.9	2165.2	2798.4
3	1.1432e-002	198.34	1114.6	1648.9	2181.9
4	2.5975e-002	173.	880.07	1266.7	1618.6
5	4.0518e-002	147.66	645.54	884.53	1055.4
6	7.7077e-002	129.41	529.72	695.1	736.86
7	0.11364	111.16	413.91	505.66	418.32
8	0.16249	92.064	326.09	399.2	346.9
9	0.21134	72.964	238.27	292.74	275.49
10	0.26085	68.713	193.43	219.51	191.46
11	0.31035	64.461	148.6	146.29	107.42
12	0.36163	58.063	121.79	103.06	28.386
13	0.41292	51.666	94.976	59.832	-50.652
14	0.4642	43.328	75.152	53.774	-13.557
15	0.51549	34.99	55.328	47.717	23.538
16	0.56677	30.276	37.368	14.646	15.261
17	0.61806	25.561	19.407	-18.424	6.9845
18	0.66934	2.3744	-4.1745	-71.815	-39.006
19	0.72062	-20.812	-27.756	-125.21	-84.997
20	0.77165	-39.731	-18.878	-134.18	-53.691
21	0.82268	-58.649	-9.9997	-143.15	-22.384
22	0.87083	-32.257	46.856	-54.452	134.05
23	0.91899	-5.8647	103.71	34.247	290.48
24	0.94876	30.647	164.76	174.14	440.82
25	0.97853	67.158	225.81	314.03	591.15
26	0.98915	84.597	262.88	412.45	655.36
27	0.99977	102.04	299.94	510.88	719.57
28	1.0049	119.48	337.	609.3	783.78
29	1.01	119.48	337.	609.3	783.78

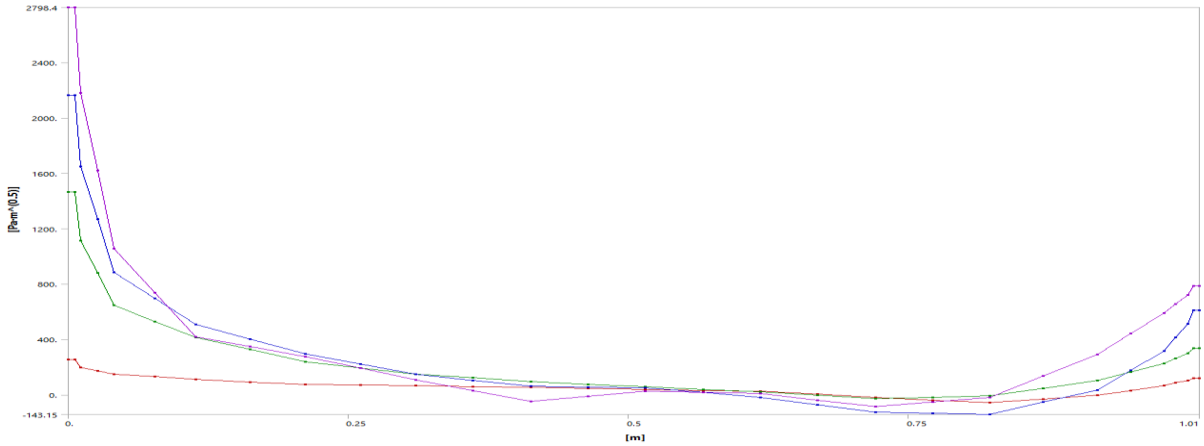

Crack 5 – J-Integral

Tabular Data

	Length [m]	J-Integral (JINT) Contour 1 [J/m²]	J-Integral (JINT) Contour 2 [J/m²]	J-Integral (JINT) Contour 3 [J/m²]	J-Integral (JINT) Contour 4 [J/m²]
1	0.	-6.6704e-002	-0.21689	-0.32402	-0.4511
2	5.7162e-003	-6.6704e-002	-0.21689	-0.32402	-0.4511
3	1.1432e-002	-5.3727e-002	-0.18868	-0.27296	-0.41109
4	2.5975e-002	-4.296e-002	-0.15287	-0.21483	-0.37979
5	4.0518e-002	-3.2194e-002	-0.11706	-0.15669	-0.34849
6	7.7077e-002	-2.6706e-002	-9.513e-002	-0.11324	-0.33929
7	0.11364	-2.1219e-002	-7.3206e-002	-6.9784e-002	-0.33009
8	0.16249	-1.8646e-002	-6.3957e-002	-4.2287e-002	-0.30317
9	0.21134	-1.6073e-002	-5.4709e-002	-1.4791e-002	-0.27625
10	0.26085	-1.5029e-002	-4.2195e-002	1.7336e-002	-0.19765
11	0.31035	-1.3986e-002	-2.9681e-002	4.9464e-002	-0.11904
12	0.36163	-1.2286e-002	-2.0558e-002	4.6187e-002	-8.3246e-002
13	0.41292	-1.0586e-002	-1.1435e-002	4.2911e-002	-4.7451e-002
14	0.4642	-9.5254e-003	-8.7656e-003	1.343e-002	-5.0474e-002
15	0.51549	-8.4645e-003	-6.0963e-003	-1.6051e-002	-5.3497e-002
16	0.56677	-9.2219e-003	-2.5068e-003	-3.3806e-002	-5.2447e-002
17	0.61806	-9.9793e-003	1.0827e-003	-5.1562e-002	-5.1397e-002
18	0.66934	-1.1415e-002	4.6704e-003	-5.3986e-002	-4.5839e-002
19	0.72062	-1.285e-002	8.2581e-003	-5.641e-002	-4.0282e-002
20	0.77165	-1.2716e-002	1.4393e-002	-3.339e-002	-5.9446e-003
21	0.82268	-1.2582e-002	2.0529e-002	-1.0369e-002	2.8392e-002
22	0.87083	-5.4717e-003	3.9501e-002	3.5569e-002	7.9398e-002
23	0.91899	1.6388e-003	5.8473e-002	8.1508e-002	0.1304
24	0.94876	1.3121e-002	9.1892e-002	0.14919	0.20428
25	0.97853	2.4603e-002	0.12531	0.21687	0.27815
26	0.98915	3.2736e-002	0.15371	0.27511	0.34643
27	0.99977	4.0868e-002	0.18211	0.33335	0.41472
28	1.0049	4.9001e-002	0.2105	0.39159	0.483
29	1.01	4.9001e-002	0.2105	0.39159	0.483

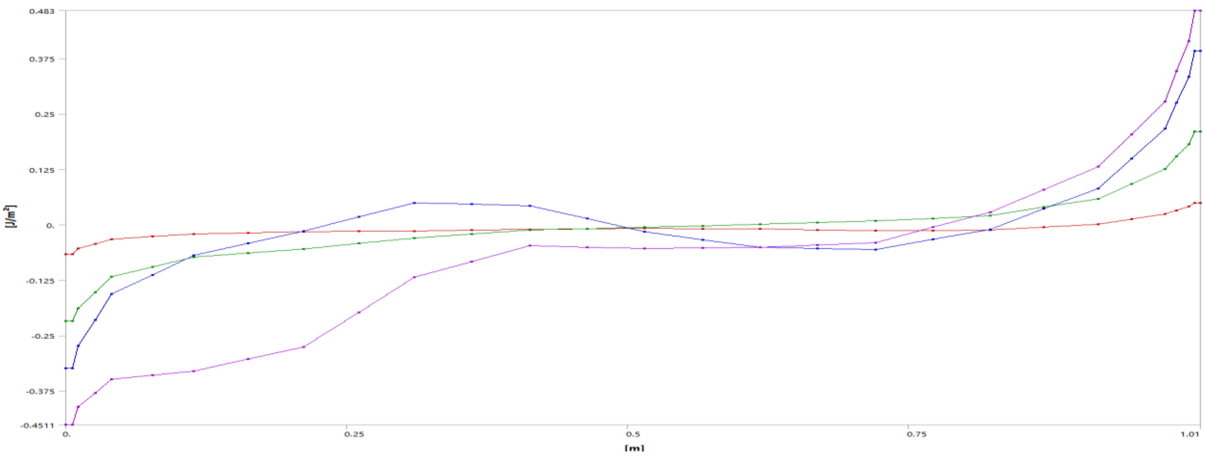

Crack 6 – Stress intensity factors

Crack 6 – SIF, K1

Tabular Data

	Length [m]	SIFS (K1) Contour 1 [Pa·m^(0.5)]	SIFS (K1) Contour 2 [Pa·m^(0.5)]	SIFS (K1) Contour 3 [Pa·m^(0.5)]	SIFS (K1) Contour 4 [Pa·m^(0.5)]
1	0.	2.7954e+005	3.1949e+005	3.2518e+005	3.2874e+005
2	2.9824e-003	2.7954e+005	3.1949e+005	3.2518e+005	3.2874e+005
3	5.9648e-003	3.0498e+005	3.4211e+005	3.4406e+005	3.5303e+005
4	1.376e-002	3.2235e+005	3.5294e+005	3.5388e+005	3.635e+005
5	2.1555e-002	3.3973e+005	3.6376e+005	3.6371e+005	3.7398e+005
6	4.7817e-002	3.2603e+005	3.4447e+005	3.4369e+005	3.5162e+005
7	7.4078e-002	3.1234e+005	3.2517e+005	3.2366e+005	3.2926e+005
8	0.14832	2.9062e+005	3.0146e+005	2.9899e+005	3.0399e+005
9	0.22256	2.6889e+005	2.7776e+005	2.7431e+005	2.7871e+005
10	0.32723	2.5703e+005	2.6617e+005	2.6265e+005	2.6622e+005
11	0.4319	2.4517e+005	2.5458e+005	2.5099e+005	2.5374e+005
12	0.53588	2.3592e+005	2.4464e+005	2.4069e+005	2.4235e+005
13	0.63986	2.2666e+005	2.347e+005	2.3038e+005	2.3096e+005
14	0.75223	2.184e+005	2.2398e+005	2.1963e+005	2.2001e+005
15	0.86461	2.1014e+005	2.1326e+005	2.0888e+005	2.0906e+005
16	0.97699	2.0542e+005	2.0645e+005	2.0287e+005	2.0276e+005
17	1.0894	2.0071e+005	1.9965e+005	1.9687e+005	1.9646e+005
18	1.2017	2.0154e+005	2.0014e+005	1.978e+005	1.9718e+005
19	1.3141	2.0237e+005	2.0063e+005	1.9872e+005	1.9791e+005
20	1.4265	2.0531e+005	2.042e+005	2.0239e+005	2.0163e+005
21	1.5389	2.0825e+005	2.0778e+005	2.0606e+005	2.0535e+005
22	1.6513	2.0568e+005	2.0529e+005	2.0387e+005	2.0313e+005
23	1.7636	2.031e+005	2.028e+005	2.0168e+005	2.0091e+005
24	1.876	1.9677e+005	1.962e+005	1.954e+005	1.9465e+005
25	1.9884	1.9044e+005	1.896e+005	1.8912e+005	1.8838e+005
26	2.1008	1.8725e+005	1.856e+005	1.8547e+005	1.8483e+005
27	2.2131	1.8405e+005	1.8161e+005	1.8182e+005	1.8128e+005
28	2.3255	1.8374e+005	1.7994e+005	1.8033e+005	1.7958e+005
29	2.4379	1.8343e+005	1.7828e+005	1.7883e+005	1.7789e+005
30	2.5503	1.8337e+005	1.7719e+005	1.778e+005	1.763e+005
31	2.6627	1.8331e+005	1.7611e+005	1.7676e+005	1.7472e+005
32	2.775	1.8428e+005	1.7818e+005	1.7889e+005	1.7721e+005
33	2.8874	1.8525e+005	1.8024e+005	1.8102e+005	1.7971e+005
34	2.9998	1.9285e+005	1.9208e+005	1.9231e+005	1.9261e+005
35	3.1122	2.0045e+005	2.0393e+005	2.0361e+005	2.055e+005
36	3.2245	2.1977e+005	2.2909e+005	2.2789e+005	2.3094e+005
37	3.3369	2.3908e+005	2.5426e+005	2.5217e+005	2.5637e+005
38	3.4389	2.667e+005	2.8577e+005	2.8429e+005	2.8918e+005
39	3.5409	2.9433e+005	3.1729e+005	3.1641e+005	3.2199e+005
40	3.6423	3.5229e+005	3.7383e+005	3.741e+005	3.802e+005
41	3.7438	4.1025e+005	4.3037e+005	4.3178e+005	4.384e+005
42	3.8292	5.1377e+005	5.4061e+005	5.4197e+005	5.4897e+005
43	3.9146	6.1729e+005	6.5086e+005	6.5216e+005	6.5953e+005
44	3.9554	6.9784e+005	7.4758e+005	7.5061e+005	7.5855e+005
45	3.9962	7.7838e+005	8.443e+005	8.4906e+005	8.5758e+005
46	4.0353	7.742e+005	8.4203e+005	8.5206e+005	8.5969e+005
47	4.0744	7.7002e+005	8.3976e+005	8.5505e+005	8.6181e+005
48	4.1322	7.1664e+005	7.7792e+005	7.9869e+005	8.0386e+005
49	4.1901	6.6326e+005	7.1609e+005	7.4233e+005	7.4592e+005
50	4.2102	6.1964e+005	6.6771e+005	6.9727e+005	7.0012e+005
51	4.2302	5.7601e+005	6.1934e+005	6.5221e+005	6.5433e+005
52	4.2401	5.3238e+005	5.7096e+005	6.0714e+005	6.0853e+005
53	4.25	5.3238e+005	5.7096e+005	6.0714e+005	6.0853e+005

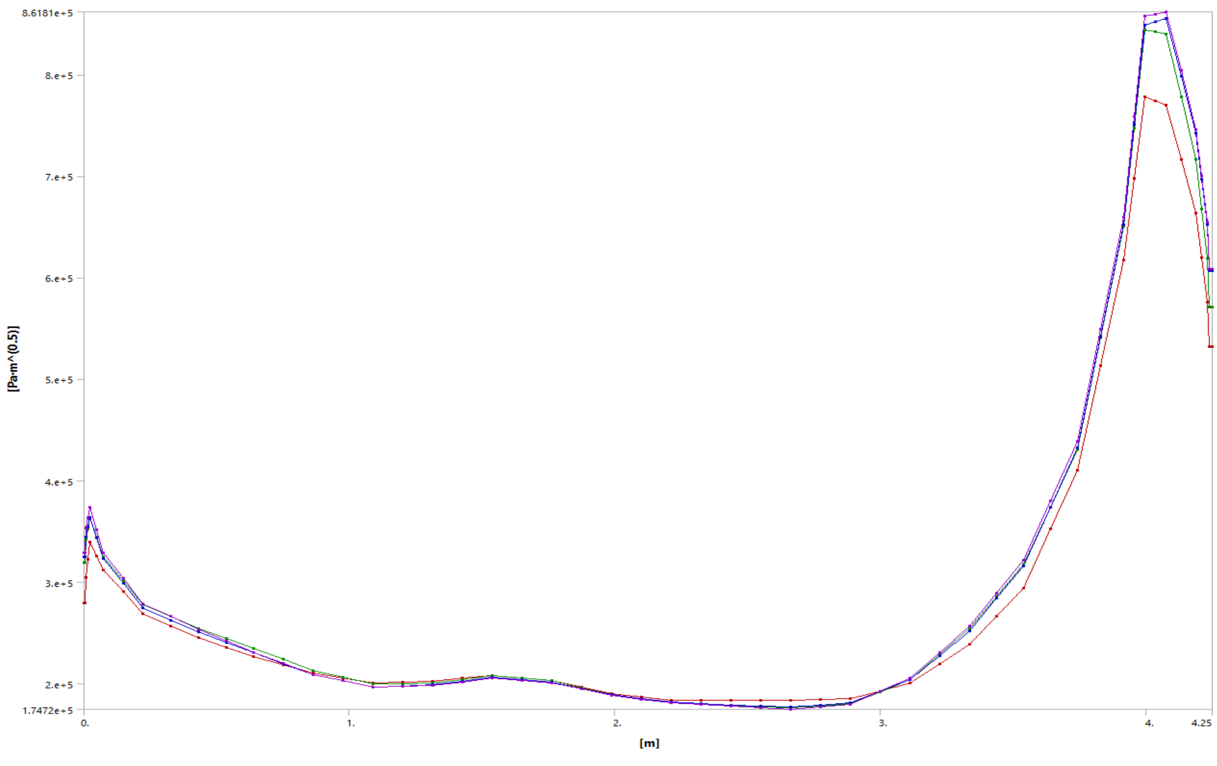

Crack 6 – SIF, K2

Tabular Data

	Length [m]	SIFS (K2) Contour 1 [Pa·m^(0.5)]	SIFS (K2) Contour 2 [Pa·m^(0.5)]	SIFS (K2) Contour 3 [Pa·m^(0.5)]	SIFS (K2) Contour 4 [Pa·m^(0.5)]
1	0.	-70578	-78281	-78995	-76548
2	2.9824e-003	-70578	-78281	-78995	-76548
3	5.9648e-003	-74391	-84960	-86604	-82236
4	1.376e-002	-80813	-92898	-95005	-91256
5	2.1555e-002	-87236	-1.0084e+005	-1.0341e+005	-1.0028e+005
6	4.7817e-002	-98487	-1.1378e+005	-1.1595e+005	-1.1455e+005
7	7.4078e-002	-1.0974e+005	-1.2673e+005	-1.2849e+005	-1.2882e+005
8	0.14832	-1.2336e+005	-1.3839e+005	-1.4111e+005	-1.4186e+005
9	0.22256	-1.3698e+005	-1.5005e+005	-1.5374e+005	-1.5491e+005
10	0.32723	-1.4249e+005	-1.4865e+005	-1.5406e+005	-1.5535e+005
11	0.4319	-1.4801e+005	-1.4724e+005	-1.5439e+005	-1.558e+005
12	0.53588	-1.4465e+005	-1.3935e+005	-1.4647e+005	-1.4801e+005
13	0.63986	-1.4129e+005	-1.3145e+005	-1.3855e+005	-1.4023e+005
14	0.75223	-1.3576e+005	-1.2559e+005	-1.3195e+005	-1.3363e+005
15	0.86461	-1.3022e+005	-1.1974e+005	-1.2535e+005	-1.2703e+005
16	0.97699	-1.2878e+005	-1.199e+005	-1.2481e+005	-1.263e+005
17	1.0894	-1.2734e+005	-1.2007e+005	-1.2426e+005	-1.2557e+005
18	1.2017	-1.3384e+005	-1.2944e+005	-1.3295e+005	-1.3397e+005
19	1.3141	-1.4034e+005	-1.388e+005	-1.4163e+005	-1.4237e+005
20	1.4265	-1.4862e+005	-1.5003e+005	-1.525e+005	-1.5317e+005
21	1.5389	-1.569e+005	-1.6126e+005	-1.6336e+005	-1.6398e+005
22	1.6513	-1.6185e+005	-1.6777e+005	-1.6945e+005	-1.6996e+005
23	1.7636	-1.6681e+005	-1.7428e+005	-1.7554e+005	-1.7594e+005
24	1.876	-1.6489e+005	-1.7201e+005	-1.7293e+005	-1.7302e+005
25	1.9884	-1.6296e+005	-1.6974e+005	-1.7032e+005	-1.701e+005
26	2.1008	-1.5367e+005	-1.5941e+005	-1.5995e+005	-1.5952e+005
27	2.2131	-1.4437e+005	-1.4907e+005	-1.4958e+005	-1.4894e+005
28	2.3255	-1.3256e+005	-1.3646e+005	-1.3699e+005	-1.3642e+005
29	2.4379	-1.2075e+005	-1.2384e+005	-1.2441e+005	-1.239e+005
30	2.5503	-1.1092e+005	-1.1264e+005	-1.1311e+005	-1.1324e+005
31	2.6627	-1.0108e+005	-1.0144e+005	-1.0182e+005	-1.0259e+005
32	2.775	-1.03e+005	-1.0174e+005	-1.0218e+005	-1.0335e+005
33	2.8874	-1.0492e+005	-1.0204e+005	-1.0253e+005	-1.0411e+005
34	2.9998	-1.1749e+005	-1.1466e+005	-1.1417e+005	-1.1361e+005
35	3.1122	-1.3005e+005	-1.2727e+005	-1.258e+005	-1.2311e+005
36	3.2245	-1.3546e+005	-1.3348e+005	-1.2984e+005	-1.2505e+005
37	3.3369	-1.4087e+005	-1.3968e+005	-1.3388e+005	-1.27e+005
38	3.4389	-1.3328e+005	-1.3135e+005	-1.2418e+005	-1.1907e+005
39	3.5409	-1.2568e+005	-1.2302e+005	-1.1449e+005	-1.1114e+005
40	3.6423	-1.2927e+005	-1.2541e+005	-1.1705e+005	-1.1441e+005
41	3.7438	-1.3286e+005	-1.278e+005	-1.1962e+005	-1.1768e+005
42	3.8292	-1.6666e+005	-1.6057e+005	-1.5381e+005	-1.4979e+005
43	3.9146	-2.0046e+005	-1.9334e+005	-1.88e+005	-1.8189e+005
44	3.9554	-2.3088e+005	-2.2369e+005	-2.2028e+005	-2.1352e+005
45	3.9962	-2.613e+005	-2.5405e+005	-2.5256e+005	-2.4516e+005
46	4.0353	-2.5386e+005	-2.4919e+005	-2.4879e+005	-2.4239e+005
47	4.0744	-2.4642e+005	-2.4433e+005	-2.4502e+005	-2.3961e+005
48	4.1322	-2.2074e+005	-2.2226e+005	-2.2196e+005	-2.1879e+005
49	4.1901	-1.9506e+005	-2.0018e+005	-1.989e+005	-1.9797e+005
50	4.2102	-1.7708e+005	-1.8462e+005	-1.8169e+005	-1.8307e+005
51	4.2302	-1.591e+005	-1.6907e+005	-1.6449e+005	-1.6818e+005
52	4.2401	-1.4113e+005	-1.5351e+005	-1.4728e+005	-1.5328e+005
53	4.25	-1.4113e+005	-1.5351e+005	-1.4728e+005	-1.5328e+005

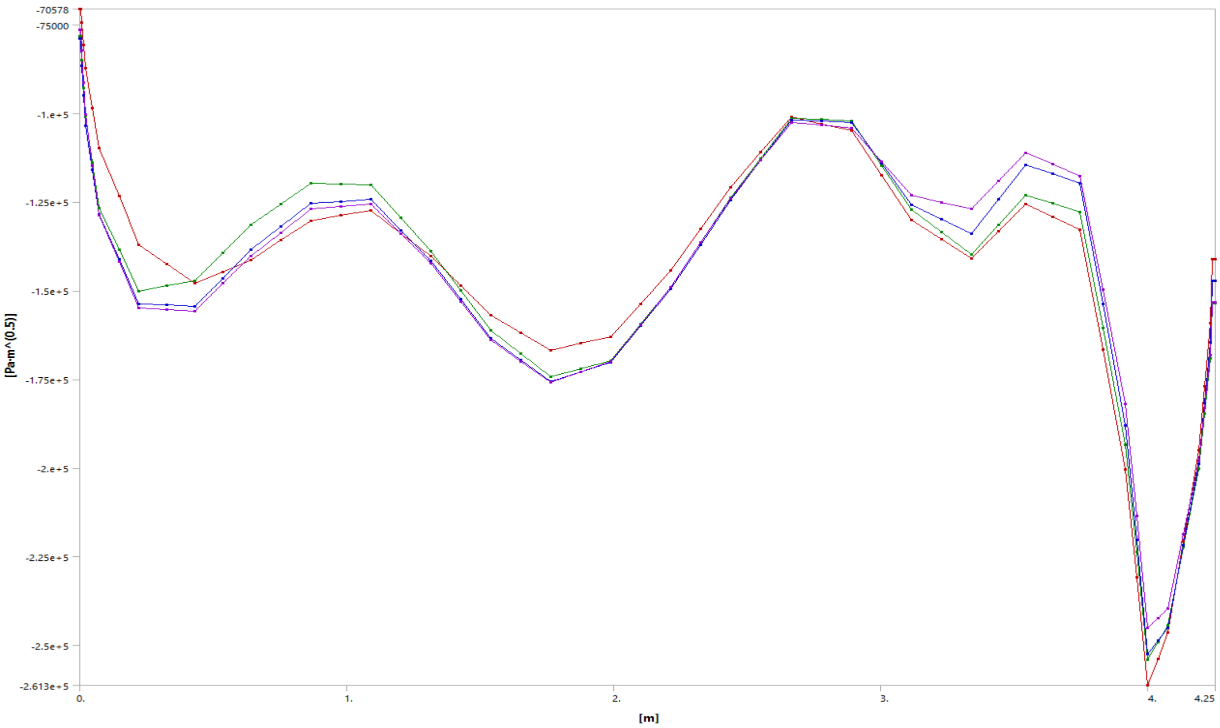

Crack 6 – SIF, K3

Tabular Data

	Length [m]	SIFS (K3) Contour 1 [Pa·m^(0.5)]	SIFS (K3) Contour 2 [Pa·m^(0.5)]	SIFS (K3) Contour 3 [Pa·m^(0.5)]	SIFS (K3) Contour 4 [Pa·m^(0.5)]
1	0.	-1.3164e+005	-1.297e+005	-1.3485e+005	-1.3781e+005
2	2.9824e-003	-1.3164e+005	-1.297e+005	-1.3485e+005	-1.3781e+005
3	5.9648e-003	-1.4556e+005	-1.4456e+005	-1.4728e+005	-1.4958e+005
4	1.376e-002	-1.5206e+005	-1.5366e+005	-1.5617e+005	-1.5686e+005
5	2.1555e-002	-1.5857e+005	-1.6276e+005	-1.6506e+005	-1.6415e+005
6	4.7817e-002	-1.4424e+005	-1.4994e+005	-1.5287e+005	-1.5155e+005
7	7.4078e-002	-1.299e+005	-1.3713e+005	-1.4069e+005	-1.3895e+005
8	0.14832	-1.0682e+005	-1.1286e+005	-1.163e+005	-1.1466e+005
9	0.22256	-83739	-88598	-91906	-90365
10	0.32723	-62979	-66510	-69932	-68082
11	0.4319	-42219	-44421	-47958	-45799
12	0.53588	-23560	-25245	-28303	-26727
13	0.63986	-4901.2	-6069.4	-8648.5	-7654.7
14	0.75223	8437.8	7860.4	6269.4	6636.4
15	0.86461	21777	21790	21187	20928
16	0.97699	26552	26755	26456	26329
17	1.0894	31326	31720	31725	31730
18	1.2017	30069	30304	30274	30277
19	1.3141	28812	28888	28822	28823
20	1.4265	24827	24942	24910	24830
21	1.5389	20841	20996	20997	20838
22	1.6513	14644	14649	14684	14553
23	1.7636	8447.2	8301.4	8370.	8266.9
24	1.876	1775.5	1268.	1208.6	1053.7
25	1.9884	-4896.3	-5765.4	-5952.7	-6159.5
26	2.1008	-10097	-11000	-11344	-11370
27	2.2131	-15298	-16234	-16736	-16580
28	2.3255	-20611	-21450	-21895	-21392
29	2.4379	-25923	-26666	-27054	-26203
30	2.5503	-31134	-31956	-32344	-31497
31	2.6627	-36345	-37246	-37635	-36792
32	2.775	-37271	-38007	-38390	-37584
33	2.8874	-38197	-38768	-39145	-38376
34	2.9998	-31706	-32467	-32971	-31951
35	3.1122	-25215	-26167	-26796	-25527
36	3.2245	-10208	-10779	-11856	-10543
37	3.3369	4799.	4609.4	3085.2	4440.4
38	3.4389	24840	26619	24895	26419
39	3.5409	44880	48629	46705	48398
40	3.6423	69823	74686	72786	74382
41	3.7438	94767	1.0074e+005	98868	1.0037e+005
42	3.8292	1.211e+005	1.2758e+005	1.2604e+005	1.2654e+005
43	3.9146	1.4744e+005	1.5441e+005	1.532e+005	1.5272e+005
44	3.9554	1.5905e+005	1.6635e+005	1.6618e+005	1.6532e+005
45	3.9962	1.7067e+005	1.7829e+005	1.7915e+005	1.7792e+005
46	4.0353	1.637e+005	1.6963e+005	1.7043e+005	1.7018e+005
47	4.0744	1.5674e+005	1.6096e+005	1.6171e+005	1.6243e+005
48	4.1322	1.4229e+005	1.4386e+005	1.421e+005	1.4433e+005
49	4.1901	1.2785e+005	1.2676e+005	1.2249e+005	1.2623e+005
50	4.2102	1.1642e+005	1.1356e+005	1.0664e+005	1.1157e+005
51	4.2302	1.05e+005	1.0037e+005	90795	96909
52	4.2401	93584	87171	74949	82246
53	4.25	93584	87171	74949	82246

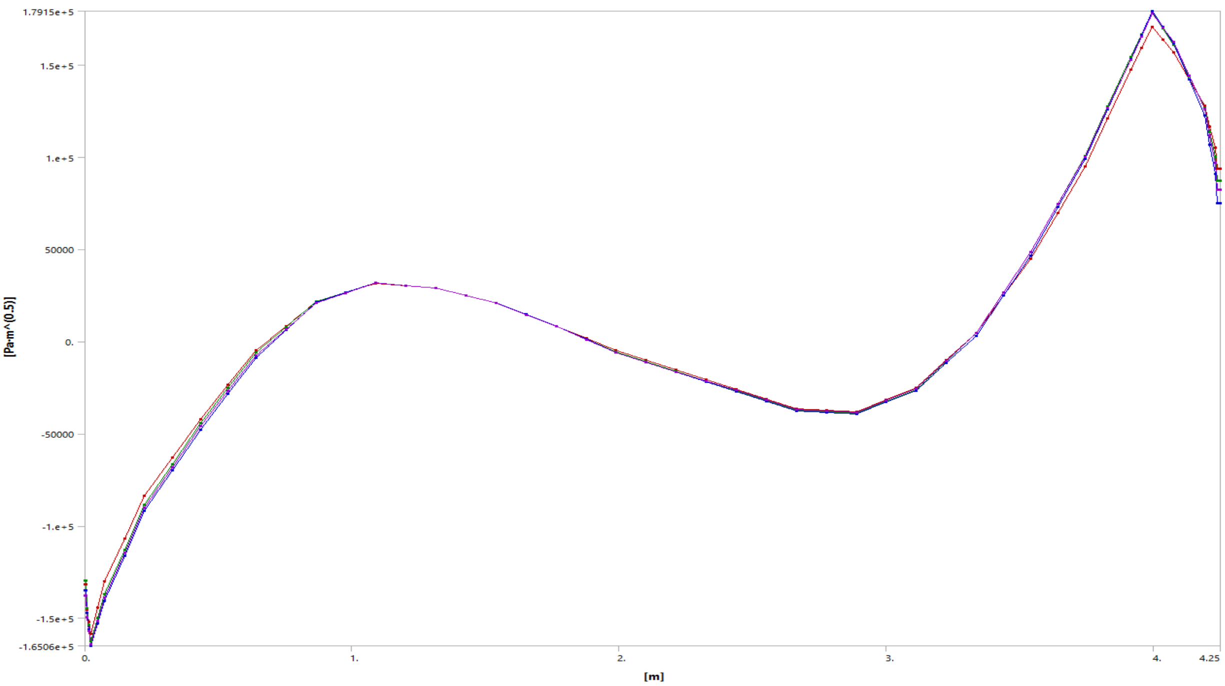

Crack 6 – J-Integral

Tabular Data

	Length [m]	J-Integral (JINT) Contour 1 [J/m²]	J-Integral (JINT) Contour 2 [J/m²]	J-Integral (JINT) Contour 3 [J/m²]	J-Integral (JINT) Contour 4 [J/m²]
1	0.	1.2895	3.7331	4.1088	3.838
2	2.9824e-003	1.2895	3.7331	4.1088	3.838
3	5.9648e-003	0.7017	3.0237	3.7731	3.2438
4	1.376e-002	-0.31168	3.2119	4.3508	3.8303
5	2.1555e-002	-1.3251	3.4	4.9284	4.4168
6	4.7817e-002	-0.75958	5.7006	7.3223	7.5482
7	7.4078e-002	-0.19411	8.0012	9.7162	10.68
8	0.14832	1.2383	8.8029	10.668	12.349
9	0.22256	2.6707	9.6045	11.621	14.018
10	0.32723	2.0396	6.7847	9.0742	11.88
11	0.4319	1.4084	3.9649	6.5279	9.7425
12	0.53588	-0.39069	1.1857	3.9302	6.9082
13	0.63986	-2.1898	-1.5934	1.3324	4.0739
14	0.75223	-2.363	-1.8302	1.3756	3.7814
15	0.86461	-2.5361	-2.0671	1.4189	3.489
16	0.97699	-1.4119	-1.2158	2.1115	4.0465
17	1.0894	-0.2876	-0.36445	2.8041	4.6041
18	1.2017	0.37623	0.30976	2.7062	4.1606
19	1.3141	1.0401	0.98396	2.6082	3.7171
20	1.4265	1.2589	1.5596	2.4841	3.3803
21	1.5389	1.4777	2.1352	2.36	3.0436
22	1.6513	1.7671	2.5993	2.4274	2.9197
23	1.7636	2.0565	3.0633	2.4947	2.7959
24	1.876	1.824	2.6522	1.9851	1.9741
25	1.9884	1.5914	2.241	1.4755	1.1523
26	2.1008	0.76817	0.98234	0.34016	-0.10322
27	2.2131	-5.5094e-002	-0.27635	-0.79514	-1.3588
28	2.3255	-1.1687	-1.6531	-1.8697	-2.337
29	2.4379	-2.2824	-3.0299	-2.9444	-3.3152
30	2.5503	-3.4276	-3.9749	-3.4068	-3.5729
31	2.6627	-4.5728	-4.9199	-3.8693	-3.8307
32	2.775	-4.6709	-4.625	-3.3794	-3.2872
33	2.8874	-4.769	-4.3301	-2.8896	-2.7437
34	2.9998	-3.7421	-2.4333	-2.045	-3.4946
35	3.1122	-2.7151	-0.53656	-1.2004	-4.2454
36	3.2245	-1.39	2.2402	-0.16768	-4.8584
37	3.3369	-6.5e-002	5.017	0.86505	-5.4713
38	3.4389	0.90275	6.4802	1.3781	-3.278
39	3.5409	1.8705	7.9433	1.8911	-1.0846
40	3.6423	3.8026	8.9214	2.9204	1.0454
41	3.7438	5.7347	9.8994	3.9497	3.1753
42	3.8292	10.385	14.532	9.7649	7.4165
43	3.9146	15.036	19.165	15.58	11.658
44	3.9554	18.217	23.688	21.362	16.93
45	3.9962	21.398	28.212	27.144	22.203
46	4.0353	19.216	25.547	25.32	21.21
47	4.0744	17.033	22.882	23.496	20.217
48	4.1322	13.079	16.833	18.98	16.88
49	4.1901	9.126	10.784	14.465	13.544
50	4.2102	6.719	6.9375	12.124	12.261
51	4.2302	4.3121	3.0906	9.7832	10.978
52	4.2401	1.9051	-0.75631	7.4425	9.6944
53	4.25	1.9051	-0.75631	7.4425	9.6944

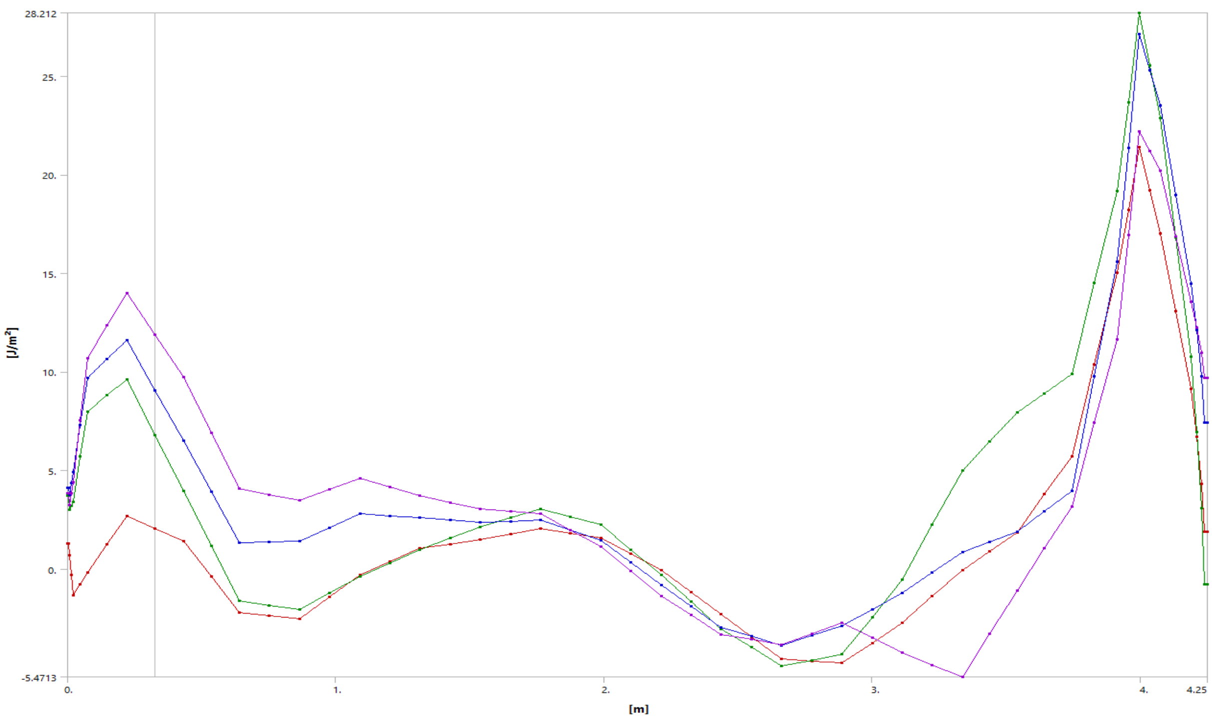

Crack 7 – Stress intensity factors

Crack 7 – SIF, K1

Tabular Data

	Length [m]	SIFS (K1) Contour 1 [Pa·m^(0.5)]	SIFS (K1) Contour 2 [Pa·m^(0.5)]	SIFS (K1) Contour 3 [Pa·m^(0.5)]	SIFS (K1) Contour 4 [Pa·m^(0.5)]
1	0.	1.0792e+005	1.0727e+005	1.1116e+005	1.1352e+005
2	4.9873e-003	1.0792e+005	1.0727e+005	1.1116e+005	1.1352e+005
3	9.9755e-003	1.1484e+005	1.1667e+005	1.2006e+005	1.227e+005
4	2.0276e-002	1.2434e+005	1.288e+005	1.3184e+005	1.3436e+005
5	3.0579e-002	1.3385e+005	1.4094e+005	1.4362e+005	1.4602e+005
6	4.531e-002	1.409e+005	1.5062e+005	1.5298e+005	1.5496e+005
7	6.0043e-002	1.4795e+005	1.603e+005	1.6235e+005	1.6389e+005
8	7.5461e-002	1.5156e+005	1.6535e+005	1.6706e+005	1.6816e+005
9	9.0881e-002	1.5517e+005	1.704e+005	1.7178e+005	1.7243e+005
10	0.10621	1.5461e+005	1.6874e+005	1.7043e+005	1.71e+005
11	0.12154	1.5406e+005	1.6708e+005	1.6907e+005	1.6958e+005
12	0.13672	1.474e+005	1.5772e+005	1.6099e+005	1.6148e+005
13	0.1519	1.4073e+005	1.4836e+005	1.5291e+005	1.5337e+005
14	0.1666	1.3128e+005	1.3668e+005	1.4241e+005	1.4243e+005
15	0.18129	1.2183e+005	1.25e+005	1.3191e+005	1.3148e+005
16	0.19094	1.1505e+005	1.1709e+005	1.2453e+005	1.2365e+005
17	0.20059	1.0827e+005	1.0918e+005	1.1714e+005	1.1581e+005
18	0.20529	1.0149e+005	1.0126e+005	1.0976e+005	1.0798e+005
19	0.21	1.0149e+005	1.0126e+005	1.0976e+005	1.0798e+005

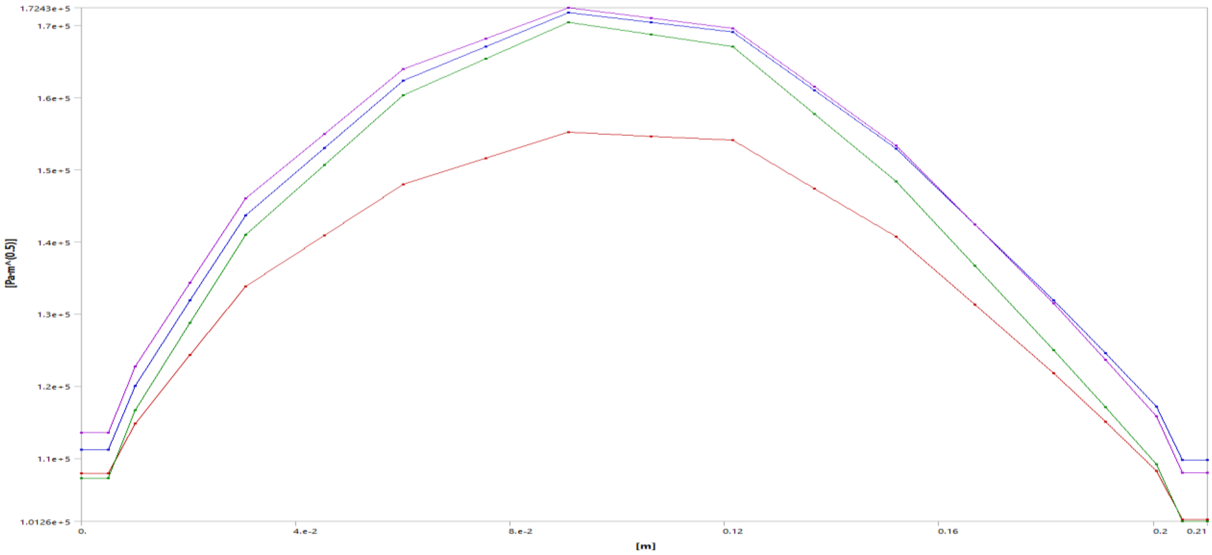

Crack 7 – SIF, K2

Tabular Data

	Length [m]	SIFS (K2) Contour 1 [Pa·m^(0.5)]	SIFS (K2) Contour 2 [Pa·m^(0.5)]	SIFS (K2) Contour 3 [Pa·m^(0.5)]	SIFS (K2) Contour 4 [Pa·m^(0.5)]
1	0.	-3420.2	-4043.3	-3587.5	-5175.4
2	4.9873e-003	-3420.2	-4043.3	-3587.5	-5175.4
3	9.9755e-003	-1774.9	-2034.3	-1709.4	-2906.
4	2.0276e-002	-1085.2	-729.81	-507.85	-1293.1
5	3.0579e-002	-395.42	574.72	693.73	319.74
6	4.531e-002	-654.42	515.11	475.93	272.38
7	6.0043e-002	-913.42	455.5	258.13	225.01
8	7.5461e-002	-808.29	544.62	88.976	10.404
9	9.0881e-002	-703.16	633.75	-80.177	-204.2
10	0.10621	-359.92	1375.7	429.04	182.12
11	0.12154	-16.678	2117.7	938.25	568.45
12	0.13672	549.08	2960.2	1644.8	1304.7
13	0.1519	1114.8	3802.7	2351.3	2041.
14	0.1666	2049.8	4367.6	2869.2	2798.6
15	0.18129	2984.7	4932.6	3387.	3556.2
16	0.19094	3728.2	5193.3	3641.4	4030.5
17	0.20059	4471.6	5454.	3895.8	4504.8
18	0.20529	5215.1	5714.8	4150.1	4979.2
19	0.21	5215.1	5714.8	4150.1	4979.2

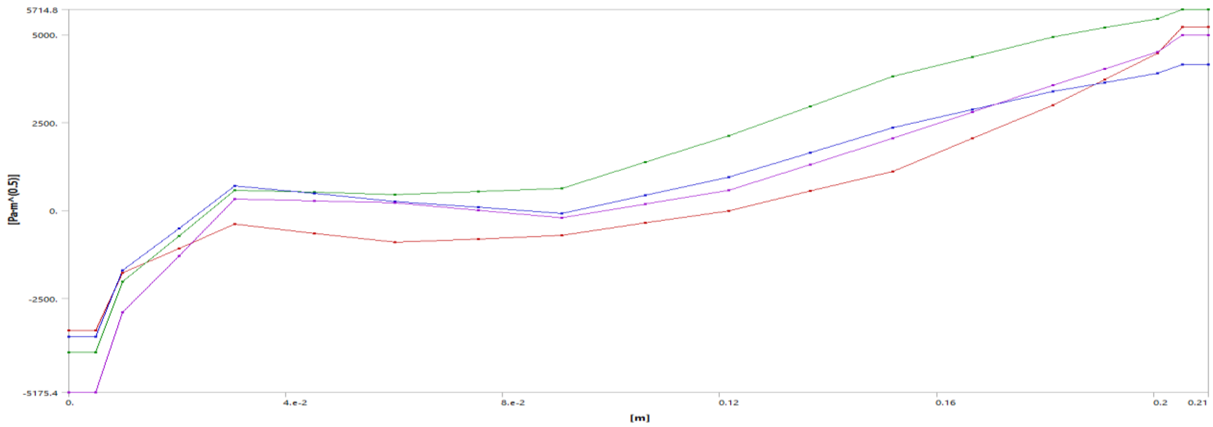

Crack 7 – SIF, K3

Tabular Data

	Length [m]	SIFS (K3) Contour 1 [Pa·m^(0.5)]	SIFS (K3) Contour 2 [Pa·m^(0.5)]	SIFS (K3) Contour 3 [Pa·m^(0.5)]	SIFS (K3) Contour 4 [Pa·m^(0.5)]
1	0.	25119	21142	20152	20925
2	4.9873e-003	25119	21142	20152	20925
3	9.9755e-003	28178	24761	24091	24700
4	2.0276e-002	32899	30121	29697	30173
5	3.0579e-002	37620	35482	35302	35645
6	4.531e-002	42483	40884	40832	41155
7	6.0043e-002	47345	46286	46362	46666
8	7.5461e-002	52041	51227	51383	51740
9	9.0881e-002	56736	56167	56404	56814
10	0.10621	60572	59534	59897	60334
11	0.12154	64408	62901	63389	63853
12	0.13672	65444	63140	63955	64432
13	0.1519	66479	63380	64521	65012
14	0.1666	64993	61510	63038	63574
15	0.18129	63507	59640	61555	62135
16	0.19094	61910	57971	60128	60751
17	0.20059	60313	56302	58702	59366
18	0.20529	58717	54633	57275	57981
19	0.21	58717	54633	57275	57981

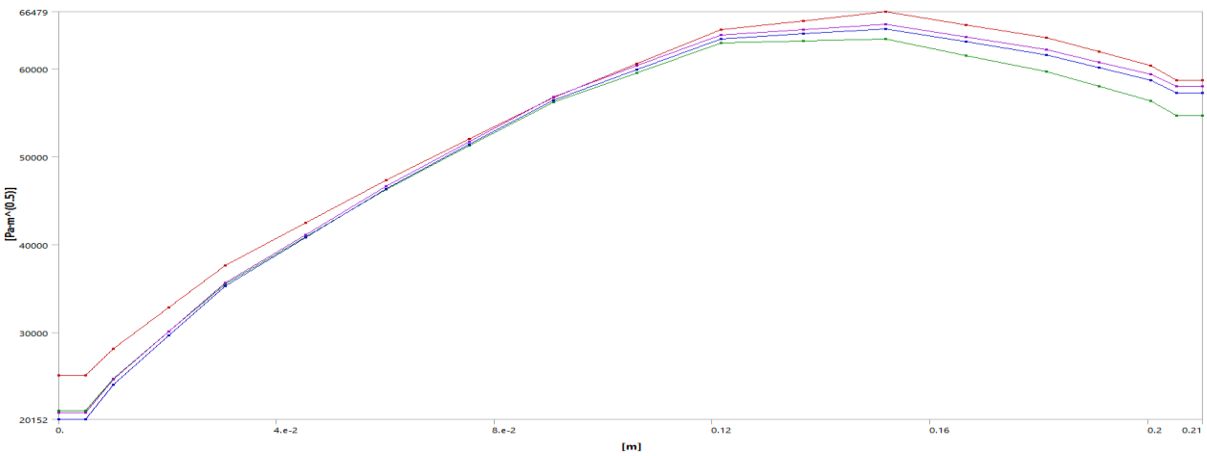

Crack 7 – J-Integral

Tabular Data

	Length [m]	J-Integral (JINT) Contour 1 [J/m²]	J-Integral (JINT) Contour 2 [J/m²]	J-Integral (JINT) Contour 3 [J/m²]	J-Integral (JINT) Contour 4 [J/m²]
1	0.	-0.38465	-0.28879	-0.19773	-0.12156
2	4.9873e-003	-0.38465	-0.28879	-0.19773	-0.12156
3	9.9755e-003	-0.43464	-0.22269	-0.13955	-6.6695e-002
4	2.0276e-002	-0.41707	-6.288e-002	1.4305e-002	8.0821e-002
5	3.0579e-002	-0.3995	9.6931e-002	0.16816	0.22834
6	4.531e-002	-0.35759	0.29469	0.36117	0.41352
7	6.0043e-002	-0.31568	0.49245	0.55419	0.59871
8	7.5461e-002	-0.25326	0.61773	0.67574	0.70995
9	9.0881e-002	-0.19083	0.74302	0.79728	0.82119
10	0.10621	-0.12918	0.70952	0.76946	0.78997
11	0.12154	-6.7534e-002	0.67602	0.74165	0.75875
12	0.13672	-6.5699e-002	0.5313	0.6195	0.63952
13	0.1519	-6.3864e-002	0.38657	0.49736	0.52029
14	0.1666	-7.8477e-002	0.26571	0.40139	0.42153
15	0.18129	-9.3091e-002	0.14486	0.30541	0.32277
16	0.19094	-9.4493e-002	8.4573e-002	0.25934	0.27144
17	0.20059	-9.5896e-002	2.429e-002	0.21326	0.22011
18	0.20529	-9.7298e-002	-3.5993e-002	0.16719	0.16878
19	0.21	-9.7298e-002	-3.5993e-002	0.16719	0.16878

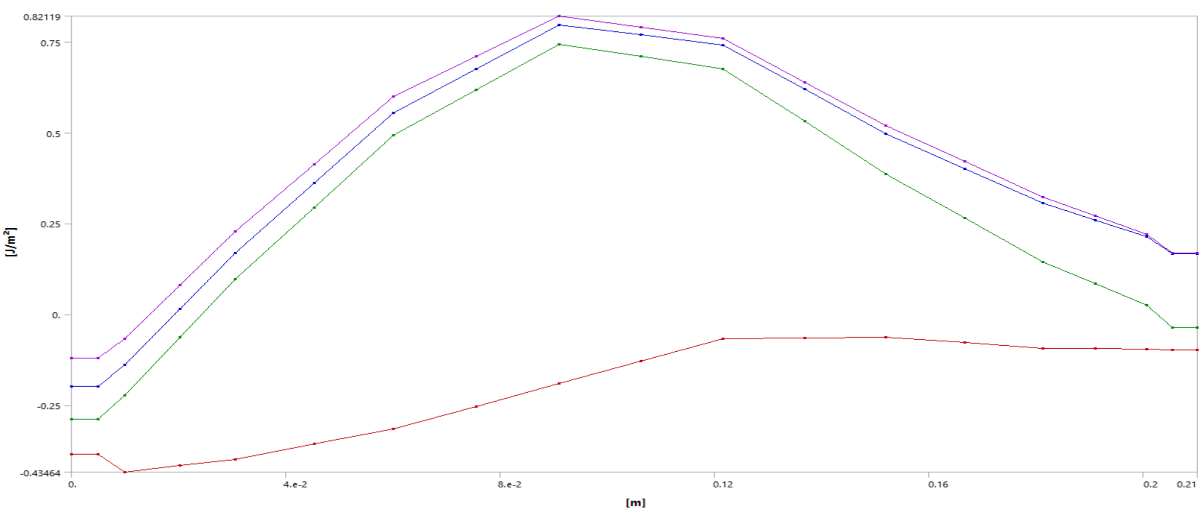

All Cracks – Stress intensity factors

All Cracks – SIF, K1

Tabular Data

	Length [m]	SIFS (K1) Contour 1 [Pa·m^(0.5)]	SIFS (K1) Contour 2 [Pa·m^(0.5)]	SIFS (K1) Contour 3 [Pa·m^(0.5)]	SIFS (K1) Contour 4 [Pa·m^(0.5)]	Crack Front Number
1	0.	-6.1491e+005	-6.6795e+005	-6.8059e+005	-6.9293e+005	1
2	9.5153e-003	-6.1491e+005	-6.6795e+005	-6.8059e+005	-6.9293e+005	1
3	1.9031e-002	-6.2348e+005	-6.7476e+005	-6.8849e+005	-6.9633e+005	1
4	3.7929e-002	-6.2886e+005	-6.8157e+005	-6.9503e+005	-6.9893e+005	1
5	5.6827e-002	-6.3424e+005	-6.8838e+005	-7.0158e+005	-7.0153e+005	1
6	8.778e-002	-6.3982e+005	-6.9667e+005	-7.0691e+005	-7.0521e+005	1
7	0.11873	-6.454e+005	-7.0496e+005	-7.1225e+005	-7.0889e+005	1
8	0.15202	-6.5757e+005	-7.197e+005	-7.2349e+005	-7.205e+005	1
9	0.18531	-6.6975e+005	-7.3445e+005	-7.3473e+005	-7.321e+005	1
10	0.22014	-6.8205e+005	-7.4793e+005	-7.4608e+005	-7.4456e+005	1
11	0.25497	-6.9436e+005	-7.6141e+005	-7.5742e+005	-7.5702e+005	1
12	0.2898	-7.0072e+005	-7.6406e+005	-7.5919e+005	-7.5967e+005	1
13	0.32463	-7.0708e+005	-7.6671e+005	-7.6095e+005	-7.6233e+005	1
14	0.35946	-7.1122e+005	-7.6517e+005	-7.5827e+005	-7.6032e+005	1
15	0.39429	-7.1536e+005	-7.6363e+005	-7.5558e+005	-7.583e+005	1
16	0.42912	-7.1989e+005	-7.6467e+005	-7.5593e+005	-7.5816e+005	1
17	0.46395	-7.2441e+005	-7.6572e+005	-7.5628e+005	-7.5801e+005	1
18	0.49878	-7.1992e+005	-7.6014e+005	-7.5266e+005	-7.5277e+005	1
19	0.53361	-7.1542e+005	-7.5457e+005	-7.4904e+005	-7.4753e+005	1
20	0.56537	-6.9806e+005	-7.377e+005	-7.3545e+005	-7.3253e+005	1
21	0.59712	-6.8069e+005	-7.2083e+005	-7.2186e+005	-7.1752e+005	1
22	0.61476	-6.646e+005	-7.0543e+005	-7.0876e+005	-7.0361e+005	1
23	0.63239	-6.485e+005	-6.9004e+005	-6.9566e+005	-6.8969e+005	1
24	0.6412	-6.324e+005	-6.7465e+005	-6.8256e+005	-6.7578e+005	1
25	0.65	-6.324e+005	-6.7465e+005	-6.8256e+005	-6.7578e+005	1

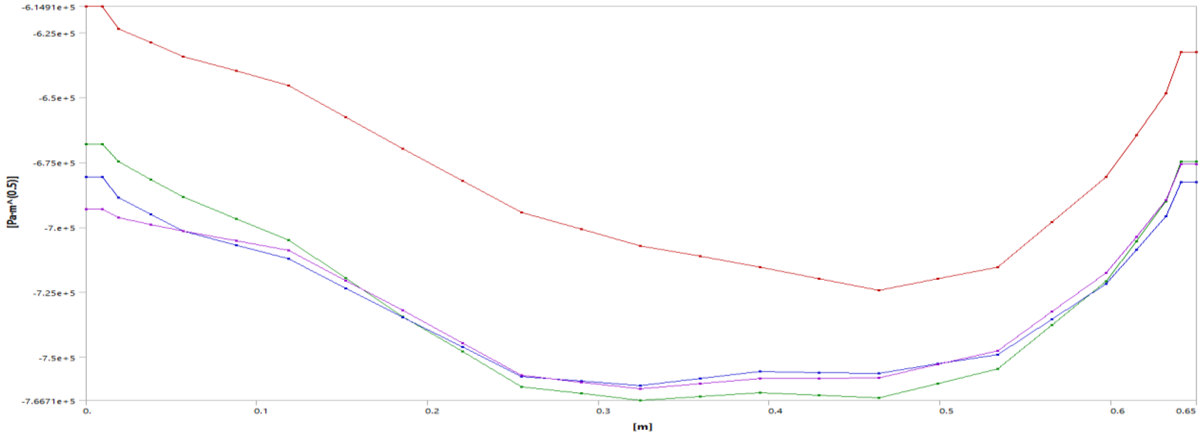

All Cracks – SIF, K2

Tabular Data

	Length [m]	SIFS (K2) Contour 1 [Pa·m^(0.5)]	SIFS (K2) Contour 2 [Pa·m^(0.5)]	SIFS (K2) Contour 3 [Pa·m^(0.5)]	SIFS (K2) Contour 4 [Pa·m^(0.5)]	Crack Front Number
1	0.	-62626	-53376	-53980	-48227	1
2	9.5153e-003	-62626	-53376	-53980	-48227	1
3	1.9031e-002	-60634	-51260	-49578	-44688	1
4	3.7929e-002	-58871	-49042	-45270	-41011	1
5	5.6827e-002	-57109	-46824	-40961	-37333	1
6	8.778e-002	-57421	-46387	-41110	-37709	1
7	0.11873	-57733	-45950	-41259	-38086	1
8	0.15202	-59356	-47960	-45680	-41793	1
9	0.18531	-60978	-49970	-50102	-45500	1
10	0.22014	-61764	-53219	-54971	-49340	1
11	0.25497	-62550	-56467	-59841	-53180	1
12	0.2898	-62025	-58353	-61434	-55127	1
13	0.32463	-61499	-60238	-63027	-57074	1
14	0.35946	-64019	-64134	-65846	-60910	1
15	0.39429	-66539	-68030	-68666	-64747	1
16	0.42912	-72601	-79090	-79475	-75999	1
17	0.46395	-78663	-90151	-90285	-87251	1
18	0.49878	-80832	-1.0129e+005	-99807	-96612	1
19	0.53361	-83000	-1.1243e+005	-1.0933e+005	-1.0597e+005	1
20	0.56537	-80719	-1.1472e+005	-1.075e+005	-1.0334e+005	1
21	0.59712	-78438	-1.1702e+005	-1.0567e+005	-1.007e+005	1
22	0.61476	-76378	-1.1504e+005	-1.0015e+005	-94343	1
23	0.63239	-74318	-1.1306e+005	-94624	-87983	1
24	0.6412	-72258	-1.1108e+005	-89102	-81624	1
25	0.65	-72258	-1.1108e+005	-89102	-81624	1

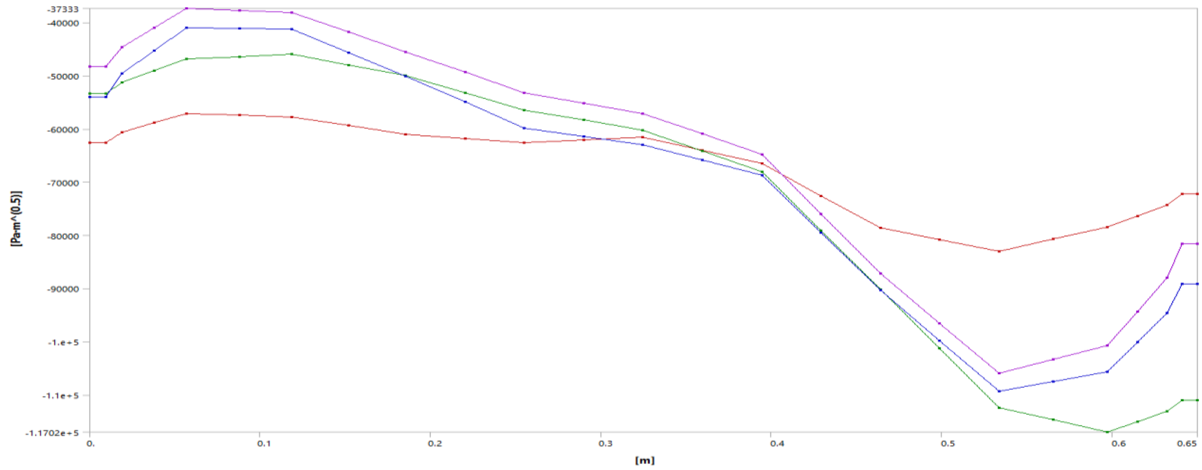

All Cracks – SIF, K3

Tabular Data

	Length [m]	SIFS (K3) Contour 1 [Pa·m^(0.5)]	SIFS (K3) Contour 2 [Pa·m^(0.5)]	SIFS (K3) Contour 3 [Pa·m^(0.5)]	SIFS (K3) Contour 4 [Pa·m^(0.5)]	Crack Front Number
1	0.	16288	21895	20483	27031	1
2	9.5153e-003	16288	21895	20483	27031	1
3	1.9031e-002	17180	21226	19553	24817	1
4	3.7929e-002	18171	20862	19121	23124	1
5	5.6827e-002	19161	20499	18689	21432	1
6	8.778e-002	19536	20349	18786	20564	1
7	0.11873	19910	20199	18882	19697	1
8	0.15202	19438	19578	18880	19258	1
9	0.18531	18965	18957	18878	18818	1
10	0.22014	18435	18328	18771	18741	1
11	0.25497	17905	17700	18665	18664	1
12	0.2898	17458	17250	18266	18287	1
13	0.32463	17011	16799	17867	17910	1
14	0.35946	16266	16040	16965	16950	1
15	0.39429	15521	15281	16064	15990	1
16	0.42912	14733	14528	15244	15094	1
17	0.46395	13945	13775	14424	14198	1
18	0.49878	12732	12583	13239	13050	1
19	0.53361	11518	11391	12054	11901	1
20	0.56537	9856.6	9553.7	9970.4	10070	1
21	0.59712	8195.4	7716.5	7886.8	8239.9	1
22	0.61476	6976.7	6302.1	6114.5	6722.8	1
23	0.63239	5758.	4887.7	4342.2	5205.7	1
24	0.6412	4539.2	3473.2	2569.9	3688.6	1
25	0.65	4539.2	3473.2	2569.9	3688.6	1

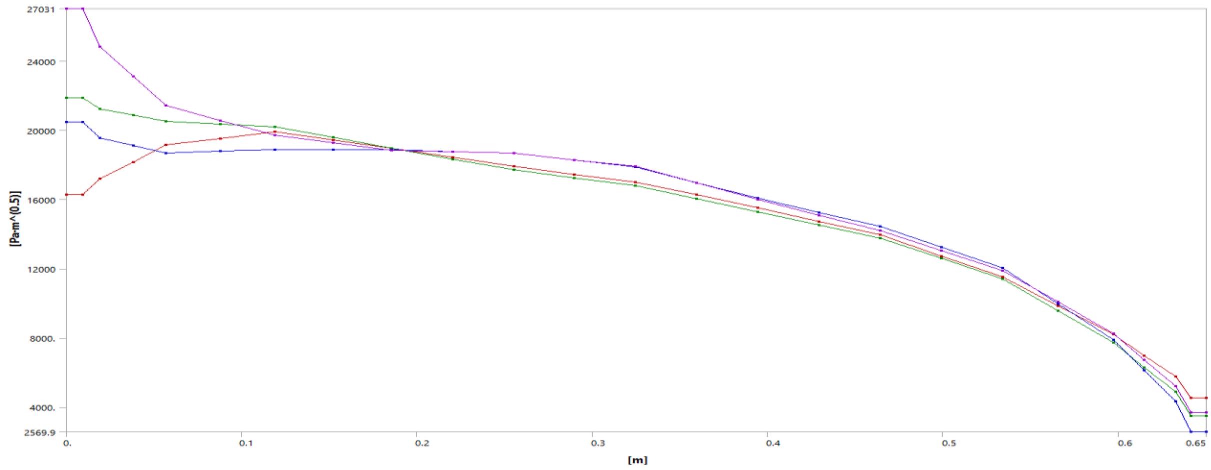

All Cracks – J-Integral

Tabular Data

	Length [m]	J-Integral (JINT) Contour 1 [J/m²]	J-Integral (JINT) Contour 2 [J/m²]	J-Integral (JINT) Contour 3 [J/m²]	J-Integral (JINT) Contour 4 [J/m²]	Crack Front Number
1	0.	4.5684	8.5242	10.631	7.6001	1
2	9.5153e-003	4.5684	8.5242	10.631	7.6001	1
3	1.9031e-002	4.8663	9.8956	10.988	8.6816	1
4	3.7929e-002	4.2707	10.478	10.406	8.2936	1
5	5.6827e-002	3.6752	11.06	9.8245	7.9056	1
6	8.778e-002	3.0117	11.347	10.04	8.0633	1
7	0.11873	2.3483	11.634	10.256	8.2211	1
8	0.15202	2.6175	13.623	12.985	10.644	1
9	0.18531	2.8866	15.612	15.715	13.066	1
10	0.22014	3.4859	17.881	18.217	15.344	1
11	0.25497	4.0851	20.151	20.72	17.621	1
12	0.2898	4.5763	21.26	21.145	18.685	1
13	0.32463	5.0676	22.369	21.57	19.748	1
14	0.35946	6.3663	23.357	21.855	20.726	1
15	0.39429	7.665	24.345	22.141	21.704	1
16	0.42912	9.5997	24.92	22.634	22.135	1
17	0.46395	11.534	25.495	23.128	22.565	1
18	0.49878	11.362	23.893	21.126	20.298	1
19	0.53361	11.189	22.292	19.124	18.031	1
20	0.56537	8.2417	18.396	13.999	12.765	1
21	0.59712	5.2948	14.501	8.8739	7.4997	1
22	0.61476	2.4906	11.049	4.312	2.8358	1
23	0.63239	-0.31364	7.5972	-0.24985	-1.828	1
24	0.6412	-3.1178	4.1452	-4.8117	-6.4919	1
25	0.65	-3.1178	4.1452	-4.8117	-6.4919	1

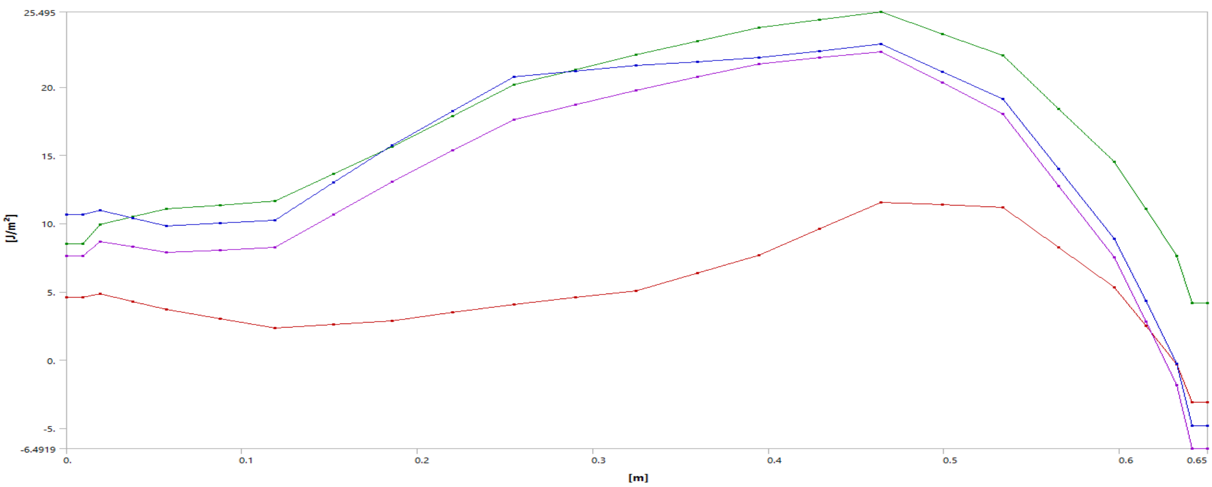

9.4 Appendix D: Mode Shapes

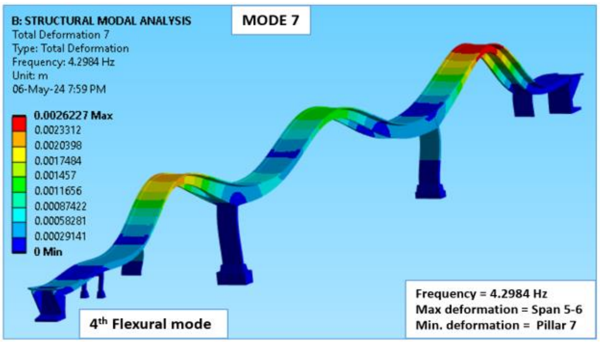

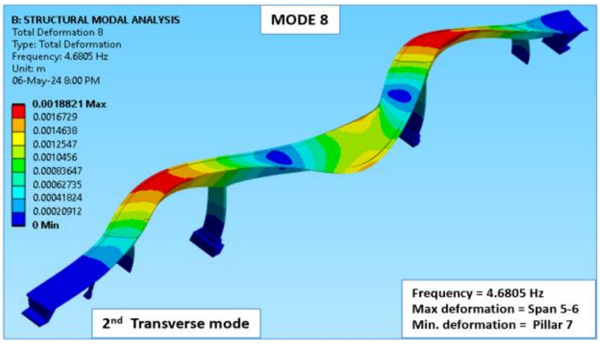

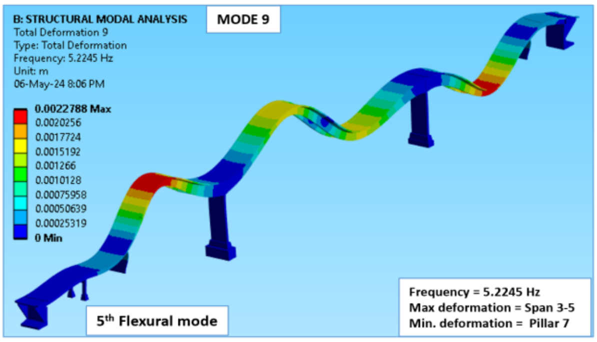

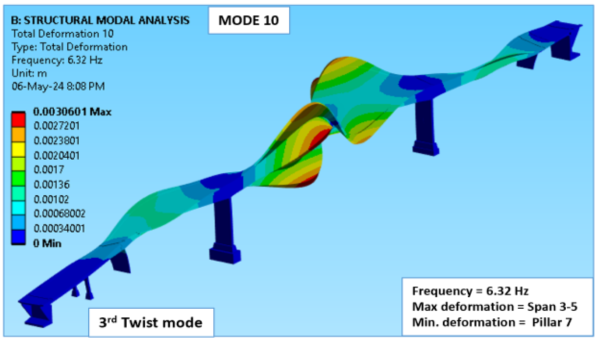

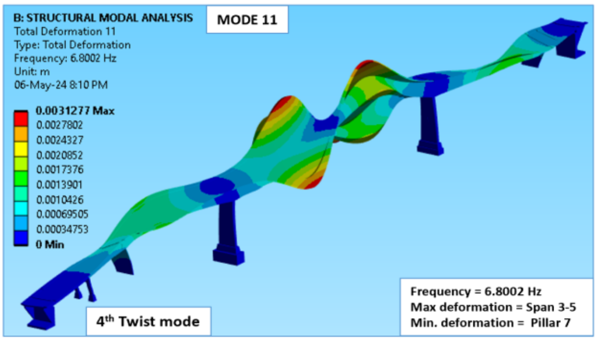

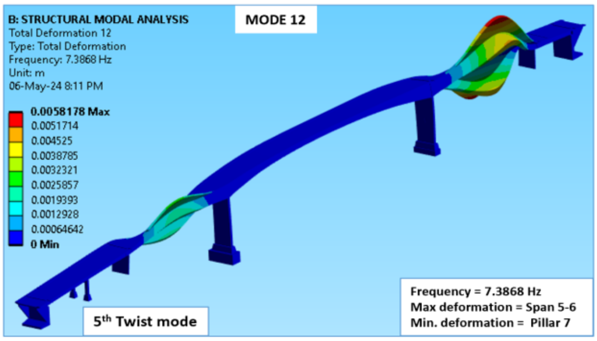

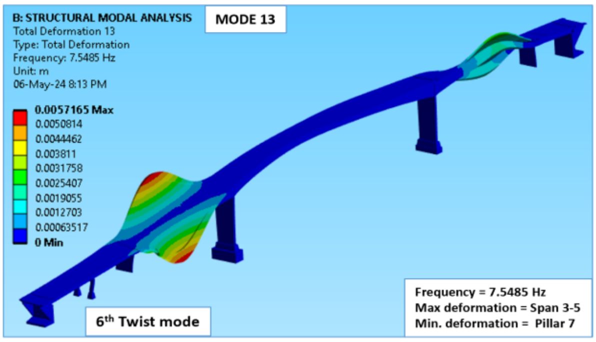

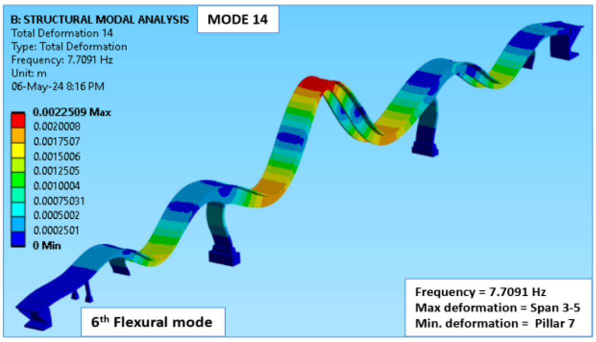

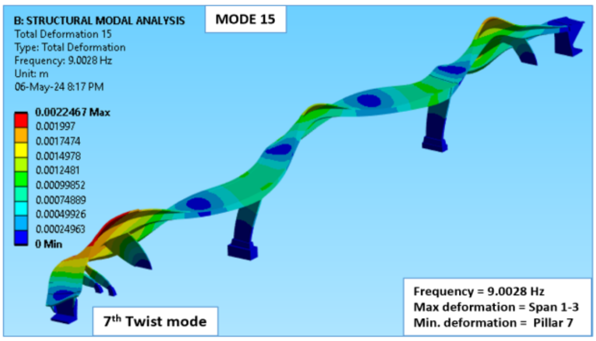

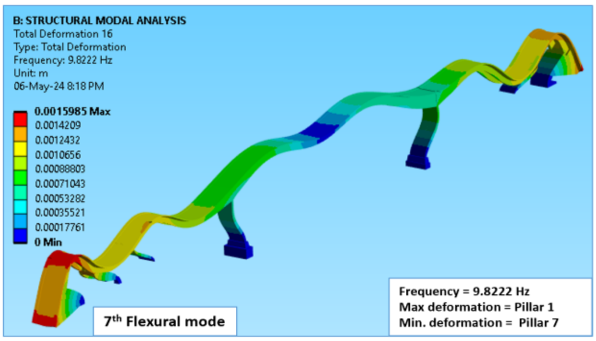

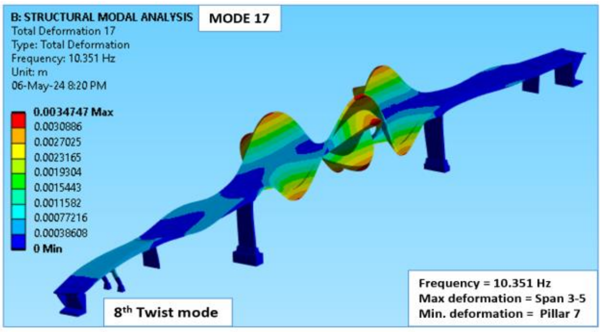

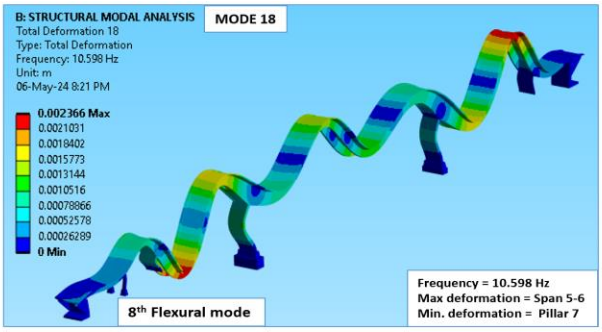

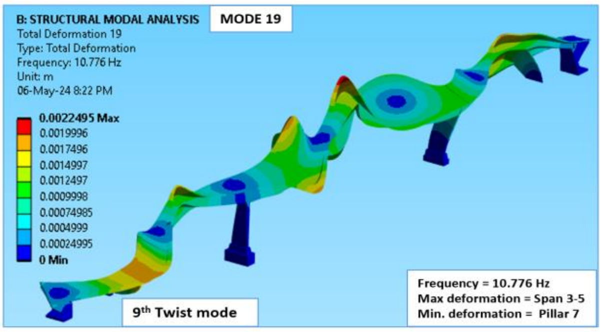

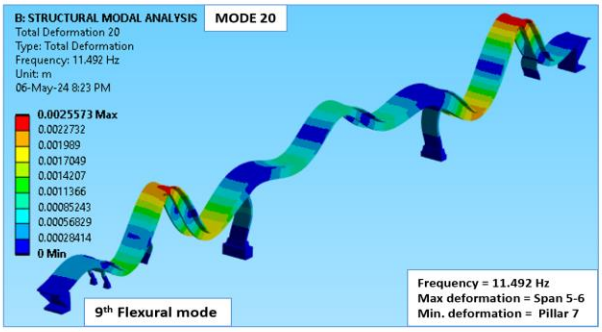

9.5 Appendix E: Frequencies, Modes, and Participation Factors

```
*** FREQUENCIES FROM BLOCK LANCZOS ITERATION ***

 MODE     FREQUENCY (HERTZ)

   1      1.423184300011
   2      1.680061539020
   3      2.945488008021
   4      3.311105972921
   5      3.545195569981
   6      3.587596883478
   7      4.298359348574
   8      4.680471118272
   9      5.224482407800
  10      6.319955655232
  11      6.800238271649
  12      7.386795661011
  13      7.548495871534
  14      7.709131248653
  15      9.002826030348
  16      9.822172458353
  17     10.35125455007
  18     10.59754815427
  19     10.77607982294
  20     11.49223316087
```

Cumulative Effective Mass Fraction

Mode	Frequency [Hz]	X Direction	Y Direction	Z Direction	Rotation X	Rotation Y	Rotation Z
1	1.4232	1.916e-003	0.25007	3.0933e-005	4.0063e-002	5.2247e-005	0.23171
2	1.6801	1.9169e-003	0.25007	0.56539	0.69069	0.53258	0.23171
3	2.9455	3.8711e-002	0.25031	0.56539	0.69073	0.53266	0.25116
4	3.3111	3.8729e-002	0.25034	0.56541	0.69287	0.62652	0.25121
5	3.5452	0.90938	0.28573	0.56541	0.69888	0.62816	0.29513
6	3.5876	0.90938	0.28574	0.56667	0.70318	0.62961	0.29514
7	4.2984	0.98579	0.67191	0.5667	0.76746	0.62969	0.64751
8	4.6805	0.9858	0.67193	0.86561	0.89298	0.90631	0.64751
9	5.2245	0.98971	0.67296	0.86564	0.89307	0.90632	0.72525
10	6.32	0.98971	0.67297	0.86656	0.89389	0.91634	0.72525
11	6.8002	0.98971	0.67297	0.86841	0.89602	0.94444	0.72525
12	7.3868	0.98971	0.67298	0.87872	0.89712	0.95352	0.72526
13	7.5485	0.98971	0.67304	0.87904	0.89923	0.95446	0.72532
14	7.7091	0.99194	0.85338	0.87904	0.93024	0.95449	0.88011
15	9.0028	0.99194	0.85338	0.97462	0.97346	0.97507	0.88011
16	9.8222	0.99868	0.90202	0.97464	0.98131	0.97509	0.9168
17	10.351	0.99868	0.90202	0.99217	0.98132	0.97847	0.9168
18	10.598	0.99945	0.90445	0.99226	0.98194	0.97856	0.91878
19	10.776	0.99946	0.90446	0.99996	0.98292	0.99998	0.91878
20	11.492	1.	1.	1.	1.	1.	1.

Ratio of Effective Mass to Total Mass

Mode	Frequency [Hz]	X Direction	Y Direction	Z Direction	Rotation X	Rotation Y	Rotation Z
1	1.4232	1.6002e-003	0.10119	2.0776e-005	2.7437e-002	2.9471e-005	8.4531e-002
2	1.6801	7.4005e-007	9.8448e-007	0.37971	0.44559	0.30039	5.2413e-007
3	2.9455	3.0729e-002	9.8608e-005	1.0555e-007	2.5984e-005	4.222e-005	7.0935e-003
4	3.3111	1.469e-005	1.0817e-005	1.4988e-005	1.4649e-003	5.2947e-002	1.893e-005
5	3.5452	0.72713	1.4322e-002	1.95e-008	4.1169e-003	9.2455e-004	1.6025e-002
6	3.5876	5.0225e-006	1.6456e-006	8.4684e-004	2.9499e-003	8.1825e-004	1.7296e-006
7	4.2984	6.3811e-002	0.15626	1.5101e-005	4.4019e-002	4.2887e-005	0.12855
8	4.6805	1.2366e-005	7.763e-006	0.20076	8.5964e-002	0.15603	3.9739e-008
9	5.2245	3.2578e-003	4.1745e-004	2.0686e-005	6.4575e-005	9.0994e-006	2.8362e-002
10	6.32	2.3595e-007	5.1453e-007	6.2027e-004	5.628e-004	5.6482e-003	1.9382e-007
11	6.8002	5.3914e-007	1.4313e-006	1.2434e-003	1.4557e-003	1.5853e-002	1.3248e-006
12	7.3868	6.1193e-008	2.9107e-006	6.9205e-003	7.5169e-004	5.1202e-003	2.6367e-006
13	7.5485	4.7836e-008	2.6957e-005	2.1744e-004	1.4443e-003	5.3054e-004	2.0921e-005
14	7.7091	1.8683e-003	7.2971e-002	1.4659e-006	2.1239e-002	1.7433e-005	5.6469e-002
15	9.0028	6.0524e-007	2.4069e-007	6.4195e-002	2.9604e-002	1.161e-002	6.7947e-008
16	9.8222	5.6294e-003	1.9682e-002	8.1136e-006	5.3706e-003	8.9084e-006	1.3385e-002
17	10.351	1.086e-007	2.6631e-007	1.178e-002	1.2316e-005	1.9087e-003	2.5343e-007
18	10.598	6.4218e-004	9.8396e-004	6.0343e-005	4.1844e-004	5.2575e-005	7.2183e-004
19	10.776	4.3575e-006	1.411e-006	5.1653e-003	6.7701e-004	1.2083e-002	1.0468e-006
20	11.492	4.5173e-004	3.866e-002	2.9937e-005	1.1695e-002	9.323e-006	2.9631e-002
Sum		0.83516	0.40464	0.67162	0.68486	0.56408	0.36481

NOTE: The data displayed in the current worksheet is with respect to the solver unit system.

***** PARTICIPATION FACTOR CALCULATION ***** X DIRECTION

MODE	FREQUENCY	PERIOD	PARTIC.FACTOR	RATIO	EFFECTIVE MASS	CUMULATIVE MASS FRACTION	RATIO EFF.MASS TO TOTAL MASS
1	1.42318	0.70265	47.080	0.046911	2216.55	0.191601E-02	0.160017E-02
2	1.68006	0.59522	-1.0125	0.001009	1.02512	0.191690E-02	0.740052E-06
3	2.94549	0.33950	206.32	0.205575	42566.0	0.387114E-01	0.307292E-01
4	3.31111	0.30201	-4.5109	0.004495	20.3483	0.387290E-01	0.146898E-04
5	3.54520	0.28207	1003.6	1.000000	0.100722E+07	0.909378	0.727127
6	3.58760	0.27874	-2.6376	0.002628	6.95710	0.909384	0.502245E-05
7	4.29836	0.23265	-297.31	0.296239	88390.9	0.985790	0.638109E-01
8	4.68047	0.21365	4.1388	0.004124	17.1296	0.985805	0.123662E-04
9	5.22448	0.19141	-67.177	0.066936	4512.71	0.989706	0.325780E-02
10	6.31996	0.15823	-0.57169	0.000570	0.326835	0.989706	0.235948E-06
11	6.80024	0.14705	-0.86419	0.000861	0.746822	0.989706	0.539144E-06
12	7.38680	0.13538	-0.29114	0.000290	0.847650E-01	0.989707	0.611934E-07
13	7.54850	0.13248	-0.25742	0.000256	0.662630E-01	0.989707	0.478364E-07
14	7.70913	0.12972	50.871	0.050689	2587.91	0.991944	0.186826E-02
15	9.00283	0.11108	-0.91563	0.000912	0.838377	0.991944	0.605239E-06
16	9.82217	0.10181	88.305	0.087988	7797.83	0.998685	0.562939E-02
17	10.3513	0.96607E-01	0.38785	0.000386	0.150429	0.998685	0.108598E-06
18	10.5975	0.94361E-01	29.825	0.029718	889.541	0.999454	0.642175E-03
19	10.7761	0.92798E-01	-2.4568	0.002448	6.03603	0.999459	0.435752E-05
20	11.4922	0.87015E-01	-25.015	0.024925	625.738	1.00000	0.451731E-03
sum					0.115686E+07		0.835155

***** PARTICIPATION FACTOR CALCULATION ***** Y DIRECTION

MODE	FREQUENCY	PERIOD	PARTIC.FACTOR	RATIO	EFFECTIVE MASS	CUMULATIVE MASS FRACTION	RATIO EFF.MASS TO TOTAL MASS
1	1.42318	0.70265	374.38	0.804702	140164.	0.250066	0.101187
2	1.68006	0.59522	-1.1678	0.002510	1.36371	0.250068	0.984485E-06
3	2.94549	0.33950	11.687	0.025121	136.591	0.250312	0.986076E-04
4	3.31111	0.30201	-3.8709	0.008320	14.9837	0.250339	0.108170E-04
5	3.54520	0.28207	140.85	0.302748	19839.4	0.285734	0.143224E-01
6	3.58760	0.27874	-1.5098	0.003245	2.27944	0.285738	0.164557E-05
7	4.29836	0.23265	465.25	1.000000	216454.	0.671913	0.156262
8	4.68047	0.21365	-3.2792	0.007048	10.7533	0.671932	0.776298E-05
9	5.22448	0.19141	24.047	0.051686	578.247	0.672964	0.417447E-03
10	6.31996	0.15823	-0.84423	0.001815	0.712724	0.672965	0.514528E-06
11	6.80024	0.14705	-1.4080	0.003026	1.98258	0.672969	0.143126E-05
12	7.38680	0.13538	2.0080	0.004316	4.03188	0.672976	0.291068E-05
13	7.54850	0.13248	6.1108	0.013134	37.3415	0.673043	0.269575E-04
14	7.70913	0.12972	-317.93	0.683360	101080.	0.853379	0.729713E-01
15	9.00283	0.11108	-0.57741	0.001241	0.333400	0.853380	0.240687E-06
16	9.82217	0.10181	165.12	0.354905	27264.0	0.902021	0.196824E-01
17	10.3513	0.96607E-01	-0.60736	0.001305	0.368889	0.902022	0.266308E-06
18	10.5975	0.94361E-01	36.919	0.079353	1362.98	0.904454	0.983958E-03
19	10.7761	0.92798E-01	-1.3980	0.003005	1.95452	0.904457	0.141100E-05
20	11.4922	0.87015E-01	-231.41	0.497401	53552.4	1.00000	0.386604E-01
sum					560507.		0.404640

***** PARTICIPATION FACTOR CALCULATION ***** Z DIRECTION

MODE	FREQUENCY	PERIOD	PARTIC.FACTOR	RATIO	EFFECTIVE MASS	CUMULATIVE MASS FRACTION	RATIO EFF.MASS TO TOTAL MASS
1	1.42318	0.70265	5.3645	0.007397	28.7783	0.309333E-04	0.207755E-04
2	1.68006	0.59522	725.24	1.000000	525973.	0.565390	0.379709
3	2.94549	0.33950	0.38238	0.000527	0.146213	0.565390	0.105554E-06
4	3.31111	0.30201	4.5565	0.006283	20.7616	0.565413	0.149881E-04
5	3.54520	0.28207	-0.16435	0.000227	0.270117E-01	0.565413	0.195002E-07
6	3.58760	0.27874	34.250	0.047225	1173.05	0.566674	0.846843E-03
7	4.29836	0.23265	4.5736	0.006306	20.9175	0.566696	0.151007E-04
8	4.68047	0.21365	527.34	0.727123	278086.	0.865606	0.200755
9	5.22448	0.19141	5.3529	0.007381	28.6539	0.865637	0.206857E-04
10	6.31996	0.15823	29.312	0.040417	859.202	0.866560	0.620273E-03
11	6.80024	0.14705	41.502	0.057225	1722.43	0.868412	0.124345E-02
12	7.38680	0.13538	-97.910	0.135003	9586.29	0.878716	0.692051E-02
13	7.54850	0.13248	-17.355	0.023930	301.198	0.879039	0.217440E-03
14	7.70913	0.12972	1.4250	0.001965	2.03061	0.879042	0.146593E-05
15	9.00283	0.11108	298.20	0.411174	88923.0	0.974623	0.641951E-01
16	9.82217	0.10181	3.3525	0.004623	11.2389	0.974635	0.811358E-05
17	10.3513	0.96607E-01	127.74	0.176135	16317.5	0.992175	0.117799E-01
18	10.5975	0.94361E-01	-9.1426	0.012606	83.5870	0.992265	0.603429E-04
19	10.7761	0.92798E-01	-84.587	0.116633	7154.93	0.999955	0.516527E-02
20	11.4922	0.87015E-01	6.4396	0.008879	41.4688	1.00000	0.299370E-04
sum					930334.		0.671625

***** PARTICIPATION FACTOR CALCULATION *****ROTX DIRECTION

MODE	FREQUENCY	PERIOD	PARTIC.FACTOR	RATIO	EFFECTIVE MASS	CUMULATIVE MASS FRACTION	RATIO EFF.MASS TO TOTAL MASS
1	1.42318	0.70265	-1236.5	0.248144	0.152904E+07	0.400626E-01	0.274374E-01
2	1.68006	0.59522	4983.2	1.000000	0.248319E+08	0.690689	0.445590
3	2.94549	0.33950	-38.053	0.007636	1448.02	0.690727	0.259836E-04
4	3.31111	0.30201	285.72	0.057337	81636.3	0.692866	0.146490E-02
5	3.54520	0.28207	-478.99	0.096121	229430.	0.698877	0.411694E-02
6	3.58760	0.27874	-405.45	0.081364	164391.	0.703184	0.294987E-02
7	4.29836	0.23265	-1566.2	0.314305	0.245309E+07	0.767458	0.440188E-01
8	4.68047	0.21365	2188.7	0.439229	0.479063E+07	0.892978	0.859640E-01
9	5.22448	0.19141	-59.989	0.012038	3598.67	0.893072	0.645754E-04
10	6.31996	0.15823	177.10	0.035539	31363.8	0.893894	0.562799E-03
11	6.80024	0.14705	284.82	0.057157	81124.3	0.896020	0.145571E-02
12	7.38680	0.13538	204.67	0.041073	41890.6	0.897117	0.751694E-03
13	7.54850	0.13248	-283.70	0.056932	80486.8	0.899226	0.144427E-02
14	7.70913	0.12972	1087.9	0.218323	0.118361E+07	0.930238	0.212389E-01
15	9.00283	0.11108	1284.4	0.257756	0.164979E+07	0.973464	0.296043E-01
16	9.82217	0.10181	-547.08	0.109785	299296.	0.981306	0.537063E-02
17	10.3513	0.96607E-01	26.199	0.005257	686.372	0.981324	0.123164E-04
18	10.5975	0.94361E-01	-152.71	0.030644	23319.2	0.981935	0.418444E-03
19	10.7761	0.92798E-01	-194.24	0.038979	37728.5	0.982924	0.677008E-03
20	11.4922	0.87015E-01	807.30	0.162005	651731.	1.00000	0.116948E-01
sum					0.381662E+08		0.684863

***** PARTICIPATION FACTOR CALCULATION *****ROTY DIRECTION

MODE	FREQUENCY	PERIOD	PARTIC.FACTOR	RATIO	EFFECTIVE MASS	CUMULATIVE MASS FRACTION	RATIO EFF.MASS TO TOTAL MASS
1	1.42318	0.70265	585.72	0.009905	343073.	0.522470E-04	0.294713E-04
2	1.68006	0.59522	59134.	1.000000	0.349680E+10	0.532584	0.300388
3	2.94549	0.33950	701.06	0.011855	491479.	0.532659	0.422199E-04
4	3.31111	0.30201	-24826.	0.419835	0.616349E+09	0.626524	0.529468E-01
5	3.54520	0.28207	3280.7	0.055479	0.107627E+08	0.628163	0.924555E-03
6	3.58760	0.27874	3086.3	0.052192	0.952523E+07	0.629614	0.818253E-03
7	4.29836	0.23265	-706.57	0.011949	499240.	0.629690	0.428866E-04
8	4.68047	0.21365	42619.	0.720718	0.181636E+10	0.906306	0.156032
9	5.22448	0.19141	325.46	0.005504	105925.	0.906322	0.909935E-05
10	6.31996	0.15823	-8108.7	0.137125	0.657509E+08	0.916335	0.564825E-02
11	6.80024	0.14705	-13585.	0.229729	0.184546E+09	0.944440	0.158532E-01
12	7.38680	0.13538	-7720.3	0.130557	0.596037E+08	0.953517	0.512019E-02
13	7.54850	0.13248	2485.2	0.042026	0.617604E+07	0.954457	0.530545E-03
14	7.70913	0.12972	450.48	0.007618	202936.	0.954488	0.174329E-04
15	9.00283	0.11108	11625.	0.196594	0.135149E+09	0.975070	0.116098E-01
16	9.82217	0.10181	322.03	0.005446	103702.	0.975086	0.890839E-05
17	10.3513	0.96607E-01	4713.7	0.079712	0.222186E+08	0.978470	0.190866E-02
18	10.5975	0.94361E-01	782.32	0.013230	612020.	0.978563	0.525748E-04
19	10.7761	0.92798E-01	11860.	0.200559	0.140655E+09	0.999983	0.120828E-01
20	11.4922	0.87015E-01	329.44	0.005571	108529.	1.00000	0.932303E-05
sum					0.656636E+10		0.564075

***** PARTICIPATION FACTOR CALCULATION *****ROTZ DIRECTION

MODE	FREQUENCY	PERIOD	PARTIC.FACTOR	RATIO	EFFECTIVE MASS	CUMULATIVE MASS FRACTION	RATIO EFF.MASS TO TOTAL MASS
1	1.42318	0.70265	-31393.	0.810915	0.985532E+09	0.231711	0.845312E-01
2	1.68006	0.59522	78.171	0.002019	6110.77	0.231712	0.524134E-06
3	2.94549	0.33950	-9094.0	0.234907	0.827015E+08	0.251157	0.709348E-02
4	3.31111	0.30201	469.79	0.012135	220704.	0.251209	0.189303E-04
5	3.54520	0.28207	-13669.	0.353070	0.186828E+09	0.295134	0.160247E-01
6	3.58760	0.27874	142.00	0.003668	20165.1	0.295139	0.172960E-05
7	4.29836	0.23265	-38713.	1.000000	0.149872E+10	0.647507	0.128548
8	4.68047	0.21365	21.525	0.000556	463.309	0.647507	0.397390E-07
9	5.22448	0.19141	18184.	0.469716	0.330667E+09	0.725251	0.283620E-01
10	6.31996	0.15823	47.536	0.001228	2259.71	0.725251	0.193820E-06
11	6.80024	0.14705	124.28	0.003210	15445.6	0.725255	0.132480E-05
12	7.38680	0.13538	-175.33	0.004529	30741.0	0.725262	0.263672E-05
13	7.54850	0.13248	-493.88	0.012757	243919.	0.725320	0.209214E-04
14	7.70913	0.12972	25658.	0.662781	0.658355E+09	0.880107	0.564685E-01
15	9.00283	0.11108	-28.146	0.000727	792.180	0.880107	0.679470E-07
16	9.82217	0.10181	-12492.	0.322680	0.156050E+09	0.916797	0.133847E-01
17	10.3513	0.96607E-01	54.357	0.001404	2954.68	0.916797	0.253429E-06
18	10.5975	0.94361E-01	-2901.0	0.074935	0.841561E+07	0.918776	0.721825E-03
19	10.7761	0.92798E-01	110.47	0.002854	12204.4	0.918779	0.104680E-05
20	11.4922	0.87015E-01	18586.	0.480106	0.345457E+09	1.00000	0.296306E-01
sum					0.425328E+10		0.364813

9.6 Appendix F: Harmonic Response Results

Phase Response Data

1	Sweeping Phase [°]	Output [m]	Rail and Asphalt Load [y]	TEDTL Traffic Load 1 [y]	TTLC Traffic Load 2 [y]
2	0	3.04E-02	-1.08E+06	-4.84E+06	-1.15E+05
3	7.2	-4.34E-02	-1.07E+06	-4.80E+06	-1.14E+05
4	14.4	-0.11645	-1.05E+06	-4.68E+06	-1.11E+05
5	21.6	-0.18771	-1.01E+06	-4.50E+06	-1.07E+05
6	28.8	-0.25601	-9.48E+05	-4.24E+06	-1.01E+05
7	36	-0.32027	-8.75E+05	-3.91E+06	-93037
8	43.2	-0.37948	-7.89E+05	-3.53E+06	-83831
9	50.4	-0.43271	-6.90E+05	-3.08E+06	-73304
10	57.6	-0.47911	-5.80E+05	-2.59E+06	-61620
11	64.8	-0.51796	-4.61E+05	-2.06E+06	-48965
12	72	-0.54864	-3.34E+05	-1.49E+06	-35537
13	79.2	-0.57066	-2.03E+05	-9.06E+05	-21549
14	86.4	-0.58369	-67939	-3.04E+05	-7220.9
15	93.6	-0.58751	67939	3.04E+05	7220.9
16	100.8	-0.58206	2.03E+05	9.06E+05	21549
17	108	-0.56744	3.34E+05	1.49E+06	35537
18	115.2	-0.54387	4.61E+05	2.06E+06	48965
19	122.4	-0.51172	5.80E+05	2.59E+06	61620
20	129.6	-0.4715	6.90E+05	3.08E+06	73304
21	136.8	-0.42384	7.89E+05	3.53E+06	83831
22	144	-0.3695	8.75E+05	3.91E+06	93037
23	151.2	-0.30933	9.48E+05	4.24E+06	1.01E+05
24	158.4	-0.24429	1.01E+06	4.50E+06	1.07E+05
25	165.6	-0.17539	1.05E+06	4.68E+06	1.11E+05
26	172.8	-0.10372	1.07E+06	4.80E+06	1.14E+05
27	180	-3.04E-02	1.08E+06	4.84E+06	1.15E+05
28	187.2	4.34E-02	1.07E+06	4.80E+06	1.14E+05
29	194.4	0.11645	1.05E+06	4.68E+06	1.11E+05
30	201.6	0.18771	1.01E+06	4.50E+06	1.07E+05
31	208.8	0.25601	9.48E+05	4.24E+06	1.01E+05
32	216	0.32027	8.75E+05	3.91E+06	93037
33	223.2	0.37948	7.89E+05	3.53E+06	83831
34	230.4	0.43271	6.90E+05	3.08E+06	73304
35	237.6	0.47911	5.80E+05	2.59E+06	61620
36	244.8	0.51796	4.61E+05	2.06E+06	48965
37	252	0.54864	3.34E+05	1.49E+06	35537
38	259.2	0.57066	2.03E+05	9.06E+05	21549
39	266.4	0.58369	67940	3.04E+05	7221
40	273.6	0.58751	-67939	-3.04E+05	-7220.8
41	280.8	0.58206	-2.03E+05	-9.06E+05	-21549
42	288	0.56744	-3.34E+05	-1.49E+06	-35537
43	295.2	0.54387	-4.61E+05	-2.06E+06	-48965
44	302.4	0.51172	-5.80E+05	-2.59E+06	-61620
45	309.6	0.4715	-6.90E+05	-3.08E+06	-73304
46	316.8	0.42384	-7.89E+05	-3.53E+06	-83831
47	324	0.3695	-8.75E+05	-3.91E+06	-93037
48	331.2	0.30933	-9.48E+05	-4.24E+06	-1.01E+05
49	338.4	0.24429	-1.01E+06	-4.50E+06	-1.07E+05
50	345.6	0.17539	-1.05E+06	-4.68E+06	-1.11E+05
51	352.8	0.10372	-1.07E+06	-4.80E+06	-1.14E+05
52	360	3.04E-02	-1.08E+06	-4.84E+06	-1.15E+05
53	367.2	-4.34E-02	-1.07E+06	-4.80E+06	-1.14E+05
54	374.4	-0.11645	-1.05E+06	-4.68E+06	-1.11E+05
55	381.6	-0.18771	-1.01E+06	-4.50E+06	-1.07E+05
56	388.8	-0.25601	-9.48E+05	-4.24E+06	-1.01E+05
57	396	-0.32027	-8.75E+05	-3.91E+06	-93037
58	403.2	-0.37948	-7.89E+05	-3.53E+06	-83831
59	410.4	-0.43271	-6.90E+05	-3.08E+06	-73304
60	417.6	-0.47911	-5.80E+05	-2.59E+06	-61620
61	424.8	-0.51796	-4.61E+05	-2.06E+06	-48965
62	432	-0.54864	-3.34E+05	-1.49E+06	-35537
63	439.2	-0.57066	-2.03E+05	-9.06E+05	-21549
64	446.4	-0.58369	-67941	-3.04E+05	-7221.1
65	453.6	-0.58751	67938	3.04E+05	7220.8
66	460.8	-0.58206	2.03E+05	9.06E+05	21549
67	468	-0.56744	3.34E+05	1.49E+06	35537
68	475.2	-0.54387	4.61E+05	2.06E+06	48964
69	482.4	-0.51172	5.80E+05	2.59E+06	61620
70	489.6	-0.4715	6.90E+05	3.08E+06	73304
71	496.8	-0.42384	7.89E+05	3.53E+06	83831
72	504	-0.3695	8.75E+05	3.91E+06	93037
73	511.2	-0.30933	9.48E+05	4.24E+06	1.01E+05
74	518.4	-0.24429	1.01E+06	4.50E+06	1.07E+05
75	525.6	-0.17539	1.05E+06	4.68E+06	1.11E+05
76	532.8	-0.10372	1.07E+06	4.80E+06	1.14E+05
77	540	-3.04E-02	1.08E+06	4.84E+06	1.15E+05
78	547.2	4.34E-02	1.07E+06	4.80E+06	1.14E+05
79	554.4	0.11645	1.05E+06	4.68E+06	1.11E+05
80	561.6	0.18771	1.01E+06	4.50E+06	1.07E+05
81	568.8	0.25601	9.48E+05	4.24E+06	1.01E+05
82	576	0.32027	8.75E+05	3.91E+06	93037
83	583.2	0.37948	7.89E+05	3.53E+06	83832
84	590.4	0.43271	6.90E+05	3.08E+06	73304
85	597.6	0.47911	5.80E+05	2.59E+06	61620
86	604.8	0.51796	4.61E+05	2.06E+06	48965
87	612	0.54864	3.34E+05	1.49E+06	35537
88	619.2	0.57066	2.03E+05	9.06E+05	21549
89	626.4	0.58369	67941	3.04E+05	7221.1
90	633.6	0.58751	-67937	-3.04E+05	-7220.7
91	640.8	0.58206	-2.03E+05	-9.06E+05	-21549
92	648	0.56744	-3.34E+05	-1.49E+06	-35537
93	655.2	0.54387	-4.61E+05	-2.06E+06	-48964
94	662.4	0.51172	-5.80E+05	-2.59E+06	-61620
95	669.6	0.4715	-6.90E+05	-3.08E+06	-73304
96	676.8	0.42384	-7.89E+05	-3.53E+06	-83831
97	684	0.3695	-8.75E+05	-3.91E+06	-93037
98	691.2	0.30933	-9.48E+05	-4.24E+06	-1.01E+05
99	698.4	0.24429	-1.01E+06	-4.50E+06	-1.07E+05
100	705.6	0.17539	-1.05E+06	-4.68E+06	-1.11E+05
101	712.8	0.10372	-1.07E+06	-4.80E+06	-1.14E+05
102	720	3.04E-02	-1.08E+06	-4.84E+06	-1.15E+05

Phase Response Graph

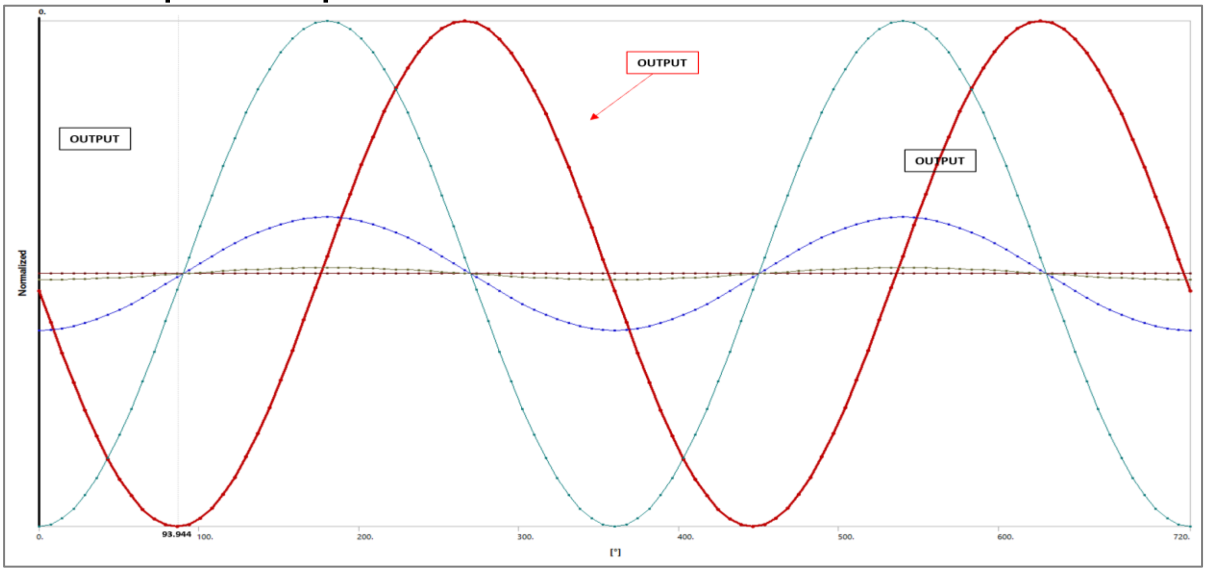

Frequency Response Deformation

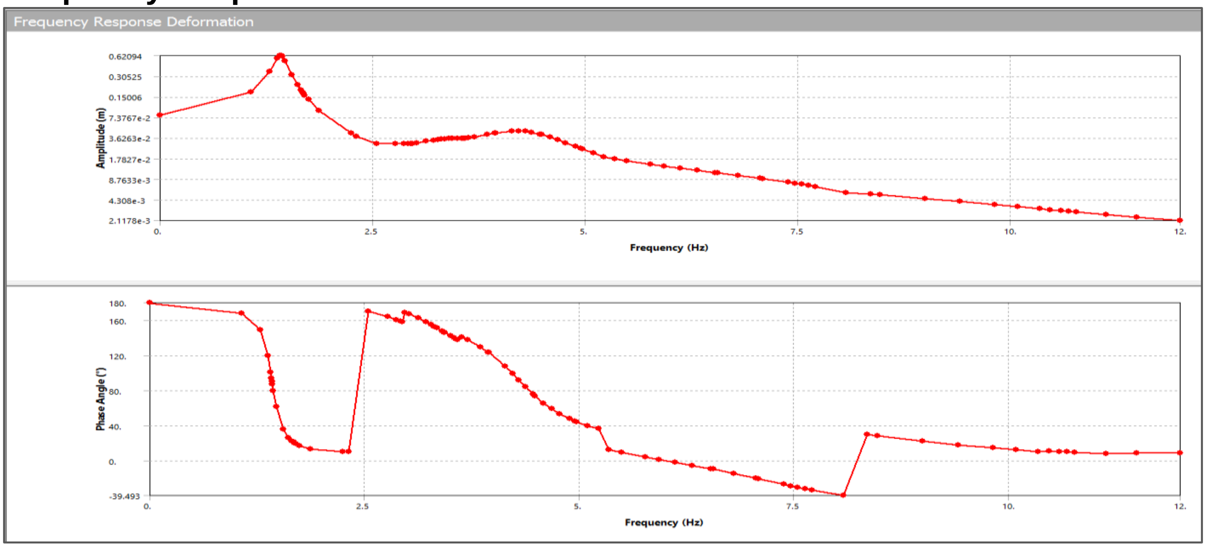

Frequency Response Velocity Data

Tabular Data

	Frequency [Hz]	Amplitude [m/s]	Phase Angle [°]
1	0.	0.	180.
2	1.0735	1.1814	-101.75
3	1.2866	2.8838	-120.58
4	1.3756	4.8526	-150.26
5	1.4073	5.4555	-169.05
6	1.418	5.5322	-176.06
7	1.4232	5.5395	-179.51
8	1.4284	5.5265	177.03
9	1.4392	5.4385	170.03
10	1.4724	4.8068	151.24
11	1.5516	3.1346	125.63
12	1.617	2.3192	116.03
13	1.6581	1.9803	112.3
14	1.6726	1.8827	111.26
15	1.6801	1.8354	110.76
16	1.6876	1.7902	110.28
17	1.7023	1.708	109.43
18	1.7456	1.5036	107.36
19	1.8733	1.109	103.59
20	2.2499	0.6086	100.33
21	2.3128	0.56192	100.3
22	2.5463	0.47744	-99.838
23	2.7734	0.52548	-106.18
24	2.8748	0.54262	-109.63
25	2.9171	0.54759	-110.94
26	2.9455	0.55053	-111.7
27	2.9741	0.56058	-101.28
28	3.0179	0.58372	-102.8
29	3.1283	0.64037	-107.61
30	3.2199	0.68418	-112.18

Tabular Data

	Frequency [Hz]	Amplitude [m/s]	Phase Angle [°]
31	3.2731	0.70819	-115.
32	3.3111	0.72461	-116.83
33	3.3496	0.74041	-119.01
34	3.4049	0.7609	-122.31
35	3.4282	0.76859	-123.66
36	3.4392	0.77203	-124.3
37	3.5	0.78863	-127.73
38	3.5452	0.79895	-130.14
39	3.5664	0.80347	-131.21
40	3.5876	0.80796	-132.25
41	3.6348	0.82939	-129.23
42	3.6998	0.87336	-132.07
43	3.8544	0.99261	-140.33
44	3.943	1.0655	-146.27
45	3.9492	1.0705	-146.73
46	4.1355	1.198	-162.44
47	4.2242	1.2278	-171.02
48	4.2984	1.2306	-178.37
49	4.3738	1.2125	174.25
50	4.4676	1.1646	165.55
51	4.4894	1.1503	163.64
52	4.5879	1.0765	155.65
53	4.6805	1.0001	149.13
54	4.7749	0.92171	143.42
55	4.8865	0.83393	137.8
56	4.9525	0.78582	135.04
57	4.9711	0.77277	134.3
58	5.101	0.68878	129.84
59	5.2245	0.61973	126.58
60	5.351	0.59282	102.36

Tabular Data

	Frequency [Hz]	Amplitude [m/s]	Phase Angle [°]
61	5.4907	0.56851	99.412
62	5.7722	0.52835	94.295
63	5.9283	0.51004	91.547
64	6.1152	0.49076	88.33
65	6.32	0.47183	84.741
66	6.5316	0.45349	80.862
67	6.5601	0.45105	80.323
68	6.8002	0.43007	75.605
69	7.0588	0.40541	70.11
70	7.0935	0.40185	69.369
71	7.3868	0.36906	63.068
72	7.4676	0.35918	61.363
73	7.5485	0.34898	59.694
74	7.6288	0.33859	58.084
75	7.7091	0.328	56.532
76	8.0746	0.2792	50.507
77	8.356	0.27485	119.56
78	8.473	0.27231	118.14
79	9.0028	0.25608	112.06
80	9.4125	0.24104	107.99
81	9.8222	0.22574	104.47
82	10.087	0.21609	102.45
83	10.351	0.20672	100.61
84	10.474	0.20258	101.35
85	10.598	0.19854	100.64
86	10.687	0.19566	100.15
87	10.776	0.19282	99.671
88	11.134	0.18182	97.927
89	11.492	0.17195	98.431
90	12.	0.15967	98.991

Frequency Response Velocity Graph

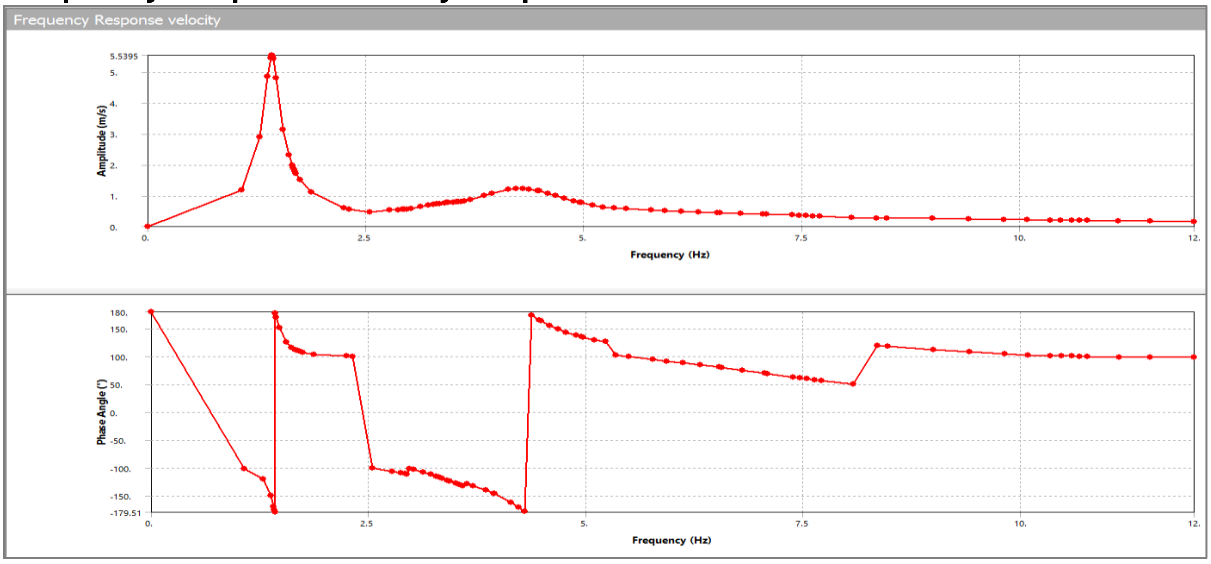

Frequency Response Acceleration Data

Tabular Data

	Frequency [Hz]	Amplitude [m/s²]	Phase Angle [°]
1	0.	0.	0.
2	1.0735	7.9681	-11.748
3	1.2866	23.313	-30.581
4	1.3756	41.942	-60.256
5	1.4073	48.24	-79.051
6	1.418	49.289	-86.056
7	1.4232	49.535	-89.511
8	1.4284	49.6	-92.966
9	1.4392	49.18	-99.971
10	1.4724	44.469	-118.76
11	1.5516	30.56	-144.37
12	1.617	23.562	-153.97
13	1.6581	20.632	-157.7
14	1.6726	19.785	-158.74
15	1.6801	19.375	-159.24
16	1.6876	18.982	-159.72
17	1.7023	18.268	-160.57
18	1.7456	16.491	-162.64
19	1.8733	13.053	-166.41
20	2.2499	8.6035	-169.67
21	2.3128	8.1656	-169.7
22	2.5463	7.6387	-9.838
23	2.7734	9.1567	-16.179
24	2.8748	9.8015	-19.634
25	2.9171	10.037	-20.937
26	2.9455	10.189	-21.704
27	2.9741	10.476	-11.276
28	3.0179	11.068	-12.804
29	3.1283	12.587	-17.608
30	3.2199	13.842	-22.178
31	3.2731	14.564	-25.004
32	3.3111	15.075	-26.83
33	3.3496	15.583	-29.007
34	3.4049	16.278	-32.307
35	3.4282	16.555	-33.657
36	3.4392	16.683	-34.295
37	3.5	17.343	-37.729
38	3.5452	17.797	-40.139
39	3.5664	18.004	-41.214
40	3.5876	18.213	-42.251
41	3.6348	18.942	-39.231
42	3.6998	20.303	-42.073
43	3.8544	24.039	-50.326
44	3.943	26.397	-56.274
45	3.9492	26.564	-56.73
46	4.1355	31.129	-72.443
47	4.2242	32.589	-81.02
48	4.2984	33.236	-88.372
49	4.3738	33.32	-95.755
50	4.4676	32.69	-104.45
51	4.4894	32.449	-106.36
52	4.5879	31.033	-114.35
53	4.6805	29.41	-120.87
54	4.7749	27.653	-126.58
55	4.8865	25.604	-132.2
56	4.9525	24.452	-134.96
57	4.9711	24.137	-135.7
58	5.101	22.075	-140.16
59	5.2245	20.343	-143.42
60	5.351	19.931	-167.64
61	5.4907	19.613	-170.59
62	5.7722	19.162	-175.71
63	5.9283	18.998	-178.45
64	6.1152	18.856	178.33
65	6.32	18.736	174.74
66	6.5316	18.611	170.86
67	6.5601	18.591	170.32
68	6.8002	18.376	165.61
69	7.0588	17.981	160.11
70	7.0935	17.911	159.37
71	7.3868	17.129	153.07
72	7.4676	16.853	151.36
73	7.5485	16.552	149.69
74	7.6288	16.23	148.08
75	7.7091	15.888	146.53
76	8.0746	14.165	140.51
77	8.356	14.43	-150.44
78	8.473	14.497	-151.86
79	9.0028	14.486	-157.94
80	9.4125	14.255	-162.01
81	9.8222	13.931	-165.53
82	10.087	13.695	-167.55
83	10.351	13.445	-169.39
84	10.474	13.332	-168.65
85	10.598	13.22	-169.36
86	10.687	13.138	-169.85
87	10.776	13.055	-170.33
88	11.134	12.72	-172.07
89	11.492	12.416	-171.57
90	12.	12.039	-171.01

Frequency Response Acceleration Graph

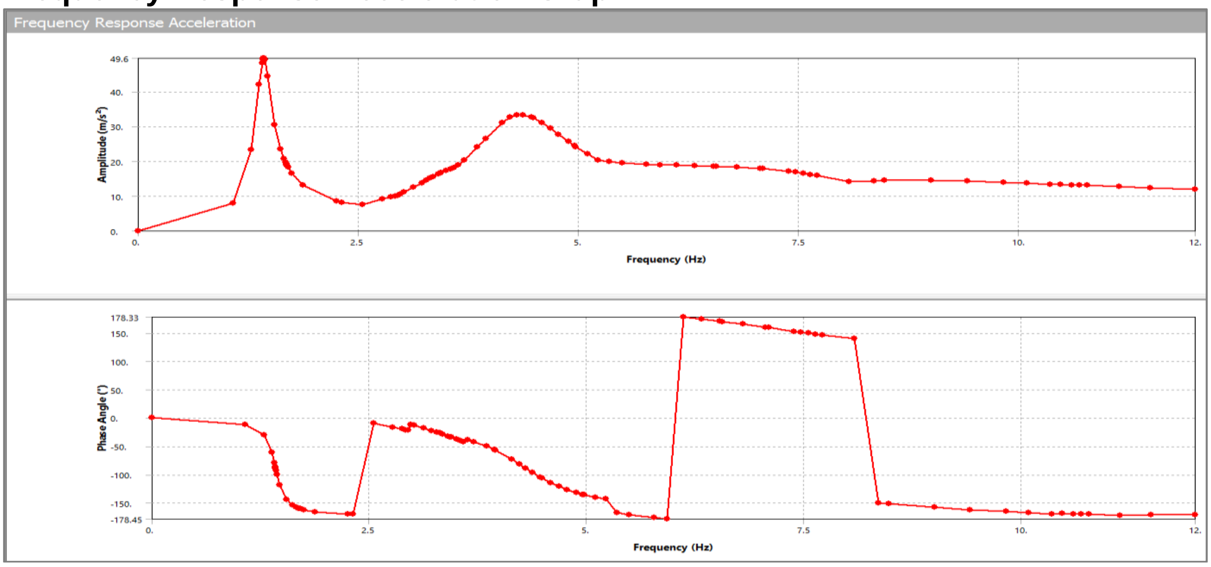

Phase Response Stress

1	Sweeping Phase [°]	Output [Pa]	Rail and Asphalt Load [y] [N]	TEDTL Traffic Load 1 [y] [N]	TTLC Traffic Load 2 [y] [N]
2	0	-2.99E+06	-1.08E+06	-4.84E+06	-1.15E+05
3	7.2	-1.03E+07	-1.07E+06	-4.80E+06	-1.14E+05
4	14.4	-1.74E+07	-1.05E+06	-4.68E+06	-1.11E+05
5	21.6	-2.42E+07	-1.01E+06	-4.50E+06	-1.07E+05
6	28.8	-3.07E+07	-9.48E+05	-4.24E+06	-1.01E+05
7	36	-3.66E+07	-8.75E+05	-3.91E+06	-93037
8	43.2	-4.20E+07	-7.89E+05	-3.53E+06	-83831
9	50.4	-4.68E+07	-6.90E+05	-3.08E+06	-73304
10	57.6	-5.08E+07	-5.80E+05	-2.59E+06	-61620
11	64.8	-5.40E+07	-4.61E+05	-2.06E+06	-48965
12	72	-5.63E+07	-3.34E+05	-1.49E+06	-35537
13	79.2	-5.78E+07	-2.03E+05	-9.06E+05	-21549
14	86.4	-5.83E+07	-67939	-3.04E+05	-7220.9
15	93.6	-5.79E+07	67939	3.04E+05	7220.9
16	100.8	-5.66E+07	2.03E+05	9.06E+05	21549
17	108	-5.45E+07	3.34E+05	1.49E+06	35537
18	115.2	-5.14E+07	4.61E+05	2.06E+06	48965
19	122.4	-4.76E+07	5.80E+05	2.59E+06	61620
20	129.6	-4.30E+07	6.90E+05	3.08E+06	73304
21	136.8	-3.77E+07	7.89E+05	3.53E+06	83831
22	144	-3.18E+07	8.75E+05	3.91E+06	93037
23	151.2	-2.54E+07	9.48E+05	4.24E+06	1.01E+05
24	158.4	-1.87E+07	1.01E+06	4.50E+06	1.07E+05
25	165.6	-1.16E+07	1.05E+06	4.68E+06	1.11E+05
26	172.8	-4.33E+06	1.07E+06	4.80E+06	1.14E+05
27	180	2.99E+06	1.08E+06	4.84E+06	1.15E+05
28	187.2	1.03E+07	1.07E+06	4.80E+06	1.14E+05
29	194.4	1.74E+07	1.05E+06	4.68E+06	1.11E+05
30	201.6	2.42E+07	1.01E+06	4.50E+06	1.07E+05
31	208.8	3.07E+07	9.48E+05	4.24E+06	1.01E+05
32	216	3.66E+07	8.75E+05	3.91E+06	93037
33	223.2	4.20E+07	7.89E+05	3.53E+06	83831
34	230.4	4.68E+07	6.90E+05	3.08E+06	73304
35	237.6	5.08E+07	5.80E+05	2.59E+06	61620
36	244.8	5.40E+07	4.61E+05	2.06E+06	48965
37	252	5.63E+07	3.34E+05	1.49E+06	35537
38	259.2	5.78E+07	2.03E+05	9.06E+05	21549
39	266.4	5.83E+07	67940	3.04E+05	7221
40	273.6	5.79E+07	-67939	-3.04E+05	-7220.8
41	280.8	5.66E+07	-2.03E+05	-9.06E+05	-21549
42	288	5.45E+07	-3.34E+05	-1.49E+06	-35537
43	295.2	5.14E+07	-4.61E+05	-2.06E+06	-48965
44	302.4	4.76E+07	-5.80E+05	-2.59E+06	-61620
45	309.6	4.30E+07	-6.90E+05	-3.08E+06	-73304
46	316.8	3.77E+07	-7.89E+05	-3.53E+06	-83831
47	324	3.18E+07	-8.75E+05	-3.91E+06	-93037
48	331.2	2.54E+07	-9.48E+05	-4.24E+06	-1.01E+05
49	338.4	1.87E+07	-1.01E+06	-4.50E+06	-1.07E+05
50	345.6	1.16E+07	-1.05E+06	-4.68E+06	-1.11E+05
51	352.8	4.33E+06	-1.07E+06	-4.80E+06	-1.14E+05
52	360	-2.99E+06	-1.08E+06	-4.84E+06	-1.15E+05
53	367.2	-1.03E+07	-1.07E+06	-4.80E+06	-1.14E+05
54	374.4	-1.74E+07	-1.05E+06	-4.68E+06	-1.11E+05
55	381.6	-2.42E+07	-1.01E+06	-4.50E+06	-1.07E+05
56	388.8	-3.07E+07	-9.48E+05	-4.24E+06	-1.01E+05
57	396	-3.66E+07	-8.75E+05	-3.91E+06	-93037
58	403.2	-4.20E+07	-7.89E+05	-3.53E+06	-83831
59	410.4	-4.68E+07	-6.90E+05	-3.08E+06	-73304
60	417.6	-5.08E+07	-5.80E+05	-2.59E+06	-61620
61	424.8	-5.40E+07	-4.61E+05	-2.06E+06	-48965
62	432	-5.63E+07	-3.34E+05	-1.49E+06	-35537
63	439.2	-5.78E+07	-2.03E+05	-9.06E+05	-21549
64	446.4	-5.83E+07	-67941	-3.04E+05	-7221.1
65	453.6	-5.79E+07	67938	3.04E+05	7220.8
66	460.8	-5.66E+07	2.03E+05	9.06E+05	21549
67	468	-5.45E+07	3.34E+05	1.49E+06	35537
68	475.2	-5.14E+07	4.61E+05	2.06E+06	48964
69	482.4	-4.76E+07	5.80E+05	2.59E+06	61620
70	489.6	-4.30E+07	6.90E+05	3.08E+06	73304
71	496.8	-3.77E+07	7.89E+05	3.53E+06	83831
72	504	-3.18E+07	8.75E+05	3.91E+06	93037
73	511.2	-2.54E+07	9.48E+05	4.24E+06	1.01E+05
74	518.4	-1.87E+07	1.01E+06	4.50E+06	1.07E+05
75	525.6	-1.16E+07	1.05E+06	4.68E+06	1.11E+05
76	532.8	-4.33E+06	1.07E+06	4.80E+06	1.14E+05
77	540	2.99E+06	1.08E+06	4.84E+06	1.15E+05
78	547.2	1.03E+07	1.07E+06	4.80E+06	1.14E+05
79	554.4	1.74E+07	1.05E+06	4.68E+06	1.11E+05
80	561.6	2.42E+07	1.01E+06	4.50E+06	1.07E+05
81	568.8	3.07E+07	9.48E+05	4.24E+06	1.01E+05
82	576	3.66E+07	8.75E+05	3.91E+06	93037
83	583.2	4.20E+07	7.89E+05	3.53E+06	83832
84	590.4	4.68E+07	6.90E+05	3.08E+06	73304
85	597.6	5.08E+07	5.80E+05	2.59E+06	61620
86	604.8	5.40E+07	4.61E+05	2.06E+06	48965
87	612	5.63E+07	3.34E+05	1.49E+06	35537
88	619.2	5.78E+07	2.03E+05	9.06E+05	21549
89	626.4	5.83E+07	67941	3.04E+05	7221.1
90	633.6	5.79E+07	-67937	-3.04E+05	-7220.7
91	640.8	5.66E+07	-2.03E+05	-9.06E+05	-21549
92	648	5.45E+07	-3.34E+05	-1.49E+06	-35537
93	655.2	5.14E+07	-4.61E+05	-2.06E+06	-48964
94	662.4	4.76E+07	-5.80E+05	-2.59E+06	-61620
95	669.6	4.30E+07	-6.90E+05	-3.08E+06	-73304
96	676.8	3.77E+07	-7.89E+05	-3.53E+06	-83831
97	684	3.18E+07	-8.75E+05	-3.91E+06	-93037
98	691.2	2.54E+07	-9.48E+05	-4.24E+06	-1.01E+05
99	698.4	1.87E+07	-1.01E+06	-4.50E+06	-1.07E+05
100	705.6	1.16E+07	-1.05E+06	-4.68E+06	-1.11E+05
101	712.8	4.33E+06	-1.07E+06	-4.80E+06	-1.14E+05
102	720	-2.99E+06	-1.08E+06	-4.84E+06	-1.15E+05

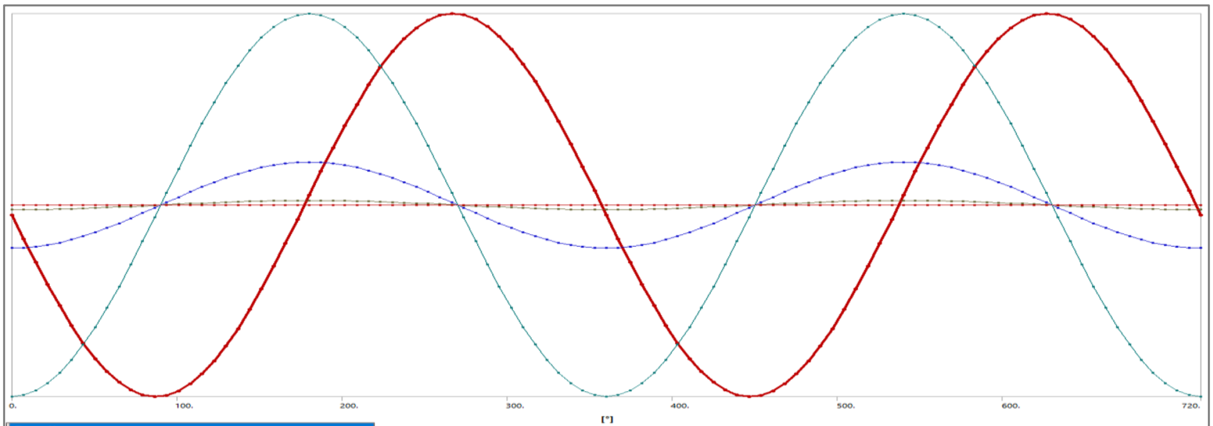

Results	
Amplitude	6.1116e+007 Pa
Phase Angle	92.935 °
Real	-3.1293e+006 Pa
Imaginary	6.1036e+007 Pa
Reported Frequency	1.418 Hz

9.7 Appendix G: Random Vibration Results

SUMMARY OF TERMS INCLUDED IN MODE COMBINATIONS
(MODAL COVARIANCE MATRIX TERMS ONLY)

*** DISPLACEMENT-TYPE QUANTITY ***

MAXIMUM TERM = 0.22671E+06

MODE I	MODE J	COVARIANCE TERM	COVARIANCE RATIO
1	1	46.017	0.20298E-03
2	1	-1.0147	0.44759E-05
2	2	0.22383E-01	0.98731E-07
3	1	265.22	0.11699E-02
3	2	-5.8755	0.25916E-04
3	3	1630.3	0.71910E-02
4	1	-6.9510	0.30660E-04
4	2	0.15464	0.68212E-06
4	3	-45.402	0.20027E-03
4	4	1.3425	0.59214E-05
5	1	1995.0	0.87996E-02
5	2	-44.698	0.19716E-03
5	3	14444.	0.63712E-01
5	4	-477.08	0.21044E-02
5	5	0.22671E+06	1.0000
6	1	-5.3631	0.23656E-04
6	2	0.12022	0.53030E-06
6	3	-39.129	0.17260E-03
6	4	1.3111	0.57832E-05
6	5	-700.41	0.30895E-02
6	6	2.4178	0.10665E-04
7	1	-360.84	0.15916E-02
7	2	7.8567	0.34655E-04
7	3	-1631.7	0.71974E-02
7	4	29.515	0.13019E-03
7	5	-2411.3	0.10636E-01
7	6	6.0779	0.26809E-04
7	7	39171.	0.17278
8	1	4.7010	0.20736E-04
8	2	-0.10194	0.44964E-06
8	3	20.383	0.89908E-04
8	4	-0.37090	0.16360E-05
8	5	39.819	0.17564E-03
8	6	-0.96145E-01	0.42409E-06
8	7	-110.58	0.48776E-03
8	8	7.7305	0.34099E-04
9	1	-71.414	0.31500E-03
9	2	1.5436	0.68085E-05
9	3	-303.03	0.13366E-02
9	4	5.6926	0.25109E-04
9	5	-792.34	0.34950E-02
9	6	1.9646	0.86658E-05
9	7	677.36	0.29878E-02
9	8	-19.349	0.85346E-04
9	9	2084.6	0.91950E-02
10	1	-0.62869	0.27731E-05
10	2	0.13583E-01	0.59913E-07
10	3	-2.7372	0.12074E-04
10	4	0.55607E-01	0.24528E-06
10	5	-10.220	0.45082E-04
10	6	0.26305E-01	0.11603E-06
10	7	4.5477	0.20059E-04
10	8	-0.74738E-01	0.32966E-06
10	9	1.8554	0.81839E-05
10	10	0.16697	0.73649E-06
11	1	-0.97466	0.42992E-05
11	2	0.21067E-01	0.92925E-07
11	3	-4.2974	0.18955E-04
11	4	0.89143E-01	0.39320E-06
11	5	-17.266	0.76159E-04
11	6	0.44729E-01	0.19730E-06
11	7	7.0149	0.30942E-04
11	8	-0.11027	0.48637E-06
11	9	2.3563	0.10394E-04
11	10	0.92499E-01	0.40801E-06
11	11	0.46617	0.20562E-05
12	1	-0.26896	0.11863E-05
12	2	0.58022E-02	0.25593E-07
12	3	-1.1623	0.51268E-05
12	4	0.23883E-01	0.10534E-06
12	5	-4.5828	0.20214E-04
12	6	0.11848E-01	0.52262E-07
12	7	1.8068	0.79699E-05
12	8	-0.27585E-01	0.12167E-06
12	9	0.54612	0.24089E-05
12	10	0.11281E-01	0.49759E-07
12	11	0.46809E-01	0.20647E-06
12	12	0.67515E-01	0.29780E-06
13	1	-0.20838	0.91914E-06
13	2	0.44894E-02	0.19802E-07
13	3	-0.88547	0.39057E-05
13	4	0.17953E-01	0.79189E-07
13	5	-3.3621	0.14830E-04
13	6	0.86612E-02	0.38204E-07
13	7	1.3420	0.59194E-05
13	8	-0.20372E-01	0.89858E-07
13	9	0.39906	0.17602E-05
13	10	0.76558E-02	0.33769E-07
13	11	0.28719E-01	0.12668E-06
13	12	0.51779E-01	0.22839E-06
13	13	0.56022E-01	0.24711E-06
14	1	33.692	0.14861E-03
14	2	-0.72424	0.31946E-05
14	3	138.87	0.61254E-03
14	4	-2.7406	0.12089E-04
14	5	486.02	0.21438E-02
14	6	-1.2418	0.54774E-05
14	7	-201.63	0.88938E-03
14	8	3.0456	0.13434E-04
14	9	-59.360	0.26183E-03
14	10	-1.1020	0.48609E-05
14	11	-3.9371	0.17366E-04
14	12	-7.1385	0.31487E-04
14	13	-9.6653	0.42633E-04
14	14	2310.3	0.10191E-01
15	1	1.1864	0.52331E-05
15	2	-0.25927E-01	0.11436E-06
15	3	6.0632	0.26744E-04
15	4	-0.14265	0.62923E-06
15	5	34.322	0.15139E-03
15	6	-0.91185E-01	0.40221E-06
15	7	-10.783	0.47562E-04
15	8	0.16008	0.70611E-06
15	9	-2.8844	0.12723E-04
15	10	-0.32737E-01	0.14440E-06
15	11	-0.56288E-01	0.24828E-06
15	12	-0.18451E-01	0.81387E-07
15	13	-0.14569E-01	0.64263E-07
15	14	2.2402	0.98811E-05
15	15	0.41881	0.18473E-05
16	1	-98.508	0.43451E-03
16	2	2.1497	0.94824E-05
16	3	-496.81	0.21914E-02
16	4	11.623	0.51270E-04
16	5	-2783.1	0.12276E-01
16	6	7.3885	0.32590E-04
16	7	864.16	0.38117E-02
16	8	-12.722	0.56117E-04
16	9	226.01	0.99691E-03
16	10	2.4701	0.10895E-04
16	11	4.1946	0.18502E-04
16	12	1.4471	0.63831E-05
16	13	1.2244	0.54007E-05
16	14	-221.05	0.97502E-03
16	15	-10.228	0.45113E-04
16	16	2574.4	0.11355E-01
17	1	-0.50152	0.22122E-05
17	2	0.10924E-01	0.48186E-07
17	3	-2.4801	0.10940E-04
17	4	0.57408E-01	0.25322E-06
17	5	-13.574	0.59873E-04
17	6	0.35979E-01	0.15870E-06
17	7	4.2133	0.18584E-04
17	8	-0.61665E-01	0.27200E-06
17	9	1.0853	0.47871E-05
17	10	0.11543E-01	0.50916E-07
17	11	0.19435E-01	0.85724E-07
17	12	0.69015E-02	0.30442E-07
17	13	0.60053E-02	0.26489E-07
17	14	-1.1394	0.50259E-05
17	15	-0.99993E-02	0.44106E-07
17	16	4.2148	0.18591E-04
17	17	0.27838E-01	0.12279E-06
18	1	-35.380	0.15606E-03
18	2	0.77074	0.33997E-05
18	3	-175.13	0.77250E-03
18	4	4.0565	0.17893E-04
18	5	-960.13	0.42351E-02
18	6	2.5452	0.11227E-04
18	7	297.42	0.13119E-02
18	8	-4.3503	0.19189E-04
18	9	76.473	0.33732E-03
18	10	0.81082	0.35765E-05
18	11	1.3627	0.60109E-05
18	12	0.48325	0.21316E-05
18	13	0.42078	0.18560E-05
18	14	-79.998	0.35286E-03
18	15	-0.45502	0.20070E-05
18	16	168.78	0.74446E-03
18	17	1.4800	0.65283E-05
18	18	90.322	0.39840E-03
19	1	2.6363	0.11628E-04
19	2	-0.57445E-01	0.25339E-06
19	3	13.086	0.57719E-04
19	4	-0.30361	0.13392E-05
19	5	72.031	0.31772E-03
19	6	-0.19100	0.84247E-06
19	7	-22.261	0.98192E-04
19	8	0.32555	0.14360E-05
19	9	-5.7201	0.25231E-04
19	10	-0.60590E-01	0.26726E-06
19	11	-0.10171	0.44862E-06
19	12	-0.35878E-01	0.15826E-06
19	13	-0.31165E-01	0.13746E-06
19	14	5.9065	0.26053E-04
19	15	0.34824E-01	0.15361E-06
19	16	-10.245	0.45191E-04
19	17	-0.93924E-01	0.41429E-06
19	18	-6.0322	0.26608E-04
19	19	0.41233	0.18188E-05
20	1	18.850	0.83146E-04
20	2	-0.41111	0.18134E-05
20	3	94.466	0.41668E-03
20	4	-2.2054	0.97280E-05
20	5	527.82	0.23282E-02
20	6	-1.4009	0.61791E-05
20	7	-161.57	0.71266E-03
20	8	2.3601	0.10410E-04
20	9	-41.368	0.18247E-03
20	10	-0.43598	0.19231E-05
20	11	-0.72790	0.32107E-05
20	12	-0.25128	0.11084E-05
20	13	-0.21598	0.95269E-06
20	14	40.369	0.17806E-03
20	15	0.34585	0.15255E-05
20	16	-58.582	0.25840E-03
20	17	-0.49277	0.21736E-05
20	18	-33.740	0.14883E-03
20	19	2.3930	0.10556E-04
20	20	14.901	0.65729E-04

FREQUENCIES USED FOR RANDOM VIBRATION SOLUTION

MODE	FREQUENCY
1	1.42318
2	1.68006
3	2.94549
4	3.31111
5	3.54520
6	3.58760
7	4.29836
8	4.68047
9	5.22448
10	6.31996
11	6.80024
12	7.38680
13	7.54850
14	7.70913
15	9.00283
16	9.82217
17	10.3513
18	10.5975
19	10.7761
20	11.4922

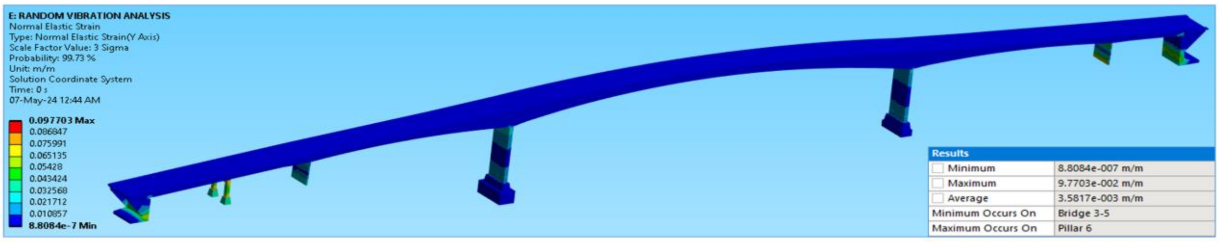

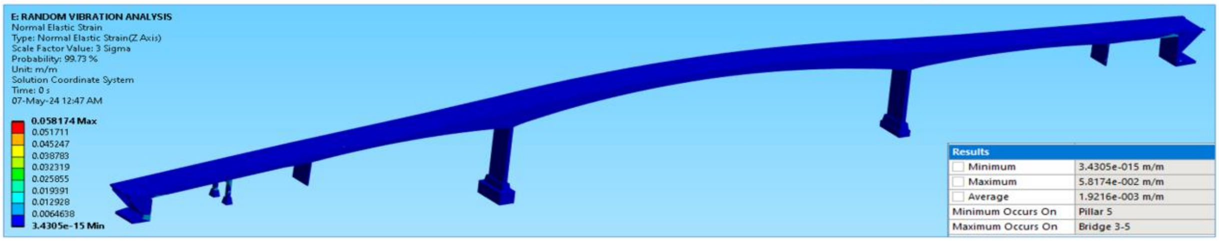

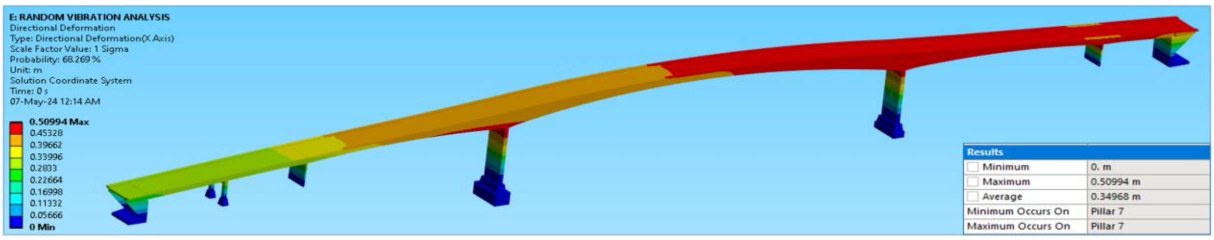

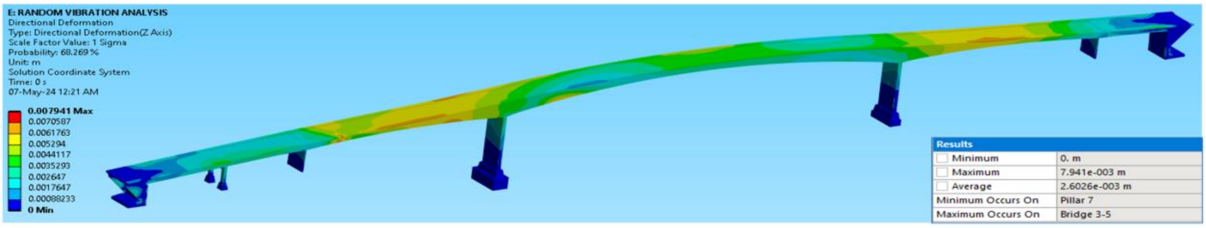
E: RANDOM VIBRATION ANALYSIS
Directional Deformation
Type: Directional Deformation(Z Axis)
Scale Factor Value: 1 Sigma
Probability: 68.269 %
Unit: m
Solution Coordinate System
Time: 0 s
07-May-24 12:21 AM
0.007941 Max
0.0070587
0.0061763
0.005294
0.0044117
0.0035293
0.002647
0.0017647
0.00088233
0 Min
Results
Minimum 0. m
Maximum 7.941e-003 m
Average 2.6026e-003 m
Minimum Occurs On Pillar 7
Maximum Occurs On Bridge 3-5

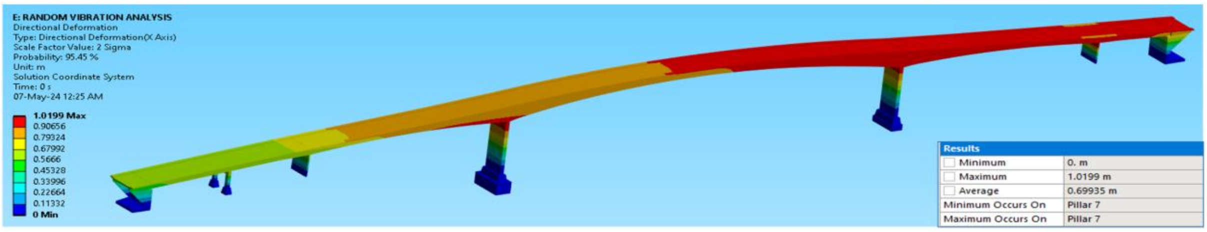
E: RANDOM VIBRATION ANALYSIS
Directional Deformation
Type: Directional Deformation(X Axis)
Scale Factor Value: 2 Sigma
Probability: 95.45 %
Unit: m
Solution Coordinate System
Time: 0 s
07-May-24 12:25 AM
1.0199 Max
0.90656
0.79324
0.67992
0.5666
0.45328
0.33996
0.22664
0.11332
0 Min
Results
Minimum 0. m
Maximum 1.0199 m
Average 0.69935 m
Minimum Occurs On Pillar 7
Maximum Occurs On Pillar 7

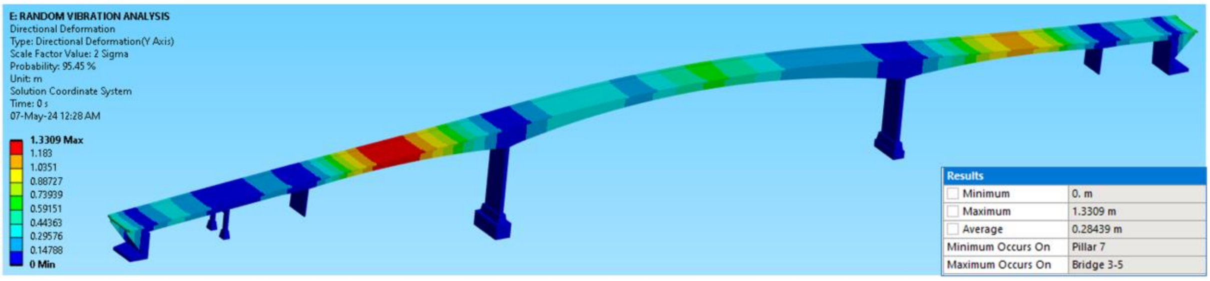
E: RANDOM VIBRATION ANALYSIS
Directional Deformation
Type: Directional Deformation(Y Axis)
Scale Factor Value: 2 Sigma
Probability: 95.45 %
Unit: m
Solution Coordinate System
Time: 0 s
07-May-24 12:28 AM
1.3309 Max
1.183
1.0351
0.88727
0.73939
0.59151
0.44363
0.29576
0.14788
0 Min
Results
Minimum 0. m
Maximum 1.3309 m
Average 0.28439 m
Minimum Occurs On Pillar 7
Maximum Occurs On Bridge 3-5


E: RANDOM VIBRATION ANALYSIS
Equivalent Stress
Type: Equivalent Stress
Scale Factor Value: 1 Sigma
Probability: 68.269 %
Unit: Pa
Time: 0 s
07-May-24 12:36 AM
1.8868e9 Max
1.6772e9
1.4675e9
1.2579e9
1.0482e9
8.386e8
6.2896e8
4.1931e8
2.0967e8
33021 Min
Results
Minimum 33021 Pa
Maximum 1.8868e+009 Pa
Average 8.1406e+007 Pa
Minimum Occurs On Bridge 3-5
Maximum Occurs On Load Bearing Steel Plate 2


E: RANDOM VIBRATION ANALYSIS
Equivalent Stress
Type: Equivalent Stress
Scale Factor Value: 2 Sigma
Probability: 95.45 %
Unit: Pa
Time: 0 s
07-May-24 12:34 AM
3.7736e9 Max
3.3543e9
2.935e9
2.5158e9
2.0965e9
1.6772e9
1.2579e9
8.3863e8
4.1935e8
66042 Min
Results
Minimum 66042 Pa
Maximum 3.7736e+009 Pa
Average 1.6281e+008 Pa
Minimum Occurs On Bridge 3-5
Maximum Occurs On Load Bearing Steel Plate 2


E: RANDOM VIBRATION ANALYSIS
Normal Elastic Strain
Type: Normal Elastic Strain(X Axis)
Scale Factor Value: 1 Sigma
Probability: 68.269 %
Unit: m/m
Solution Coordinate System
Time: 0 s
07-May-24 12:15 AM
0.034954 Max
0.03107
0.027186
0.023303
0.019419
0.015535
0.011651
0.0077675
0.0038838
2.9449e-14 Min
Results
Minimum 2.9449e-014 m/m
Maximum 3.4954e-002 m/m
Average 2.9311e-003 m/m
Minimum Occurs On Pillar 1
Maximum Occurs On Bridge 6-7


E: RANDOM VIBRATION ANALYSIS
Normal Elastic Strain
Type: Normal Elastic Strain(X Axis)
Scale Factor Value: 2 Sigma
Probability: 95.45 %
Unit: m/m
Solution Coordinate System
Time: 0 s
07-May-24 12:27 AM
0.069908 Max
0.06214
0.054373
0.046605
0.038838
0.03107
0.023303
0.015535
0.0077675
5.8899e-14 Min
Results
Minimum 5.8899e-014 m/m
Maximum 6.9908e-002 m/m
Average 5.8623e-003 m/m
Minimum Occurs On Pillar 1
Maximum Occurs On Bridge 6-7

Response PSD results

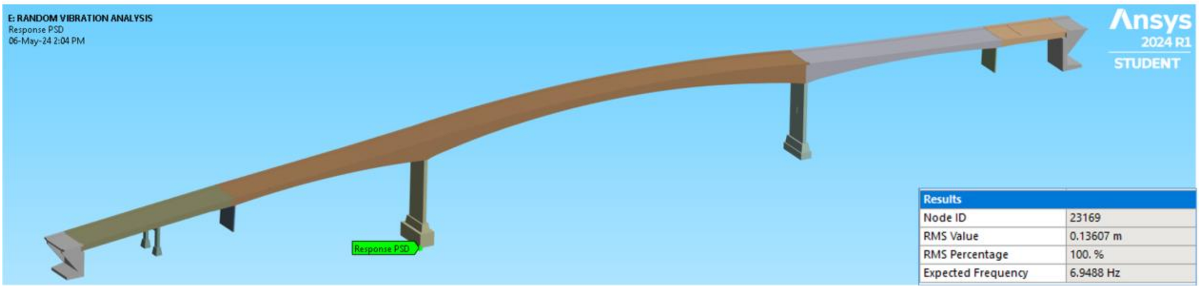

Tabular Data

	Frequency [Hz]	Response PSD [(m²)/Hz]
1	3.589	4.4784e-003
2	3.6173	4.2625e-003
3	3.824	3.0031e-003
4	3.9475	2.4583e-003
5	3.9737	2.4534e-003
6	4.0788	2.4342e-003
7	4.1512	2.4214e-003
8	4.2003	2.4128e-003
9	4.2332	2.4072e-003
10	4.2552	2.4034e-003
11	4.2698	2.4009e-003
12	4.2795	2.3993e-003
13	4.2859	2.3982e-003
14	4.2902	2.3975e-003
15	4.293	2.397e-003
16	4.2948	2.3967e-003
17	4.296	2.3965e-003
18	4.2968	2.3964e-003
19	4.2984	2.3961e-003
20	4.2999	2.3959e-003
21	4.3007	2.3957e-003
22	4.3019	2.3955e-003
23	4.3038	2.3952e-003
24	4.3066	2.3948e-003
25	4.3108	2.3941e-003
26	4.3173	2.393e-003
27	4.3184	2.3928e-003
28	4.327	2.3914e-003
29	4.3419	2.3889e-003
30	4.3645	2.3852e-003
31	4.3987	2.3796e-003
32	4.4345	2.3738e-003
33	4.4507	2.3712e-003
34	4.5148	2.361e-003
35	4.5297	2.3587e-003
36	4.5695	2.3525e-003
37	4.6065	2.3468e-003
38	4.6312	2.343e-003
39	4.6478	2.3405e-003
40	4.6495	2.3402e-003
41	4.6588	2.3388e-003
42	4.6661	2.3377e-003
43	4.671	2.337e-003
44	4.6742	2.3365e-003
45	4.6763	2.3362e-003
46	4.6777	2.336e-003
47	4.6786	2.3358e-003
48	4.6805	2.3355e-003
49	4.6823	2.3353e-003
50	4.6832	2.3351e-003
51	4.6846	2.3349e-003
52	4.6868	2.3346e-003
53	4.69	2.3341e-003
54	4.6949	2.3334e-003
55	4.7022	2.3323e-003
56	4.7134	2.3306e-003
57	4.7302	2.3281e-003
58	4.7557	2.3244e-003
59	4.7941	2.3188e-003
60	4.8069	2.3169e-003
61	4.8523	2.3104e-003
62	4.939	2.2981e-003
63	4.9401	2.2979e-003
64	5.0309	2.2854e-003
65	5.0729	2.2797e-003
66	5.0941	2.2768e-003
67	5.137	2.2711e-003
68	5.1659	2.2672e-003
69	5.1854	2.2647e-003
70	5.1984	2.263e-003
71	5.2071	2.2618e-003
72	5.2129	2.2611e-003
73	5.2168	2.2606e-003
74	5.2193	2.2602e-003
75	5.2211	2.26e-003
76	5.2222	2.2599e-003
77	5.2245	2.2596e-003
78	5.2268	2.2593e-003
79	5.2279	2.2591e-003
80	5.2296	2.2589e-003
81	5.2322	2.2586e-003
82	5.2361	2.2581e-003
83	5.2419	2.2573e-003
84	5.2453	2.2569e-003
85	5.2507	2.2562e-003
86	5.2639	2.2545e-003
87	5.2837	2.2519e-003
88	5.3135	2.2481e-003
89	5.3582	2.2425e-003
90	5.4255	2.2341e-003
91	5.5265	2.2217e-003
92	5.5543	2.2183e-003
93	5.6783	2.2037e-003
94	5.7836	2.1915e-003
95	5.9064	2.1777e-003
96	5.9488	2.173e-003
97	6.0653	2.1604e-003
98	6.1464	2.1518e-003
99	6.2021	2.1459e-003
100	6.2402	2.142e-003
101	6.2492	2.1411e-003
102	6.2661	2.1393e-003
103	6.2836	2.1375e-003
104	6.2954	2.1363e-003
105	6.3034	2.1355e-003
106	6.3065	2.1352e-003
107	6.3088	2.1378e-003
108	6.3125	2.1418e-003
109	6.3149	2.1445e-003
110	6.3166	2.1463e-003
111	6.32	2.1501e-003
112	6.3233	2.1539e-003
113	6.325	2.1557e-003
114	6.3274	2.1584e-003
115	6.3311	2.1625e-003
116	6.3365	2.1685e-003
117	6.3446	2.1775e-003
118	6.3565	2.1909e-003
119	6.3743	2.211e-003
120	6.389	2.2276e-003
121	6.4007	2.2411e-003
122	6.44	2.2863e-003
123	6.4984	2.3546e-003
124	6.5167	2.3763e-003
125	6.5853	2.4588e-003
126	6.606	2.4841e-003
127	6.6678	2.5607e-003
128	6.7101	2.6141e-003
129	6.7143	2.6194e-003
130	6.7391	2.6511e-003
131	6.7588	2.6765e-003
132	6.7722	2.6938e-003
133	6.7812	2.7056e-003
134	6.7874	2.7136e-003
135	6.7915	2.719e-003
136	6.7944	2.7227e-003
137	6.7963	2.7252e-003
138	6.8002	2.7304e-003
139	6.8042	2.7356e-003
140	6.8061	2.7381e-003
141	6.8089	2.7418e-003
142	6.8131	2.7473e-003
143	6.8193	2.7554e-003
144	6.8284	2.7675e-003
145	6.8419	2.7854e-003
146	6.8619	2.812e-003
147	6.8915	2.8518e-003
148	6.9245	2.8966e-003
149	6.9353	2.9113e-003
150	7.0001	3.001e-003
151	7.0664	3.0946e-003
152	7.0961	3.1372e-003
153	7.166	3.2393e-003
154	7.2354	3.3427e-003
155	7.238	3.3466e-003
156	7.2833	3.4154e-003
157	7.3161	3.4659e-003
158	7.3386	3.5008e-003
159	7.354	3.5248e-003
160	7.3645	3.5412e-003
161	7.3716	3.5524e-003
162	7.3765	3.56e-003
163	7.3798	3.5652e-003
164	7.382	3.5688e-003
165	7.3868	3.5763e-003
166	7.3915	3.5838e-003
167	7.3917	3.584e-003
168	7.3938	3.5874e-003
169	7.3971	3.5926e-003
170	7.402	3.6003e-003
171	7.4091	3.6117e-003
172	7.4197	3.6285e-003
173	7.4352	3.6534e-003
174	7.4411	3.6628e-003
175	7.4581	3.6902e-003
176	7.4751	3.7177e-003
177	7.4918	3.7448e-003
178	7.4984	3.7556e-003
179	7.5143	3.7817e-003
180	7.5252	3.7996e-003
181	7.5327	3.8118e-003
182	7.5377	3.8202e-003
183	7.5412	3.8259e-003
184	7.5414	3.8262e-003
185	7.5435	3.8298e-003
186	7.5485	3.8381e-003
187	7.5535	3.8463e-003
188	7.5558	3.8502e-003
189	7.5593	3.856e-003
190	7.5644	3.8644e-003
191	7.5718	3.8769e-003
192	7.5828	3.8952e-003
193	7.5978	3.9205e-003
194	7.5989	3.9223e-003
195	7.6226	3.9624e-003
196	7.6329	3.9799e-003
197	7.6571	4.0211e-003
198	7.6574	4.0217e-003
199	7.6736	4.0495e-003
200	7.6849	4.0689e-003
201	7.6926	4.0823e-003
202	7.6979	4.0914e-003
203	7.7014	4.0976e-003
204	7.7039	4.1019e-003
205	7.7087	4.1101e-003
206	7.7091	4.1109e-003
207	7.7144	4.1201e-003
208	7.7168	4.1243e-003
209	7.7204	4.1306e-003
210	7.7257	4.1398e-003
211	7.7334	4.1534e-003
212	7.7448	4.1734e-003
213	7.7615	4.2028e-003
214	7.7861	4.2463e-003
215	7.7983	4.2682e-003
216	7.8221	4.3107e-003
217	7.8749	4.4065e-003
218	7.9525	4.5497e-003
219	8.0665	4.7658e-003
220	8.1377	4.9045e-003
221	8.2337	5.0958e-003
222	8.389	5.416e-003
223	8.4793	5.6084e-003
224	8.5587	5.7816e-003
225	8.5712	5.5557e-003
226	8.7012	3.6808e-003
227	8.7931	2.7625e-003
228	8.8397	2.3903e-003
229	8.8574	2.2633e-003
230	8.9022	1.9715e-003
231	8.9333	1.7921e-003
232	8.9549	1.6779e-003
233	8.9698	1.6034e-003
234	8.9801	1.554e-003
235	8.9871	1.5208e-003
236	8.992	1.4984e-003
237	8.9954	1.4832e-003
238	9.0028	1.45e-003
239	9.0061	1.4357e-003
240	9.0103	1.4363e-003
241	9.0136	1.4368e-003
242	9.0185	1.4376e-003
243	9.0257	1.4386e-003
244	9.036	1.4401e-003
245	9.051	1.4424e-003
246	9.0729	1.4456e-003
247	9.1046	1.4503e-003
248	9.1255	1.4534e-003
249	9.1507	1.4572e-003
250	9.2176	1.4671e-003
251	9.3149	1.4816e-003
252	9.329	1.4837e-003
253	9.4562	1.5025e-003
254	9.4753	1.5053e-003
255	9.5793	1.5208e-003
256	9.6527	1.5316e-003
257	9.6616	1.5329e-003
258	9.7042	1.5392e-003
259	9.7402	1.5446e-003
260	9.7653	1.5483e-003
261	9.7827	1.5508e-003
262	9.7948	1.5526e-003
263	9.8032	1.5539e-003
264	9.809	1.5547e-003
265	9.8131	1.5553e-003
266	9.8222	1.5567e-003
267	9.8313	1.558e-003
268	9.8353	1.5586e-003
269	9.8412	1.5595e-003
270	9.8496	1.5607e-003
271	9.8618	1.5625e-003
272	9.8794	1.5651e-003
273	9.9048	1.5689e-003
274	9.9416	1.5743e-003
275	9.9736	1.5791e-003
276	9.9946	1.5822e-003
277	10.071	1.5935e-003
278	10.086	1.5956e-003
279	10.165	1.6073e-003
280	10.182	1.6098e-003
281	10.221	1.6156e-003
282	10.261	1.6214e-003
283	10.288	1.6254e-003
284	10.307	1.6283e-003
285	10.321	1.6302e-003
286	10.33	1.6316e-003
287	10.336	1.6326e-003
288	10.341	1.6332e-003
289	10.341	1.6333e-003
290	10.351	1.6348e-003
291	10.357	1.6356e-003